EXPERIMENTS IN AXISYMMETRIC SUPERSONIC JETS

Thesis by

Cyrille Dennis Moore

In Partial Fufillment of the Requirements

for the Degree of

Doctor of Philosophy

California Institute of Technology

Pasadena, California

1996

(Submitted September 29, 1995)

Acknowledgments

I would first and foremost like to thank my advisor, Professor Anatol Roshko, for his patience and guidance during the course of this research. He has made the difficulties encountered my graduate work not only bearable but enjoyable.

I am also indebted to other members of the GALCIT faculty for their assistance and suggestions during the course of this research. In particular, Professors Donald Coles, Ed Zukoski, and Mory Gharib greatly aided this research. The Aero Shop was very helpful, often allowing me to take over one of their lathes for a week at a time.

Fellow graduate students Sid Valluri, Derek Lisoski, and Flavio Noca were instrumental in helping to keep my spirits up when Murphy seemed to have taken up residence in the Firestone basement. I am also grateful to Elliot and Jill Andrews for their encouragement, and to Sam Wheeler for helping with the machining of some of the components of the facility.

This project was sponsored by ONR, whose support we gratefully acknowledge.

I would also like to thank my family for supporting and encouraging me during my stay at GALCIT, and my wife Wei, without whom I could not have finished.

Abstract

An experimental study of the effects of exit Mach number and density ratio on the development of axisymmetric jets is described in this thesis. Jet exit Mach numbers of 1.41, 2.0, and 3.0, were studied for jets of helium, argon, and nitrogen. The jets exit into a gas at rest (velocity ratio = 0), in order to better isolate the effects of compressibility and density ratio. Density ratios vary from 0.23 to 5.5.

In order to generate shock free-jets, unique nozzles were designed and constructed for each gas and Mach number combination. A plating method for the construction of the nozzles was developed to ensure high-accuracy and a good surface finish at a cost significantly less than direct-machining techniques.

The spreading rate of the jet for several downstream locations is measured with a pitot probe. Centerline data are used to characterise the length of the potential core of the jet, which correlates well with the relative spreading rates. Limited frequency data is obtained through the use of piezo-resistive pressure probes. This method is promising for flows that are not conducive to hot-wire probes.

Spark shadography is used to visualize both the mean and instantaneous flow, with the minimum spark time being 20 nanoseconds. The convection velocity of large-scale disturbances is estimated from the visible Mach-type acoustic waves emanating from the jet.

For a wide range of jet Mach and Reynolds numbers, the convection velocity of the large scale disturbances in the potential core region of the jet is approximately 0.8 times the jet velocity, the approximate velocity of the first helical instability mode of the jet.

The main objectives of the present work were to investigate the effects of compressibility and density on the initial development of the axisymmetric jet. Although the data are not sufficient to determine if the convective Mach number concept used in 2-d shear layer research will work in the case of an axisymmetric jet, it is clear that the axisymmetric data do not collapse onto the 2-d curve. However, the density ratio scaling used for the 2-d shear layer appears to work well for the axisymmetric jet, based on the available data.

The data appear to indicate that the initial development of the jet is dominated by instability modes of the jet as a whole, rather than the shear layers.

One anomaly noted was that there were long period variations in the centerline total pressure, with times on the order of 3000 jet time scales. The fluctuations did not appear to be experimental artifacts.

Contents

List of Figures

List of Tables

Chapter 1

Introduction

1.1 Motivation

Turbulent mixing is an important physical process that has a profound influence in our daily lives. The efficiency of every combustion system is directly influenced by the mixing processes between the fuel and oxidizer, and even things as mundane as the escape slides on aircraft rely on mixing in the ejectors for proper inflation. In the literature, the word 'mixing' has generally been used to indicate that fluid has been entrained into a mixing region of some sort, rather than being mixed on a molecular level. Herein, 'mixing' will be used to designate the entanglement or engulfment of fluid, and 'molecular mixing' will be used to designate mixing on a molecular level.

There has been long-term scientific interest in turbulent compressible mixing and on attempting to quantify the difference between density and compressibility effects on mixing. Birch and Eggers [1] gathered data which showed that as the Mach number increased, for the case of one stream at rest, the spreading rate decreased, with the spreading rate being assumed as indicative of the level of mixing. However, since the experiments performed up to that point generally involved two streams of air mixing together, with the same total temperatures, there was a question as to whether the mixing differences were due to the compressibility of the flow per se, or to the density difference, since the higher Mach number stream was colder and more dense.

In an attempt to answer this question, Brown and Roshko [2] built an apparatus for conducting research into the effect of density differences on the development of an incompressible (M = 0) two-dimensional shear layer. In addition to identifying large scale structures as important in the mixing process, they found that although density ratio did affect mixing, it was a much smaller effect than observed experimentally with compressible shear layers having the same density ratio. Compressibility, therefore, had to be an important parameter in the growth of the turbulent mixing layer.

The intervening 20 years between that paper and the present has been filled with various studies of the compressible shear layer. However, the vast majority of these studies have focused on the two-dimensional shear layer, primarily because after a

short region dominated by the wake component, the shear layer is expected to be self-similar and so lends itself to well-defined experimental conditions that are also amenable to theoretical treatments. Brown and Roshko chose a two-dimensional shear layer to study in part because it was a much more clear-cut experiment than one done with a jet, although experimentally more difficult. Traditionally, experimenters have used Bradshaw's estimate of several hundred initial momentum thicknesses as far enough to be in the self-similar region [3]. However, Dimotakis [4] has more recently argued that the planar shear layer can be affected by its initial conditions several thousand momentum thicknesses downstream of the splitter plate. This may be a large part of the reason for the wide scatter in the experimental data.

Although the results obtained by the various experimenters have been very useful and have greatly enhanced our understanding of the mixing process in the case of a two-dimensional shear layer, they do not necessarily apply to the case of an axisymmetric shear layer, which is very common in the physical world. Jet and rocket motors, plumes, gaseous injectors and ejectors, for example, all have an axisymmetric geometry. Unlike a two-dimensional shear layer, however, the axisymmetric shear layer, typically formed by an axisymmetric jet, does not become self-similar. Axisymmetric jets do not become self-similar until the jet fluid is so dilute that the jet core disappears, the velocity and mass profiles form the typical gaussian-like profiles [5],

and the only experimentally determinable quantity associated with the jet is its initial momentum flux.

In the case of a supersonic axisymmetric jet, for instance, the jet initially forms an annular shear layer between unmixed jet fluid and unmixed ambient fluid. One expects that the shear layer would entrain fluid in a similar ratio to the two-dimensional shear layer initially (i.e., biased towards the high-speed side) but as the shear layer grows the entrainment ratio would shift towards the ambient fluid, due to the different circumferences on the inside and outside of the annulus. Furthermore, as the shear layer grows, the unmixed jet fluid disappears and one is left with a jet of varying velocity and composition at a supersonic Mach number. At a sufficiently far distance, the flow becomes subsonic and the jet gas dilute enough, that the jet is self-similar, with only the momentum input distinguishable as an input. However, by this point there is no effect of either compressibility or density ratio on the downstream development of the jet.

Furthermore, for gaseous injectors and other important physical processes, the combustion, if any, and noise production take place within a relatively few jet diameters of the exit. This requires that experimental studies of density of compressibility effects on jets be done in a non-self similar environment, which raises the experimental complexity and the difficulty of achieving repeatable, comparable results. As a res-

ult, compressible mixing in axisymmetric supersonic jets has not been a well studied problem, and there are many questions unanswered.

The goal of this research therefore became to quantify the role that density ratio and compressibility play in the mixing of axisymmetric supersonic jets.

1.2 Previous Research

1.2.1 Planar Shear Layers

Although the focus of this thesis is axisymmetric jets, some of the results from two-dimensional shear layers are important in that they lend some physical intuition into what we would expect in the axisymmetric case. Specifically, the effects of density ratio and compressibility on planar shear layers would be expected to be qualitatively similar to that of axisymmetric jets. The nomenclature traditionally used to describe planar shear layers is as shown in figure 1.1, taken from [6], where $U_1 > U_2$.

Brown and Roshko [2], as mentioned above, investigated the effects of density ratio on an incompressible two-dimensional shear layer, with the density ratio varying from 1/7 to 7. They found that the shear layer spread less rapidly with a denser high-speed fluid and more rapidly with a lighter high-speed fluid, for the same velocity ratio, although this difference in the spreading rate was less than observed for a compressible

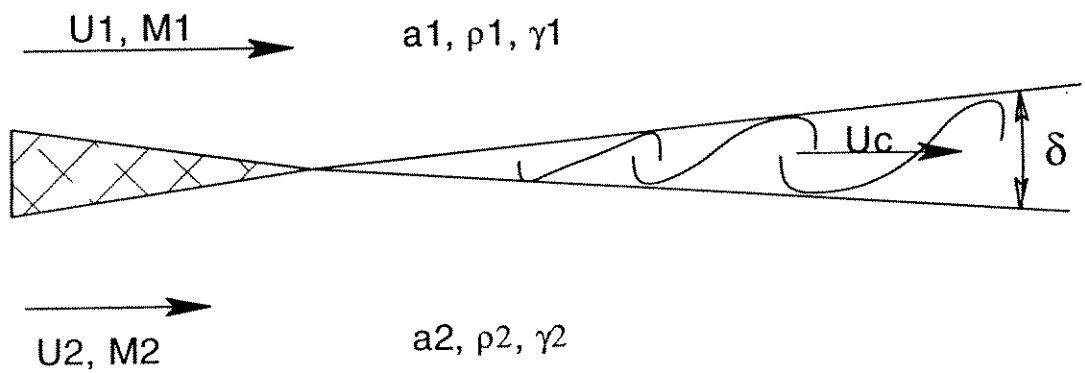

Figure 1.1: Planar Shear Layer Nomenclature

shear layer generating the same density difference.

Brown found, when analyzing the data, that the total entrainment for a given density ratio was the same regardless of which fluid was on the high-speed side, and that the individual entrainment rates for a given gas combination and velocity ratio depended only on the gases used. The entrainment, therefore, depended only on the density ratio and not on whether the light gas, for instance, was the high-speed or low-speed fluid [7]. He argued using an analogy of a temporally growing layer, which obviously is independent of the individual gas velocities and depends solely on the velocity difference and gases. The only possible frame of reference in this case is one

fixed on the large structures, which would be expected to convect at a velocity closer to the high density side than to the low density side. The following argument is taken largely from his paper, with some notation changes.

In a temporally growing layer, with the frame of reference fixed on a large structure, $u_2 = -k * u_1$, and the growth rate of the layer is proportional to $u_1 - u_2$. For $s = \frac{\rho_2}{\rho_1}$, the expression for the growth rate can be expressed as

$$\frac{d\delta}{dt} = c(s)(u_1 - u_2) = c(s)(1 + k(s))u_1 \tag{1.1}$$

where c(s) and k(s) express the dependence of the growth rate on the density ratio. For an observer moving at a speed U_0 with respect to the large structures, so that $U_1 = u_1 + U_0$, $U_2 = u_2 + U_0$, $r = \frac{U_2}{U_1}$, and $\delta' = \frac{d\delta}{dx}$:

$$\delta' = \frac{c(s)(1 + k(s))u_1}{U_0} = \frac{c(s)(1 + k(s))(U_1 - U_2)}{U_1 k(s) + U_2} = \frac{c(s)(1 + k(s))(1 - r)}{k(s) + r} \tag{1.2}$$

Brown then argues that if the gases, or equivalently, the velocities, are interchanged, the growth rate does not change for the temporal layer. The convection velocity of the large structures remains the same with respect to the individual gases. For example, in the temporal case it makes no difference to a helium-nitrogen shear layer whether the helium or the nitrogen is stationary with respect to the laboratory frame of reference. The large-scale structures will have the same velocity with respect to the two sides of the shear layer independent of the reference frame of the observer.

Therefore, $c(s) = c(\frac{1}{s})$ and $k(\frac{1}{s}) = \frac{1}{k(s)}$. This requires that k(s) have the form of a power law, and that c(s) be an even function with a minimum at $s = 1$. Furthermore, since molecular diffusion is expected to be unimportant for turbulent flow, c(s) = c, a universal constant. The data that Brown used was very limited (5 data points) and he concluded that $k(s) = s^{-n}$, where n was between 0.5 and 0.6 and c = 0.178. As a note, for a frame of reference moving so that the dynamic pressures of each stream are identical, n = 0.5. Under the assumption that the dynamic pressures are approximately equal, for $U_2 \equiv 0$, $r \equiv 0$ (i.e., half jet), and the above equation becomes:

$$\delta' = c(s)(\frac{1}{k(s)} + 1) = 0.178(s^{\frac{1}{2}} + 1) \tag{1.3}$$

Experiments performed by Konrad [8], however, showed that the amount of fluid entrained did depend on which fluid was on the high-speed side. Dimotakis [9] proposed to account for the difference based on the observed assymetry of the large structures in a spatially growing shear layer. Specifically, it would be expected that the high-speed fluid would be preferentially entrained into the layer, since the 'scoop' was larger on the high-speed side of a large structure than on the low-speed side, since the high-speed fluid was entrained downstream of the structure, where the mixing layer was thicker and the distance to the next structure was larger than on the upstream side.

The modified expression for growth rate becomes:

$$\delta' = c\frac{(1-r)(1+s^{1/2})}{1+s^{1/2}r}\left[1-\frac{(1-s^{1/2})/(1+s^{1/2})}{1+2.9(1+r)/(1-r)}\right] \tag{1.4}$$

where the factor in brackets accounts for the spatial asymmetry, for typically- observed structure spacing.

For the present work, $U_2 \equiv 0$, $r \equiv 0$, and the expression reduces to :

$$\delta' = c(1+s^{1/2})\left[1-\frac{(1-s^{1/2})}{3.9(1+s^{1/2})}\right] \tag{1.5}$$

Although it may seem very surprising, very little work was done subsequent to the work of Brown and Roshko to quantify the effect of compressibility on the growth of mixing layers, until the analysis of Bogdanoff [10] and Papamoschou's Ph.D. thesis [6] and associated papers. In his work, Papamoschou made use of the 'convective Mach number' concept, where the inherent compressibility of the shear layer is measured from a frame of reference that moves with a speed between that of the two layers such that when the two flows are isentropically brought to rest in the chosen frame of reference the total pressures match. This avoids the problems with a laboratory frame of reference, where two streams that are supersonic with respect to the laboratory may be subsonic with respect to each other and will therefore behave as a subsonic shear layer with respect to growth rate. In order to isolate the effects of compressibility, he measured the growth rates of various compressible shear layers and compared

them with Brown's model for the incompressible shear layer, at the same density and velocity ratios. The data used for the normalization was the existing literature data for incompressible flow. He found that there was little or no effect of compressibility on the growth rate of the shear layer until the convective mach number reached about 0.4, whereupon the growth rate dropped dramatically to about 0.2 at a convective Mach number of 0.8. Dimotakis [4] used data from Papamoschou and subsequent experimenters to arrive at the following equation:

$$f(M_{c1}) = \frac{\delta'(r, s, M_{c1})}{\delta'(r, s, M = 0)} = (1 - f_\infty)e^{-3M_{c1}^2} + f_\infty \tag{1.6}$$

with f_∞= 0.2.

1.2.2 Incompressible Homogeneous Jets

Any attempt to understand mixing in axisymmetric jets must have, as a basis, an understanding of the fundamental problem, in this case the development of incompressible, homogeneous, axisymmetric jets. A summary of experiments up to 1950 is given in [11]. Abramovich, in his book [12], reviews the basic theories and formulas. A diagram of the traditional jet nomenclature is given in figure 1.2. For incompressible, homogeneous, non-coflowing jets, the potential core length is 4 jet diameters, and the centerline velocity is proportional to $\frac{1}{x}$ in the far field.

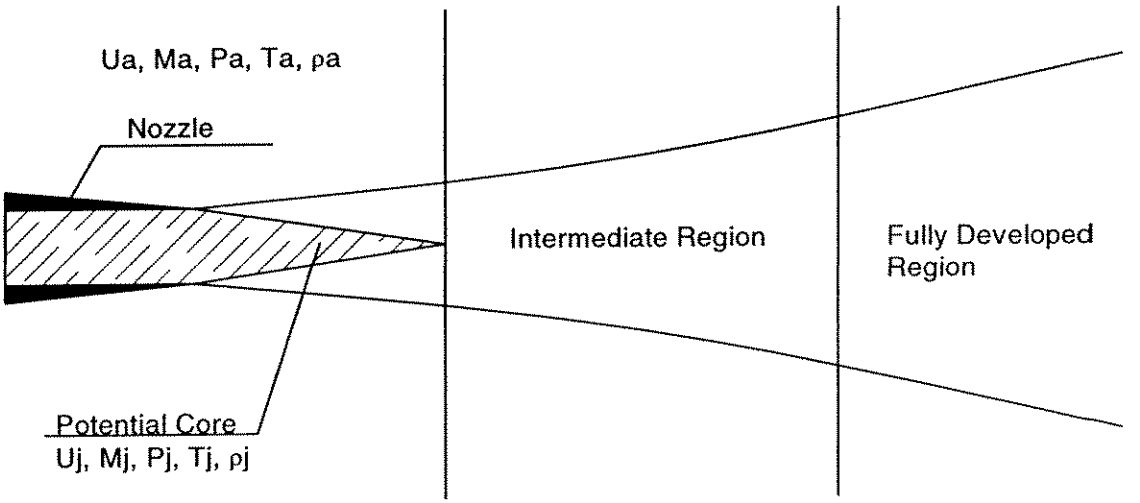

Figure 1.2: Axisymmetric Jet Nomenclature

One of the more useful studies was done by Forstall and Shapiro [11]. They studied jets, both with and without coflow, using a small percentage of helium in the jet in order to determine the spreading rates of jet fluid as well as the jet momentum. They found that the spreading rate of both mass and momentum was proportional to $x^{1-\lambda}$ where $\lambda = \frac{U_a}{U_j}$. Furthermore, the radial profiles were well approximated by either a cosine or gaussian curve whose maximum value decayed as $\frac{1}{x}$. The potential core length, L, was found to be $L = 4 + 12\lambda$. The ratio of the momentum to mass mixing widths was .70, which is a direct measure of the 'turbulent Schmidt number' of the jet. By examining the data of previous researchers, they came to the conclusion that

the turbulent Prandtl and Schmidt numbers were nearly equal for axisymmetric jets.

1.2.3 Incompressible Inhomogeneous Jets

There has been long term scientific interest and experimentation in inhomogeneous axisymmetric jets, here taken to mean those jets where the density difference is due to some factor other than temperature difference due to isentropic expansion of the jet. The density difference could be due to heating or cooling the jet gas so that the stagnation temperatures were different or to the use of different gases. Unfortunately, nearly all the experiments have concentrated on the far-field development of the jet, after similarity had been achieved.

Among the first inhomogeneous jet experiments reported in the open literature were those of Corrsin and Uberoi in 1949 [13]. They investigated heated air jets and found that the jets, once fully developed, had the same form as homogeneous jets, i.e., the velocity distribution was gaussian. The temperature profiles were also gaussian, although they were wider than the velocity. Similar results were obtained by Keagy and Weller [14] who studied jets of helium, nitrogen, and carbon dioxide into air. The velocity and concentration profiles were gaussian, beyond the end of the potential core, with the concentration profiles being wider than the velocity profiles. Unfortunately, they only reported traverses made at 16 and 24 diameters. The meas-

ured turbulent Schmidt number in their experiments varied linearly with density of the jet fluid $Sc_T = .464 + m/114$, where m is the molecular weight. An interesting result of their experiments was that for a homogeneous jet, the centerline values of concentration and velocity, relative to the initial values were nearly identical; for a heavy jet, the concentration decayed more rapidly than the velocity; and for a light jet, the concentration decayed much more slowly than the velocity. This is a result of the fact that in order to conserve both mass and momentum, where the profiles can both be well approximated by a gaussian, then the mean centerline velocity and concentration are related by $\overline{C_c U_c} = constant/x^2$, where the constant is determined by initial conditions.

In 1953, Thring and Newby [15] proposed that the jet data would collapse if scaled by an effective radius $r_\varepsilon = r_o(\rho_o/\rho_\infty)^{1/2}$, which is the radius of a jet composed of ambient fluid having the same mass and momentum flux as the inhomogeneous jet. In his Ph.D. thesis, Tombach investigated jets composed of helium into air, air into helium, air into air, and helium into SF_6, although he only examined velocity and not concentration. He also found that despite a very large range of density differences, the jets all developed a gaussian profile as their asymptotic form, and that they had a centerline decay of $\frac{1}{x}$, as expected [5]. The primary result of the density difference was a shift in the virtual origin of the jet for the far-field behavior. Recent

experiments by Pitts [16] confirmed the $\frac{1}{x}$ decay of both velocity and concentration, and provided a fairly exhaustive list of other references. A companion paper [17] examined Reynolds number dependence and found that as Reynolds number increased, there was a downstream shift in the virtual origin of the jet, but that no shift was observed as the Reynolds number was increased beyond 50000 or so.

Abramovich et al. [18] conducted experiments with air, helium, and freon-12, with and without a coflow. It is the only paper that I am aware of that attempted to examine density and velocity effects on the initial region of a jet. The paper covers a wide variety and range of parameters, and there are few details provided. However, there are a few pertinent results that can be gleaned from the data. The first is that a coflow substantially changes the character of the jet. The second is that in a jet without coflow, the entrainment ratio of the jet is a very weak function of density: the ratio of growth of the mixing region into the ambient fluid to the growth of the mixing region into the jet fluid changes from 0.63 to 0.57 as the ratio of the jet to ambient density ratio changes from 3.7 to 0.143. Furthermore, as the jet density increases, the spreading rate of the shear layer decreases, roughly as $1 + (\frac{\rho_a}{\rho_j})^{.5}$, where a and j denote ambient and jet conditions, respectively. By definition, the jet fluid has a higher velocity than the ambient fluid, and so, in accordance with the conventions mentioned previously for planar shear layers, this equation can be written as $\delta' \propto 1 + s^{\frac{1}{2}}$. This

is in agreement with results from planar shear layers, expressed in equation 1.3.

1.2.4 Homogeneous Compressible Jets

Although there has been a large number of papers written about homogeneous, axisymmetric, compressible jets, the vast majority of them focus on the noise properties of the jet, rather than on the mixing between the jet and the free-stream. Since, as discussed in the following section, the data for compressible, inhomogeneous jets are both scarce and not easily comparable, it is important to glean as much information as possible about Mach number effects from the homogeneous data. While the following discussion is by no means exhaustive, it should serve to illuminate the current state of knowledge.

One of the earliest investigations of compressible jets was conducted by Johannesen, under the auspices of the British A.R.C., in 1957. He investigated a Mach 1.40 jet of Air into Air, using pitot and static pressure probes and schlieren and shadowgraph flow visualization as diagnostics [19, 20]. One of the most important points to come out of his work was the demonstration that Foelsch nozzles are inadequate for use in axisymmetric flows. His 'Jet 1' was a Foelsch design for parallel, ideally expanded flow at Mach 1.40. However, pressure measurements and pictures both showed a very strong shock pattern in the jet. He subsequently made four more nozzles of sim-

ilar design to investigate the problem. He found that the Foelsch design resulted in a Mach-disk type of shock in the nozzle just downstream of the throat. This shock could not be eliminated, although it could be reduced in intensity by using a larger inlet radius. Johannesen concluded that the Foelsch method's difficulties resulted from the discontinuity in curvature inherent in the method, leading to the shock in the nozzle. Furthermore, the details of the inlet shape were, in fact, important in determining the quality of flow through the nozzle; using a smooth contraction was not sufficient. The shape of the inlet influences the shape of the sonic line at the throat, and since supersonic nozzle design methods use the throat and sonic line as starting points for the characteristics, the inlet must be shaped so as to give a sonic line as close as possible to the assumed shape. Johannesen then manufactured a nozzle using the Clippinger method, which avoided the discontinuity inherent in the Foelsch approach. This jet, designated 'Jet 6', had much improved flow characteristics.

In addition to the surprisingly difficult task of designing and building a shock-free, ideally-expanded nozzle, Johannesen had a hard time measuring static pressure in Jet 6, and could not measure any static pressures in Jet 1. For Jet 6, except in the exit plane of the nozzle, there was a local maximum on the jet axis and two minima at the inflection points of the velocity profile. These minima gradually merged and became a single minimum on the axis. In the exit plane of the nozzle, there is a

local minimum on the axis and local maxima about 0.2 jet radii from the axis. The pressure variations were small enough that the assumption of a constant static pressure equal to the ambient value did not noticably change the velocities calculated from the pitot measurements. Johannesen was doubtful that the static pressure traverses were reliable; the shock wave from the tip of the static probe could either be interfering with the jet or reflecting from the shear layer, and the effect of large shear and turbulence on static probes had not been sufficiently addressed experimentally to provide reasonable confidence in or corrections to the data.

There were several unexpected experimental results in his research. The strong shocks in Jet 1 shortened the potential core to $\frac{x_c}{D_j} = 3$ as compared to 4 for an incompressible jet. While the shortening of the potential core in the presence of strong shocks is not unexpected, the jet was symmetric and the shear layers had an initial spreading rate of only $\frac{1}{2}$ of the incompressible value. At the approximate location where the lip shock encountered the opposite shear layer, the spreading rate of the layer abruptly switched to the incompressible value. A shorter potential core combined with a reduced spreading rate requires that the shear layers be tilted more towards the axis than for the subsonic jet. In Jet 6, however, where there was no significant exit shock, the jet was asymmetric, and the spreading of the shear layer was constant, at about 80% of the incompressible value. The potential core length

was found to be about 7 jet diameters. Furthermore, although the stagnation pressure was kept constant to within 0.2%, long-time runs of Jet 1 showed significant 'bursts' in the pitot pressure on the jet centerline, with durations of up to 10 seconds. No explanation for either the asymmetry of Jet 6 or the pressure fluctuations of Jet 1 were found. The large variation in jet development due to the quality of the initial flow is also quite surprising, since the velocities derived from pitot and static pressure traverses in the potential core of Jet 1 were less than 5% different from the ideal value.

Researchers since Johannesen have frequently used simple conical nozzles for low-supersonic Mach numbers, assuming that the shock pattern had no effect on the development of the jet. Although this approach may produce results that are useful for, say, examining the effects of stagnation temperature or Reynold's Number on the jet development, neither a conical nor a Foelsch nozzle is adequate for studying ideally-expanded jets.

Warren [21, 22] investigated jets of air into air, using a 5:1 contraction with an exit diameter of 2.5 inches for subsonic jets, and installing rings designed using the Foelsch method on the interior of the contraction to form a throat for Mach numbers 1.5 and 2.6, again with a 2.5 in exit diameter. This method of constructing a supersonic nozzle did not work well; the Mach 2.6 nozzle had shock waves internal to the nozzle, and the flow produced by the Mach 1.5 nozzle was so poor that Warren deemed it unusable in

the experiments. His subsonic tests, consisting of Mach 0.690 and 0.970 air heated to keep the jet density at the ambient value, did show a definite increase in the potential core length with increasing jet Mach number. Furthermore, Warren's data show that the centerline data for any given density ratio tend to collapse when plotted against $\frac{x}{x_c}$, with the jet Mach number affecting the potential core length, and the density ratio determining the incompressible core length and the shape of the curve after the end of the potential core.

As did Johannesen, Warren attempted to measure the static pressure in his jets, and met with similar problems. His data showed a maximum in static pressure on the axis of the jet, and a static pressure minimum located within the shear region. The minima spread and merged to form a single minimum on the axis after the end of the potential core. However, the static pressure profiles at the nozzle exit were not uniform, and the interaction of the probe with the jet was not addressed. The measured static pressure variations did not result in an observable difference between the calculated velocity profile with the static pressure assumed to be constant and equal to the ambient pressure and that calculated with the measured static pressure.

In 1963, Maydew and Reed investigated jets of unheated air with exit diameters of 3 inches, and Mach numbers of 0.7, 0.85, 0.95, 1.49, and 1.96, exhausting into still air, [23]. Unfortunately for comparison purposes with the present work, their paper

does not explain how they designed the nozzle and it neither exits flush with a wall nor has a smooth outer contour, but rather appears to exit from a square tube whose dimensions are about 20% larger than the nozzle exit diameter. The purpose of their investigation was to determine the effect of the exit Mach number on the spreading rate of the shear layers. They traversed the shear layer at $\frac{x}{D} = 0.5, 1, 2, 3$, and 4, and found that although the error function profile fit the velocity curve fairly well through the center of the shear layer, the profiles suggested by Crane [24] worked better towards the edges of the layer. The growth was constant throughout the length of the potential core. Furthermore, ignoring a data point at Mach 3 from a private communication, the spreading rate of the jet was constant up until a Mach number of about 1, where it began to decrease nearly linearly with Mach number. The line is in good agreement with Johannesen's Jet 6.

Eggers [25] investigated a Mach 2.2 jet of air into air, for the primary purpose of developing eddy-viscosity coefficients. He used a 'minimum length' nozzle and his schlieren photographs clearly show a shock wave in the flow, emanating from within the nozzle. Unlike the other investigators, he provides the raw data in tabular form, as an appendix, rather than simply giving a result. The potential core length was 8.5 diameters.

In 1979, Lau, Morris and Fisher studied jets of Mach 0.28, 0.90, and 1.37 heated

air into still air, with a laser velocimeter [26]. The air was heated so that there was no density difference between the jet and ambient fluid. No details on the facility are given, beyond the exit diameter of the jet (51 mm), and the statement that the supersonic nozzle was designed with the method of characteristics. Both mean and fluctuating quantities were measured, at 2, 4, 8, 12, and 16 jet diameters downstream of the nozzle. They found that their data also collapsed when plotted non-dimensionalized by the potential core length for the centerline values, or by the local thickness for the profiles. Their estimate for the potential core length is $x_c = 4.2 + 1.1M_j^2$, and for the growth rate is $\delta' = 0.165 - 0.045M_j^2$. However, these results are somewhat suspect, since the value of the spreading rate at Mach 1.37 is nearly identical to that of Johannesen's Jet 1, which had extremely poor (shock-dominated) flow, but the potential core length is close to that of Jet 6. Their formula, if it is valid, only applies in the transonic range, since the results imply a spreading rate of 0 for Mach numbers of 1.91 or above, but with a finite potential core length.

1.2.5 Inhomogeneous Compressible Jets

There are only two sets of experiments that I am aware of that attempt to examine heterogeneous compressible jets. One set was conducted at the Polytechnic Institute of Brooklyn (PIB), under the direction of A. Ferri, and culminated in the report

by Zakkay et al. [27]. More recently, some experiments were conducted at Calspan [28, 29], using the Ludweig tube facility.

The experiments conducted at PIB appear, at first, to be very useful, since they examined the mixing between hydrogen, helium, argon, carbon dioxide, and air. However, the utility of the experiments to other experimenters was severely compromised by the basic assumptions of the PIB researchers. The basic assumption that they made was that all jet data could be characterized solely by the ratio of the mass flux of the jet and outer fluids, with the spreading angle increasing as the jet mass flux increased. If this were true, then a jet would spread more rapidly as the jet fluid were made denser, for the same velocity, and two streams of equal velocity and density would have the same mixing characteristics as a light, fast jet in a slowly moving outer fluid. These implications are contradicted by all other experimenters as well as by accepted jet theory.

The abnormal PIB results may have been a result of the experimental setup used in the conduct of their experiments. All experiments were conducted in a facility with a Mach 1.6 air outer stream of 3.44 inches diameter, with an inner nozzle of .3 or .6 inches diameter. Both streams exited into a 12 in diameter tube where the measurements were taken. As a result, the outer momentum was fixed, and the geometry was that of a constrained double coflow. This did not allow them to check their basic assumptions

regarding the physics of the mixing in the jet. In their analysis, no distinction was made between a jet and a wake. While they did achieve reproducible results, the results are not useful in a comparative study, due to their correlation solely by mass flux and the uncommon geometry.

The experiments at Calspan examined jets of a varying mixture of hydrogen and nitrogen, ranging from 0% to 100% H_2. The effects of density ratio were examined for Mach 4.0 into Mach 2.0 air and Mach 3.0 into still air. The effects of Mach number were examined for fixed jet/ambient density ratios of 1.67 and 0.1, for exit Mach numbers of 2, 3, and 4, in an outer stream of Mach 2.0 air. This set of experiments was intended to be used to generate constants for use in rocket plume codes. Therefore, most of the data was taken well downstream of the potential core, with the goal of being able to fit a universal cosine curve to the velocity and concentration data. The jet can therefore be described solely by centerline values and half-widths [28].

The nozzle flow was generated using a Ludwig tube. In order to fit the inner nozzles into the facility without affecting the outer flow, the entrance of the subsonic contraction and the exit of the nozzles were given the same diameter. This resulted in nozzles with boundary layers thicknesses up to 0.5 nozzle radii. The experiments into 'still air' were conducted by simply turning the outer flow off, without systematically measuring the velocity of the induced coflow. Induced velocities of up to 300 m/s were

measured, on one of the occasionbs when the induced outer flow was measured. Due to the incomplete information on the outer flow velocity, the data reduction process ignores any coflow effects.

Potential core lengths were estimated by extrapolating from two or three farfield centerline measurements back to the initial value. While this is an accepted method, given the goals of the research, the data set did not allow this to be done in every case. In the case of the Mach 3 jet into still air, for example, the potential core length was extrapolated from a measurement from a single downstream location, assuming that the decay would be similar to that of the Mach 4 jet into the Mach 2 stream.

Controlling density by adding hydrogen, the method used in the experiments, increases the jet velocity as the density is decreased. The data reduction ignored the velocity ratio, however, and the conclusion was drawn that for the coflowing jet, density ratio did not affect the mixing and for the jet into 'still' air, the core length increased as density of the jet decreased. The information contained in the published papers concerning this set of experiments does not allow a correlation of the spreading rate as a function of velocity ratio as well as density, and there is no information on the development of the jet within the potential core. Except for the last series of experiments performed, no comparison with the present experiments is useful. The last series of experiments that were performed, holding the density ratio constant with

a Mach 2.0 outer flow, showed that as the jet Mach number increased, the potential core length increased for both light and heavy jets.

1.2.6 Acoustics and Structure

Since recent data indicates that any large scale structures in supersonic shear layers do not convect at the convective Mach number, but at a velocity much closer to one of the streams, one of the suggestions made has been to estimate the velocity of the structures by the angle of the acoustic radiation of the flow, since the radiation would presumably be the Mach wave radiation from the structures. There has been an extensive amount of research done on the noise of axisymmetric jets, and on the various types and speeds of the structures that might be producing the noise, and it is useful to examine these results.

The idea that organized large-scale disturbances were predominantly responsible for the majority of the noise of the jet was first suggested by Mollo-Christensen and Ffowcs Williams [30, 31, 32, 33]. Tam, alone and in association with other people, has done the most work from a theoretical viewpoint [34, 35, 36, 37, 38, 39, 40]. Tam's first paper was an attempt to explain the intense, directional acoustic radiation seen on schlieren and shadowgraph pictures of supersonic jets. This radiation is often confined to a sector downstream, with a definite cut-off angle that is acute with

respect to the axis of the jet. He linearized the problem and assumed that the shear layer was infinitesimally thin, with infinitesimal, sinusoidal disturbances both in the downstream direction and circumferentially. Unstable disturbances would grow as they propagated downstream and create the observed waves. The solution is obtained in terms of Hankel and Bessel functions and the asymptotic approximation for small wave number is used to give some analytical results. They indicate that for high wave numbers there is a cut-off angle such that upstream the acoustic radiation is exponentially small. Furthermore, the phase velocity of the radiation is not necessarily equal to the sound speed, since the waves are unstable, and if the growth rate is sufficiently large, then propagation at velocities less than the sound speed is possible. There was generally good agreement between experiment and theory for the cut-off angle.

Although this prediction was successful, it did not really address the issue of noise production in supersonic jets, which had been found to have two major noise sources, neither one of which is located near the nozzle exit. In Mach number 2.0 cold air jets, for instance, the dominant noise sources occur at Strouhal numbers of about 0.4 and 0.2, based on jet exit diameter and velocity [41]. The higher frequency noise source, at $S_t = 0.4$, is located at about 6 jet diameters, while the low frequency source, which contains most of the power, is located about 10 diameters downstream

of the nozzle exit. Tam theorized that the noise was produced by large-scale helical mode instabilities of the jet [35] and derived a wavenumber-frequency relation for such modes. In order to match experiments, he imposed a selection mechanism on the flow. The wavelength of jet perturbations due to an infinitesimal pressure mismatch, as calculated using linear perturbation theory, was used to provide the mechanism[1]. A cell structure would resonantly enhance two helical modes whose wave numbers differed by the wave number of the cell, and Tam theorized that the two modes were responsible for the two separate noise sources.

In 1975, McLaughlin, Morrison, and Troutt conducted experiments in an attempt to verify whether or not the large scale motions of the flow were responsible for the dominant ($S_t = 0.2$) noise production [41]. The jets investigated were approximately Mach 2.0 air exhausting into an anechoic tank kept at 1/30 of an atmosphere. The low static pressure was used both to keep the Reynolds number low, to better experimentally approximate the infinitesimal shear layer model used by Tam, and to allow the use of hot wires without fear of breakage. They used three nozzles: a 6.35 mm conical nozzle, a 9.52 mm conical nozzle, and a 15.9 mm contoured nozzle, all of equal

[1]It should be noted that the wavelength of the cell used by Tam, which is the same as Prandtl's estimate, $\lambda \approx \pi\sqrt{M_j^2 - 1}D/\beta_1(\beta 1 = 2.40483)$ was shown to be in error some 20 years before Tam wrote his paper [42]. The minimum value for the cell is $\lambda = D\sqrt{M_j^2 - 1}$ [43]. It is unknown why Tam chose this estimate, since he cites both [42] and [43] in his paper.

length. As with other experimenters, the contoured nozzle had poor flow quality and was not extensively used in the experiments. The Reynolds number range for the experiments was 8000-107000. They investigated the instability using a glow exciter to mark the fluid, with a hot-wire and microphone as instruments. They found that the spectral peak in the radiated noise was centered around a Strouhal number of 0.18, which agreed with Tam's analysis, but that had multiple modes and broader peaks when the Reynolds number was increased. The largest single peak was obtained with the 9.52 mm jet, which had the strongest wave-cell structure, as might be expected. The wavelength of the instability was 3.9 jet diameters, and the sound radiated in a Mach-wave fashion. Further results from the same facility [44] also showed very broad peaks, rather than the single peak predicted by Tam. However, the same paper also showed that instability waves with subsonic convection velocities could still be powerful noise radiators. The only plausible mechanism for the generation of significant radiating noise from a subsonic jet seems to be the phase broadening associated with the strong growth and decay of the waves. Similar results were obtained by Laufer et al. [45] in high Reynolds number ($R_e > 10^6$) jets, although they identified the source of the acoustic radiation more generally as large-scale structures, rather than instability waves.

A later set of experiments in the same facility in 1980 [46], for a range of Mach

numbers, showed that the growth rates of the instabilities agreed with a quasi-linear, multiple scales analysis that Morris and Tam had developed in an attempt to predict the noise field itself, rather than the most dominant instability [47]. Additionally, this set of experiments showed that Tam's original mode-selection hypothesis [35] gave the wrong trend with Mach number for the Strouhal number of the dominant instability wave. The experimental curve and Tam's theoretical curve for the dominant instability frequency fortuitously crossed at Mach 2.1, giving a spurious agreement in the first set of experiments. In the 1980 set of experiments, the instability waves in the flow were examined for very low Reynolds number jets ($R_e < 10000$), to make the spectrum cleaner, for Mach numbers of 1.4, 2.1, and 2.5. They found that the Strouhal frequency of the most dominant instability decreased with Mach number, so that the modified Helmholtz number $H \equiv St * M = \frac{f*d}{a_j}$ was ≈ 0.43.(constant). The convection velocity of this instability was also constant, at around $0.7U_j$. The jet was observed to be dominated by the first helical modes ($n = \pm 1$). The glow excitation used caused the modes to be phase locked, so the jet had a flapping mode, until the end of the potential core, where coherence of the modes was lost. In a natural jet, the two helical modes would be expected to have a slowly varying random phase angle between the opposite-handed first helical modes. At increased Reynolds numbers, the apparent sound source moved upstream, the spectral peak broadened, and the axial

phase velocity was found to be nearly constant at $0.8U_j$ for Strouhal numbers between 0.3 and 0.8 [48]. A noise prediction algorithm based on the Tam and Morris analysis was shown to give excellent agreement between predicted and measured noise levels and directivity, although axial locations of the noise peak were not well predicted by theory [49]. A further improvement in the ability to predict the radiated noise field, rather than merely the frequency, was developed by Tam and Burton [37, 38], with a matched-asymptotic solution.

In addition to the traditional Mach wave radiation from high-speed structures, Oertel observed two other families of waves in axisymmetric supersonic jets [50, 51], which he named w, $w\prime$, and $w\prime\prime$. Tam and Hu [39] showed that the $w\prime$ family was the familiar Kelvin-Helmholtz instability wave and that the w and $w\prime\prime$ wave families were, in fact, both a result of the jet geometry. An axisymmetric jet can support an internal set of Mach waves when $U_j - c > a_o$, where c is the convection speed of the Mach wave system with respect to the outer flow ($c > 0$ for downstream propagation and < 0 for propagation in the upstream direction) and a_o is the ambient sound speed. Oertel's $w\prime\prime$ family occurs when $c < a_o$. Since the convection velocity is subsonic with respect to the ambient fluid, the system cannot produce Mach-wave type noise. If $c > a_o$, then the wave system can produce radiation, and this is the w family of waves. An unconfined 2-d shear layer cannot support the w or $w\prime\prime$ families, but it should be

noted that these families could occur in a typical, confined, shear-layer facility. It is also interesting to note that the w and w'' sets of waves convected at the isentropic convective Mach number in the above experiments.

Lepicovsky et al. conducted excited-jet experiments using both an LDV and a phase-locked schlieren system for flow visualization. They were thus able to visualize the unexcited and excited jet shear layers, at distinct Strouhal excitation frequencies [52, 53]. The excitation Strouhal number with the largest visual disturbances correlated well with frequencies measured with microphones by previous experimenters ($S_t = 0.4$ for $M = 1.4$). The convection velocity of the disturbances also correlated well for the peak Strouhal number, but natural jets tended to have a nearly constant phase velocity, the excited jet phase velocity decayed on either side of the peak. Visually, it is impossible to see any distinct structures in their pictures, and the visualizations seem to be instability waves, rather than the classic Brown-Roshko type of structure.

Arnette, Samimy, and Elliott [54] examined underexpanded jets and concluded that streamwise vortices that occurred in such jets were a result of a Taylor-Goertler type of instability, due to the curved jet boundary. No such vortices were seen in ideally expanded jets. Their results lead to the speculation that the scatter in the experimental results from axisymmetric jets may be due to slight under- or over-expansion.

In summary, the results from the research into jet noise indicate the following, with respect to the high Reynolds number jet structure: The largest single contributer to the jet noise is Mach-wave radiation from the Kelvin-Helmholtz type of instability wave. They initially are unstable, but, as the shear layer grows, they saturate and then become damped, resulting in a peak noise source about at the end of the potential core. The instability waves may have their growth inhibited to such an extent that they never roll up into distinct structures, or, if they do, they may not achieve coherence for any significant distance. Above a certain Strouhal frequency, the convection velocity of the waves/structures is nearly a constant, which varies depending on the jet Mach number. Instabilities that convect subsonically may still generate noise, but the mechanisms through which this is accomplished are unclear. Although other wave families are possible and have been experimentally observed, the Kelvin-Helmholtz family is the dominant instability over a wide range of jet Mach numbers and temperatures [40]. For the present experiments, the implication is that convection velocities before the end of the potential core can be estimated by assuming that the waves visible on flow visualization pictures are from Mach-wave radiation.

1.3 Statement of the Problem

If one tries to get an idea from the existing data of the effects of density ratio and Mach number on the development of an axisymmetric jet, the conclusions are very limited and qualitative. Increasing Mach number does decrease the initial growth rate of the shear layer and a denser jet has a longer potential core. The fundamental problem with the existing data is that there is a tremendous amount of scatter, due to the lack of attention paid to the initial conditions. The majority of the jet experiments had very poor flow out of the nozzle and it is difficult to distinguish between Mach number and shock-strength effects for the compressible experiments. Additionally, some experiments have intentional coflow, and some experiments don't give any details about their initial conditions at all. Since any coflow fundamentally changes the jet mixing and growth characteristics, this leads to significant interpretation difficulties. The effects of density on the initial growth of the shear layers have not been addressed to any significant degree, and the far field has been examined by very few experimenters. Unfortunately, the lack of data means that even modern models for jets and plumes are using a limited data set to verify their predictions[4].

The experiments performed for this thesis were designed to shed some light on the effects of compressibility and density ratio on the development of axisymmetric compressible jets, in the absence of a coflow or significant shock structure. In order to

ensure that there would be no coflow, it was decided that all jets would exit flush with a wall. This would ensure both that $r = \frac{U_2}{U_1} \equiv 0$ and that all jets would have similar boundary conditions. In order to reduce waves in the flow as much as possible, a considerable amount of time was spent on developing a method to design and manufacture high-precision supersonic nozzles. An abandoned arc-jet facility was resurrected and modified for the experiments. Due to the nature of its construction, only benign gases could be used, so there was no attempt made to investigate molecular mixing. It was decided to use nitrogen, helium, and argon as the jet gases, and to design nozzles for Mach 1.4, 2.0, and 3.0. With helium and argon, experiments were performed into air as well as into the same gas. This gave 9 nozzles and 12 distinct cases, since helium into helium would be expected to be the same as argon into argon.

Chapter 2

Experimental Details

2.1 General

In order to conduct the planned experiments, a new facility was built from remnants of a few older facilities. In it, flow from a variety of nozzles into a controllable outer atmosphere can be established and probed. The facility is of the blow-down type, with gas exiting into a large, sealed tank, which allows the experiments to be conducted into a variety of atmospheres. The Mach number and size of the jet are determined by the nozzle selected. The jet exits into the ambient atmosphere flush with a wall, to ensure that $U_2 = 0$. The flow diagnostics consist of pressure measurements and shadowgraph flow visualization. Each run lasts about 4 seconds, a compromise between gas use and

data gathered on the flow. During the construction of the facility, a novel method for the construction of high-precision internal shapes was developed and frequency data from the pressure probes were used to gather data on the flow. The gas supply, probe motion, and data acquisition were all computer driven in order to conduct repeatable experiments with minimum gas expenditure.

2.2 Facility Description

The facility was constructed from the remains of an arc-jet facility that had been unused for over 20 years. The external tank of the arc-jet was reused as the tank for the ambient atmosphere in the present experiments. It has a volume of approximately 200 cubic feet. A Beech-Russ 325D vacuum pump and a Speedivac diffusion pump are attached to the facility. Only the Beech-Russ pump was used on the present experiments. The hardware associated with the arc-jet was removed, and the gas supply for the nozzles installed. A diagram of the facility is shown in figure 2.2, and a photograph in figure 2.1.

The primary advantage in using the tank is that it allows the outer atmosphere to be varied at will. The vacuum pump was used to evacuate the tank, which was then filled with the desired gas for the experiment. This capability allows a significant

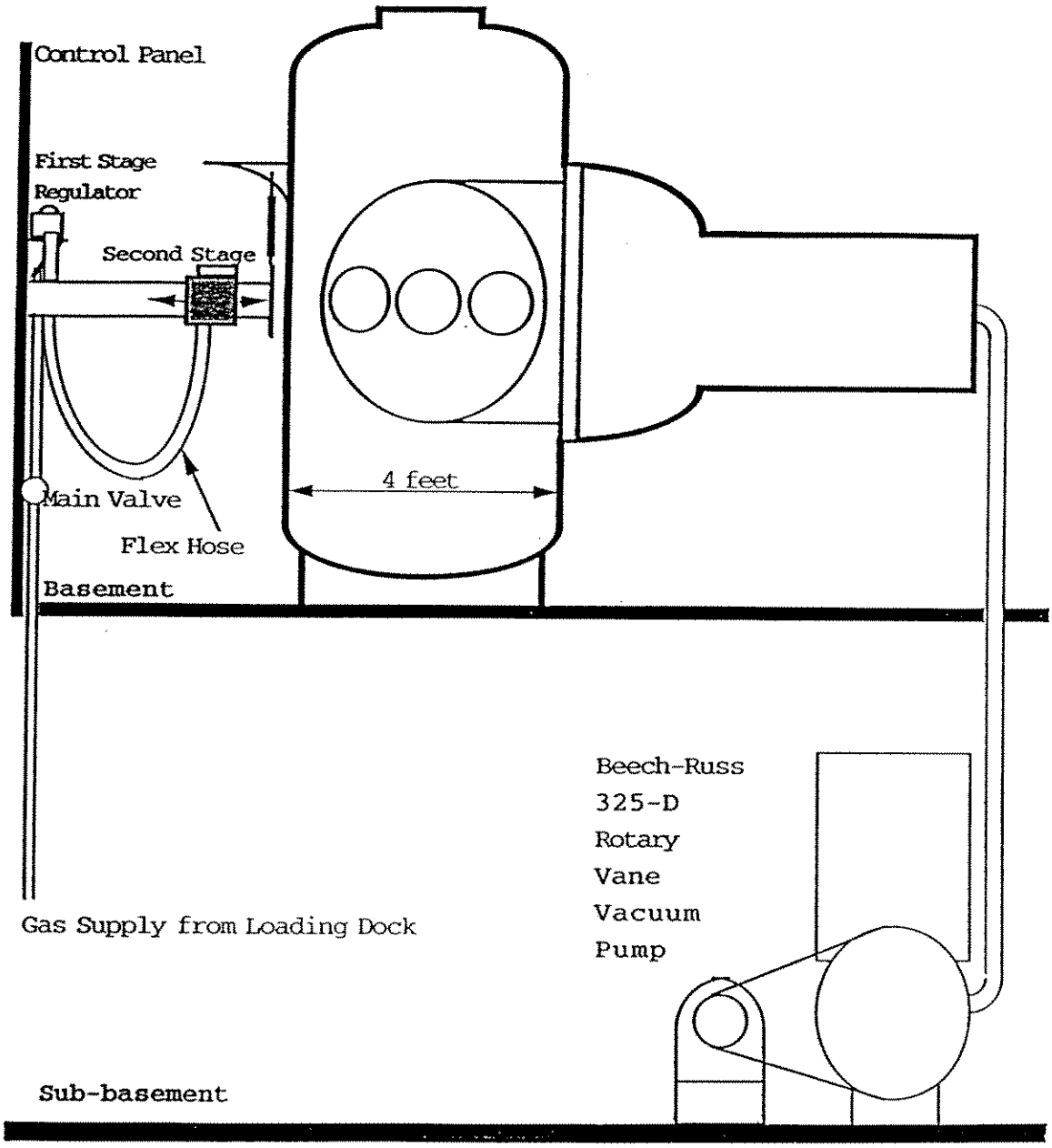

Figure 2.1: Diagram of Supersonic Jet Facility

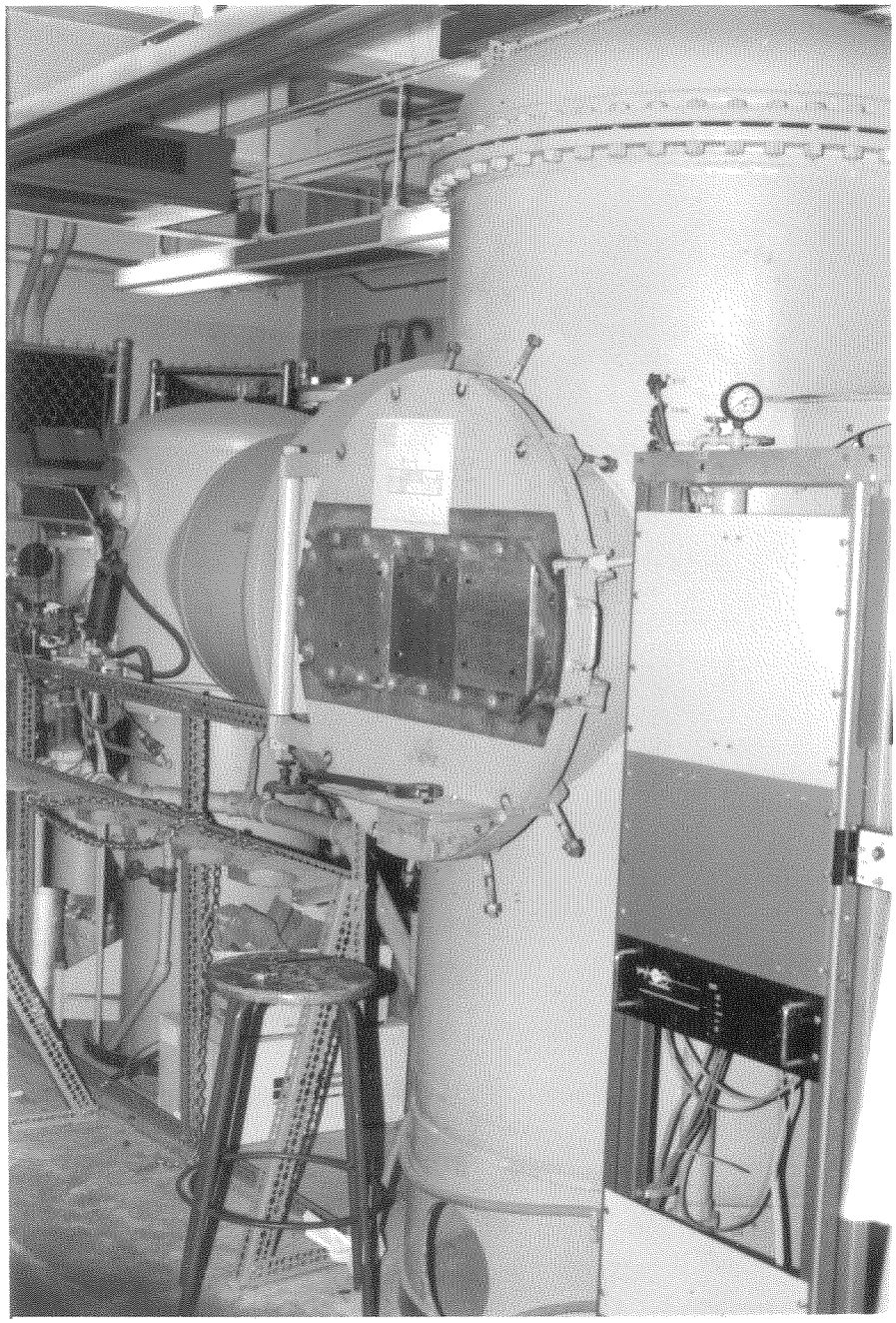

Figure 2.2: Photograph of Facility

density variation between the jet and ambient fluid, and is believed to be unique among operating supersonic jet facilities. The ability to explore the effects of density ratio depended on the tank. Although not used in the present experiments, a capability to conduct experiments at lower pressures, and hence lower Reynolds numbers, exists.

The drawbacks to the tank were the limited optical access (3 windows per side) and the inability to have an outer co-flow. The former did not significantly hinder the gathering of data, although it was a nuisance, and for the present experiments it was not desirable to have an outer flow. For future work, however, increased optical access, for better flow visualization, and coflowing data, in order to extend the parameter space, would be useful.

2.3 Gas Supply

The gas supply consists of a two-stage pressure regulation system, a settling chamber, and a means to mate the nozzles to the outlet of the settling chamber. The gas supply was designed to a minimum burst pressure of 6000 psi and has a 1500 psi safety valve located between the first and second stages to prevent overpressurization of the second stage, settling chamber, and nozzles. A schematic of the gas supply system in shown in figure 2.3. The gas for the experiments is supplied from a bottle farm located

on a loading dock adjacent to the building, shown in figure 2.4. This facilitates the quick exchange of empty and full bottles as well as enhancing safety. The gas is piped through a 3/4 in. pipe to the facility. This pipe also helped to maintain the stagnation temperature of the flow at the ambient temperature of the lab despite the adiabatic cooling of the bottles during the experiments, since the piping was nearly 150 ft. long.

The purpose of the gas supply system is to precisely regulate the settling chamber pressure to the desired value. Since previous experimenters had experienced great difficulty in getting a single stage regulation system to work precisely and repeatably [6], a two-stage pressure regulation system was adopted. A two stage system, in addition to regulating the outlet pressure more precisely, also allows both the use of higher-pressure gas bottles and the depletion of the bottles to lower pressures than would be possible with a single-stage system. These benefits significantly reduce the cost of the gas required for the experiments. The two-stage system worked well in the present experiments. The typical rms pressure fluctuation in the settling chamber was less than 0.5 psi.

The system uses dome-loaded diaphragm-type poppet valve pressure regulators. Dome loaded regulators have much better regulation characteristics, in general, than spring-loaded regulators, as well as being capable of much higher flow rates. They

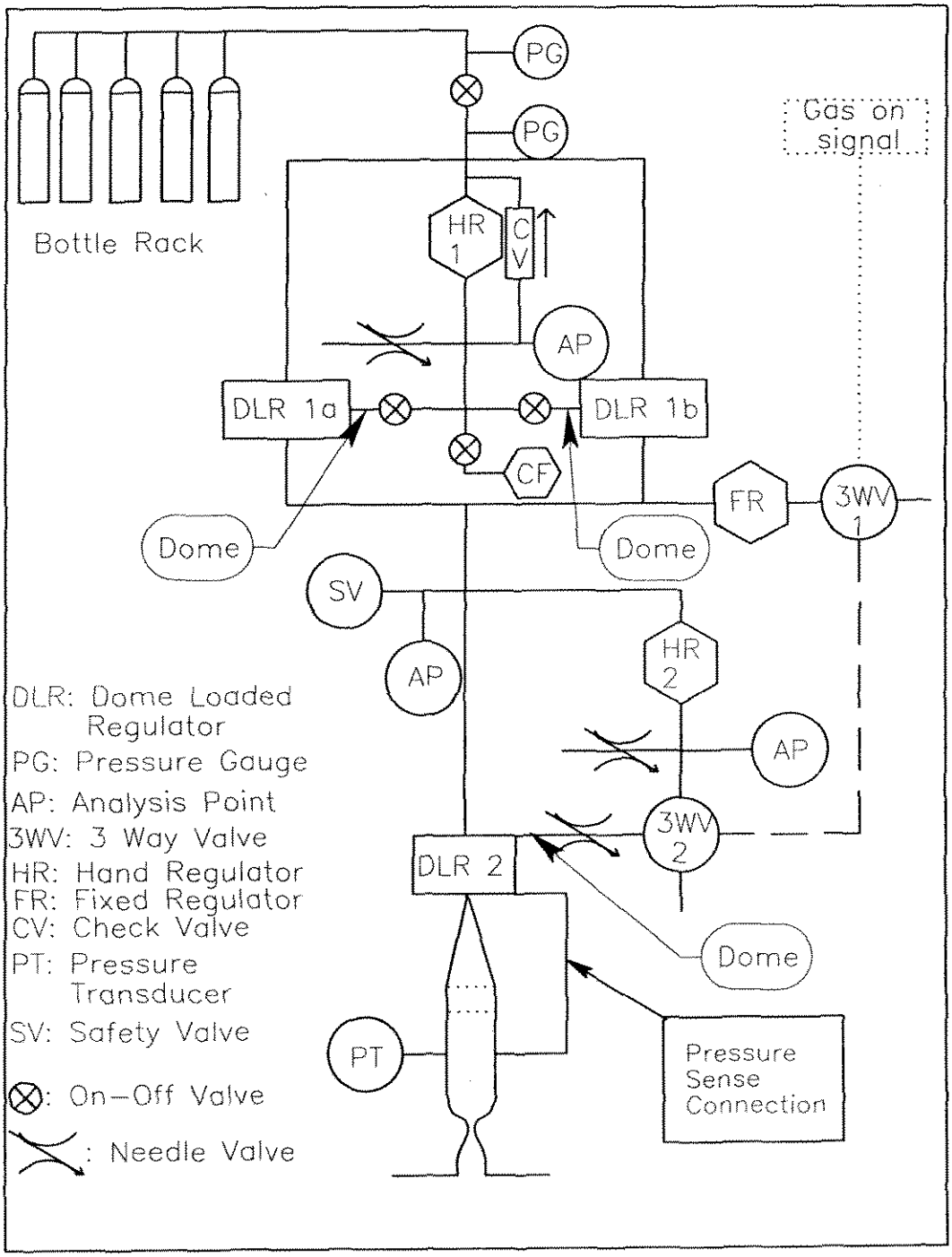

Figure 2.3: Gas Supply Schematic

are insensitive to temperature changes, and usually quite reliable. However, this type of regulator does have several characteristics which need to be understood and taken into account in a high-precision environment.

During the course of a run, the most important characteristic of dome-loaded regulators is that the outlet pressure is affected by the inlet pressure, for a constant dome pressure. The outlet pressure rises by 2.4 psi for each 100 psi drop in the inlet pressure. When the flow starts at the beginning of a run, the pressure drop in the line due to friction and the decreasing bottle pressure raise the outlet pressure of the regulator. The outlet pressure of the first stage regulators is therefore not at the expected value, but rather at some continuously increasing value above it. Unless an extremely large gas supply is used, this characteristic requires that at least two stages be used when precise regulation is required.

The second important characteristic of the regulators is that poppet valves are used for flow regulation. As a result, the regulation will be linear with the difference between the desired and actual outlet pressure only when the flow is choked around the annulus of the valve. Experimentally, it was found that good regulation only occurred when the inlet pressure exceeded the outlet pressure by a factor of two for diatomic gases and three for monatomic gases. This criterion was used for the second stage. The first stage was allowed to operate with subsonic flow through the valve, since the

pressure variations resulting from this practice were taken out by the second stage and a higher percentage of gas from each bottle could be used.

For ideal pressure regulation, the combination of flow rate and pressure drop through the regulator should be such that the poppet valve is in the middle of its operating range. At low flow rates the poppet tends to bounce off its seat, producing a very uneven, pulsed flow. This state is referred to as valve chattering. At high flow rates, the poppet hits its fully open stop, and becomes a fixed orifice.

Lastly, the precise regulator outlet pressure that will be maintained during a run, even with a constant supply pressure, is unknown, unless there is flow through the system. Without a small continuous flow, the poppet valve will close when the outlet pressure builds sufficiently so that the helper spring overcomes the force on the valve from the diaphragm. This outlet pressure may or may not be the actual run pressure corresponding to the pressure in the dome. The exact pressure at which the valve will come off its seat is unknown in this case. There will be no flow through the regulator for any pressure between the dome pressure and the dome pressure minus the helper spring force pressure equivalent, which varies with temperature. If, however, a small continuous flow is maintained through the gas supply system, the helper spring force is continuously and automatically balanced. The pressures across the valve will be close to the balance achieved during a run, except for the pressure drop and pipe friction.

The regulation will therefore be smoother and more precise.

With reference to figure 2.3, the operation of the gas supply will now be explained. The gas supply has a main valve which closes off the entire facility from the bottle rack. Pressure gauges immediately prior to, and after, the main valve monitor the inlet pressure from the bottle rack. Downstream of the main valve, the gas is directed to the inlets of the first stage regulators as well as to the first stage loader. The loader, a Grove 15LHX spring-loaded regulator, is used to set the pressure in the first stage domes, using a Heise 0-1000 psia digital pressure gauge. Although the dome pressure could be set directly, during the present experiments the dome pressure in the first stage was set to give the desired first stage outlet pressure, while maintaining a slight bleed flow through the system. The outlet of the first stage dome loader, in addition to loading the domes, is also connected to a micrometer-handled needle valve, to ensure that there was continuous flow through the dome-loader valve. A photograph of the facility control panel is shown in figure 2.5.

The first stage consists of two Grove 202G dome-loaded pressure regulators in parallel, with an on-off valve in the line leading to each dome. A photograph of the first stage is shown in figure 2.6. When the gas bottles are full, or the flow rate is small, only one regulator is used. This prevents valve chattering. As the gas is exhausted, the parallel regulator is brought on line so that the bottles may be used to a lower

pressure. The Grove 202G regulator has an internal sense connection only; the outlet pressure is sensed at the outlet port, and cannot be sensed at some point downstream. Since the purpose of the first stage is to provide the optimum inlet pressure for the second stage, insulated from variations in the gas supply pressure, the internal sense type of regulation is adequate to the task at hand.

The output from the first stage regulators is ganged together into a 1 in. i.d. flexible hose leading to the second stage, shown in figure 2.7. The hose allows the second stage regulator and attached settling chamber to move relative to the facility.

This motion is provided so that the nozzles may be easily changed. The hose also provides a settling chamber of sorts between the two stages, so that pressure variations from the first stage are minimized. An additional outlet at the hose inlet is connected to a fixed pressure regulator, which provides a constant 200 psi to the facility to power the pneumatic valves and cylinders. A check valve between the first stage outlet and the dome loading lines prevents high pressure air from being trapped in the dome if the bottles become exhausted during a run. The hose leads into a 4-way cross whose outputs are connected to a pressure relief valve, set at 1500 psi, the inlet to the second stage regulator, and to a small flex hose leading back to the control panel and another Grove 15 LHX dome-loading regulator.

The output of the second-stage dome-loading regulator is set using the same Heise

digital gauge as for the first stage, through the use of a selector valve. Another small flex hose takes the desired dome pressure to the second stage. As with the first stage, there is a micrometer handled needle valve venting the outlet of the dome loading regulator to atmosphere. This needle valve ensures that the poppets for the first stage regulators, as well as for the second stage dome loader, are always passing a small amount of flow. Rather than loading the dome of the second stage directly, however, the output of the second stage loader is connected to the inlet of a pneumatically operated three-way valve, which is used to turn the flow on and off. Various other options for starting the flow were considered, such as a diaphragm in the settling chamber, or an outlet on-off valve on the second stage regulator, in an attempt to reduce the start-up time of the jet, but they all would have interfered with the flow.

The three-way valve admits the desired pressure to the second stage dome to start the flow, and vents the dome to atmosphere to stop the flow. A needle valve located between the three-way valve and the second stage dome inlet was used to adjust the rate of dome loading and unloading to minimize rise time and overshoot of the outlet pressure. The pneumatic signal to operate the three-way valve was controlled via a computer actuated 3-way valve using the pneumatic pressure from the fixed output regulator. This may seem unnecessarily complex, but a computer-controlled valve could not be found that could withstand the dome pressures required for high Mach

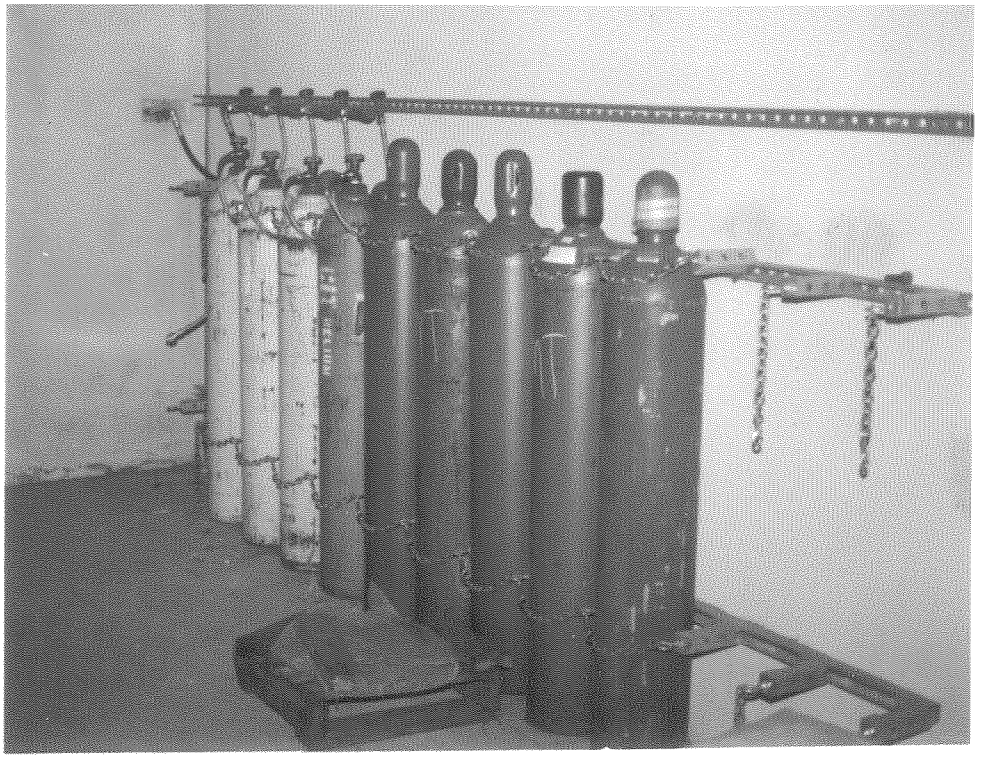

Figure 2.4: Bottle Farm

Figure 2.5 Facility Control Panel

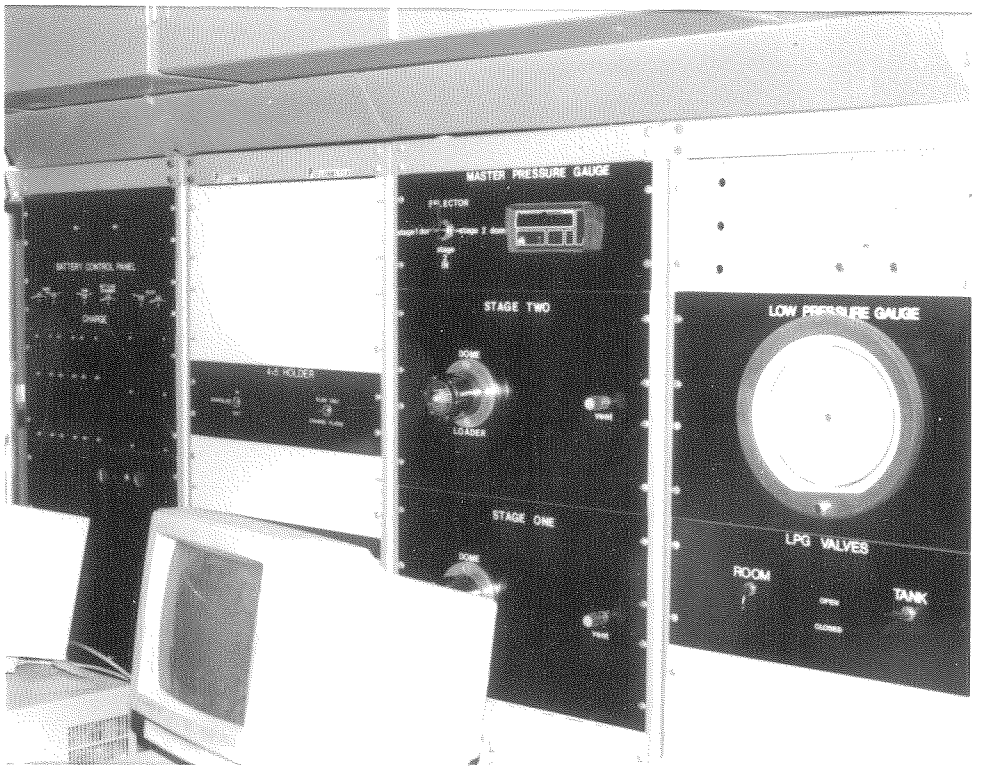

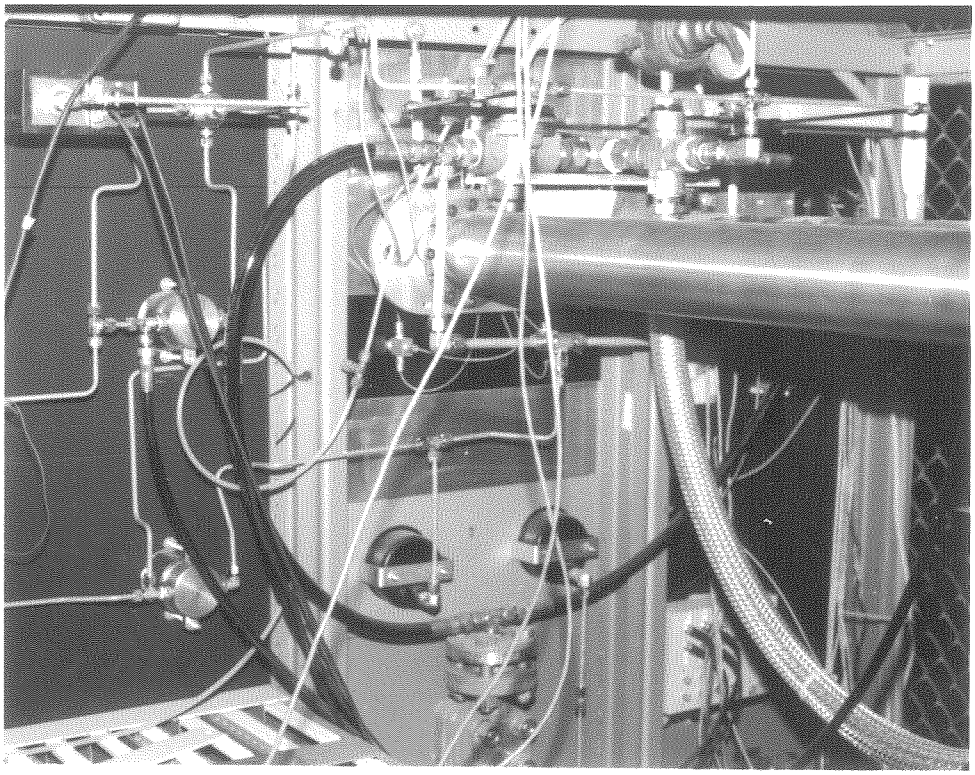

Figure 2.6: First Stage Pressure Regulators

Figure 2.7: Second Stage Pressure Regulator

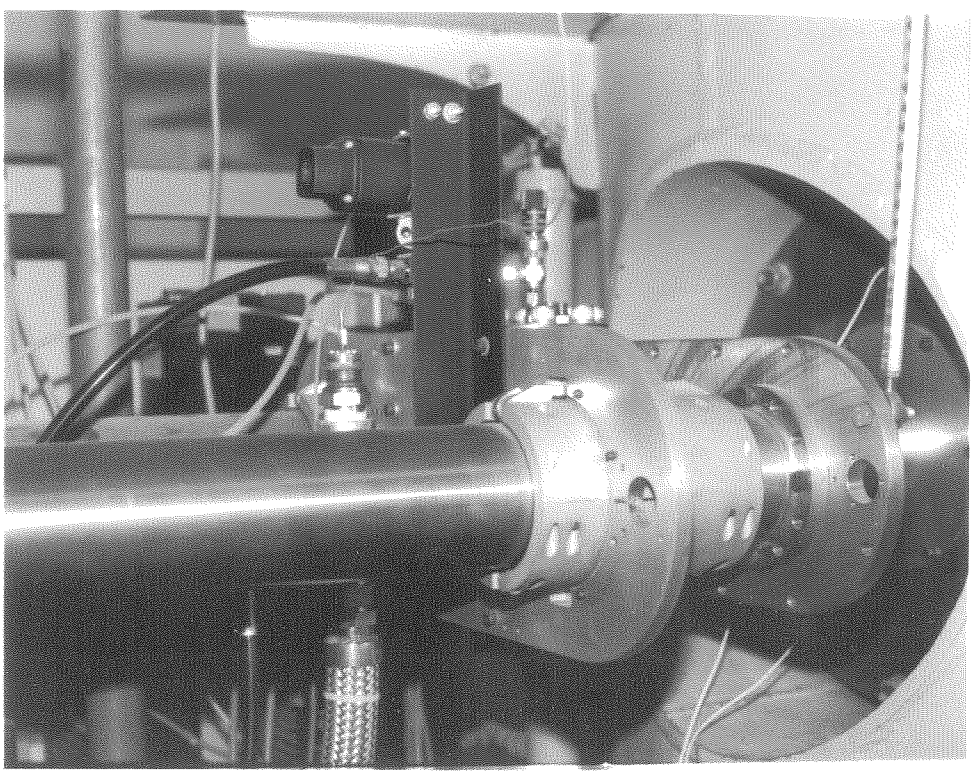

number flows.

The output of the second stage regulator is connected to a short diffuser, which enlarges the diameter from the 1 in. outlet of the second stage to the 1.5 in. diameter of the settling chamber, and has an included angle of 10 degrees. The settling chamber has a constant 1.5 in. inside diameter, and is 5 in. long. A section of honeycomb and screens at the entrance are used to reduce the turbulence of the flow, as shown in fig 2.8. The outlet end of the settling chamber is machined to hold the nozzles and is used to clamp the nozzles to the wall of the tank. The settling chamber has pressure ports for the second stage regulator outlet sense line and for the settling chamber pressure probe.

2.4 Nozzles

One of the great difficulties that previous experimenters have encountered is the construction of an axisymmetric supersonic nozzle with good flow quality. In nearly every published paper on axisymmetric compressible jet mixing, there are large centerline variations and asymmetries in the jet. In the majority of cases, strong shocks are present as well. Since shocks and asymmetries can have profound influences on the development of the jet, a great deal of effort was expended in ensuring the quality of

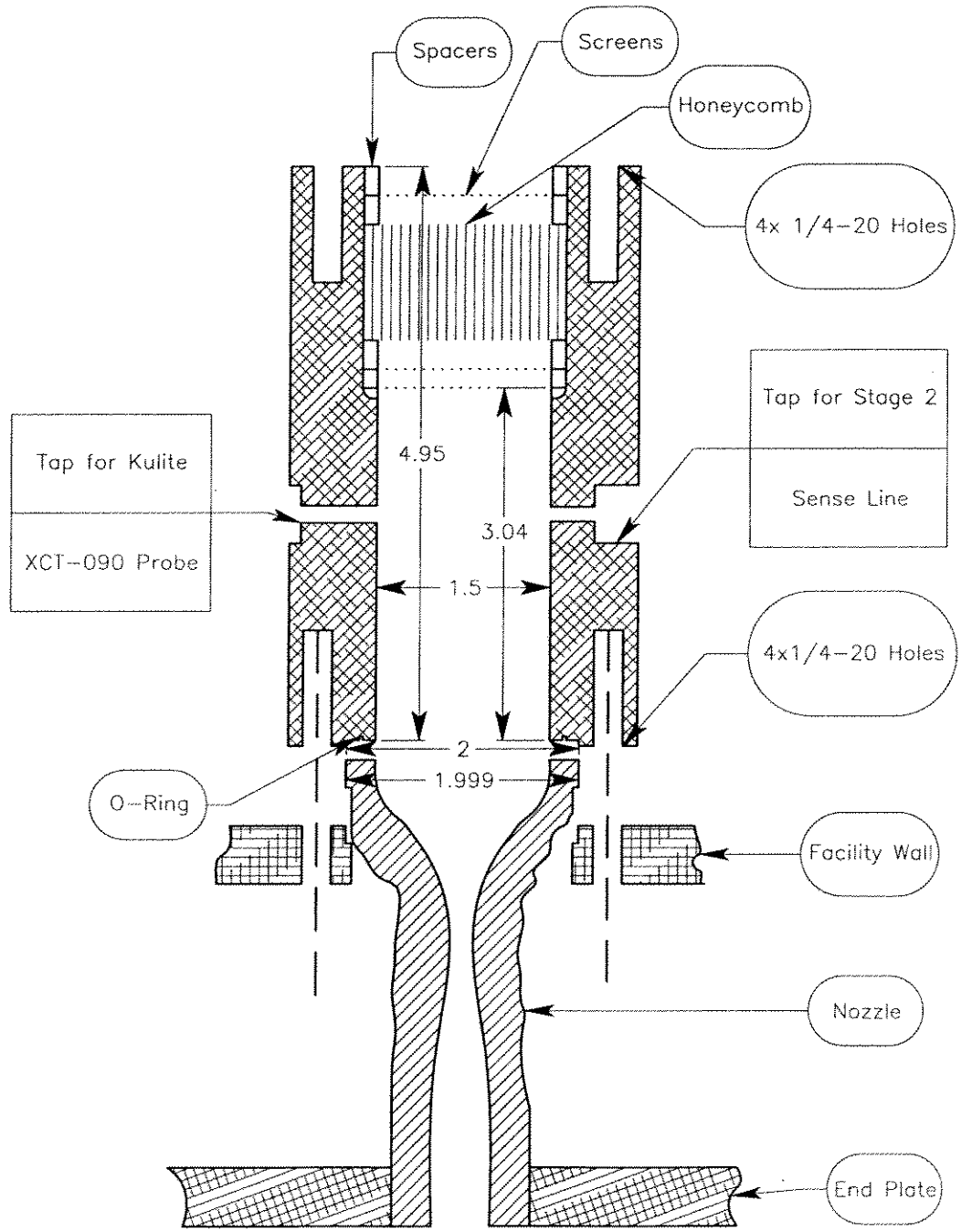

Figure 2.8: Settling Chamber

the flow.

Experimenters who have examined parallel-exit ideally expanded flows have traditionally used a Foelsch type of nozzle, since the contour is easily computed. This method has worked quite well for experiments on two-dimensional shear layers, despite the discontinuity in wall curvature inherent in this approach. In the axisymmetric case, however, the discontinuity in the wall curvature focuses a disturbance onto the axis, which can be strong enough to cause a Mach-disk type of shock to occur within the nozzle [19]. In order to avoid these difficulties, the supersonic contraction was designed using the code written by Sivels [55], with a continuous 4th order Mach number distribution from the throat to the exit.

Another problem with previous experiments is that the contractions were not designed to work well with the nozzles. Although the shape of a contraction does not significantly affect the flow in a subsonic nozzle, as long as it is sufficiently smooth, in supersonic flow the contraction has a profound effect on the flow quality, through its influence on the shape of the sonic line at the throat [19]. The contractions in the present nozzles were designed by using a continuous Mach number distribution from the settling chamber to the throat, where it matched the first four derivatives of the supersonic portion, and then obtaining the contour from the Area-Velocity relation. This approach seemed to work very well for the nozzles built for the present set of

experiments.

The construction of the nozzles is described fully in Appendix A. It is a plating method designed to reduce the expense of constructing an axisymmetric nozzle of high precision. The cost of conventional machining methods was found to be driven by the difficulty of obtaining a good surface while machining a deep, small diameter hole and the necessity of machining from both ends due to the presence of a throat. The plating method uses an aluminum mandrel that is of the shape and surface finish desired for the internal contour, which is then plated with pure nickel. The aluminum is then dissolved out and one then has a high-precision, supersonic nozzle.

The construction of nozzles using the plating method resulted in nozzles that were of higher precision than obtainable by direct manufacture, while costing about an order of magnitude less. Both the high precision, due to the flow quality requirements, and the low cost, due to the large number of nozzles needed, allowed the successful completion of the experimental program.

2.5 Instrumentation

The instrumentation used during the present set of experiments consisted primarily of piezo-resistive pressure probes and shadowgraph flow visualization. The output from

the probes was filtered, amplified and recorded in digital form. The pressure sensors were placed to measure the pressure in the settling chamber, the pitot pressure in the jet, and the ambient static pressure in the tank. In addition, the digital pressure gauge used to set the dome pressures was equipped with an electronic output, and was used to monitor and record the various pressures in the gas supply system. A thermocouple was placed at the entrance of the second stage to monitor the total temperature.

2.5.1 Pressure Probes

In a departure from common practice, where pressure probes are used to measure only the mean flow quantities, the pressure probes in the experiments described herein were used to measure fluctuating quantities in the flow. This was possible because the probes used were piezo-resistive, and therefore could provide both high frequency response and mean levels. LDV systems were prohibitively expensive for the present experiments, and require seeding of the flow. PIV techniques are as yet unproven in supersonic jet flows. Hot-wire or hot-film probes are not robust enough to survive high Reynolds number experiments. Piezo-electric probes are more robust than piezo-resistive probes, and have a higher frequency response, but cannot supply DC pressure levels. Piezo-resistive probes have a high enough frequency response to be useful in most experiments, are relatively inexpensive, reasonably robust, unaffected

by temperature, and provide reliable low-velocity signals. These factors combine to make piezo-resistive probes attractive for experimental use. The sensors used in the present experiments were obtained from Kulite Corp. An XCQ-062 0-250 psia sensor was used for the pitot probe, an XT-092 0-1000 psia sensor was used in the settling chamber, and an XT-092 0-25 psia sensor was used in the tank. The natural frequencies for the probes are 1MHz, and they produce usable data to approximately 1/3 of that value, according to the manufacturer. The probes are of strain-gauge type construction, and so require that either the power supply or the sensing instrument be electrically independent for each probe.

The initial amplifiers used, Avtech AV-143-CTAs, were not true differential amplifiers, although they did have the advantage that their frequency response was flat from 0-2MHz. The amplifier case was also the ground reference. Therefore, the power supplies for each probe needed to be independent from eachother in order to avoid ground loops and short-circuiting of the probe strain gauges. Common power supplies with floating outputs had too much noise for the experiments, due to the 10ma currents required by the pressure probes, and power supplies that were of sufficiently high quality were prohibitively expensive. Therefore, 12V Marine deep-cycle lead-acid batteries were used as the power source, since they have extremely clean output voltage, are relatively inexpensive, and are by nature floating. The output from the batteries is

clamped by zener diodes to 10V, which is the manufacturer's recommended excitation voltage. The wiring diagram for the probe system is shown in fig 2.9. Zener diodes have the good characteristic that they are very stable, but their breakdown voltage varies from diode to diode. In this case, stability was more important than a precise voltage value, since the entire system was calibrated at once; a known pressure was applied to the pressure sensor and the digital output was read off the A/D convertor. In order to alleviate any temperature dependence that the zener diode output would have, power was always applied for at least 12 hours prior to the start of data collection. The room temperature did not significantly vary, since the laboratory was in an air-conditioned basement.

The pressure sensors in the tank and the settling chamber were mounted with the sensing surface flush with their respective walls, and so they produced a full range of frequency data. The sensor used in the pitot probe, however, did not receive a full range of frequencies, due to the design compromises inherent in the tradeoff between spatial resolution and frequency response. A diagram showing the probe tips is shown in fig 2.10. A family of probe tips were constructed with inlet diameters of .010, .013, .020, .030, and .055 in., to allow a tradeoff to be made between spatial resolution and frequency response. All probe tips had a 20 degree included angle, in order to minimize flow disturbance. The frequency response of each probe was

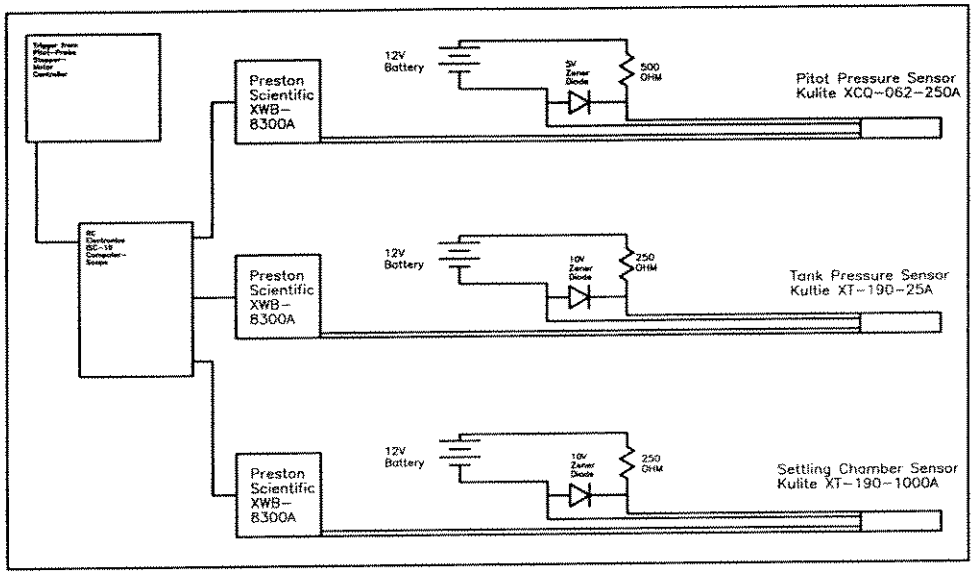

Figure 2.9: Pressure Sensor Wiring

made following the analysis of Bergh and Tijdemann [56], as described in Appendix B. Unless otherwise specified, all experimental results presented herein were taken with the .013 inch diameter probe tip.

Although the diameter of the probe base (0.5 inch) may seem large, the size was necessary due to the high dynamic pressure in order to ensure spatial precision and repeatability. There did not appear to be any upstream influence of the probe, even when the jet was subsonic downstream. There were no differences in mean measurements made with the probe and more conventional L-shaped probes of 0.125 and 0.0625 inch outside diameter in the farfield (low subsonic portion) of the jet. No

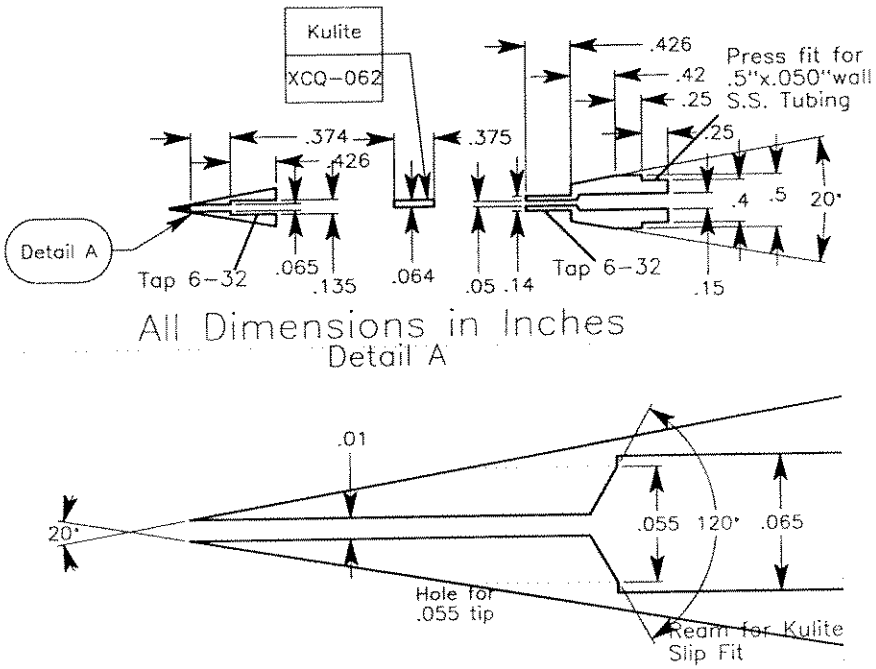

Figure 2.10: Pitot Probe Installation

comparisons could be made between the probe used in the experiments and more conventional probes in the transonic or supersonic ranges due to the structural limitations of the conventional probes. A photo of the pitot probe installation and internal tank layout is shown in figure 2.11.

2.5.2 Data Acquisition

The output from the pressure probes is filtered and amplified by Preston Scientific XWB-8300A amplifiers, which have an integral 4-pole Bessel low-pass filter. These amplifiers replaced the Avtec amplifiers and R/C filter network used initially in the

experiments. All data presented herein were taken with the Preston amplifiers. For the present experiments, the cut-off frequency was 1KHz. The output of the amplifiers is digitized and stored by an RCI Electronics Computerscope running on a Zenith 1600 (IBM PC-AT clone). Due to the limited on board storage of the Computerscope, the acquisition frequency was limited to 2kHz (1kHz Nyquist) for 4 channels for the typical 4 second duration of each run. The raw data were moved to another computer, which had a larger disk, where the data was broken down into the individual channels, converted to pressure, and stored in ASCII format for use by data analysis programs.

The data were analyzed to obtain mean and rms pressures from each run. If the data were from a run where the probe was stationary, typically on the jet centerline, the mean and rms data were calculated in a straightforward manner, over durations ranging from 1-3 seconds, depending on when the settling chamber pressure stabilized. For about 90% of the mean data, the duration of the data analyzed was 2 seconds.

If the data were from a traverse of the jet, a different approach was taken, since the probe was not stationary, and an average in time was also an average in space. For this case, the mean and rms values were calculated over 100 neighboring points, since that corresponds to the time it takes the probe to move one probe opening diameter. Rather than an arithmetic mean, the smoothing was accomplished by first taking an FFT of the data, eliminating frequencies that corresponded to ones above the 100

point window, and inverting the FFT. This "smoothed" data were then subtracted from the raw data, the result rectified, and the process repeated to obtain the "rms" data.

2.5.3 Flow Visualization

The flow visualization was accomplished through the use of a spark shadowgraph technique. A schematic diagram is shown in figure 2.13. It consisted of a Xenon Corp Nanolamp, which produces a spark of either 10 or 20ns duration, depending on the spark head used, of about 150 mJ energy. Space constraints, better sensitivity, and ease of alignment and use were the primary reasons for using a shadowgraph rather than a Schlieren type system. The flow was imaged on 4x5in Kodak T-Max film, ASA 400, and the distance to the film plane was arranged as the best compromise between sensitivity and spatial resolution. Since this distance resulted in the placement of the film inside the tank, a system using an old Speed-Graphix Graphmatic film changer and pneumatic cylinders was developed. This allowes for up to 6 pictures to be taken before the tank needed to be opened and the film changed, which was an important feature when the tank was filled with gases other than air. A photograph of the film changing mechanism is shown in figure 2.12.

The images obtained were of higher quality than expected, given the simplicity of

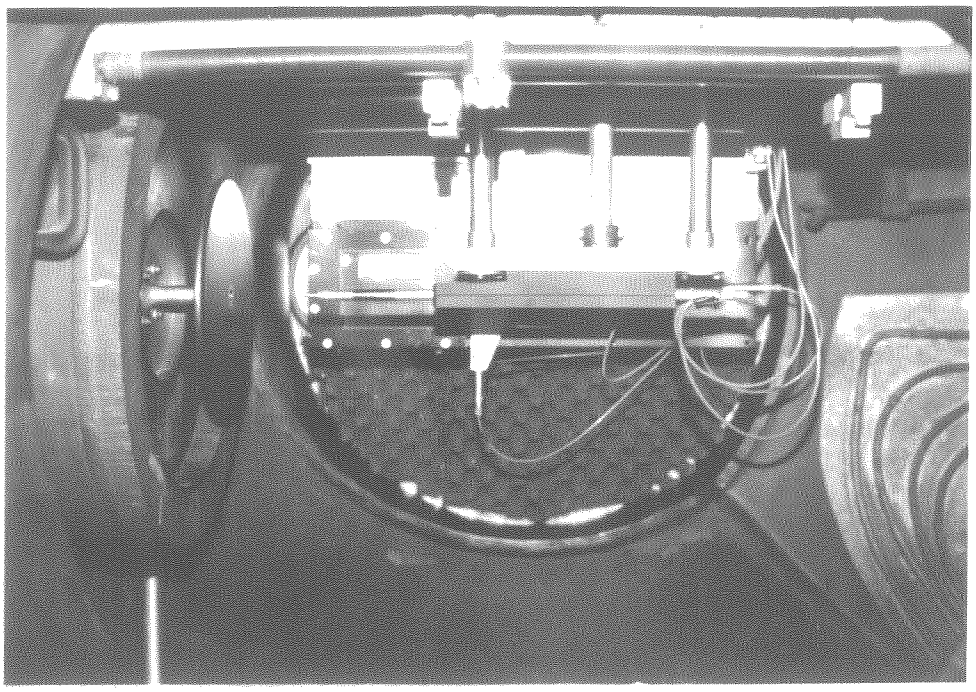

Figure 2.11: Pitot Probe and Internal Tank Layout

Figure 2.12: Film Changing System

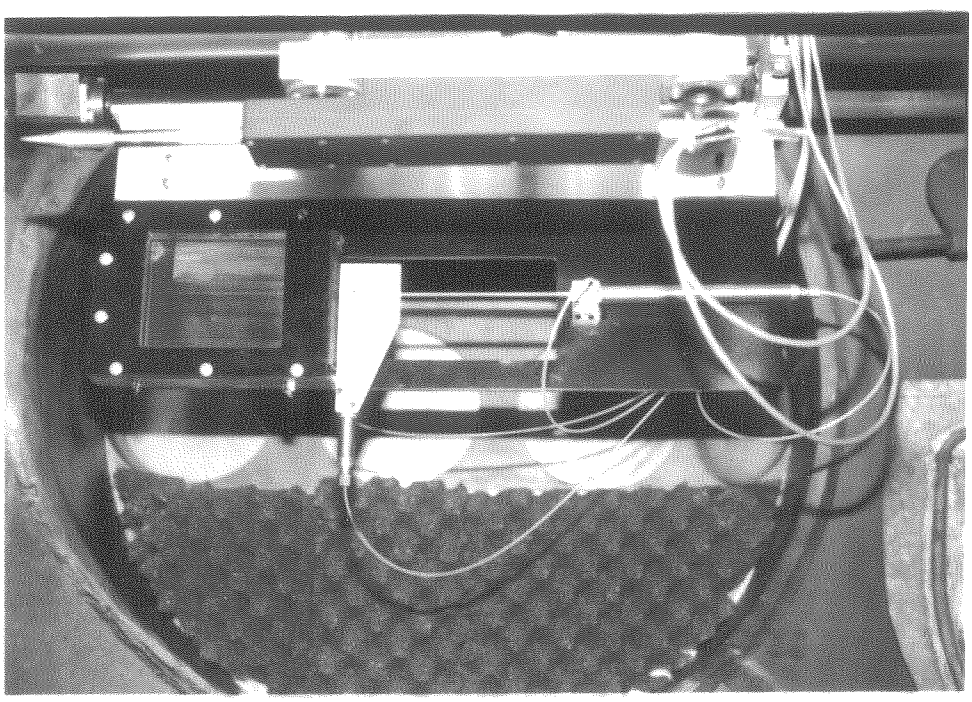

the shadowgraph system. They clearly show the stronger acoustic radiation as well as fine detail of the jet itself. This is due to the large negative used, which gives a greater number of film grains per jet feature than systems which image onto 35mm film, and to the lack of interference from the outer flow, since there are no boundary layers on the windows as there are in a 2-d shear layer or coflowing jet experiment. The use of a shadowgraph system also aided in the visualization of weak waves and acoustic radiation of the flow, since it is more sensitive than a schlieren system.

The flow visualization pictures presented herein are generally one of two types. One is a 20ns single spark shadowgraph of the flow. This type shows the fine detail and large-scale jet structure. The second type is a picture obtained by imaging 50 sparks over 1 second, with an appropriate attenuation filter placed at the output of the spark lamp. This latter provides pictures of the mean flow, and allows one to pick out stationary features that are not visible in the single-spark images.

2.6 Typical Runs

Runs were conducted in several different ways, depending on the object of the experiments. The first criterion used was whether the probe was stationary or moving. If the runs were traverses of heterogeneous jets, the desired starting point for data collection

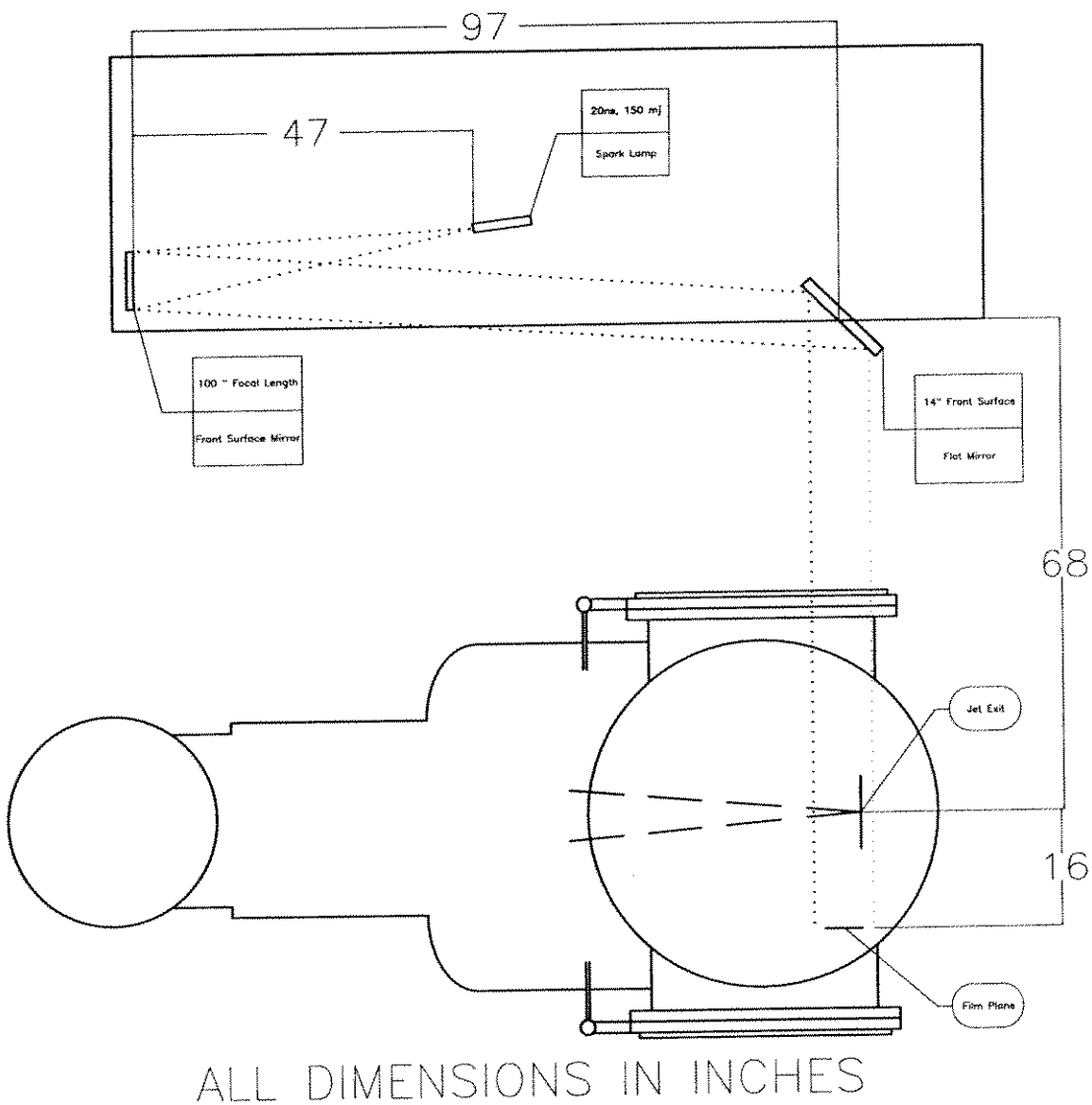

Figure 2.13: Flow Visualization System

was entered into the computer controlling the probe. This computer moved the probe to a position 1/2 inch away from the final staging point for the run, in xyz space, and then brought the probe to the staging point. This was done in order to eliminate the backlash inherent in the probe traverse design. The staging point was 1.0 inch below or to the side of the desired starting point, for vertical or horizontal traverses, respectively. The computer driving the probe traverse then was set to wait for an external trigger. Meanwhile, the computer controlling the data acquisition system was set up to take 4 seconds of data, with the start of data acquisition triggered by the traverse controller. When the probe motion was triggered, the traverse controller accelerated the probe, a process which took 2 seconds and 1 inch of probe travel. The gas flow was started when the probe was between 1 and 1.5 seconds away from the desired traverse start point, depending on the Mach number of the jet and the gas used. This was accomplished by the probe traverse controller sending a signal to the computer-controlled 3-way valve, as described above. The time lead allowed the gas supply time to pressurize the settling chamber and the jet to reach its steady-state configuration prior to the data collection process. When the probe reached the desired starting point for data collection, the data acquisition board was triggered, again by the traverse computer, and the collection process began. The collection typically began 1 inch from the jet centerline, and continued until 1 inch after the jet center-

line, a traverse which took 4 seconds at the maximum probe velocity of 1/2 inch per second. At the end point, the probe controller shut off the gas and stopped the probe motion. The vacuum pump was started and allowed to draw fresh air into the tank for 1 minute, providing a complete change of the tank atmosphere. After another minute with the pump off, to allow any significant residual eddies in the tank to decay, the next run was performed.

The second major criterion that determined the conduct of the experiments was the (in)homogeneity of the jet. In the case of a homogeneous jet, the tank was evacuated to approximately 0.1 psia using the Beech-Russ vacuum pump and then refilled with the desired gas from a bottle. Experiments then proceeded as described above, except that the vacuum pump was not used between runs. For the case of nitrogen, it was deemed sufficient to exhaust into air, rather than evacuate the tank and refill it with nitrogen.

The third criterion was whether the probe was moving or stationary. For runs to gather mean centerline data, the probe was moved initially to a point 1/2 inch from the desired measurement point and then to the desired point, to minimize backlash. The gas and data acquisition system were triggered at the same time and after 3 seconds the gas supply was turned off. The output from the stagnation pressure probe was then examined to determine when the settling chamber had reached the desired pressure

and how long it stayed there. This startup information was used to determine the minimum lead-time necessary for the gas supply during traverses. The data used for computing the centerline mean and rms were taken from the segment of the data that had steady settling chamber pressure. The typical amount of data that was usable from each run was 2 seconds.

For flow visualization runs, the probe was moved out of the way, and the film negative carrier positioned as desired. The gas supply and data acquisition were triggered at the same time, and, after 1.5 seconds, the spark lamp was triggered. If the photo was a single spark, the gas supply was then shut off, whereas if it was a multiple spark photo, the gas supply was maintained for another second and then turned off. The data were examined to ensure that the desired stagnation pressure was obtained when the picture was taken.

The data taken for all runs included the pressure probes in the stagnation chamber, tank, and pitot probe, as well as the inter-stage pressure of the gas supply system, which was useful in determining whether to use one or both of the first stage regulators. In addition, the total temperature was monitored using a J-type thermocouple, connected to a Fluke 80-TK and Fluke 87 voltmeter, which gave a temperature reading in degrees farenheit. This temperature was monitored visually, to ensure that the total temperature did not vary due to the adiabatic expansion of gas from the supply

bottles. Due to the long piping, the temperature never varied by more than 2 degrees farenheit from the ambient temperature in the lab, and was independent of both the outside temperature and the gas temperature drop as the gas was used.

2.7 Suggested Improvements

Although once the nozzles were constructed the research, in general, proceeded smoothly, there were some areas that gave some trouble and some others that could be improved in future experiments. They are discussed in this section, and will be loosely grouped into general facility, gas supply, nozzles, and instrumentation.

The facility, as a whole, performed remarkably well considering that it was constructed chiefly of cannibalized parts. No real difficulties were encountered with the operation. For continued research, some minor maintenance such as replacement of o-rings and valve seals and lubrication of the probe traverse would be desirable. There are, of course, major improvements that could be made to enhance the utility of the facility.

One such improvement would be to install an exhaust pressure regulator so that the jets could be run into differing ambient pressures, which would modify the Reynolds number. It would also ensure that no ambient air could mix with the tank atmosphere.

Currently, if the tank is not filled with air, the exhaust valve is manually opened as the gas starts to flow, and closed after the experiment. To prevent contamination of the tank, a few runs were made with slight overpressures of the facility before the data collection was begun. This ensured that the exhaust piping was filled with the same gas as the tank and minimized the chance for air to contaminate the tank.

Another improvement that could be made would be to change the optical access to the facility. The facility, as it was used for these experiments, is limited by having three discrete 7 inch windows on each side. The 1 inch steel plate that has the window holes in it could be replaced with one having a single large window, for instance. The size would be limited by the fact that the window would have to withstand the forces generated when the tank is pumped down to vacuum in order to replace the gas, while still being of optical quality. For the present experiments, since all the runs were into ambient pressure, a 1/8 inch thick optical window was used. When the tank needed to be pumped down to allow a gas change, a 1/4 inch thick aluminum plate was substituted for the window. After the tank was filled with gas, and allowing a slight gas flow to ensure a positive tank pressure, the plate was replaced with the window for the experiments.

The 2-stage gas supply regulated the pressure in the stagnation chamber to give stagnation pressures that usually only varied by 0.2% or less. However, some problems

were encountered when using helium, particularly with the Mach 1.4 and 2.0 nozzles. The best regulation was generally obtained when the pressure across the second stage would give a M=1.5 flow if ideally expanded. However, when trying to step the high pressure helium from the bottles down to this pressure across the first stage, even when using only one of the two parallel first stage regulators, the valve was barely open, and chattered. Once this happened, the valve seat was destroyed, and the regulator would leak. The regulator then needed to be torn down and rebuilt. This problem was partially ameliorated by opening the main gas valve only slightly when using new bottles of helium, and then gradually opening the main valve as the pressure history of the runs began to show signs that the regulator valve was fully open during the preceeding run. As the gas supply decreased to very low pressures, the parallel first stage regulator was turned on, by admitting gas to the dome, so the supply bottles could be used fully. The problem with manually setting a restrictive orifice by using the main valve was that the exact setting was critical to the quality of the flow. If it were opened too little, the gas pressure for the run dropped to where the stagnation pressure was not constant, and if it were opened too much, the valve chattered, destroying the regulator valve seat as well as giving useless data. A significant number of the helium runs needed to be repeated, which resulted in substantial extra expense. The improvement that could be implemented here would

be to replace the valve body in one of the regulators with a smaller capacity valve. This would both allow a better regulation with helium as well as allowing subsonic flows to be studied. A smaller valve body for the second stage valve would also be useful for studying subsonic flows.

The plating technique used for the manufacture of the nozzles worked as well as could be expected. The only problem encountered with the nozzles at all was that the boundary layer calculations are suspect, since the design Mach number did not exactly coincide with the Mach number achieved with the nozzle. However, the flow quality was still excellent and the technique could be used to build and test elliptical nozzles, or any other complex internal shape. The long lead time for the construction of nozzles by this technique remains its primary drawback.

The instrumentation used in the tests performed admirably. The only problems encountered in general was the need to keep the batteries filled with water and properly charged. Instrumentation is one area, however, that could be greatly improved with a minimal investment. The data presented herein was collected using an RC Electronics ISC-16 Computerscope. While this board has the capability to read in 1 Megasample/sec, it has only 64K samples of memory on board. The computer used to collect the data was a Zenith IBM PC-AT clone and did not have enough bandwidth capability to the hard disk to allow samples to be stored continuously. This limited

the frequency achievable with the system to 1 kHz, for the 4 seconds of data needed to complete a traverse of the jet. Current generation PCs, with a PCI bus, have the capability to transfer 200K samples/sec to disk, which would allow a bandwidth of 25 kHz for the data. If a faster data acquisition rate was coupled with the probe tips having a faster response, it would greatly enhance the information gathered on the flow. In addition, a series of pressure sensors with different ranges would be very useful and would improve the resolution and signal to noise ratio of the data at the lower Mach numbers.

Although adding new flow diagnostics, such as an LDV, would be useful, the most important additional instrumentation would be some device to measure the concentration of the ambient and jet fluid. One possibility would be to use sulfur hexafluoride as a tracer, since it can be reliably detected on the level of 100's of parts per trillion. Seeding the plow with, say, 1 ppm would give a way of reliably detecting the jet fluid and ambient fluid mean relative concentrations down to a level of .1%. Such a small amount of tracer would not be expected to affect the flow significantly, if at all. Other possibilities include PIV, which could potentially give velocity and concentration fields simultaneously (based on density of the seeding particles), or using microphones to explore the sound field.

Chapter 3

Experimental Results

3.1 General Results

This section presents the general results obtained during the experimental effort. The parametric data space explored is as shown in table 3.1.

For each jet, a series of shadowgraph pictures was taken around the calculated pressure ratio for the nozzle design and tank pressure (typically 14.4 psia). This was to allow for slight irregularities that may have occurred in the design or manufacture of the nozzle. The photographs were examined and the pressure that resulted in the weakest waves in the flow was used in the experiment. Based on the measured settling chamber pressure and the measured pitot pressure, the actual exit mach number for

Mj	Jet Gas	Ambient Gas	ρ_j/ρ_a	Mc [1]	Uj [2]	Uc [3]
3.0	Helium	Air	.55	1.79	1503	624
2.0	Helium	Air	.32	1.33	1312	467
3.0	Nitrogen	Air	2.8	1.13	622	387
1.41	Helium	Air	.23	.99	1091	351
3.0	Argon	Argon	4.0	1.00	475	317
3.0	Argon	Air	5.5	.94	475	332
2.0	Nitrogen	Air	1.8	.86	518	294
2.0	Argon	Argon	2.3	.79	415	251
2.0	Argon	Air	3.2	.75	415	265
1.41	Nitrogen	Air	1.4	.65	415	223
1.41	Argon	Argon	1.7	.62	347	196
1.41	Argon	Air	2.3	.59	347	209

[1] Average isentropic convective Mach number

[2] Meters per second relative to lab frame

[3] Meters per second relative to tank ambient fluid (theoretical)

Table 3.1: Jet Parameters

the nozzles can be calculated. The exit mach number for the nozzles was within 2% of the design condition.

For each jet, after the proper settling chamber pressure was established, two initial sets of traverses were made. The first set was a horizontal and vertical traverse, taken 0.1 inch downstream of the nozzle exit. This was used to ensure that the probe was centered with respect to the jet exit. A second set of traverses was made 4 inches downstream of the nozzle exit, to ensure that the nozzle was axially aligned with the traverse. If not, a linear correction was applied in the horizontal plane to keep the probe on the horizontal centerline of the jet. For the traversing runs, no correction was applied in the vertical direction, since the corrections were usually small (on the order of hundredths of an inch) and the probe traversed completely through the jet during the course of a run. For the centerline data collection, the probe was located on the axial centerline both horizontally and vertically.

The data were collected using the 0.013 inch diameter pitot probe tip. The acquisition rate was 2kHz, and the cut-off frequency for the 4th order Bessel filters was 1kHz. As mentioned in the previous chapter, for the vertical traverses, the data were averaged over 100 neighboring points to generate the pitot pressure profile. This profile was subtracted from the raw data, and the result rectified and smoothed again, to generate the 'RMS' data. For the data gathered on the centerline, the mean pressure

and RMS value was calculated over a two second time span.

In addition to the pitot profiles, each of the above cases had both single spark and 50 spark average pictures taken. The photos are collected into a set of photo pages in Appendix C. The first photo, figure C.1, shows single and 50 spark averages taken through the window used when the jet exhausted into an atmosphere other than air (no window was used if the ambient gas was air). After the photo pages, the complete traverse data set is presented in Appendix D. For purposes of clarity, only certain traverse data will be included in the main text, and they are repeated in the data set. Both the photo pages and the data set are organized with argon into argon data first, followed by argon into air, helium into air, and nitrogen into air. Within each set of gas data, the progression is Mach 1.41, Mach 2.0, and Mach 3.0. The smoothed pitot profile for each gas combination is paired with the associated 'RMS' data.

3.2 Density Ratio and Mach Number Effects

A difficulty encountered in the course of the research was to define an easily measurable, repeatable quantity that measured the spreading rate of the shear layer of the jet. Since neither the static pressure near the jet nor the concentration of jet and ambient fluids was known, the velocity could not be determined with certainty. The

traditional definitions of mixing layer width used in previous jet research usually depend on velocity measurements, and therefore could not be used for analysis of the present results.

Abramovich et al., experimenting in subsonic jets [18], had found that for the case where the outer flow velocity was identically zero, the only effect of density ratio was to shorten or lengthen the potential core; the relative spreading into the jet and outer fluid was nearly constant over a wide range of density ratios. Since the flow in the present experiments was set up to ensure that there was no outer flow, the possibility that this observation was true for supersonic jets was explored. The data collected were analyzed for traverses whose axial locations was approximately half of the potential core length. If two traverses appeared to have the same potential core radii, then the traverses were superimposed to see if the outer widths were the same. An example is shown in figure 3.1, which shows a traverse of Mach 3.0 argon into air at 8 jet diameters and a traverse of Mach 2.0 helium into air at 6 diameters. The traverses are quite similar despite a large density ratio difference in the jets. Similar comparisons made with a large number of traverses indicate that, indeed, the spreading into the outer flow is a constant fraction of the total mixing region width. For the present data, $\frac{R_o - R_j}{R_o - R_i} \approx 0.55$, where the subscripts o, j, and i designate the mixing layer outer radius, the jet exit radius, and the mixing layer inner radius, respectively. This

is remarkably close to the Abrahmovich et al. result of 0.57 to 0.63 for subsonic jets.

This result allows the spreading rate of the jet to be uniquely characterized by the length of the potential core, a quantity which is repeatable and which can be well defined. However, in order to address the questions concerning the effects of compressibility and density ratio on the development of the jet, more information is needed on the effects of density ratio on the development of subsonic jets. Unfortunately, as noted in Chapter 1, there is a lack of data on the effects of density ratio on the initial mixing of subsonic jets.

Examination of the test matrix shows that both Mach 1.4 helium into air and Mach 3.0 argon into argon have convective Mach numbers of 1.0, but that the density ratios are widely different. Using a definition of the potential core as the distance at which the logarithmic decay after the potential core intercepts the potential core pressure value, the potential core length for Mach 3.0 argon into argon is 12 jet diameters, while the potential core length for the Mach 1.0 helium into air jet is 6 diameters. As can be seen on figures D.11 and D.15 both jets have diameters of slightly over 2 jet exit diameters, which is consistent with the relative inner and outer spreading rates being independent of density ratio.

For an incompressible two-dimensional shear layer, the growth rate approximately

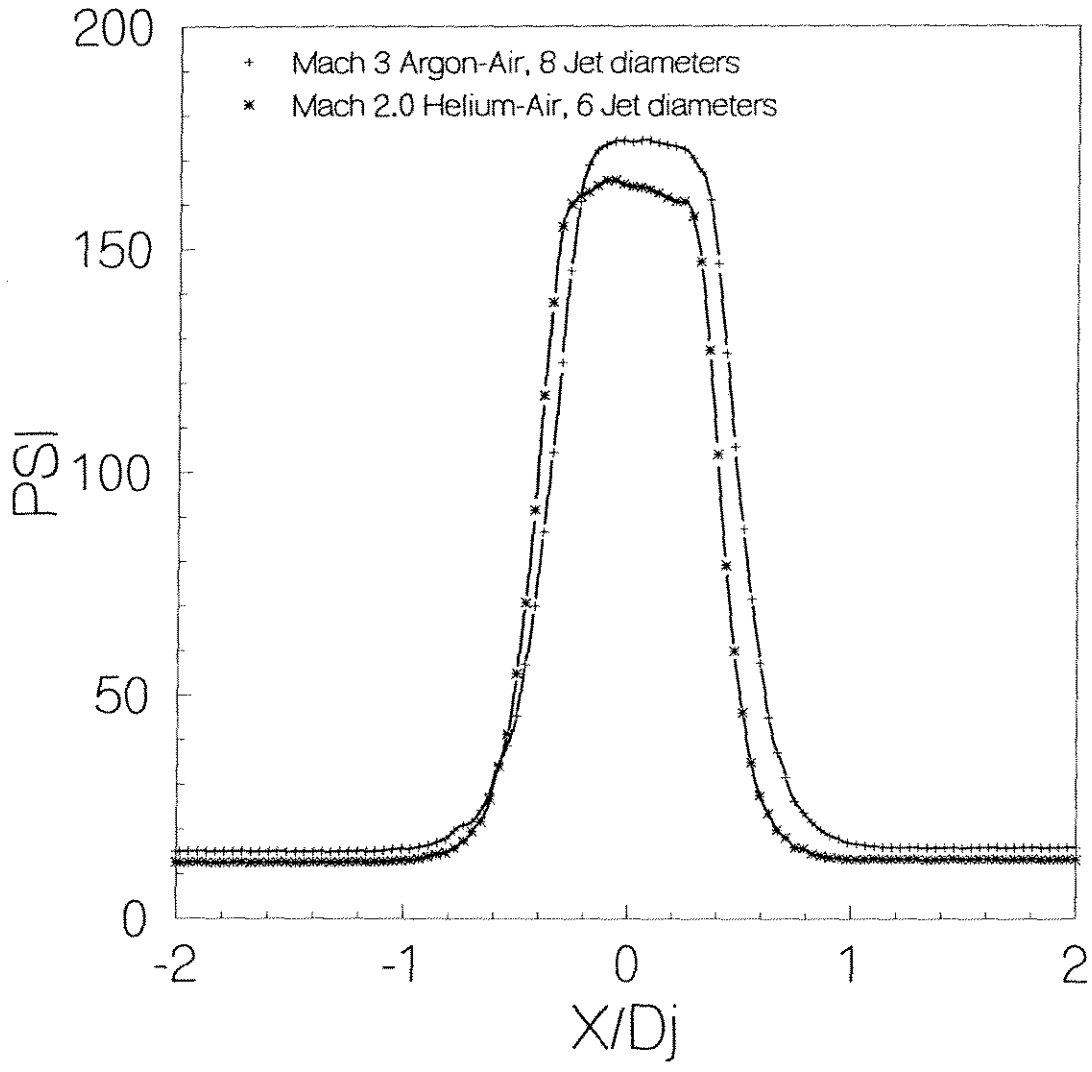

Figure 3.1: Pitot Pressures, Mach 3.0 Ar-air @ 8Dj, Mach 2.0 He-air @ 6Dj

follows the formula first proposed by Brown [7], as discussed in Chapter 1.

$$\delta' \propto \frac{(1-r)(1+s^{.5})}{1+rs^{.5}} \tag{3.1}$$

where, in this case, $s = \frac{\rho_a}{\rho_j}$ and $r = \frac{U_a}{U_j}$ with the subscripts j and a designating jet and ambient fluid, respectively. For a free jet, as in the present experiments, $r \equiv 0$ and the equation becomes:

$$\delta' \propto (1+s^{.5}) \tag{3.2}$$

When the numbers are plugged into the equation, ($s = 4.0$ and $.23$), the expected change in the potential core length is 2.03, which is well within the accuracy of the present measurements. Since Abramovich et al. found a similar scaling in their experiments [18], it seems that the above equation is a reasonable estimate of the effects of density ratio on the mixing in the potential core region of supersonic jets.

Figure 3.2 shows the centerline mean pitot pressure measurements for the homogeneous cases conducted, on a linear scale. Fig 3.3 shows the data from 5 to 20 jet diameters, plotted on a log-log scale. There are slight differences, in part attributable to the slightly different density ratios for a given mach number but different gammas, due to the pressure-temperature coupling. However, the data clearly fall into three distinct areas, with the potential core length being similar for all data with the same Mach number. The rough power-law decay after the potential core can be seen by

the fact that the points for a given Mach number and gas tend to fall on a straight line when plotted on a log-log scale. Although a power law decay is expected in the jet far field, for both the Mach 2.0 and Mach 3.0 data, the jet is still supersonic at 20 jet diameters. The power law is expected to change, as the jet transitions to subsonic flow, and eventually become $\frac{1}{x}$. The beginning of this process can be seen in the Mach 1.4 data.

Figure 3.4 shows the corresponding centerline 'RMS' data for the homogeneous cases. In this case as well, the data separates into three distinct bands. Towards the end of the potential core, an exponential growth begins, peaks and falls off. This fall off is exponential as well.

Figure 3.5 shows the centerline data for the inhomogeneous cases, with argon into argon homogeneous data also plotted as a reference. The corresponding log-log plot for 5-20 jet diameters is shown in Figure 3.6. Interestingly, Mach 1.4 helium into air and Mach 1.4 argon into air have nearly identical centerline pressure measurements. Similarly, Mach 2.0 argon into air and Mach 2.0 helium into air have very similar values until a few diameters after the end of the potential core, where the helium jet begins to decay much more quickly. As with the homogeneous jets, the decay after the end of the potential core follows a power law, based on the straight line decay as plotted on log-log axes. The corresponding 'RMS' data is shown in figure 3.7.

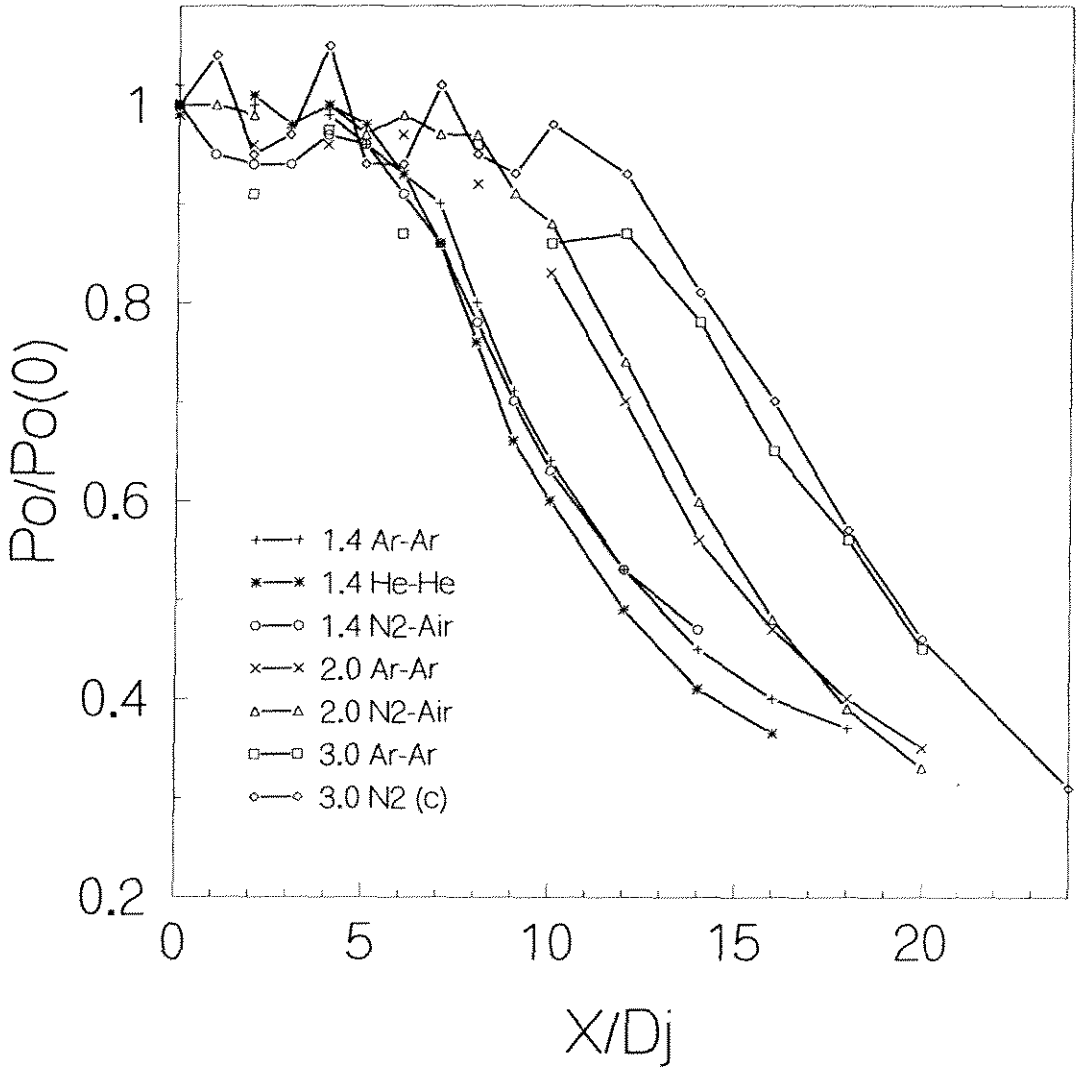

Figure 3.2: Mean Centerline Pitot Pressures, Homogeneous Data, linear scale

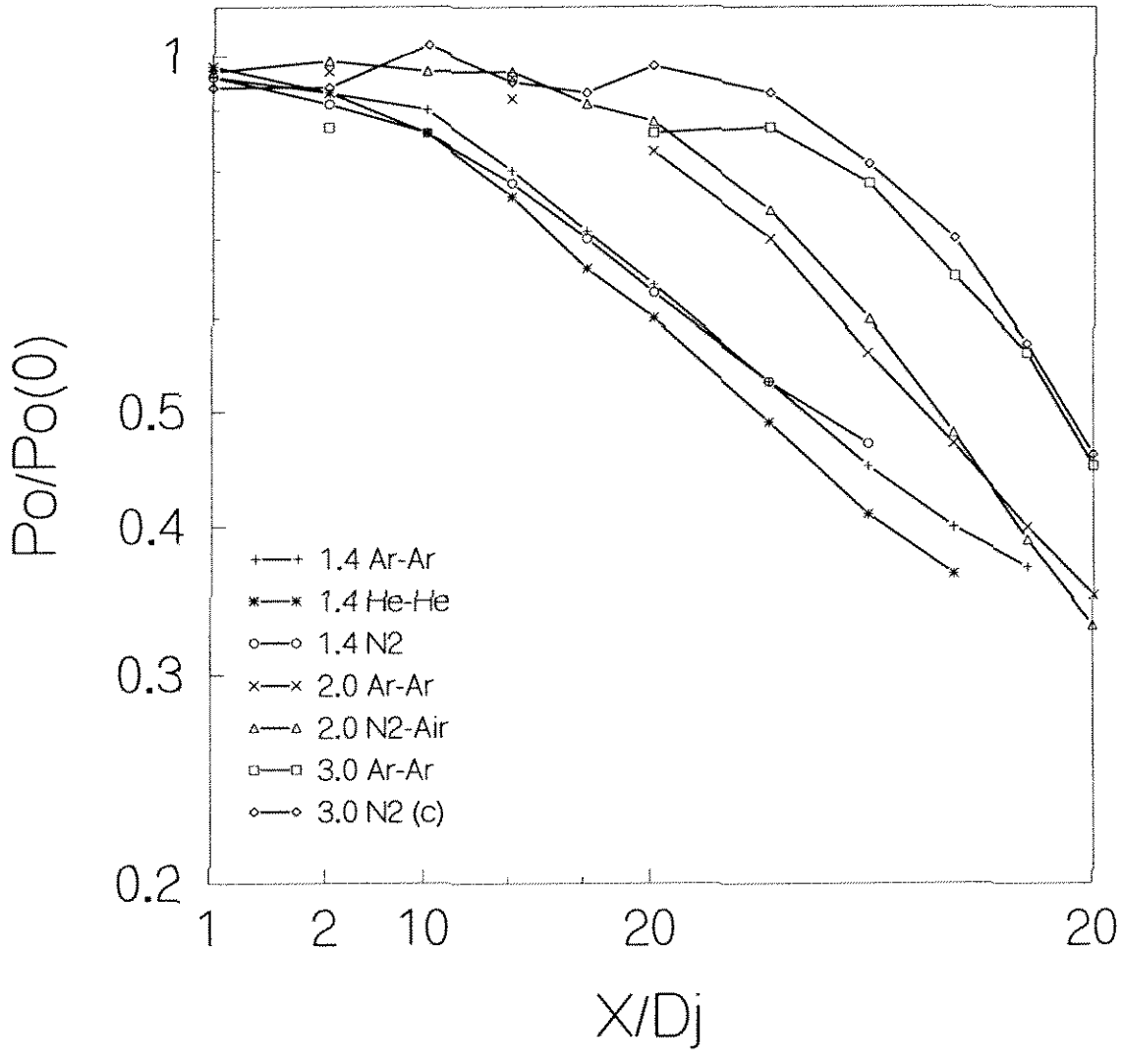

Figure 3.3: Mean Centerline Pitot Pressures, Homogeneous Data, log-log scale

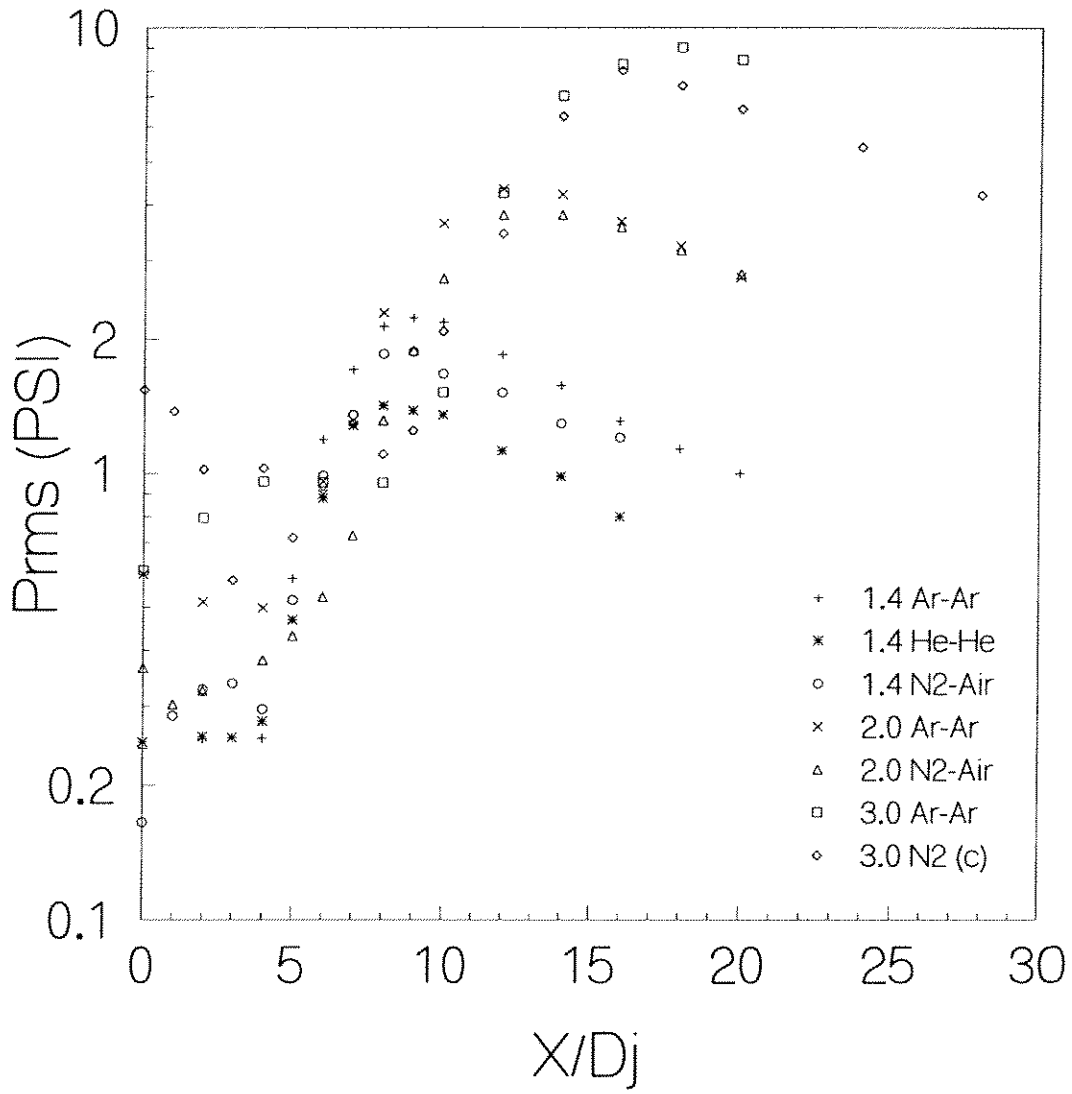

Figure 3.4: RMS Centerline Pitot Pressures, Homogeneous Data

Again, toward the end of the potential core an exponential rise occurs followed by an exponential decay, evidenced by the straight line on a log-linear axis.

The potential core lengths for the various flows were measured from the above plots. The potential core, for the purposes of the data presented herein, is defined as the distance at which the asymptote from the decay after the potential core reaches the potential core pitot pressure value. The density correction discussed above was applied to the measured values, to generate a 'density ratio normalized' potential core length. The results are shown in table 3.2. Although a general trend to have a reduced normalized potential core length as the convective Mach number is reduced can be discerned, there are significant differences visible as well. Furthermore, compressibility does not appear to affect the jet as much as it affects the compressible shear layer. For the shear layer, using the formula proposed by Dimotakis [4], for a convective Mach number of 1 or greater, the spreading rate is reduced by a factor of 4 or more, compared to an incompressible shear layer. However, in the case of the jet, the potential core length is only about 2.5 times longer than that observed for the incompressible jet. This is graphically shown in Figure 3.8. Compressibility therefore plays a less significant role in the initial growth of the shear layers in an axisymmetric jet than in the case of a two-dimensional shear layer. The location of the peak in the 'RMS' data was also measured and is included in the table. The values range from

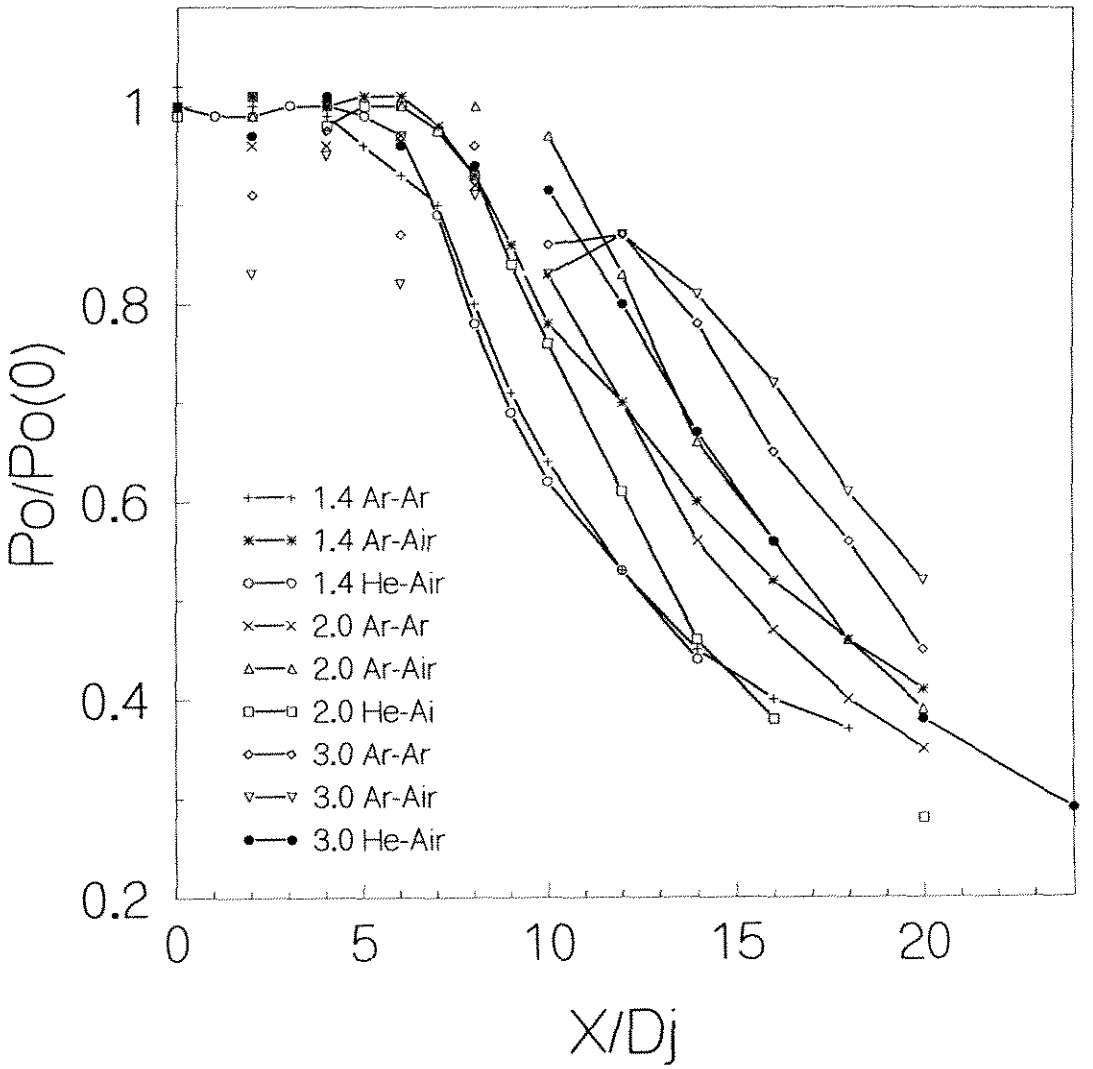

Figure 3.5: Mean Centerline Pitot Pressures, Inhomogeneous Data, linear scale

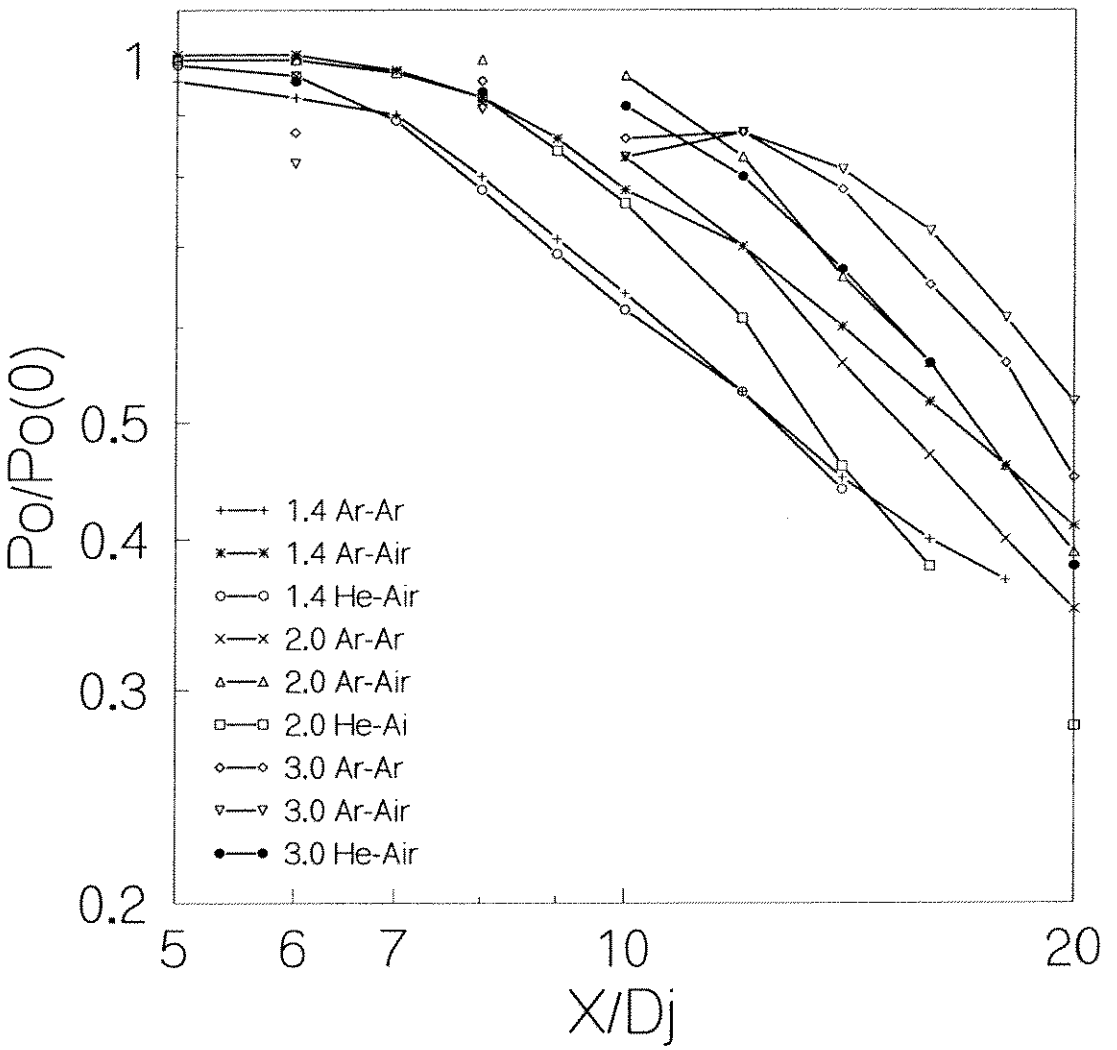

Figure 3.6: Mean Centerline Pitot Pressures, Inhomogeneous Data, log-log scale

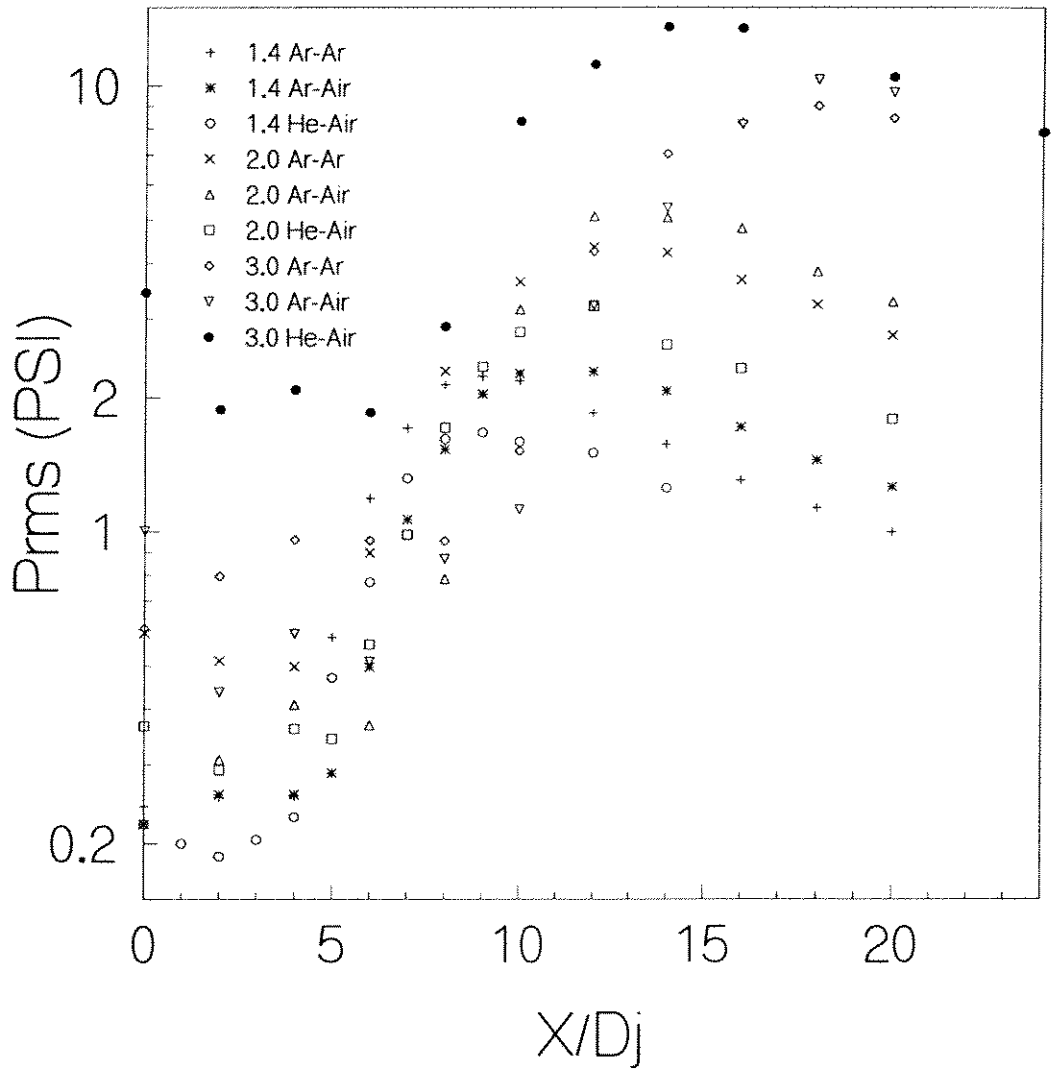

Figure 3.7: RMS Centerline Pitot Pressures, Inhomogeneous Data

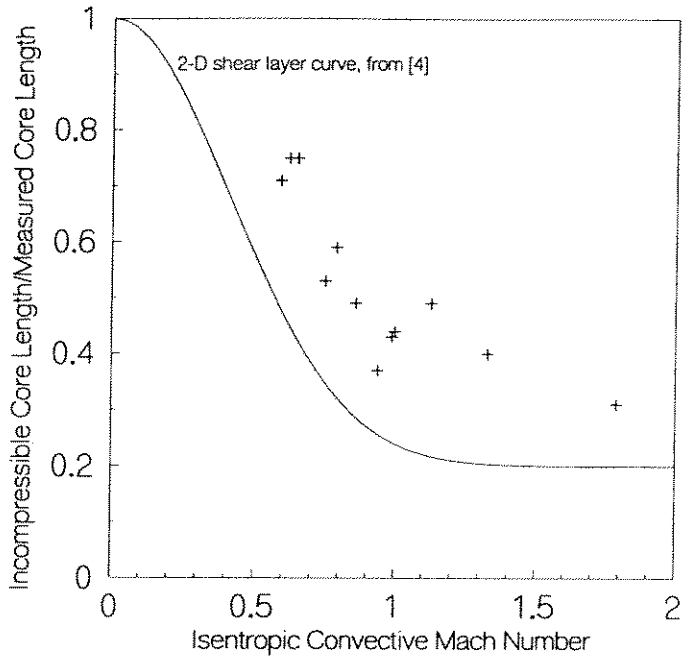

Figure 3.8: Density normalized vs Incompressible spreading rate

1.2 to 1.7 potential core lengths.

3.3 Convection Velocity

One of the most discussed questions with respect to supersonic shear layers in the last few years has been the convection velocity of the large scale structures. Experiments by Papamoschou, Dimotakis, and others have indicated that the structures that do exist convect not at the isentropic convective Mach number, but rather at a speed that is close to the speed of one of the streams. It should be pointed out, however,

Mj	Jet Gas	Ambient	ρ_j/ρ_a	Mc [1]	L(m) [2]	L(c) [3]	Peak RMS
3.0	Helium	Air	0.55	1.79	11.0	12.9	1.3
2.0	Helium	Air	0.32	1.33	7.25	10.0	1.6
3.0	Nitrogen	Air	2.8	1.13	12.5	8.1	1.3
1.41	Helium	Air	0.23	0.99	6.0	9.3	1.5
3.0	Argon	Argon	4.0	1.00	12.0	9.0	1.3
3.0	Argon	Air	5.5	0.94	15.0	10.7	1.2
2.0	Nitrogen	Air	1.8	0.86	9.25	8.1	1.4
2.0	Argon	Argon	2.3	0.79	8.25	6.8	1.5
2.0	Argon	Air	3.2	0.75	9.75	7.6	1.3
1.41	Nitrogen	Air	1.4	0.65	5.75	5.3	1.6
1.41	Argon	Argon	1.7	0.62	6.0	5.3	1.5
1.41	Argon	Air	2.3	0.59	6.75	5.6	1.7

[1] Average isentropic convective Mach number

[2] Measured potential core length

[3] Density corrected potential core length

Table 3.2: Potential Core Length

that the use of the convective Mach number as a compressibility criterion is objective, easy to implement, and, for most of the data, does seem to collapse the effects of compressibility onto a single curve.

In order to address the convective velocity question in axisymmetric jets, rather than two-dimensional shear layers, an analysis of the acoustic radiation pattern of the jets was conducted. Each jet that showed discernible radiation in the single spark photographs had the angles of the radiation measured[1]. These angles were used to calculate the speed of the convective structures, assuming that the radiation was a Mach-wave type emanating from the structures.

The results are tabulated in table 3.3. The surprising result is that for the axisymmetric supersonic jet, the structures convect at about $0.8U_j$, for a wide range of jet density ratios. The consistency of the results is suprising, since a slight variation in the angles can result in a large variation in the calculated velocity. Since $0.8U_j$ is close to the theoretical convection velocity for the most amplified instability wave in supersonic jets, the clear implication is that for axisymmetric supersonic jets the dominant mixing force is the growth of the jet instabilities, rather than the instabilities of the shear layer. The value of $0.8U_j$ is in agreement with the results of Troutt and

[1]In order to lend some objectivity to the obviously subjective process of measuring angles, the author plus two people who did not know the purpose of measuring the angles tabulated the angles independently, and the results averaged.

McLaughlin [48] for the n = 1 helical mode. It is also close to the observed value of 0.7 obtained by Morrison and McLaughlin [46]. This agreement is quite remarkable, since the Reynolds number in the present experiments is one and two orders of magnitude higher, respectively, and the measurement methods are completely different.

The acoustic radiation patterns observed in the photographs also provide further indication that the jet is dominated by helical instability waves. The radiation does not occupy the entire space around the jet, but is confined to some conical region of space downstream of the jet exit. This acoustic cut-off, which can clearly be seen on the photographs, is in close agreement with the predictions of Tam [34], who modeled the acoustic radiation from an assumed helical instability.

The idea that the mixing, as indicated by the spreading rate, is dominated by jet rather than shear layer instabilities is bolstered by the RMS centerline data. The recent jet noise theories hypothesize that some observed downstream noise sources of the jet are caused by a helical disturbance that grows exponentially, saturates, and is damped, giving up a significant amount of energy. The saturation is calculated to take place slightly downstream of the potential core [38], which would be in reasonable agreement with the measured locations of the RMS peaks.

Mj	Jet Gas	Ambient	ρ_j/ρ_a	Mc1 [1]	Mc2 [2]	Uj [3]	Angle	Uc [4]	$\frac{U_c}{U_j}$
3.0	Helium	Air	0.55	0.66	3.42	1503	17	1173	.79
2.0	Helium	Air	0.32	0.31	3.24	1312	18	1110	.83
3.0	Nitrogen	Air	2.8	0.62	1.44	622	44	494	.79
1.41	Helium	Air	0.23	0.25	2.61	1091	23	878	.80
3.0	Argon	Argon	4.0	0.60	1.19	475	51	380	.80
3.0	Argon	Air	5.5	0.63	1.09	475	66	376	.79
2.0	Nitrogen	Air	1.8	0.36	1.31	518	54	424	.81
2.0	Argon	Argon	2.3	0.48	1.05	415	70	335	.81

[1] Convective Mach number with respect to jet

[2] Convective Mach number with respect to ambient fluid

[3] Meters per second relative to lab frame

[4] Meters per second relative to tank ambient fluid (theoretical)

Table 3.3: Estimated Convection Velocities

3.4 Effect of Off-design Conditions

In order to probe the effects of slightly off-design operation on the development of the jet, a series of experiments was conducted using the Mach 3.0 nitrogen nozzle, exhausting into air. The ideally-expanded stagnation pressure was determined, as explained above, on the basis of flow visualization pictures. Data were then taken with the stagnation pressure varied to give underexpanded jets with static pressure mismatches of 0.1 and 0.2 psi, and an overexpanded jet with a static pressure mismatch of .1 psi. This gave settling chambers of 534, 491, 454, and 417 psia. The jets will be referred to as jet A, B, C, and D, respectively, throughout this section. Jet C is the "ideally expanded" jet. A Mach 3.0 jet was chosen because it allows a more precise control over the exact pressure mismatch between the jet exit and the tank, while at the same time permitting a greater mismatch without forming a mach disk on the axis.

Photos of the jets are shown in figures C.13 to C.17, in Appendix C. In addition to photos of jets A-D, an additional photo is provided for a jet with a settling chamber pressure of 380 psia, to make the effects of overexpansion more visually obvious. No data are provided for this jet.

The photos of Jet A, figure C.13, clearly show the expansion fan and the characteristic axisymmetric cell structure. The pitot profiles from 0 to 8 jet diameters, figure E.1, show that the initial profile is a top-hat and that the expansion fan reflects

back and forth inside the jet, with the effects visible through the first eight jet diameters. The reason for the increase toward the center of the jet at 1 jet diameter is that the expansion fan has not yet reached the axis. Similar features can occasionally be seen in other profiles, and their identity can be determined with reference to the photographs (the jet diameter is .5 in, and the photos are 1:1). The traces from 8 to 14 jet diameters, figure E.2, show that the potential core is about 10 jet diameters long, as well as the gradual transition to a more Gaussian profile. The first two figures have uniform scaling for all the traces, so that the decay can be judged. The third figure E.3, which shows profiles spaced every 4 jet diameters, from 0 to 28 diameters, allows the scaling to vary so that each trace fills the allotted space, to better gauge the spreading and shape of the profiles. The pressure sensor used in the pitot probe was not repeatable below 20 psia, which is the reason for the variation in the low (outside the jet) pressures. The 'RMS' profiles clearly show both the growth of the shear layer and the initial expansion fan. The data confirm that the potential core is about 10 diameters long.

As the settling chamber pressure is lowered, the expansion fan becomes weaker. The photo of Jet B, figure C.14, does shows a weaker set of cells, with the same general features. No clearly discernable effect of the different pressure on the development of the flow can be seen. The potential core also is about 10 diameters long in this case,

and the widths of the jet are nearly identical despite the difference in the strength of the expansion. The one slight difference, based on the pressure profiles, is that Jet B approaches the gaussian profile more quickly than Jet A, once downstream of the potential core (see figures E.5 and E.11).

Jet C does not have an expansion fan, but rather a weak compression wave. The effects on the flow are minimal and the pitot traverses, shown in figures E.13 to E.15, show an initial top-hat profile that decays as the shear layer grows, until the layers merge. As with Jet B, there is no distinct difference in mixing width or potential core length attributable to the expansion. The potential core is still approximately 10 jet diameters, and the approach to the gaussian profile is virtually identical to that of Jet B (slightly faster than for Jet A). The photos, on photo page 15, show that the shear layers are not bent by the incident wave and that the disturbance is, in fact, a slight compression.

Although Jet D is overexpanded, the photos, on photo page 16, seem to show less of a flow disturbance than that due to Jet C. However, an examination of the pitot traces, figures E.19 to E.21, clearly show the shock wave crossing the jet centerline at about 1 jet diameter and then reflecting from the edge of the jet as an expansion. The widths of the jet are not distinguishable from Jets C or B, but are slightly narrower than Jet A. The potential core length appears to be unaffected, and the approach to

a gaussian profile happens even more quickly in Jet D than for Jet C.

In order to illuminate possible subtle differences in the jets, since no major effects could be seen in the pitot traverses, mean centerline data was taken every jet diameter until the end of the potential core, with gradually increasing spacing thereafter. The centerline mean pitot pressure is shown in figure 3.9. The reflection of the waves within the jet are clearly discernable. The end of the potential core, based on these measurements, rather than on the traverses, gives a value of 12 diameters. After the end of the potential core, the decay becomes nearly linear, as expected from classical jet theory. It can also be seen that although the ideally expanded jet, jet C, has the slowest decay, that a slight underexpansion does not affect the flow as much as a slight overexpansion.

The RMS centerline data, plotted on a linear scale, are shown in figure 3.10. The data indicate that the potential core ends for all jets simultaneously, at about 9 or 10 jet diameters. The difference between these data and the mean data is to be expected, since initial minor fluctuations will affect the RMS without affecting the mean data. The peak in the fluctuations occurs at about 16 jet diameters, except for Jet D, the overexpanded case. The centerline RMS data also support the observation that the approach to a gaussian profile is slowest for Jet A, followed by Jet C, Jet B, and Jet D, in that order. Downstream of the peak fluctuations, the level for the various jets

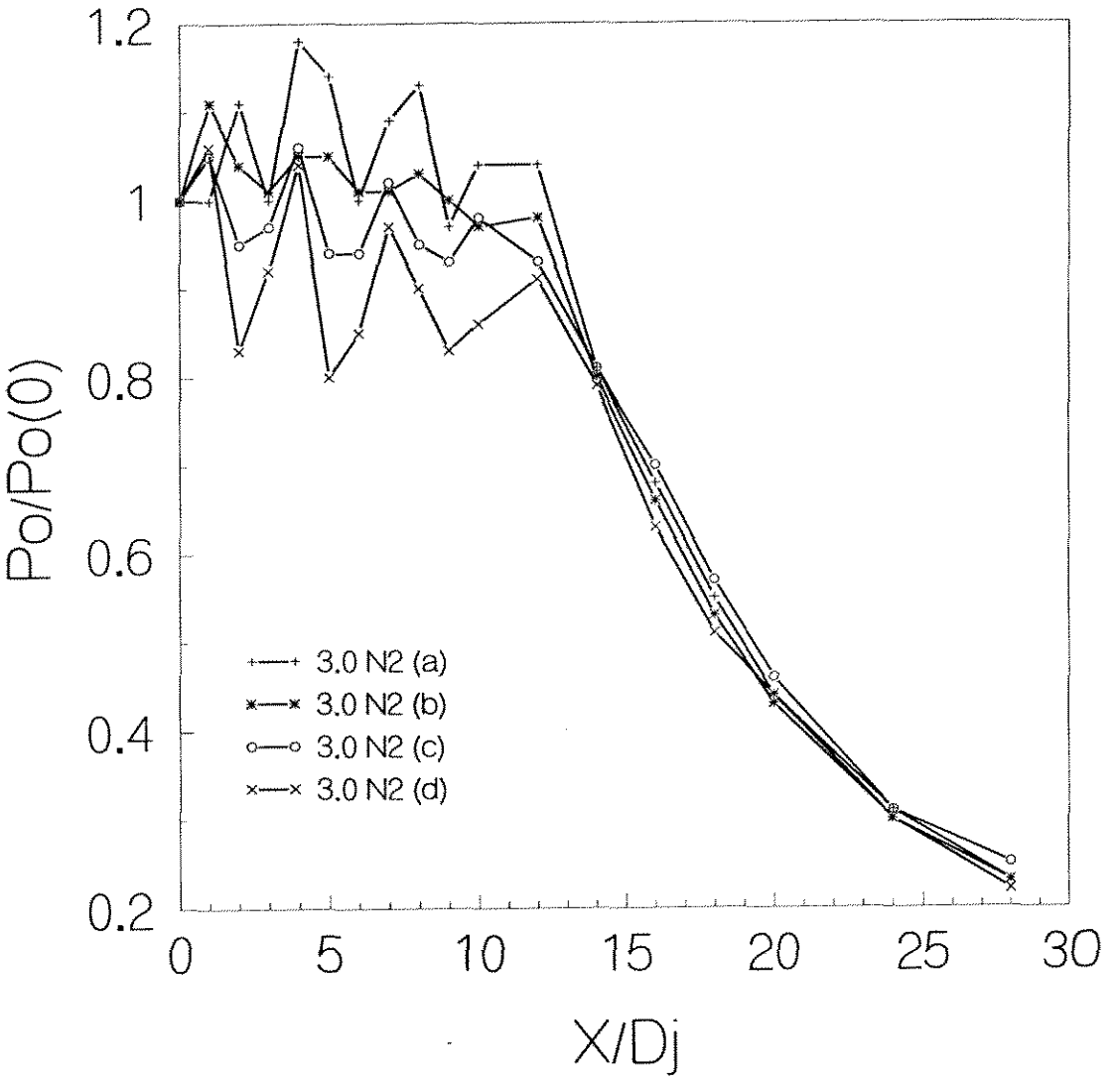

Figure 3.9: Centerline Mean Pitot Pressure, Off-Design M 3.0 Nitrogen

becomes one of inverse settling chamber pressure. Jet D has the highest fluctuation level, followed in order by Jet C, Jet B, and Jet A.

The same data, plotted on a logarithmic scale, are shown in figure 3.11. It shows that the fluctuations experience approximately exponential growth after the end of the potential core, and an approximately exponential decay after the peak fluctuations. The exponential decay is required in the far field, since it is known that after the jet reaches a subsonic asymptotic form, then the spread of the jet is linear, the velocity on the axis decays linearly, and the velocity fluctuations on the axis are a fixed level of the centerline velocity. The asymptotic level has not been reached in this case, since the flow with the highest fluctuation level is also the flow with the lowest pitot pressure, and hence velocity.

The conclusion to be drawn from the off-design experiments is that if the nozzle is designed and constructed appropriately, then the effects of small under- or over-expansion on the development of the jet is minimal. Under-expansion appears to stabilize the jet somewhat, while over-expansion leads to a more rapid decay after the end of the potential core.

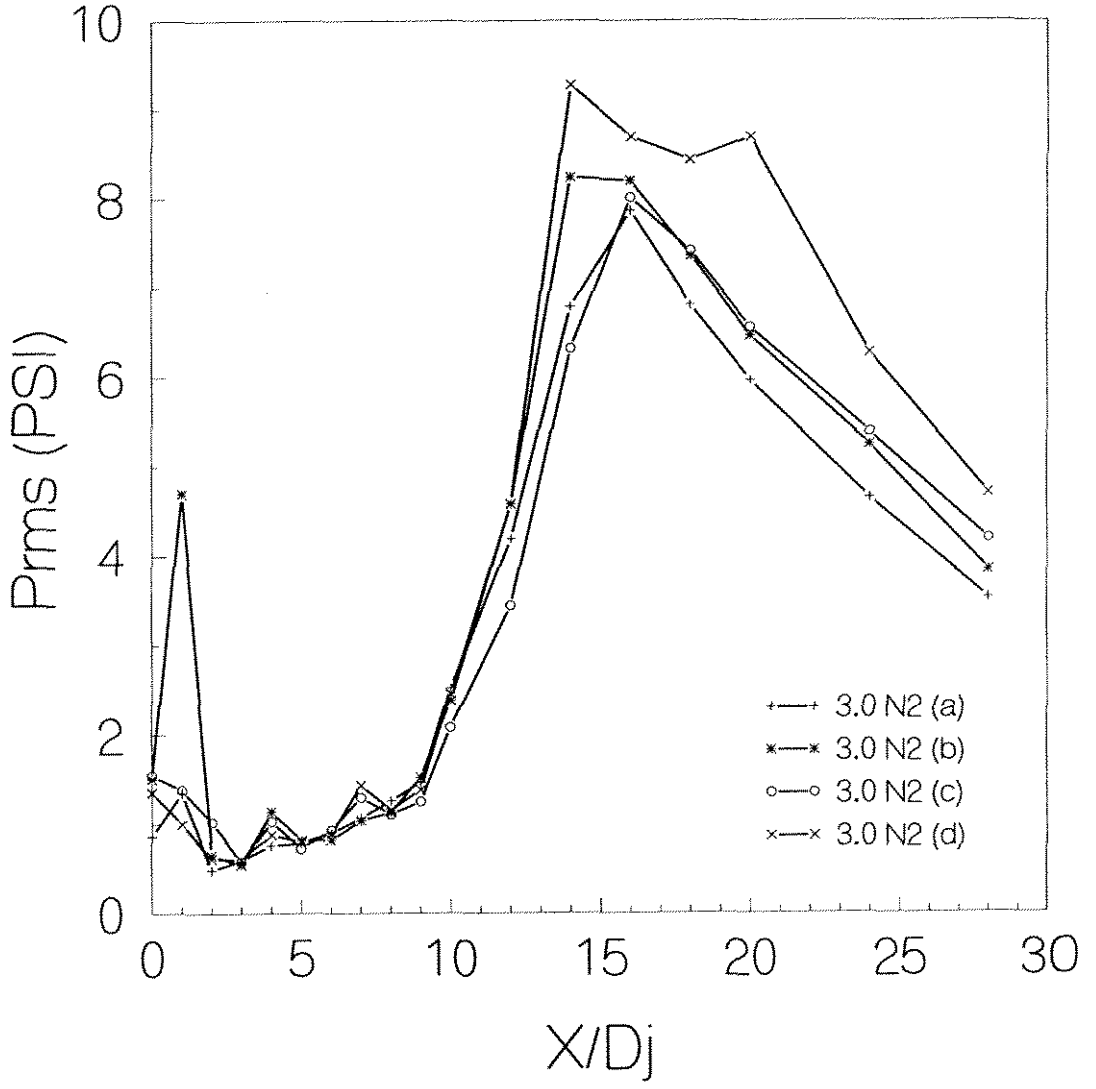

Figure 3.10: Centerline RMS Pitot Data, Off-Design Mach 3.0 Nitrogen

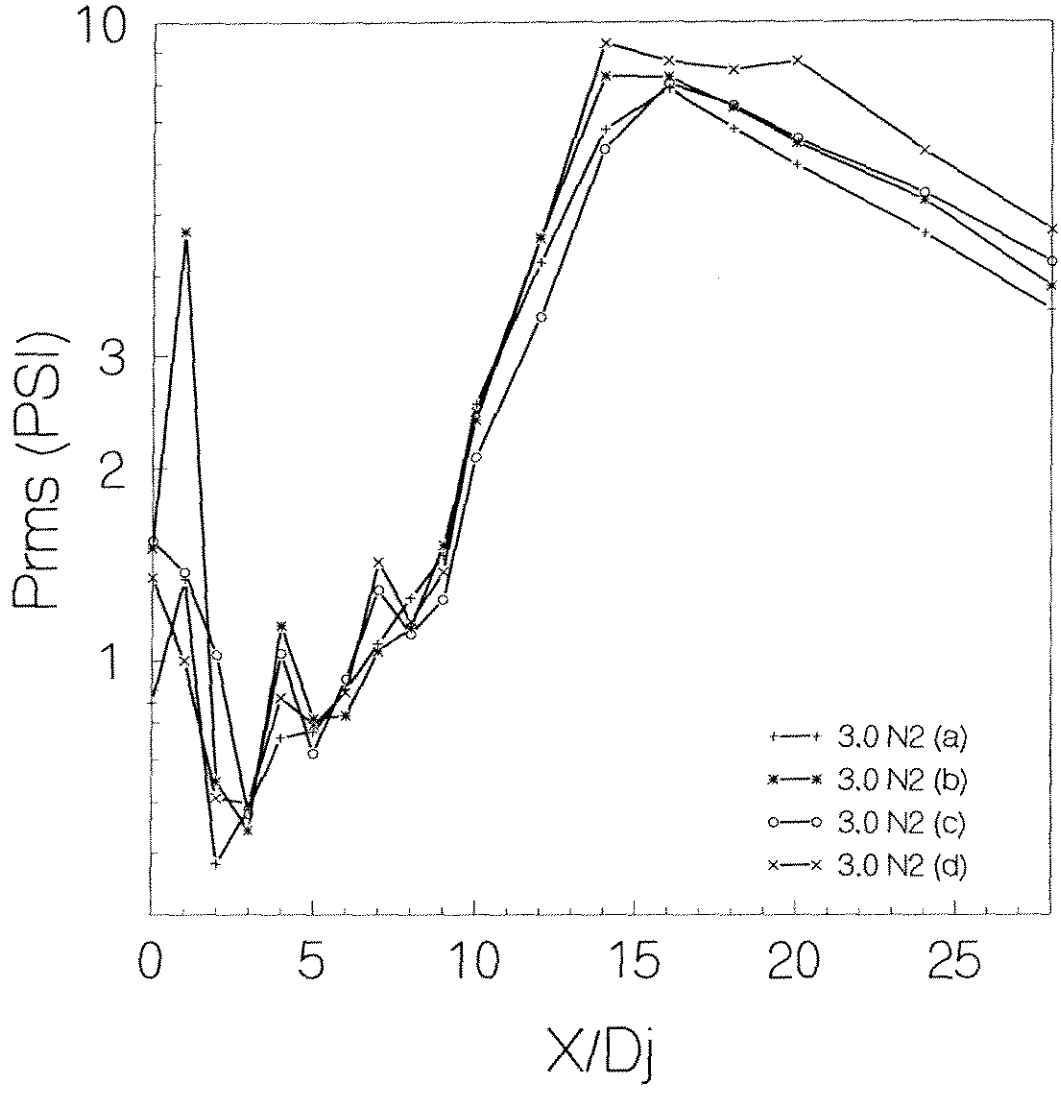

Figure 3.11: Centerline RMS Pitot Data, Off-Design Mach 3.0 N2, log scale

3.5 Anomalous Conditions

During the course of the experiments, two quite unexpected results were obtained. The results are experimentally repeatable and, to the best of our ability, have been determined to not be artifacts of the facility or experimental methodology.

3.5.1 Long-period Variations

As mentioned previously, data were gathered with the probe moving continuously during a run, rather than stopping at discrete points. At each point, the pressure is changing temporally due to the turbulent fluctuations in the flow. However, in a sheared flow the mean data also changes spatially as well. With a moving probe, temporal variations in the measured pressure would be a combination of spatial and turbulence-caused fluctuations. Smoothing over a given number of neighbor points allows the turbulent fluctuations to be averaged out, so that the mean value of the pressure may be obtained. However, the greater the number of points used the greater spatial distance the averaging represents, and, therefore, the lower the spatial resolution.

Once it was decided to use the pressure probes to obtain limited frequency data, the number of neighboring points to smooth over became a critical issue. In order to determine the optimum number of points, which is a compromise between temporal

smoothness and spatial smearing, frequency data were taken on the jet centerline downstream of the potential core. Since the mean value on the jet centerline is expected to be steady, the number of points required to achieve a steady mean value would be expected to be the appropriate number of points to smooth over. However, it was found that the average of the data never settled to a constant value, regardless of the number of points chosen. As the number of points was increased, fluctuations still existed, with frequencies corresponding to the number of points selected quite evident. In order to ensure that these results were not the artifact of either noise in the analog filter or computer post-processing, additional data were taken with a total pressure probe with a reduced entrance diameter, without using the analog filter or computer processing. The reduced entrance diameter effectively limits the frequency response of the probe. A trace from a Mach 3.0 nitrogen jet is shown in Figure 3.12. In addition to showing the low-frequency component of the pitot data, the figure also shows the inherent advantage in a two-stage regulation system. Although the interstage pressure fluctuates, the settling chamber pressure is isolated from them.

Examination of the figure shows that variations in the total pressure measurement with time-scales of 0.1 second or more are quite prevalent. For the local Mach number and jet diameter, these fluctuations correspond to durations of 3000 jet time-scales (diameter divided by velocity). The settling chamber pressure varies by less than 0.5%

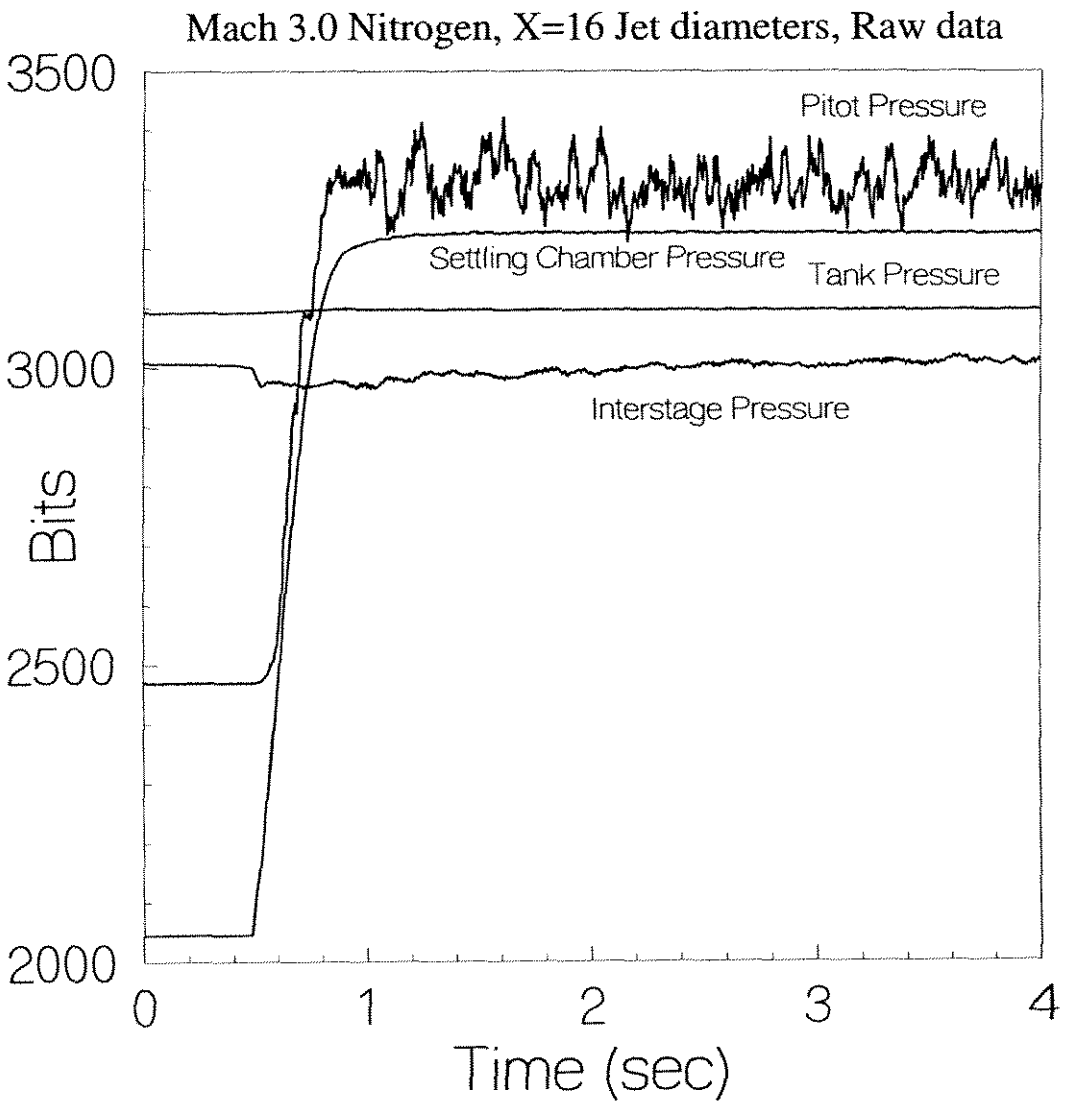

Figure 3.12: Mach 3.0 N_2 Low Frequency Data

during the same time period, and the tank ambient pressure is constant to within the accuracy of the measurements. Within the limits of the data acquisition system, and the length of time that the gas supply can run, there is a flat noise spectrum from the high-frequency cut-off of the filter to the lowest frequency with reliable data.

Since it was speculated that even low-level pressure fluctuations could have a profound influence on the jet, the jet fluctuations were checked for correlation with the minimal settling chamber variations as well as the interstage pressure fluctuations. No correlation was found. The fluctuations were also observed when data was taken with two conventional L-shaped probes, so they are unlikely to be caused by the particular shape of the probe used in these experiments. Changing the acoustic modes of the tank by opening access doors, closing off downstream piping and valves, etc. , had no effect on the fluctuations, and it is concluded that the fluctuations are an inherent part of the flow rather than an experimental artifact. The mechanism behind the fluctuations is unknown.

3.5.2 Nozzle Boundary Layers

Despite all the care taken, small waves persisted in the flow. It should be emphasized that no effect of the waves on the flow was discernable from the shadowgraph pictures and the pressure variations are extremely slight. Some waves are to be expected due

to the displacement effect of the shear layers. It is also expected that different ambient gases will interact differently, and the strength of the weak cell structure will vary as well. However, for a given nozzle and gas, the measured total pressure should be a constant fraction of the settling chamber pressure, independent of the downstream pressure. The actual data has anomalous behavior, in that the measured total pressure in the exit plane of the nozzle is apparently affected by the ambient fluid.

Figure 3.13 shows two sets of data. The first set is Mach 3.0 argon into air, while the second is Mach 3.0 argon into argon. For both sets, the settling chamber pressures were constant and equal to within 0.5%, and the ambient pressure in the tank was constant to within the accuracy of the instrumentation. The spatial variation in the pressure measurements with downstream distance, and the slightly decreasing trend, are believed to be the effect of slight variations in the static pressure of the jet. The measured total pressure is very sensitive to slight changes in the static pressure, since the strength of the bow shock of the pitot probe will be significantly affected. The variations in this case take place within the potential core of the jet, and the isentropic stagnation pressure is expected to be constant.

However, total pressure measurements made in the exit plane are theoretically independent of the downstream conditions, since the flow is supersonic. Despite the fact that the settling chamber pressure for the two subject cases is equal to within 0.5%,

the measured total pressure differs by about 4%. Somehow, the flow in the nozzle is being slightly affected by the downstream conditions, in this case by differing ambient gases. Since the only subsonic portion of the flow in the nozzle is the boundary layer, it is believed that there must be some slight effect of the downstream conditions on the displacement thickness of the nozzle wall boundary layer. No satisfactory mechanism for this boundary layer modification has been proposed.

It should be pointed out that although the pressure fluctuations are fairly large, the actual velocity fluctuations (calculated for the argon into argon jet using measured pitot pressure and tank ambient pressure) are less than 1%. This serves to illustrate the point made earlier, that total pressure measurements are inherently more sensitive than velocity measurements to variations in flow conditions.

3.5.3 Static Pressure

One assumption that has been generally made by researchers is that the static pressure is constant throughout a jet flowfield. While that may be the case for subsonic jets, it is not the case for supersonic jets. As mentioned at the beginning of this chapter, the settling chamber pressure used for each run was determined by a series of photographs, which were examined for shocks and expansion fans. The reason that this was done, rather than setting the pressure in the settling chamber appropriate to the tank and jat

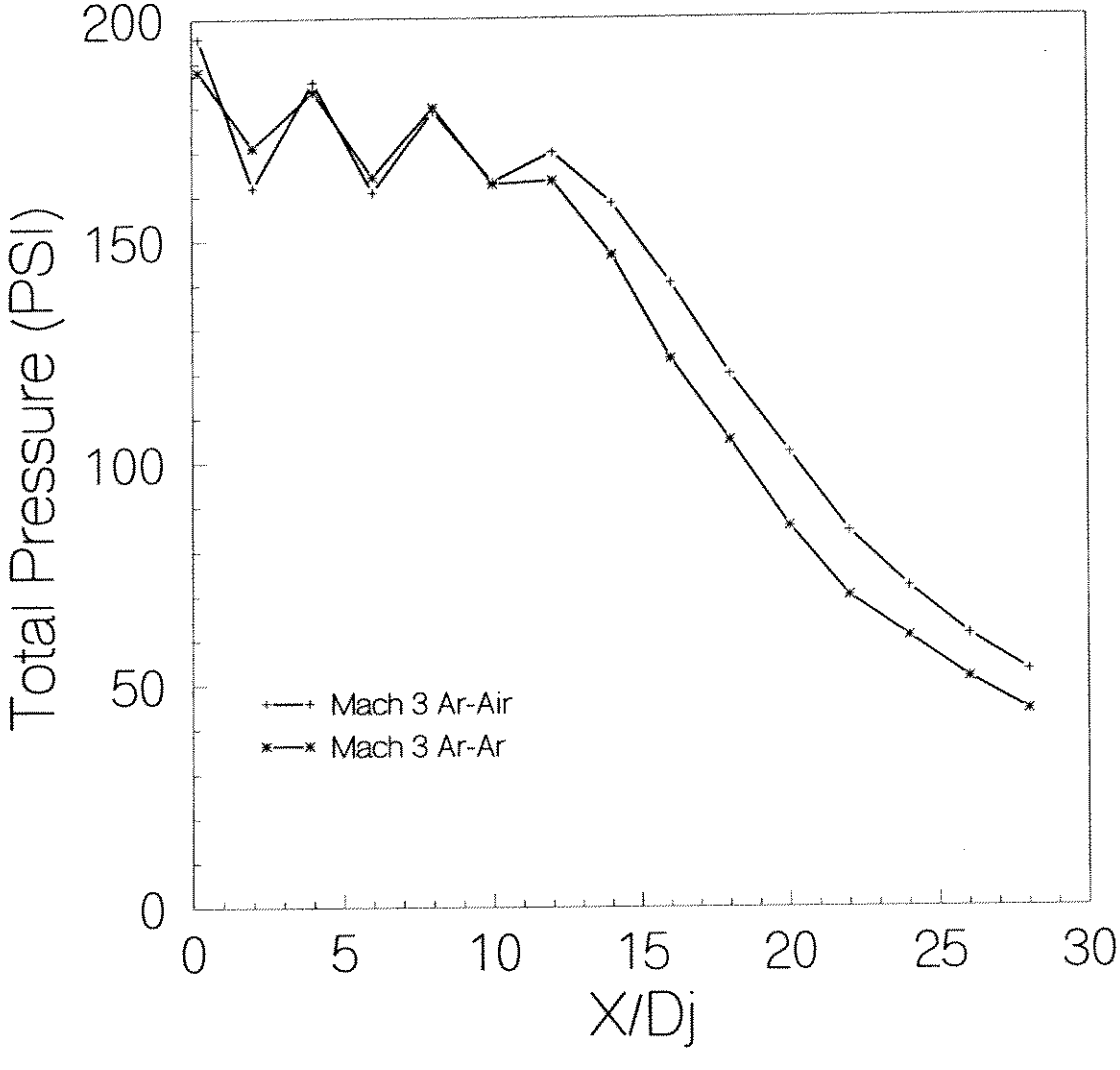

Figure 3.13: Measured Centerline Total Pressure, Mach 3.0 Argon

Mach number, was that the expected value of the pressure resulted in a mismatched jet. Both the shadowgraph pictures and pitot probe traverses would show the presence of expansion fans. When the pressure was reduced to an ideally-expanded condition, and the Mach number calculated based on the settling chamber pressure and the pitot pressure, the Mach number was at the design value. However, if the static pressure was calculated using the settling chamber pressure and the jet Mach number, the calculated static pressure was lower than the measured static pressure in the tank by as much as 2 psi.

Chapter 4

Conclusions

A parametric study of axisymmetric supersonic jets has been conducted. The jet Mach numbers ranged from 1.41 to 3.0, and the density ratio varies from 0.23 to 5.5. The experiments were conducted into an ambient gas at rest, in order to better isolate the effects of compressibility and density ratio on the jet by eliminating the velocity ratio as a parameter.

In order to conduct the study, unique nozzles had to be designed for each gas and Mach number combination. In addition, since previous researchers encountered significant flow difficulties as a result of nozzle design and construction problems, a considerable effort was expended on devising a method to manufacture the nozzles. A plating method, in which pure nickel is deposited over an aluminum mandrel and then

the aluminum dissolved out, was developed and resulted in nozzles that had mirror finishes on the interior contours as well as being an order of magnitude less costly than methods using direct machining techniques.

Pressure sensors were used to obtain limited frequency information in an environment too harsh for hot wires. Post-processing of the data allowed both a smoothed profile, similar to that obtained by traditional pitot probes, and an 'RMS' profile to be generated. the 'RMS' profiles clearly show the development of the mixing layer, and the gradual modification to a gaussian profile downstream of the potential core.

4.1 Summary of Results

(a) The primary effect of density ratio, for a free jet, is to shorten or lengthen the potential core. The relation between the inner and outer spreading of the annular mixing region is constant, with approximately 55% of the mixing layer lying outside the initial jet radius, and the remaining 45% lying inside the initial jet radius. This result is consistent with that of previous experimenters. This result also implies that for a free jet, the potential core length uniquely determines the spreading rate of the annular mixing region.

(b) Due to the lack of subsonic data to compare to, the effect of density ratio was

compared to the two-dimensional scaling for two jets with the same convective Mach number but different density ratios. The scaling appeared to be accurate, and it was used to normalize the effects of density ratio on the jet.

(c) Using the two-dimensional density normalization, the effects of compressibility on the initial development of the jet were explored. While the same general trend as for two-dimensional shear layers is found: the higher the convective Mach number of the flow, the less the mixing, significant deviations of the data from a monotonic function were noticed. Furthermore, the spreading rate ratio between high Mach numbers and the incompressible case asymptotes to about 40%, rather than 20%. The data gathered here is not sufficient to conclude whether the convective Mach number concept will collapse jet data in the same way that it has for two-dimensional data. However, it is possible to conclude that the accepted 2-d compressibility correction does not apply to jets.

(d) The convective velocity of the large scale variations in the jet were estimated by measuring Mach angles from 20 nanosecond shadowgraph pictures of the flow. All jets with visible radiation had estimated convection velocities of 0.8 Uj, which is the expected convection velocity of the first helical modes of the jet.

(e) The peak in the RMS centerline data occurs between 1.2 and 1.7 potential core lengths, follows an exponential rise, and is followed by an exponential decay. This

value is reasonably close to the literature estimates of the saturation distance for the most unstable helical instability.

(f) The above three points combine to show that the jet is not dominated by instabilities of the shear layer, but rather by instabilites of the jet itself. The shear layer growth is important through its effect on the stability of the global jet instability.

(g) For a well designed nozzle, even moderate pressure mismatches do not have a significant effect beyond the end of the potential core, despite large variations in the pitot pressure measured within the core.

(h) Long-time variations in the pitot pressure trace occur despite the lack of any fluctuations in the settling chamber pressure. The variations are thought to be caused by randomly varying phase between the helical instability modes of the jet.

(i) It is believed that the static pressures near the jet are not the same as elsewhere in the tank, as is generally assumed. The exit mach number of the jets, based on pitot pressure and settling chamber pressure, were close to the design condition, but the static pressure in the tank indicated that the jet should be overexpanded at the exit, based on the nozzle Mach number and the settling chamber pressure. Shadowgraph photographs confirmed that the nozzles were operating in a near shock-free condition and were ideally expanded.

4.2 Suggestions for Future Work

The present set of experiments has addressed some issues relating to the development of axisymmetric supersonic jets, but there are areas that still need significant data. The single most important issue to be addressed is the concentration field throughout the jet. Without a concentration field, the molecular mixing cannot be addressed, and the measurement of concentration should provide a more objective and repeatable definition of both the potential core length and the mixing layer width.

The transition from a supersonic turbulent jet to a subsonic turbulent jet needs to be addressed more fully. This would require more sensitive flow diagnostics than were used in the present experiments.

The static pressures in the jet need to be accurately measured. It is clear from the present work that the pressure should not be considered constant across the jet, but the measurement of static pressure in a yawed, highly sheared, supersonic environment is a technique that does not exist at the present time. One possible method of addressing the static pressure issue would be to make LDV or PIV measurements to obtain velocity, and then use measured concentration and pitot pressures to enable a calculation of static pressure to be made.

Appendix A

Supersonic Nozzle Details

A.1 Introduction

One of the major difficulties encountered in the course of this thesis was the design and construction of the nozzles. A parametric study over a range of density ratios and Mach numbers was planned, as shown in Table A.1. Since each gas and Mach number combination has a unique contour, this required a large number of nozzles. A review of the existing literature showed that one of the most common experimental difficulties was in obtaining good flow from the nozzle: that is, a nozzle free from internal shocks with thin boundary layers and parallel flow at the exit. Furthermore, estimates to produce such nozzles by direct machining averaged about $2000 per nozzle, a cost

Gas	M Exit	Dia.[1]	Re [2]
Ar	< 1.0	.500	$< 4.5x10^5$
He	< 1.0	.500	$< 1.1x10^5$
N_2	< 1.0	.500	$< 4.2x10^5$
SF_6	< 1.0	.500	$< 8.2x10^5$
Ar	1.4142	.500	$8.2x10^5$
He	1.4142	.500	$1.9x10^5$
N_2	1.4142	.500	$6.2x10^5$
Ar	2.0	.500	$2.1x10^6$
He	2.0	.500	$6.5x10^5$
N_2	2.0	.500	$1.4x10^6$
N_2	2.0	.125	$3.5x10^5$
SF_6	2.0	.125	$5.0x10^5$
Ar	3.0	.500	$5.0x10^6$
He	3.0	.500	$1.6x10^6$
N_2	3.0	.500	$3.4x10^6$

[1] Inviscid Exit Diameter

[2] Re based on Inviscid Exit Diameter

Table A.1: Nozzle Parameters

which was prohibitive. A different method had to be developed in order to make the proposed experiments feasible.

Experimenters traditionally have either used the Foelsch method to design nozzles, or used a conical nozzle because of machining difficulties. The experimenters [19, 21, 25, 28, 53, 41, 48, 57] found that their flow had an axial cell structure present downstream. Johannesen in particular found that the Foelsch nozzle was markedly inferior to one designed with the Clippinger method [19]. It should be pointed out that the cell structure can be caused either by a weak shock pattern or an axisymmetric instability as predicted by Tam [35] for an infinitesimal pressure mismatch. The wavelength of the instability is shorter than that of Mach wave cells. In order to conduct the desired experiments, the nozzles used needed to produce a flow with uniform exit conditions and without shocks at the desired Mach number.

A.2 Nozzle Design

Most of the nozzles of previous experimenters have been of the Foelsch type. This type is based on a radial source flow, with a conical section followed by a cancellation region designed using the method of characteristics. The advantage of the Foelsch method, particularly when it was first introduced, is that the calculation can readily

be done by hand, with the nozzle profile in the cancellation region consisting of a simple polynomial. However, the transition from the conical section to the cancellation region inherently involves a discontinuity in the curvature of the nozzle wall, which results in a converging series of compression waves being launched from that point. While this generally does not cause any problems in a 2-d flow, where Foelsch type nozzles have been used successfully, in an axisymmetric flow the geometry focuses any disturbance onto the axis, and often results in a Mach-disk being formed inside the nozzle just downstream of the throat.

In the present work, the supersonic portion of the nozzles was designed using the code developed by Sivels [55]. This code also uses the method of characteristics to calculate the contours, but unlike the Foelsch nozzle, does not involve any discontinuity of curvature. It allows the user to specify either a Mach number or velocity distribution from the throat to the exit, and includes a boundary layer correction. A computer is required to generate the contour, but that is not a serious drawback in this day and age. It was found that the convergence of the code depended strongly on the specified ratio between the throat radius (Rt) and the axial throat radius of curvature (Rc), and after some trial and error a radius of Rc/Rt = 20/Me was used. A 4th order Mach number distribution was used from the throat to the exit in the prototype nozzle.

With a supersonic contour in hand, the next task was to design the subsonic

approach section. A common choice has been to match the curvature of the throat, and specify an inflection point in the nozzle contour [6, 58], which results in a 7th order polynomial for the subsonic section. Pope, however, suggests that the appropriate contour is one that results in a continuous Mach number distribution at the throat, rather than one that simply matches curvature at the throat [59]. The two approaches will be nearly equivalent for the 2-d case, but Pope's approach will result in a slower contraction near the throat for the axisymmetric case, due to the square root relation between the diameter and the cross sectional area. Johannesen had found that the exit properties of a nozzle did, in fact, depend on the subsonic inlet design [19]. He found that the exit flow quality improved as the inlet became less curved, and the sonic line straighter. Therefore, Pope's approach was used to design the subsonic section of the nozzles described herein.

As a 4th order Mach number distribution had been used for the supersonic section, it was decided to make the Mach number distribution of the subsonic section match to 4th order at the throat. The Mach number and the first 4 derivatives were specified at the throat; a Mach number dependent on the contraction ratio and the first four derivatives equal to 0 were specified as the condition at the start of the contraction. This requires a tenth order polynomial, in Mach number, for the subsonic section. The Mach number calculated from the polynomial for a given axial location was used

to calculate the local area ratio and diameter. A linear boundary layer growth was then added so that the thickness at the throat was matched with that calculated by the supersonic code.

In addition to the supersonic nozzles, three nozzles were designed for M=1.0 flow using the same method, but with the derivatives zero at the exit as well as the entrance. Even though the constraints result in a unique Mach number distribution, three nozzles are needed because the area ratio at a given Mach number depends on γ. No boundary layer correction was added to the sonic nozzles.

A.3 Nozzle Construction

The manufacture of a nozzle by direct machining so that it matches the desired contour has been very difficult, even for the M=1.0 case. Machining must be done from a larger towards a smaller internal diameter. This requires a long, thin tool bit which tends to flex and chatter, decreasing the accuracy and leaving tool marks, respectively. In a Laval nozzle of any appreciable Mach number, the situation is worse, since it requires that the part be removed from the lathe, turned around, and the machining completed from the other side. Machine shops are only willing to guarantee accuracies of about .001" for such an operation. Although that may seem to be a small mismatch, the

throat area is extremely sensitive, and a .001" step can have large adverse affects on the flow quality at the exit. Any machining marks left in the supersonic portion of the nozzle will create patterns of waves in the nozzle, which is again undesirable.

One experimenter describes the use of grinding paste in an attempt to obtain a smoother final contour [53]. However, only one out of three of their nozzles was deemed usable, and even that one exhibited large flow asymmetries. Due to the difficulty of directly machining such nozzles, machine shops quoted about $2000 per nozzle with a .001" tolerance and a 30 microinch surface finish. Clearly, a new method was needed to make the large number of nozzles required for the desired experiments affordable.

The driver of the cost in machining a small, relatively deep internal shape like a Laval Nozzle is that a special tool bit smaller in diameter than the throat but longer in length than either the contraction or the supersonic portion must be made. Such a bit is inherently flexible because of its relative thinness, and it causes problems both with the tolerance and surface finish. Any method that hopes to do significantly better with respect to cost or accuracy must either have most of the machining performed on an external contour or use a technique that doesn't rely on a tool bit. The possibilities that were explored were plug nozzles, edm, broaching, casting, and plating.

Plug nozzles would allow all complex machining to be done on an external contour, as well as allowing for changes to flow conditions in a manner similar to swapping

nozzle blocks. The drawbacks to a plug nozzle are that there is no existing code to compute a contour, and that this geometry introduces a wake into the middle of the flow. Electron Discharge Machining (EDM) was the only direct-machining approach considered. EDM can give a very accurate contour, but cannot give a good surface finish. In addition, one still must deal with alignment problems at the throat. Broaching a nozzle, where a plug is made out of tool steel and then pressed hydraulically into aluminum to make the part, is extremely accurate, and lends itself to mass-production of nozzles. However, the nozzle must be split longitudinally and made in two halves to avoid alignment problems at the throat, and it is the most expensive method if only a single nozzle of any contour is going to be built.

The two most attractive methods are casting and plating. Both allow a male mold to be made with external machining only, a part formed around it, and then the mold eliminated. Casting has the advantage that it is very fast. Once a part is cast, it can be used almost immediately. Plating a nozzle, as described in detail in the next section, has the advantages that it has a better surface finish, since the inner surface of the nozzle is a molecular match for the outer surface of the part, and that it is cheaper, since the plating process simply requires residence time in the plating tank, with none of the complex equipment that casting requires. The primary drawback to plating is that it takes about four weeks to make a part.

It was decided to make a prototype nozzle using the plating method, both to confirm that a .250 in. thickness (the desired nozzle wall) was achievable using plating, and to test the computed contours for the desired flow properties. The prototype nozzle, a Mach 2.0 Nitrogen nozzle, was manufactured as follows: Using a CNC lathe, a nozzle mandrel was machined out of 2024 Aluminum so that the external surface matched the computed contour, and then hand polished to achieve a mirror finish. A typical, unpolished mandrel is shown in figure A.1. The mandrel was placed in a nickel plating tank and left for two weeks, the amount of time it took to build up the thickness to a .250 in. minimum. At the end of that time, it was removed from the tank and a flange machined on the external nickel surface to allow the nozzle to be mounted in the facility. The nozzle was then placed in a saturated NaOH solution to dissolve out the mandrel. This process took another two weeks. When it was finished, the nozzle was used in preliminary tests to confirm the flow properties, both by direct observation and by comparing the results with prior similar experiments. After the prototype was tested successfully, the remainder of the nozzles in the test matrix were constructed, at a cost of approximately $300 per nozzle.

A.3.1 Details of the Plating Process

The nozzles were constructed using an electroform nickel process, which deposits a pure nickel coating on an aluminum substrate. An equivalent process, using copper instead of nickel, was also considered. Nickel is extremely hard and resistant to corrosion, while pure copper is prone to corrosion and fairly soft. Both are difficult to machine; the nickel is difficult due to its extreme hardness, while the copper is so soft that it is gummy and doesn't cut well. Nickel offered a better solution to the present problem, but if heat transfer is important, copper would be a better choice. It is also possible to plate the copper and nickel in layers if, for instance, a nickel surface was needed for corrosion resistance but a copper body for heat transfer.

The thickness of the nickel is limited only by the amount of time that the mandrel sits in the plating tank. However, as the thickness builds up the rate of plating decreases, and there quickly comes a point of diminishing returns. For the prototype nozzle, since it was not known how many flaws, voids, and dislocations there would be in the nickel, and because the stagnation pressure would exceed 1000 p.s.i. for some cases, a factor of safety of 50 was used in determining the required thickness. No flaws were evident in the prototype nozzle, and a thinner one could be built without danger. The inner surface is a match on a molecular level for the outer surface of the mandrel, so that if the mandrel has a mirror finish, the finished nozzle will as well. Any shape

can be plated, with the caveat that sharp internal corners will not be smoothly plated and should be avoided.

In contrast to the inner surface, the outer surface is rough and uneven, since the plating rate varies with the local curvature, as shown in figure A.2. A means must be provided for holding the plated mandrel in a lathe so that any necessary machining can be performed on the nozzle. In the present case, an external fitting was manufactured that could be held in a lathe collet, was centered on the nozzle mandrel with a dowel pin, and had an offset screw to both secure it to the mandrel and to transmit the driving torque. Using this fitting, a flange was turned on the contraction end of the nozzle to mate it to the settling chamber, and a straight section was turned on the exit end, to allow the end-plate to be attached, as shown in figure A.3.

Once the external machining is done, the mandrel may be dissolved out, as shown in figure A.4. This is accomplished by placing the nozzle in a saturated solution of NaOH. It is important that a strong base be used, since that dissolves the aluminum via the following reaction:

$$2Al(s) + 2OH^{-}(aq) + 6H_2O(l) \rightarrow$$

$$2[Al(OH)_4]^{-}(aq) + 3H_2(g)$$

If a strong acid, instead of a strong base, is used, the corresponding reaction produces aluminum oxide solid, which is what gives anodized aluminum its hardness and cor-

rosion resistance. If an acid is used to dissolve the aluminum, a surface coating of the oxide will quickly build up and stop any further reactions. The $Al(OH)_4^-$, on the other hand, dissolves, which leaves fresh aluminum on the surface to be attacked. The nickel is not attacked by the NaOH because the aluminum acts in a similar fashion to the zincs used on boats.

When this was tried on the prototype nozzle, the initial rate at which the aluminum was dissolving was extremely slow. The solution next to the aluminum was being depleted of hydroxyl, and the reaction was slowing. The solution was to drill a through hole on the mandrel, using a diameter smaller than the throat, and to place the nozzle vertically in the solution. The hole acted as a chimney, with the bouyancy of the hydrogen providing the motive power, and the rest of the dissolving went reasonably quickly. The aluminum dissolves at the rate of .050" per day, and in this case it took about one week to completely remove it.

During this process, a black substance was also being formed and deposited on the nickel. After some thought, it was realized that the substance was copper oxide, with the copper coming from the alloy used in the mandrel (2024). Although the copper oxide was eliminated with a quick acid bath, it can be avoided altogether by using 5052, which is void of copper, or 6061, which has only a trace amount. 6061-T6 Alloy was used in the non-prototype nozzles, since 5052 is available only in billet form.

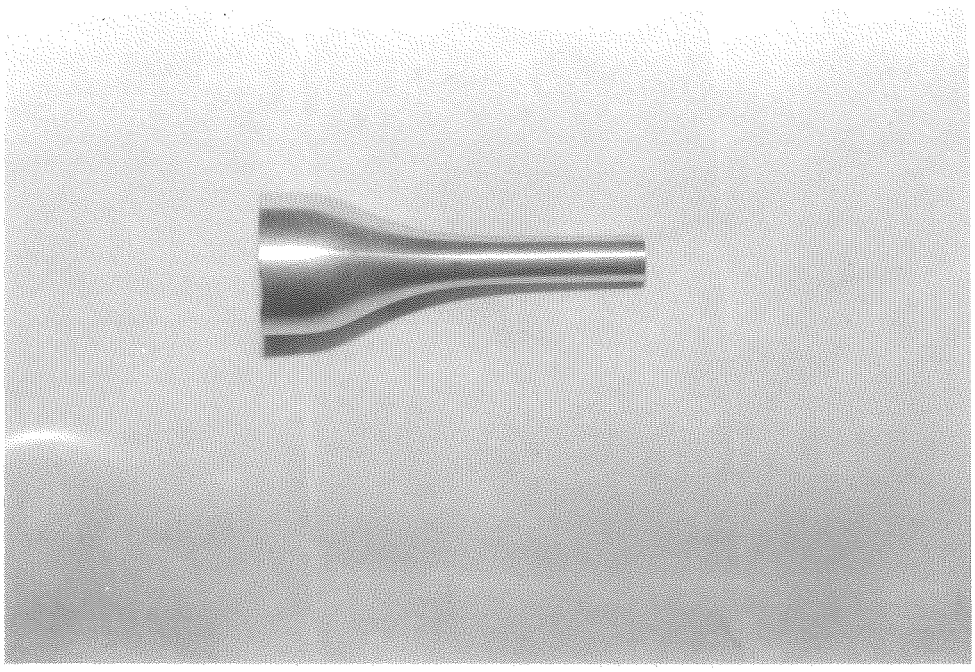

Figure A.1 Unpolished Nozzle Mandrel

Figure A.2 Plated Mandrel

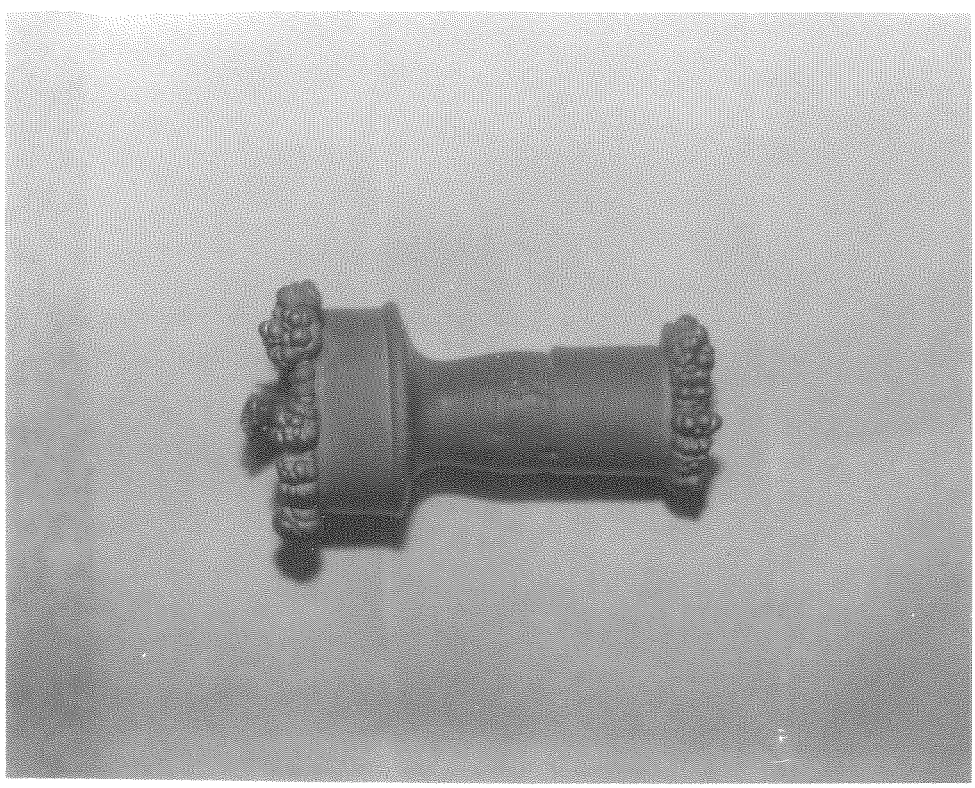

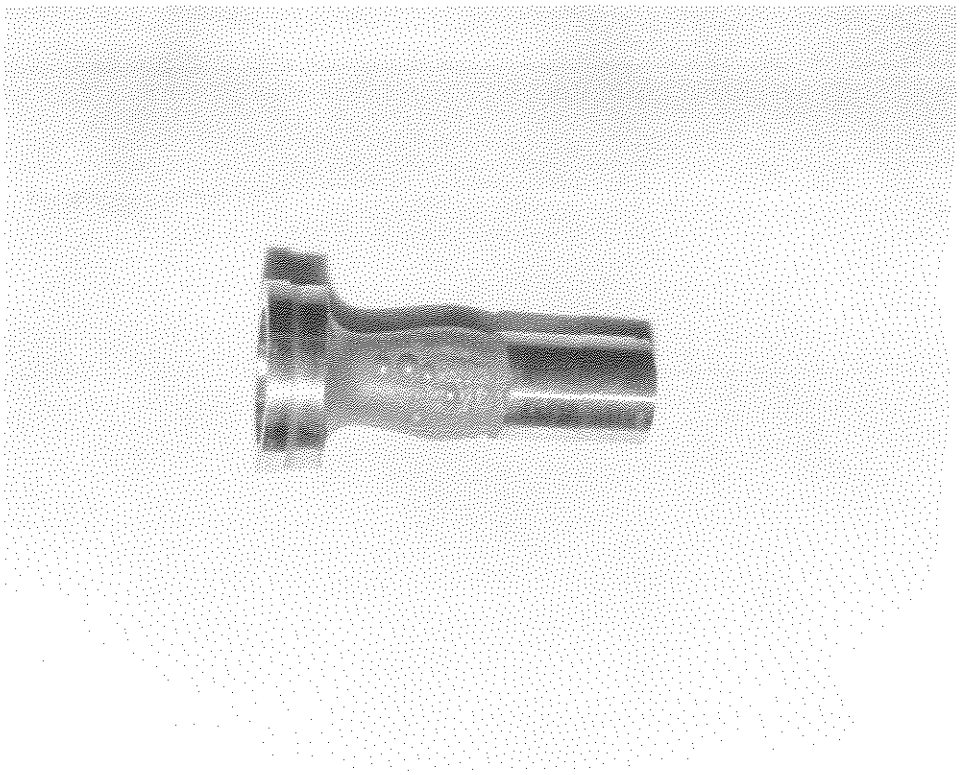

Figure A.3 Machined, Plated Mandrel

Figure A.4 Finished Nozzle

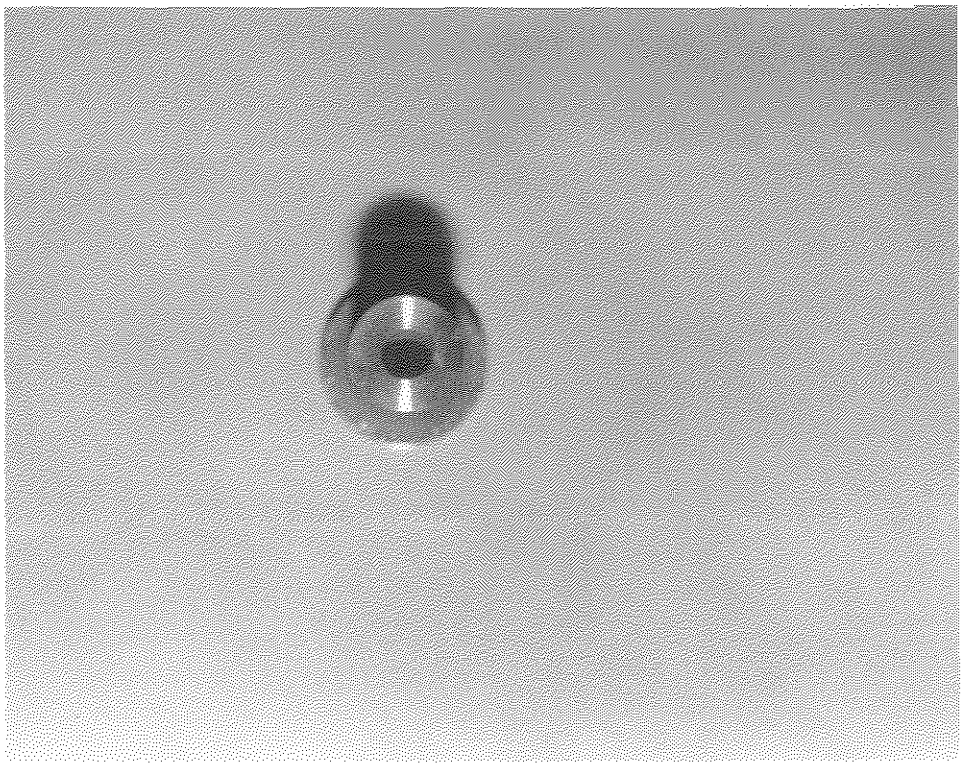

Appendix B

Pitot Probe Design

Pitot probes are one of the most widely used diagnostic instruments in fluid mechanics. They are relatively simple, robust, and inexpensive. In general, however, they have been used solely to gather information about the mean flow field, and questions about spatial resolution and frequency response have received suprisingly little attention. This has been especially true for pitot probes used in supersonic flows. Since one of the aims of this research project was to attempt to gain further information about the flow by using instantaneous pitot pressure data, it was important to understand the various affects that pitot probes had on the measurements. Although pitot probes have not, to our knowledge, been used in this fashion before, the questions are fundamentally similar to those that must be answered for the use of hot-wire, hot-film, or similar

probes. The reason that pitot probes, and not hot-wires, were used was the high dynamic pressures involved in these experiments. The questions that need to be addressed are the response of pitot probes to yaw and shear, the spatial resolution of the pitot probe, and the frequency response of the probe-transducer system.

B.1 Effects of Yaw and Probe Shape

One of the more comprehensive studies of pitot probe shapes and the effect of yaw on the pressure readings was conducted by Gracey, Letko, and Russell for N.A.C.A. in the late 1940's. They investigated 39 different probe shapes from +45 to -45 degrees of yaw, at Mach numbers ranging from .25 to 2.40. The subsonic results are reported in [60] and the supersonic results in [61]. The results that are germane to the present research are that as the ratio of the inner to outer diameter of the probe, at the probe entrance, becomes larger, the angle of attack range of the probe becomes greater; that a sharp edged probe, with either an internal or external bevel, had a greater range, with an internal bevel being slightly better; and that the size of the opening in relation to the outer diameter had no effect on either the supersonic or subsonic mean flow pressures.

Substantially similar results were obtained by Dudziniski and Kruse [62], who

investigated very small pitot tubes $0.010 < d < 0.125 inches$. They additionally determined that in order for the pressure at the tip to be unaffected by the probe support, the tip needed to be at least 2 support diameters in front of the support.

B.2 Spatial Resolution and Shear

The questions of the spatial resolution of pitot probes and their response to shear in the flow are interrelated, since if there is no shear, it is both impossible and irrelevant to determine spatial resolution. Since a jet has a very large shear in the potential core region, understanding the effects that the shear has on the pitot reading is necessary for interpreting the results.

One of the earliest systematic studies of shear was conducted by Young and Maas, in 1936 [63]. They studied a family of pitot tubes with varying outside diameters and varying inside to outside diameter ratios, although most of the probes had the i.d. = .6 o.d., traversing a small wake. They found that there was a displacement effect towards the region of higher pressure. This meant that the pitot measurements made jets seem wider, wakes appear narrower, and displaced shear layers. The displacement of the pitot tube also appeared to be independent of the strength of the gradient, and

was expressed as:

$$\frac{\delta}{D} = .131 + .082\frac{D_i}{D} \tag{B.1}$$

where D is the outer diameter, D_i, the inner diameter, and δ, the displacement of the location of the pressure reading. This displacement is only a very weak function of the inner diameter and primarily depends on the outer diameter.

One obvious problem with the above results is that they imply a discontinuity in the displacement on the centerline of a jet or wake, which is physically implausible. Davies attempted to address this paradox in 1957 [64], with a more careful investigation of a wake behind an airfoil. He also found that the displacement depended primarily on the outside diameter of the tube, and that the mean level measured in the center of the wake did not change until the tube was wider than the wake itself. He found, however, that the results changed when the near wake of the airfoil was surveyed, due to the yaw of the stream with respect to the pitot, which changed the response. He attributed the paradox of Young and Maas to the fact that their traverses were conducted fairly close to the trailing edge of their airfoil. The inner diameter of the tube did not affect the displacement, but did affect the yaw response. The overall behavior of the pitot tube was similar to the theoretical analysis of Lighthill for spheres [65], but with different constants:

$$\frac{\delta}{D} \approx .9K - 2.70K^3 \tag{B.2}$$

where $K = \frac{U_1 - U_2}{U_1 + U_2}$ and U_1 and U_2 represent the velocities at diametrically opposed points on the edge of the pitot tube.

In contrast to these results for subsonic flow, where the inner diameter of the pitot tube has little, if any, effect on the measurements, Johannesen and Mair found that in supersonic flow there was little effect of the outer diameter on the mean measurements and no displacement effect of any kind [66]. Investigating a 0.1" wake behind a wedge, they found that for the i.d. of the probe less than 0.25", and for the o.d. up to 0.7," there was no effect on the measured wake width.

B.3 Frequency Response

The frequency response of pressure measuring tube-transducer systems has been treated theoretically and experimentally by Bergh and Tijdemann [56, 67]. The results are quite applicable to the present research, although they were primarily interested in the measurement of static pressures on wind tunnel models. Analytically, the behavior of a single tube-volume system was determined to follow the relationship:

$$\frac{P_1}{P_0} = \left[cosh(\phi L) + \frac{V_v}{V_t}(\sigma + \frac{1}{k}) * n\phi L sinh(\phi L) \right]^{-1} \tag{B.3}$$

where P_1 is the observed pressure, P_0 is the applied pressure, L is the tube length, V_v is the volume of the transducer, V_t is the volume of the tube, and σ is the dimensionless

expansion of the transducer volume due to the applied pressure. k and n are polytropic factors for the volume and tube, respectively, and are equal to:

$$n(ork) = \left[1 + \frac{\gamma - 1}{\gamma} \frac{J_2(\alpha\sqrt{Pr})}{J_0(\alpha\sqrt{Pr})}\right]^{-1} \tag{B.4}$$

where γ, Pr, J_2, and J_0 have their usual definitions, and α is defined by

$$\alpha = i\sqrt{i}R\sqrt{\frac{\rho_s \nu}{\mu}} \tag{B.5}$$

where R is the tube radius, $i = \sqrt{-1}$, ρ_s is the mean density, ν is the frequency, and μ is the absolute viscosity. k and n range between 1, for an isothermal expansion or compression, to γ for an isentropic expansion or compression. ϕ is determined by:

$$\phi = \frac{\nu}{a_o}\sqrt{\frac{J_0(\alpha)}{J_2(\alpha)}}\sqrt{\frac{\gamma}{n}} \tag{B.6}$$

with a_o = local sound speed.

Multiple tube-volume systems may be calculated by successively multiplying transfer functions together. Tijdeman and Bergh also conducted experiments with single and double tube-transducer systems, and found excellent agreement between theory and experiment.

B.4 Pitot Tube Design

The aforementioned results were used to design a family of pitot probes for use in the present experiments. From the results on yaw effects, it was clear that a sharp-edged pitot entry should be used, since these gave the correct total pressure up to 20 degrees of yaw in subsonic flow and 30 degrees in supersonic flow. Furthermore, since the displacement effect scaled primarily with the diameter at the entrance of the pitot, this should be made as small as possible, to enhance the spatial resolution. However, since the pitot would be placed in flows with extremely high dynamic pressures (q=76000 p.s.f.), the base had to be made thick enough to accurately hold the probe in position. The final design consisted of a hollow 0.5" diameter tube with a 20 degree cone forming the probe entrance. The tip of the probe is removable to allow repair or replacement of the pressure transducer and allow different tips to be used to trade off between spatial resolution and frequency response. The probe tips are geometrically similar; the only difference is the size of the opening.

The response for each ot the tips was calculated following the method of Tijdeman and Bergh, and the results for the 0.013 inch diameter tip are shown in figures B.1 and B.2. The magnitude and delay, rather than phase, are given, since that gives a better picture of the step-response of the system. The probe used for most of the experiments was the one with a 0.013 inch entrance diameter.

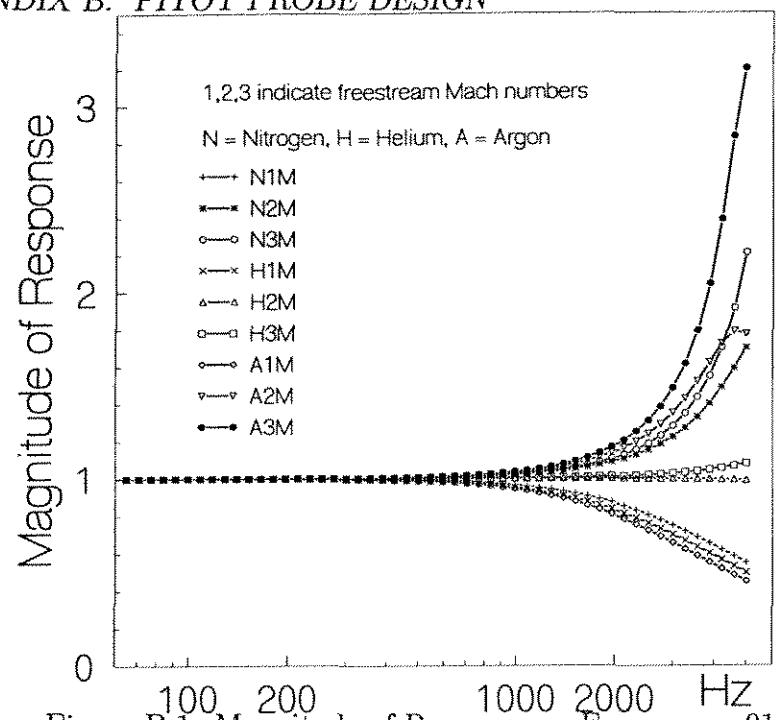

Figure B.1: Magnitude of Response vs Frequency, .013" Probe

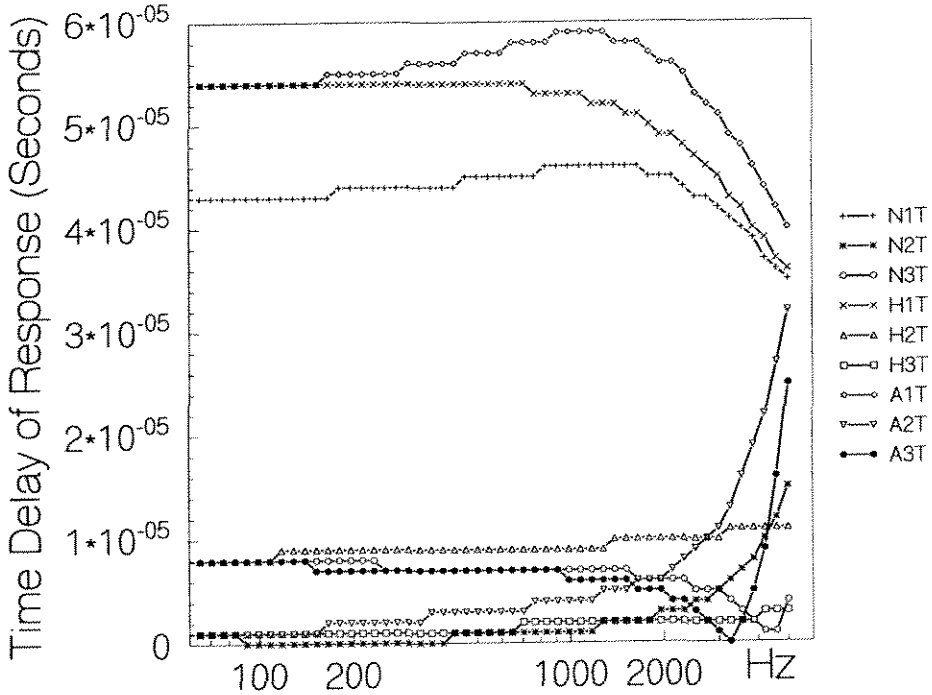

Figure B.2: Time Delay vs Frequency, .013" Probe

Appendix C

Flow Visualization Photographs

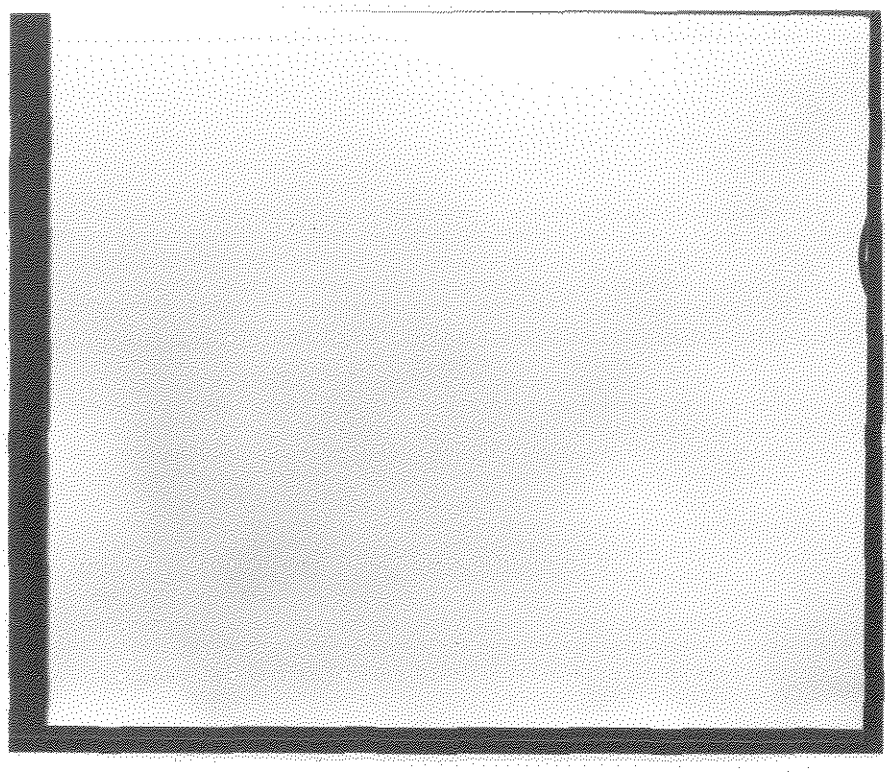

C.1 : No Flow

C.2 : Mach 1.4 Argon into Argon

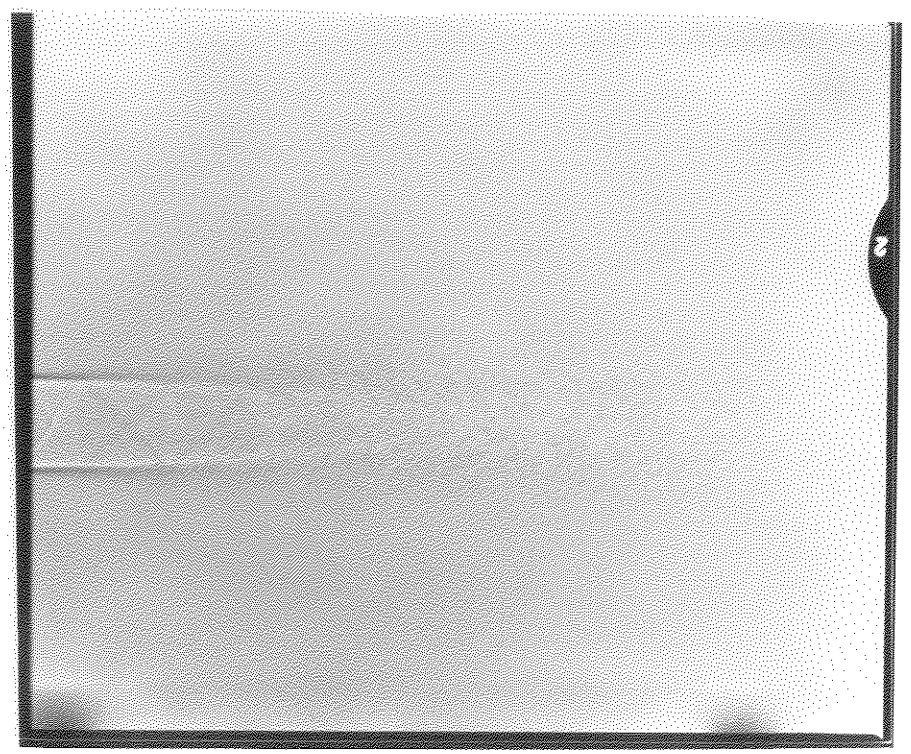

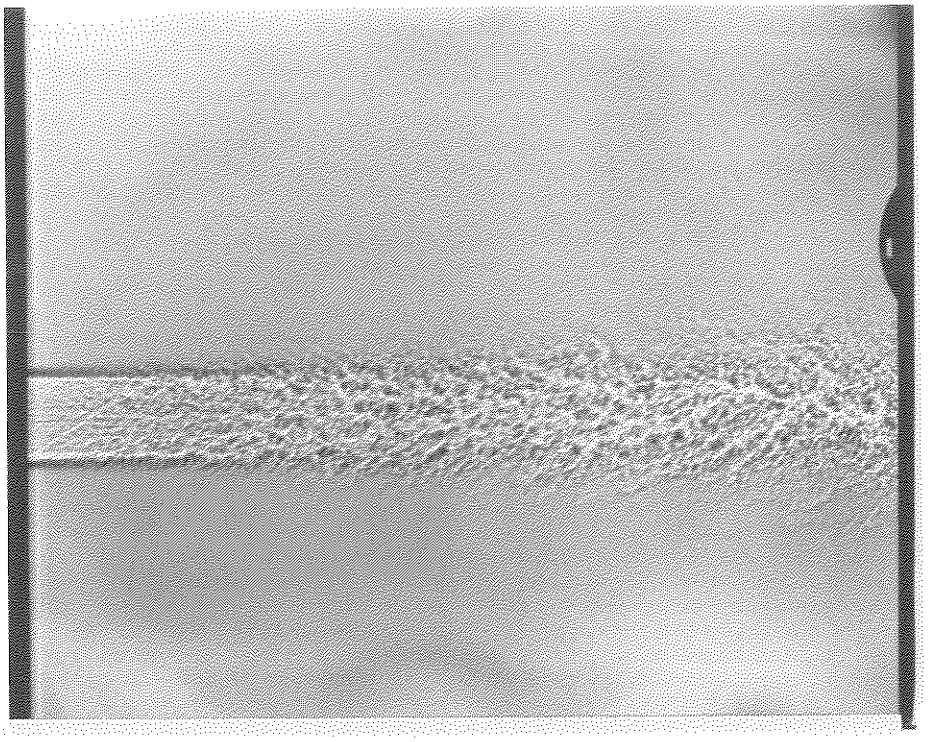

C.3 : Mach 2.0 Argon into Argon

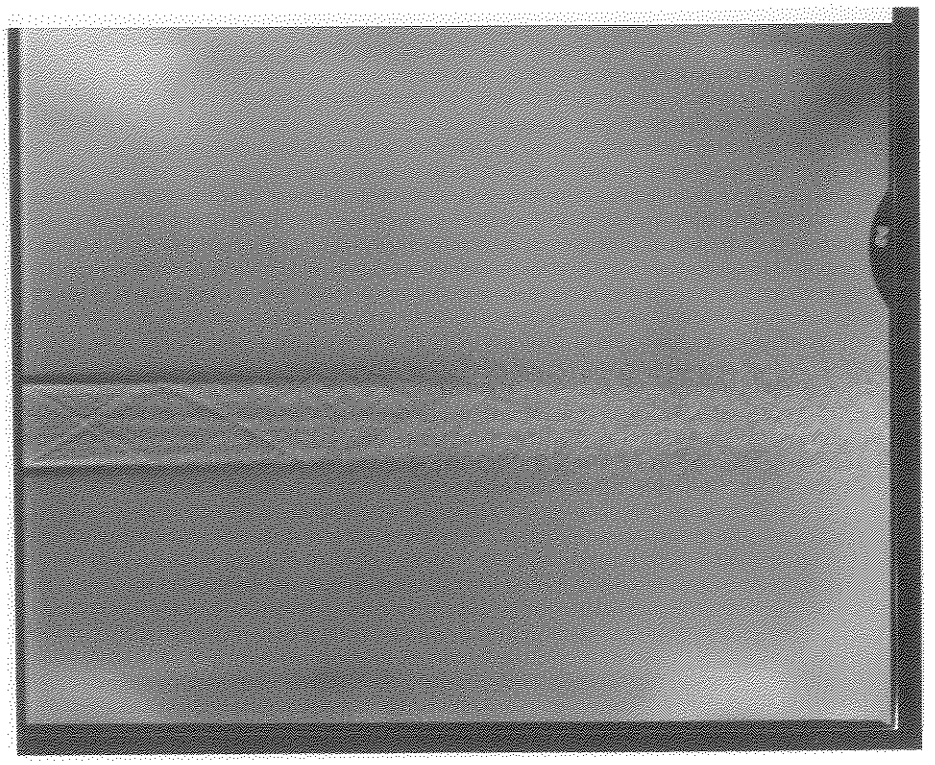

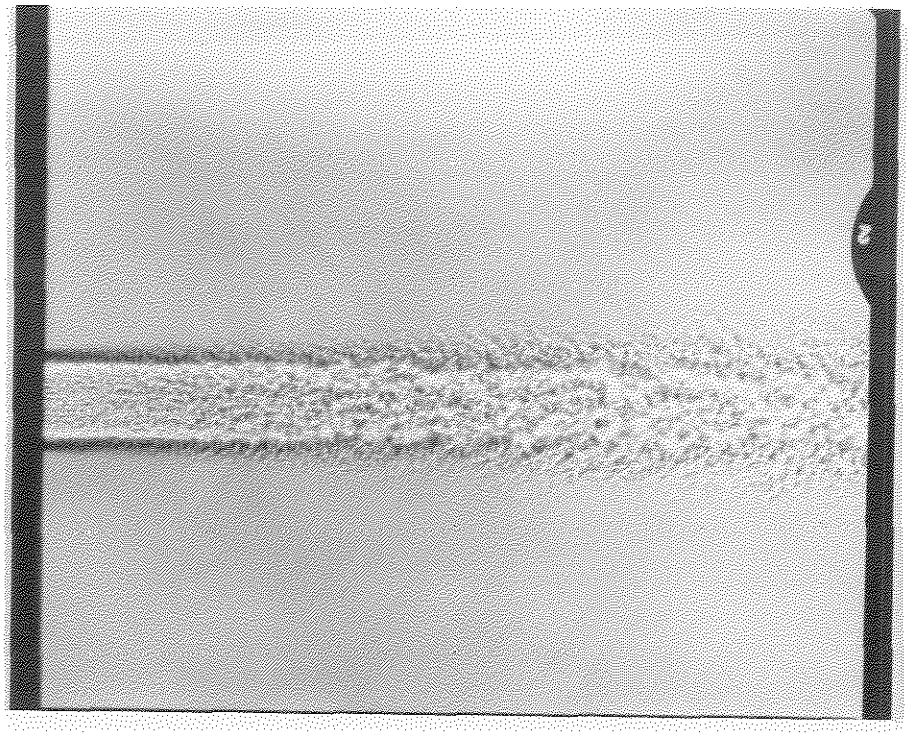

C.4 : Mach 3.0 Argon into Argon

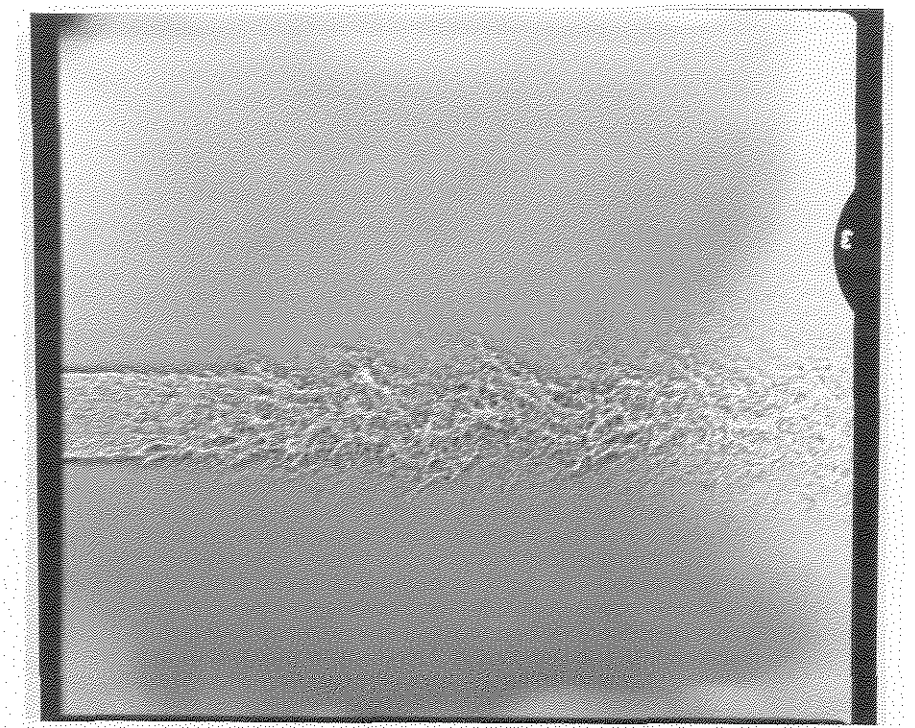

C.5 : Mach 1.4 Argon into Air

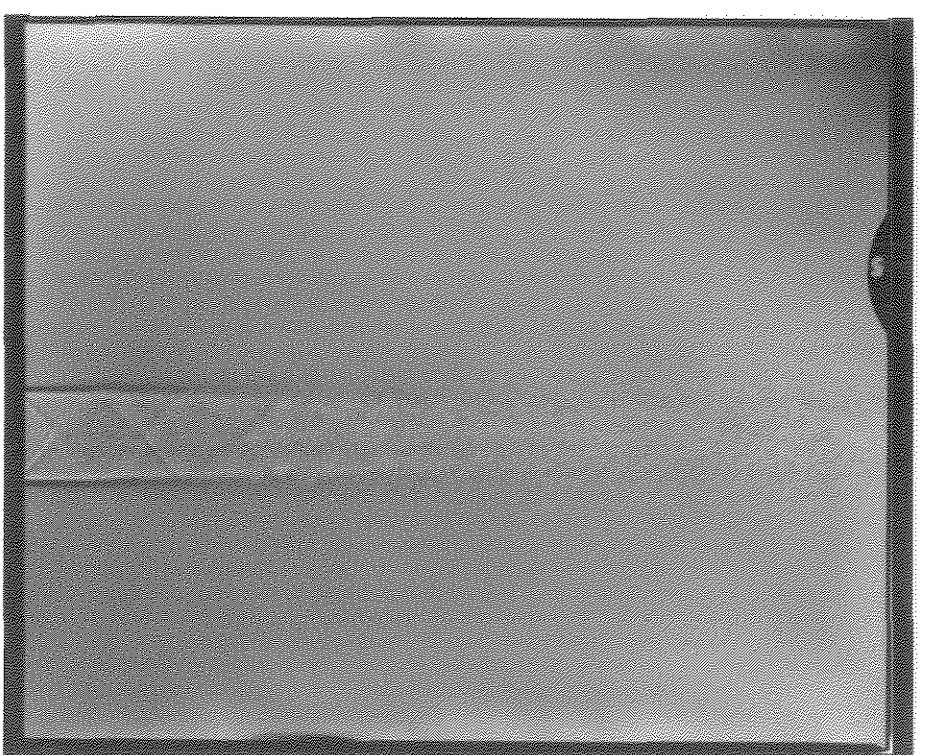

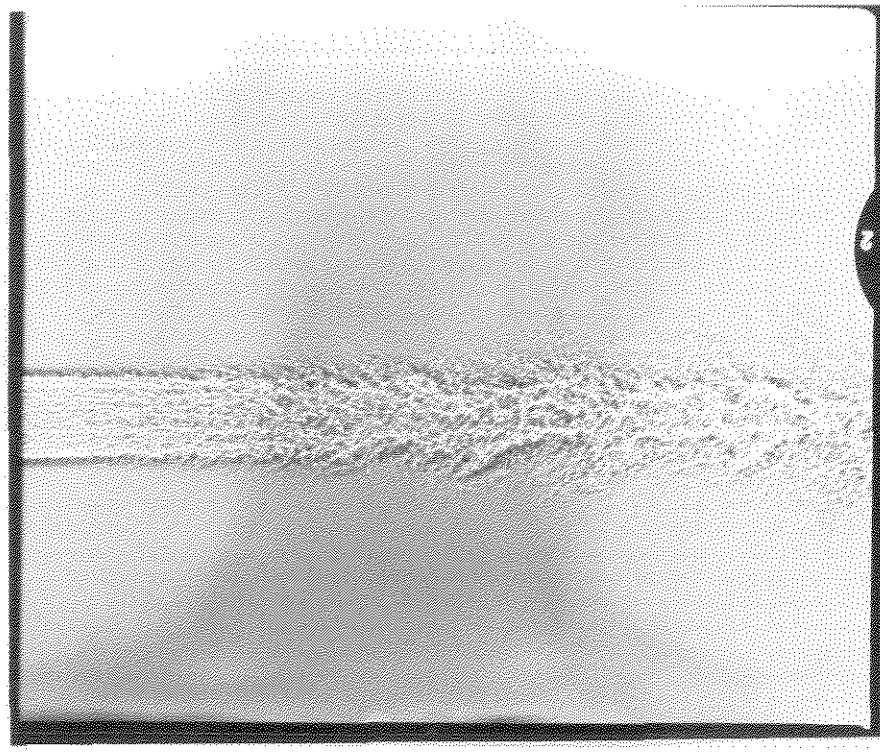

C.6 : Mach 2.0 Argon into Air

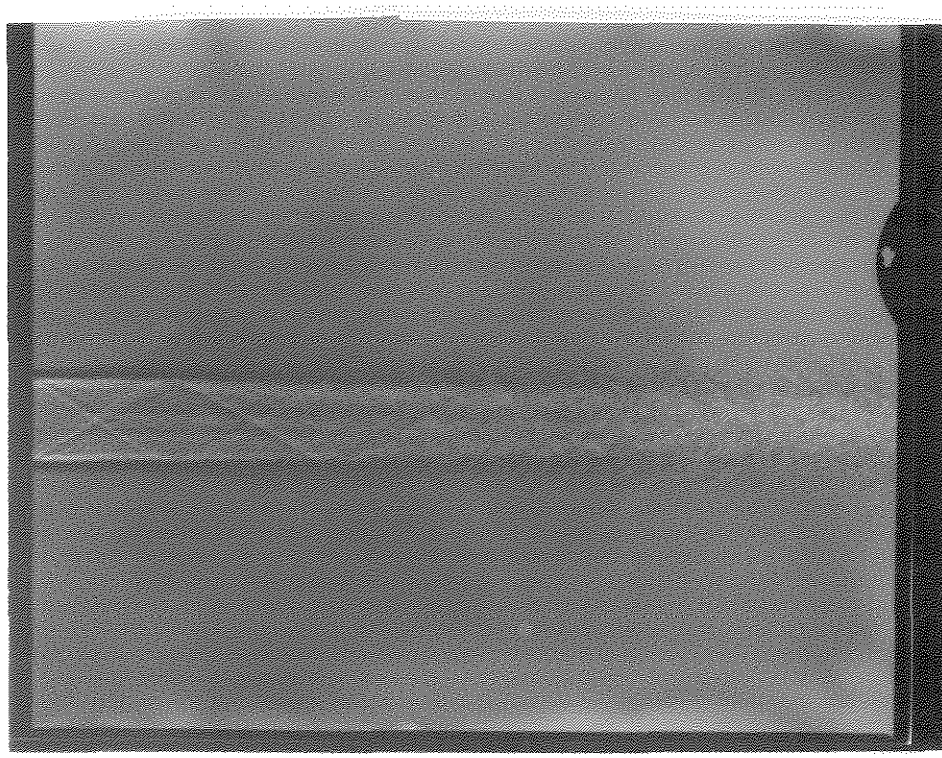

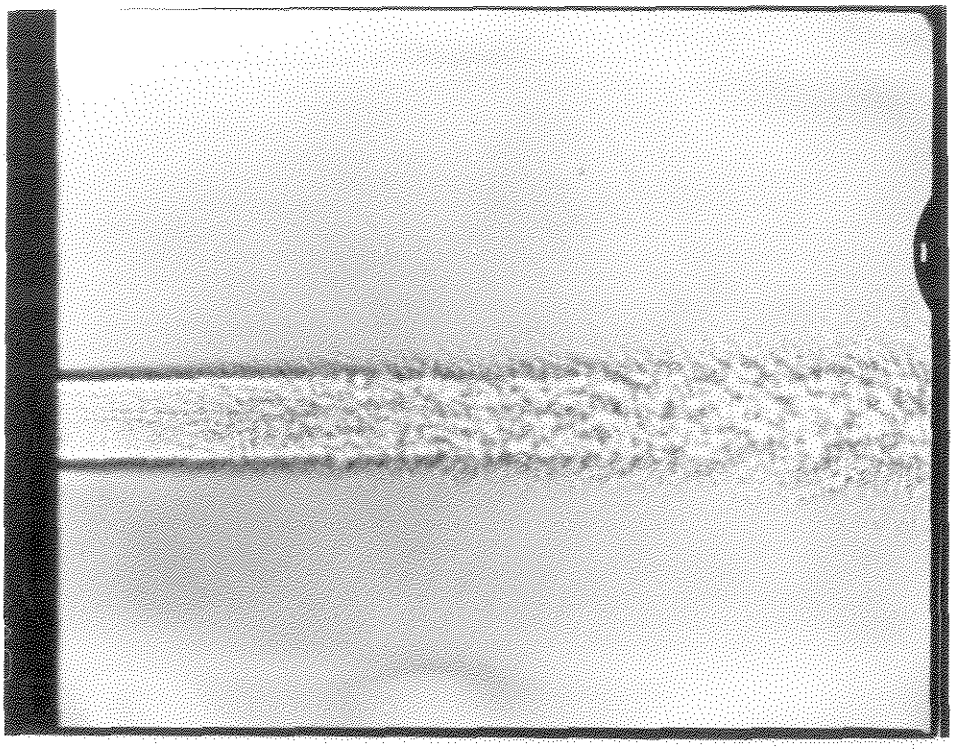

C.7 : Mach 3.0 Argon into Air

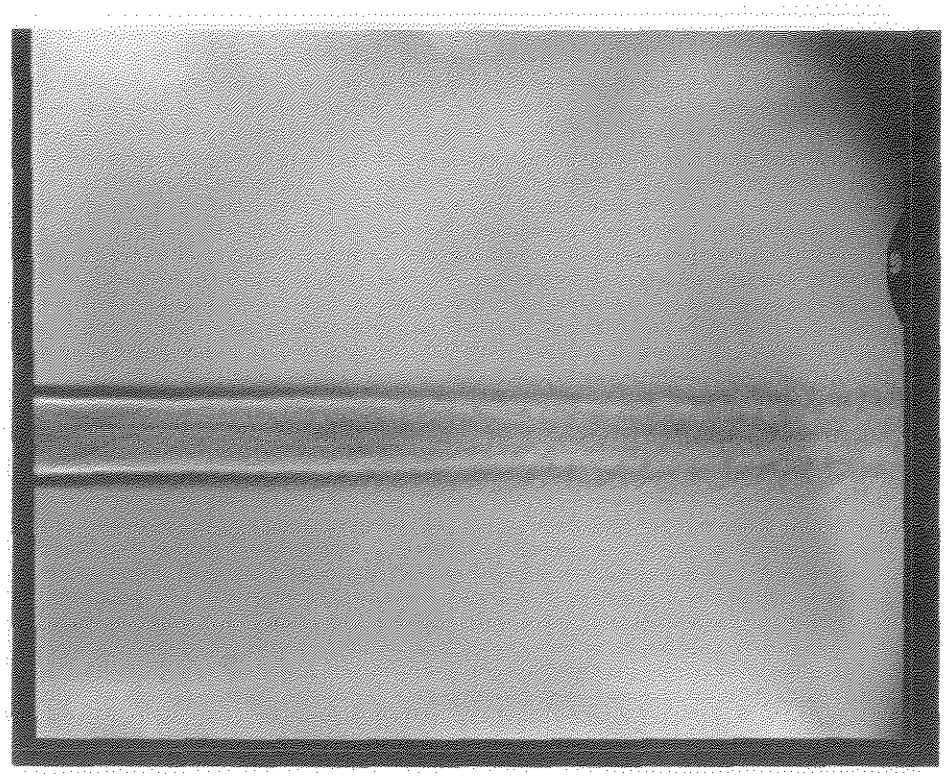

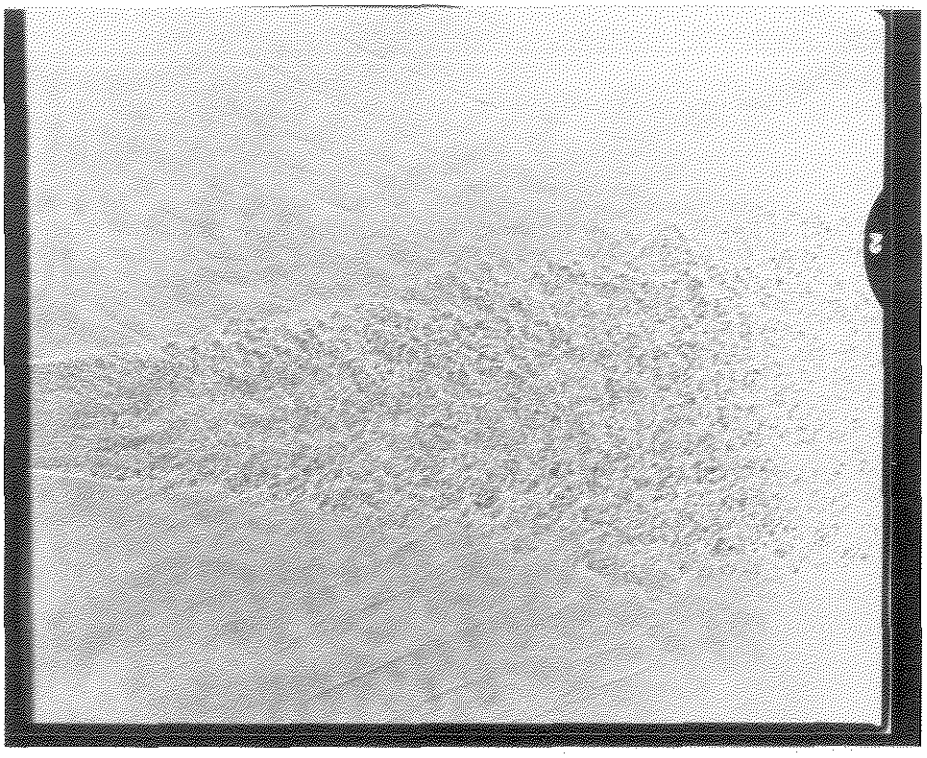

C.8 : Mach 1.4 Helium into Air

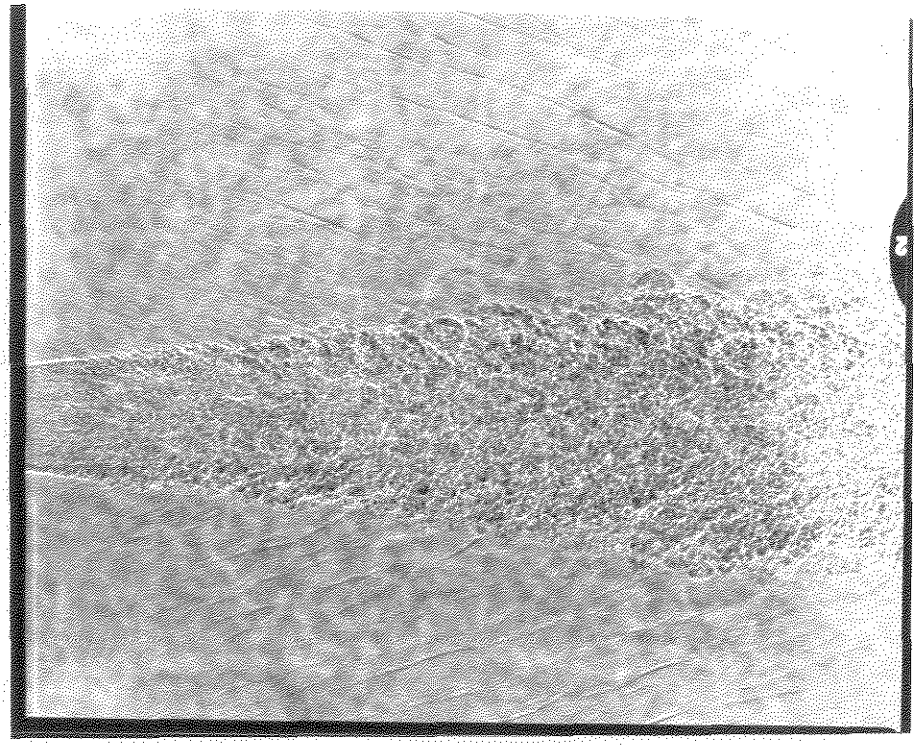

C.9 : Mach 2.0 Helium into Air

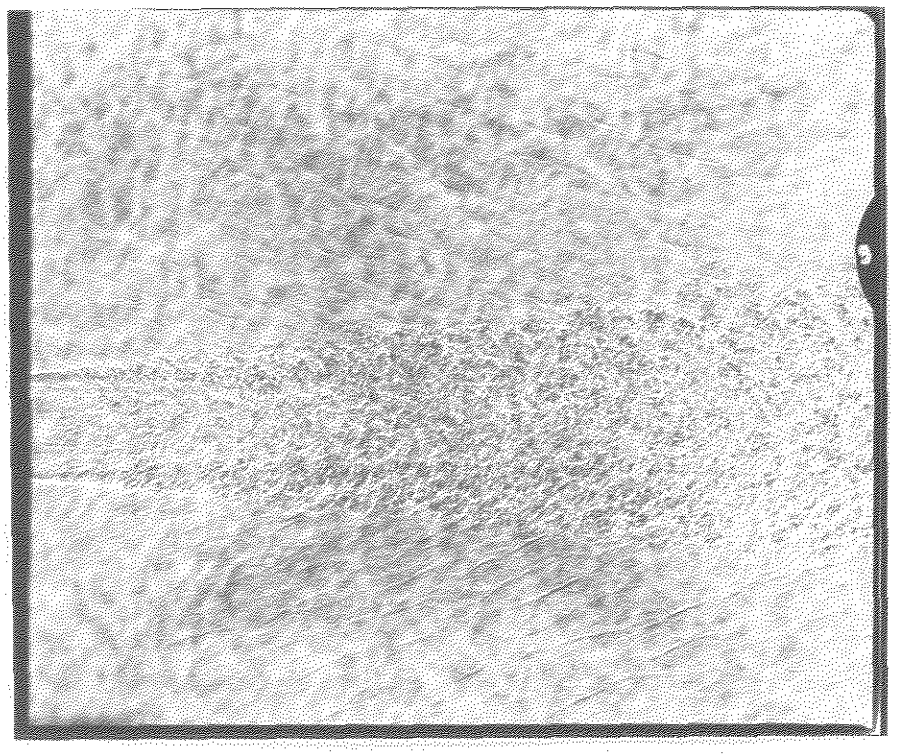

C.10 : Mach 3.0 Helium into Air

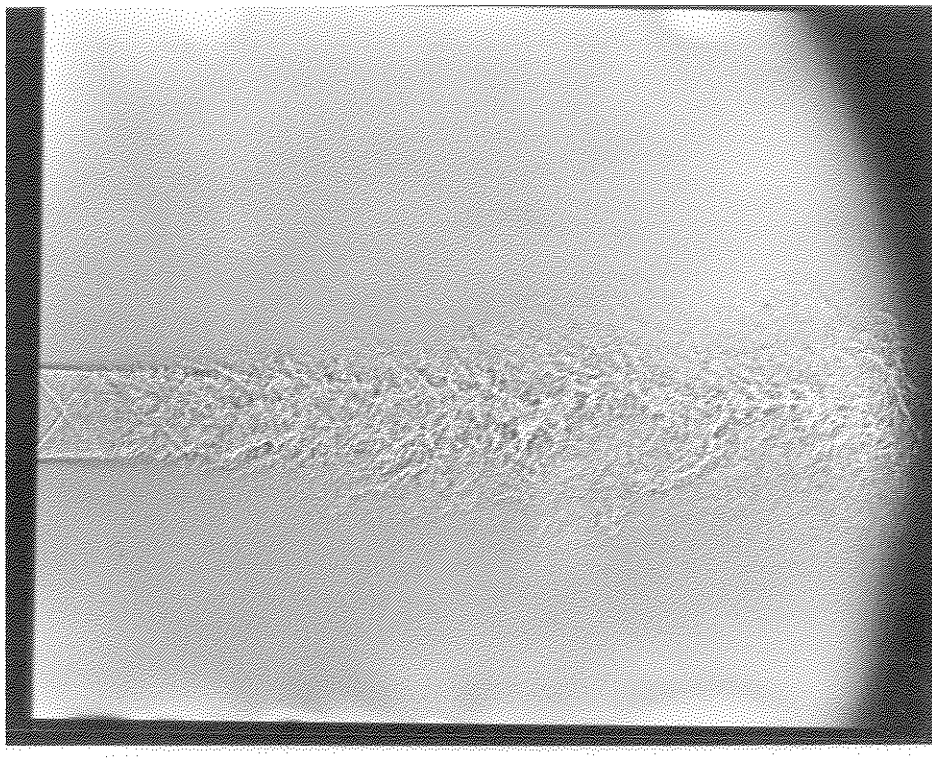

C.11 : Mach 1.4 Nitrogen into Air

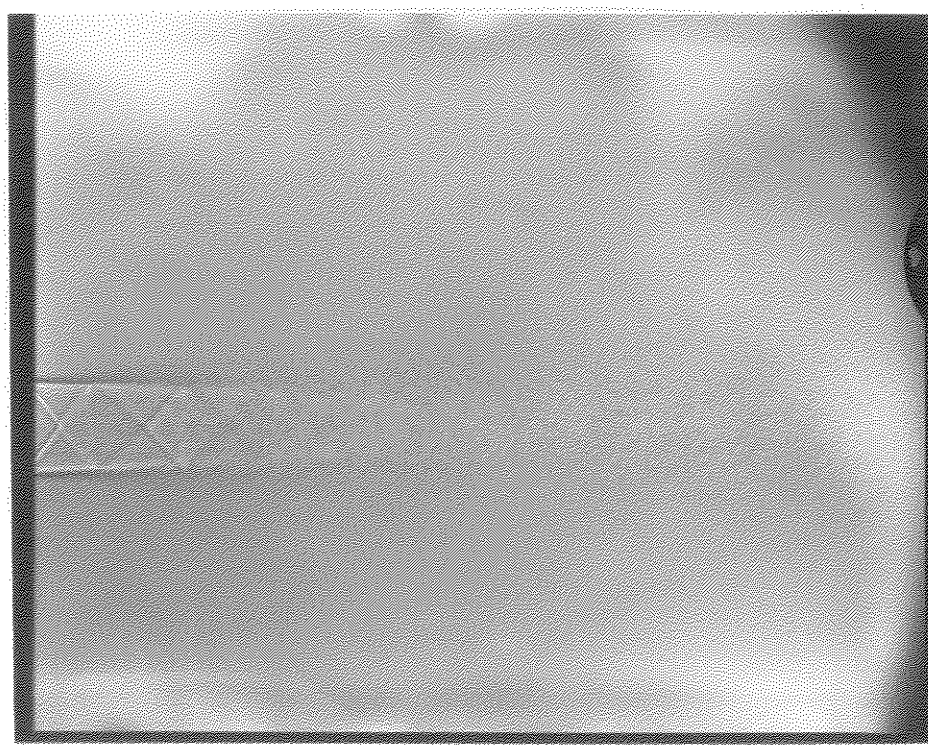

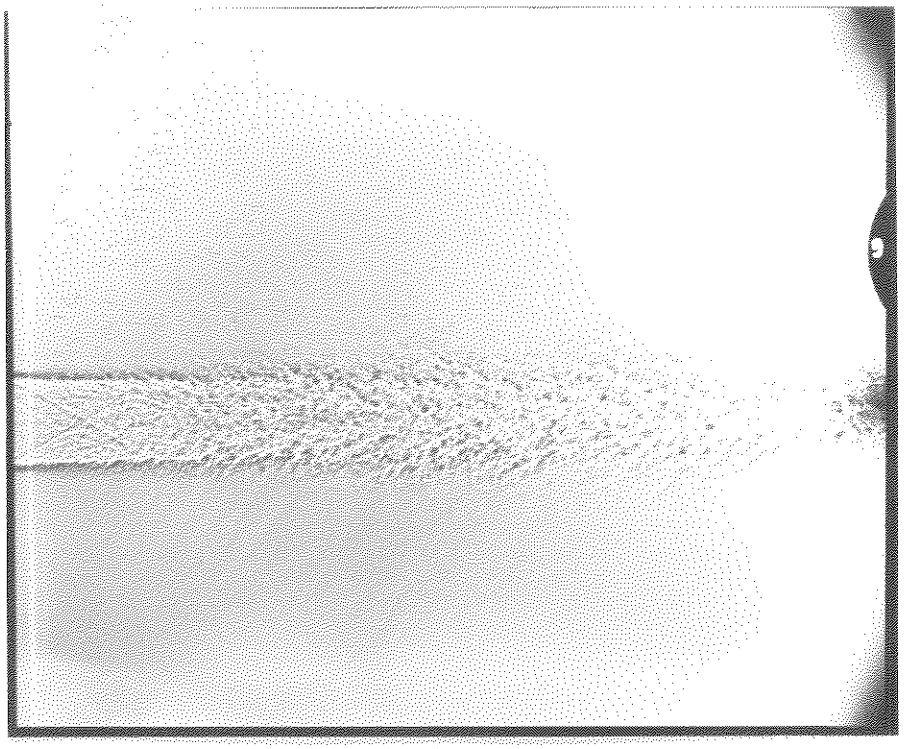

C.12 : Mach 2.0 Nitrogen into Air

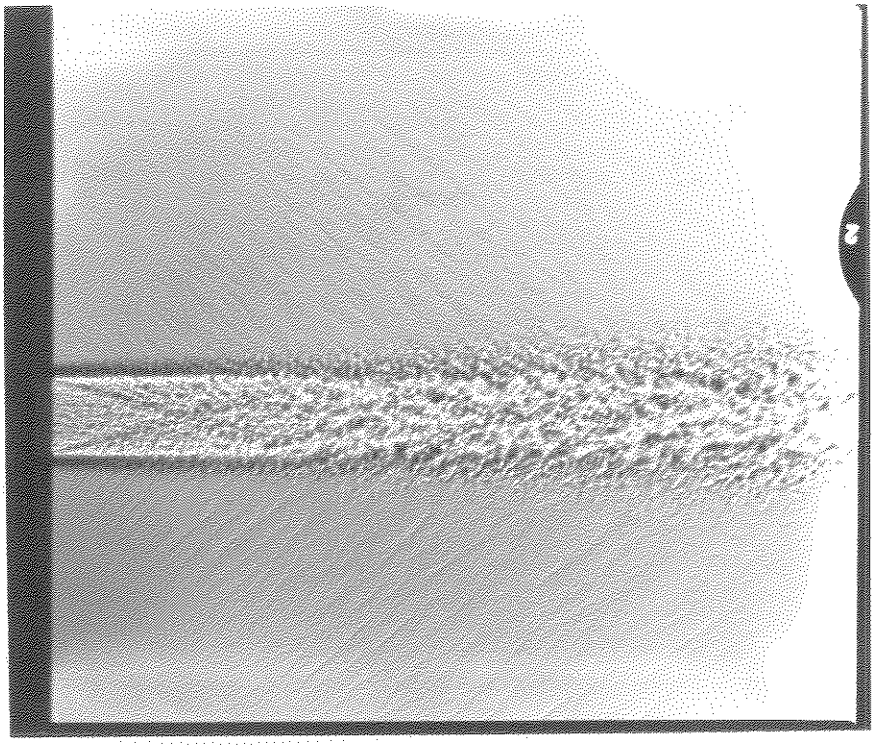

C.13 : Mach 3.0 Nitrogen into Air, 534 psia

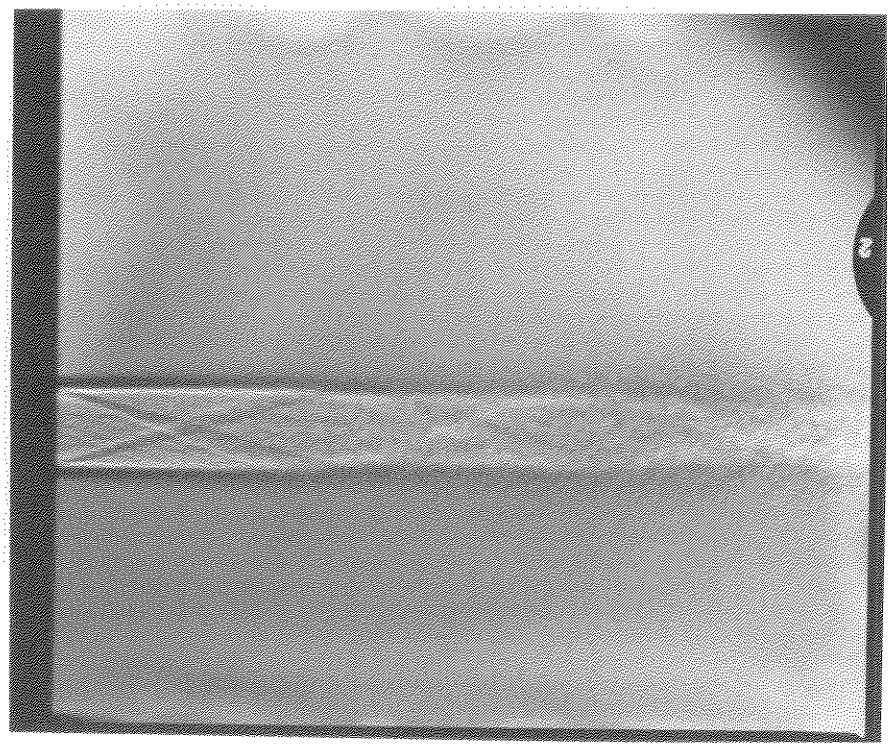

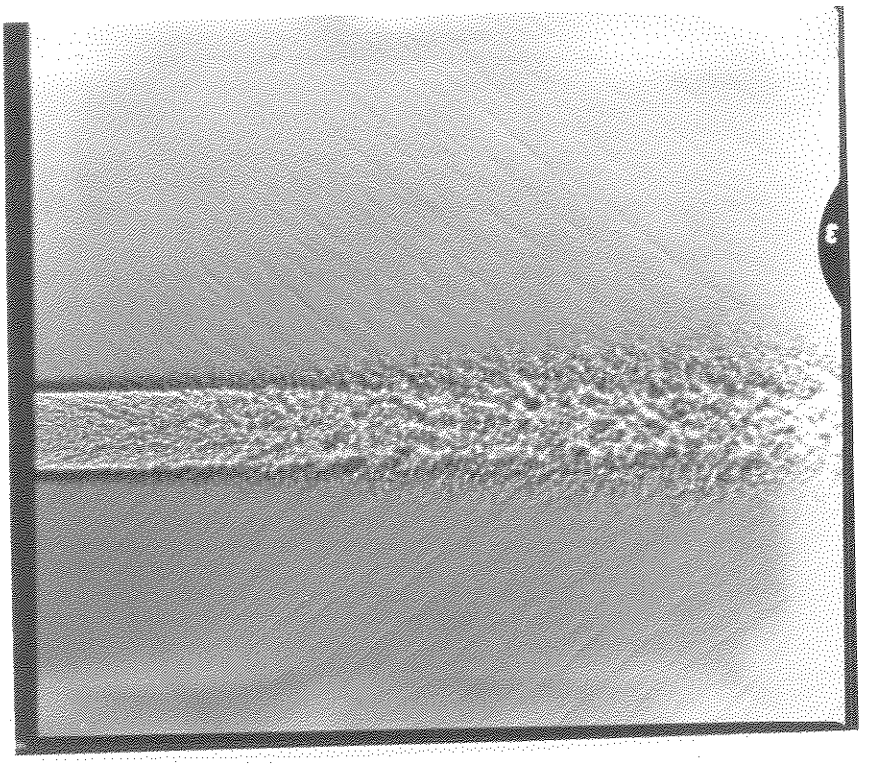

C.14 : Mach 3.0 Nitrogen into Air, 491 psia

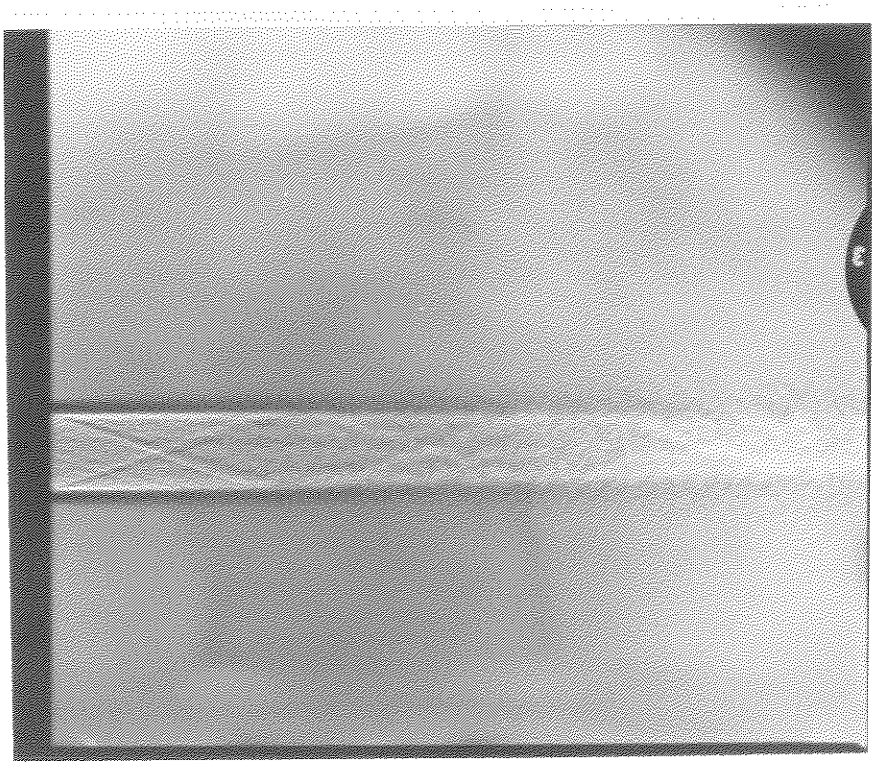

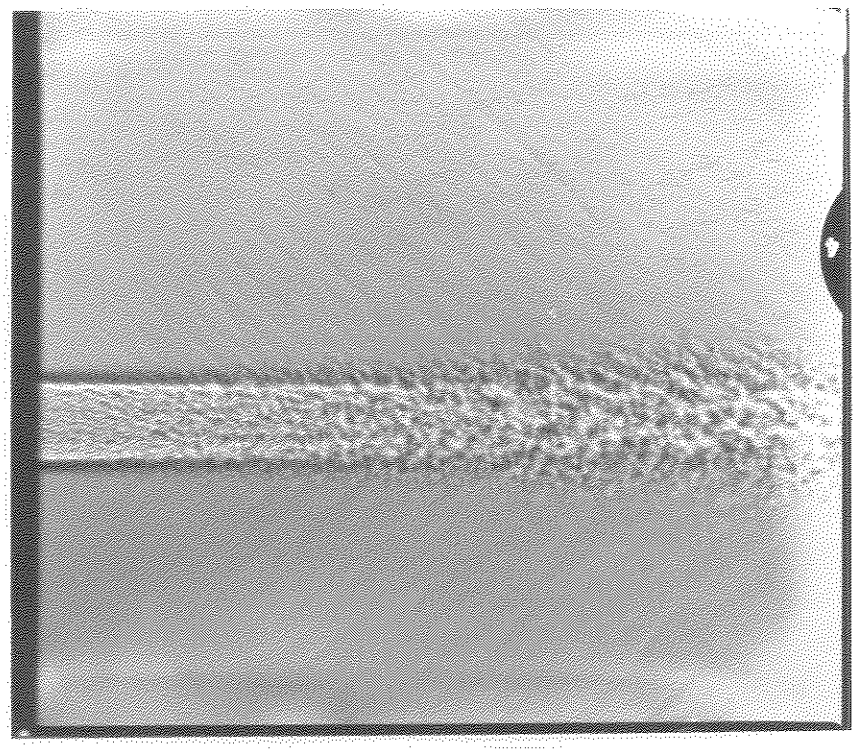

C.15 : Mach 3.0 Nitrogen into Air, 454 psia

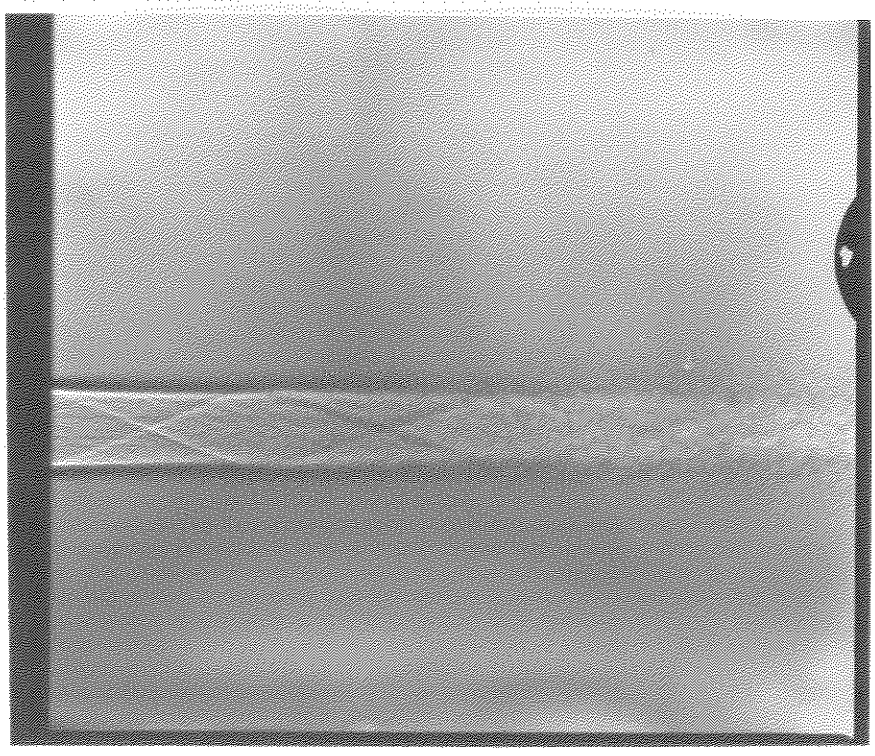

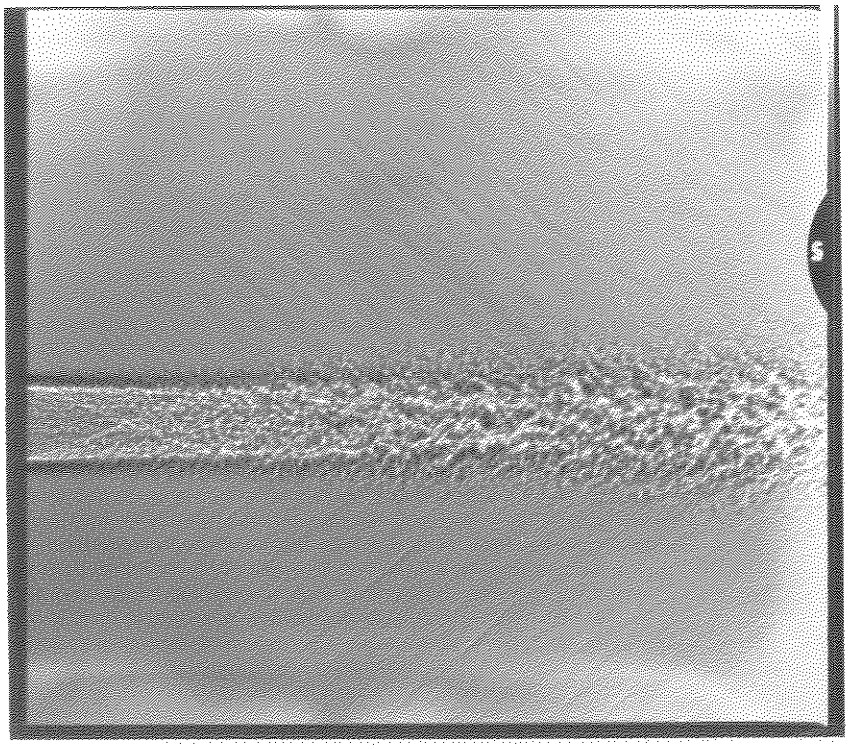

C.16 : Mach 3.0 Nitrogen into Air, 418 psia

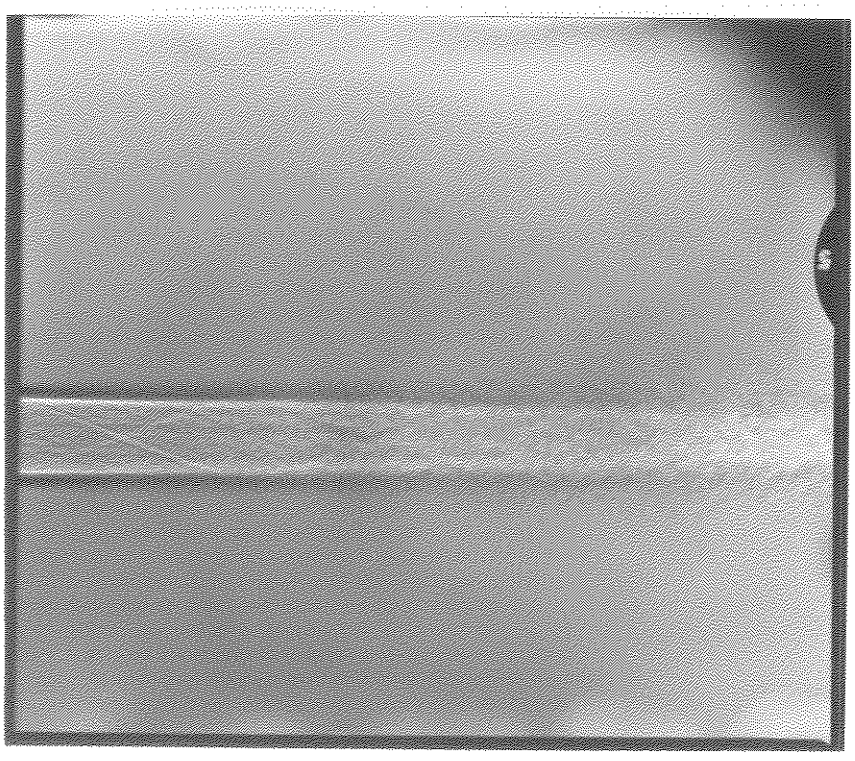

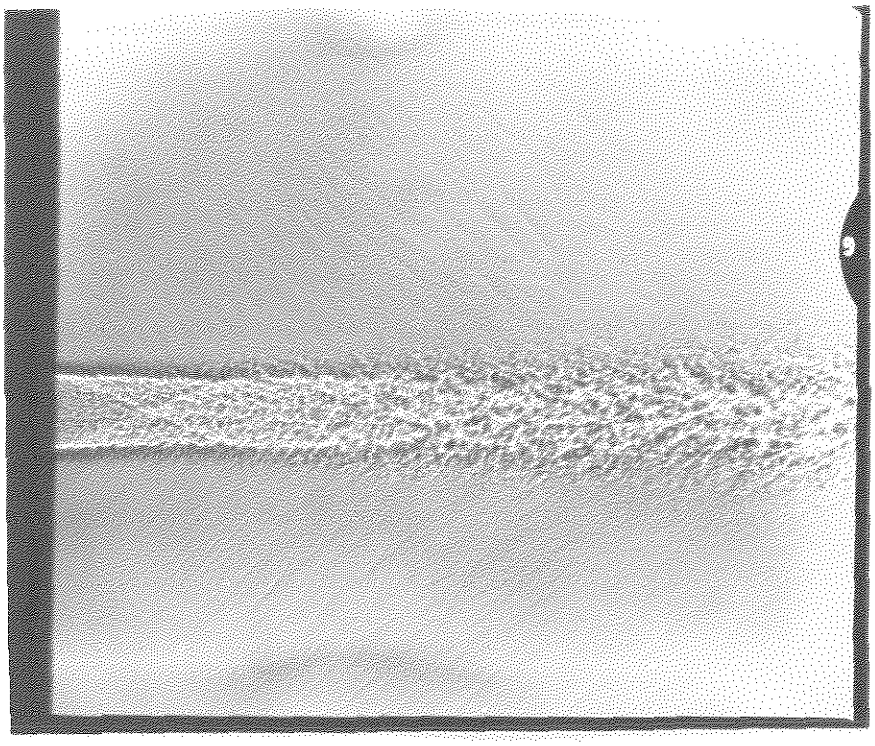

C.17 : Mach 3.0 Nitrogen into Air, 380 psia

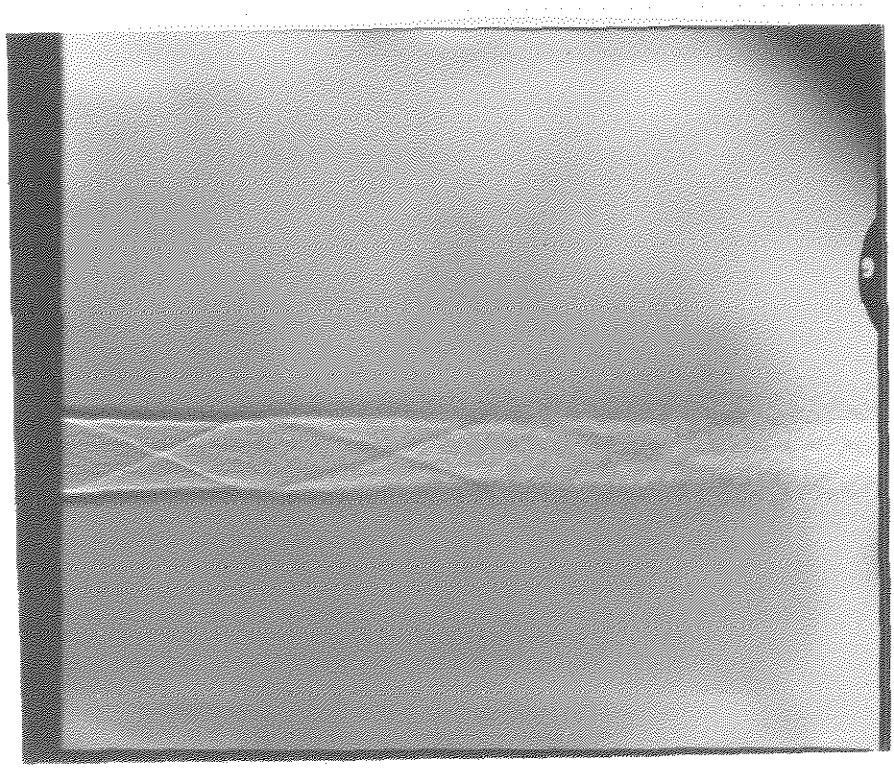

Appendix D

Pitot Traverse Data

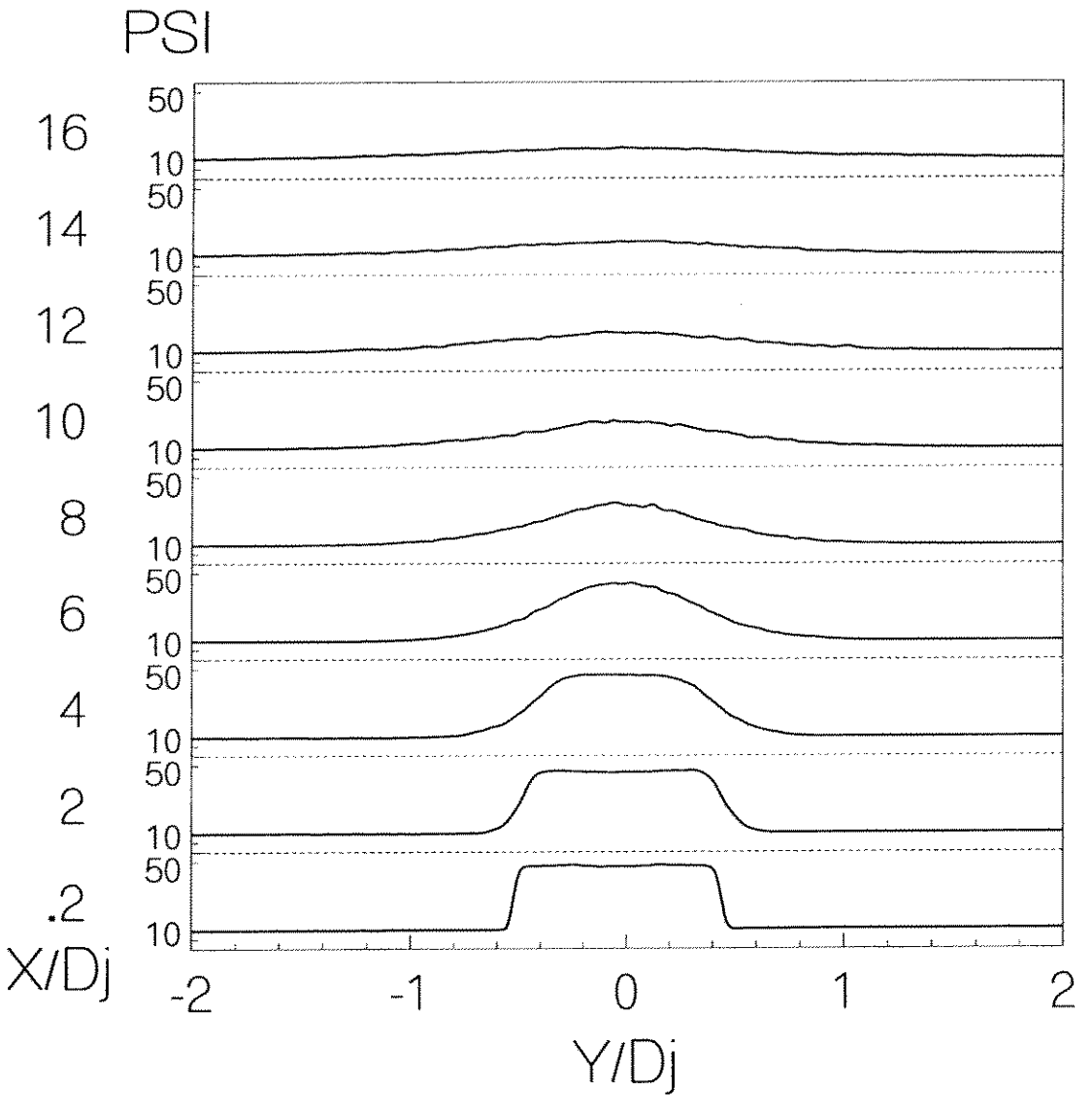

Figure D.1: Argon into Argon, Mach 1.41, Mean Pitot Pressures

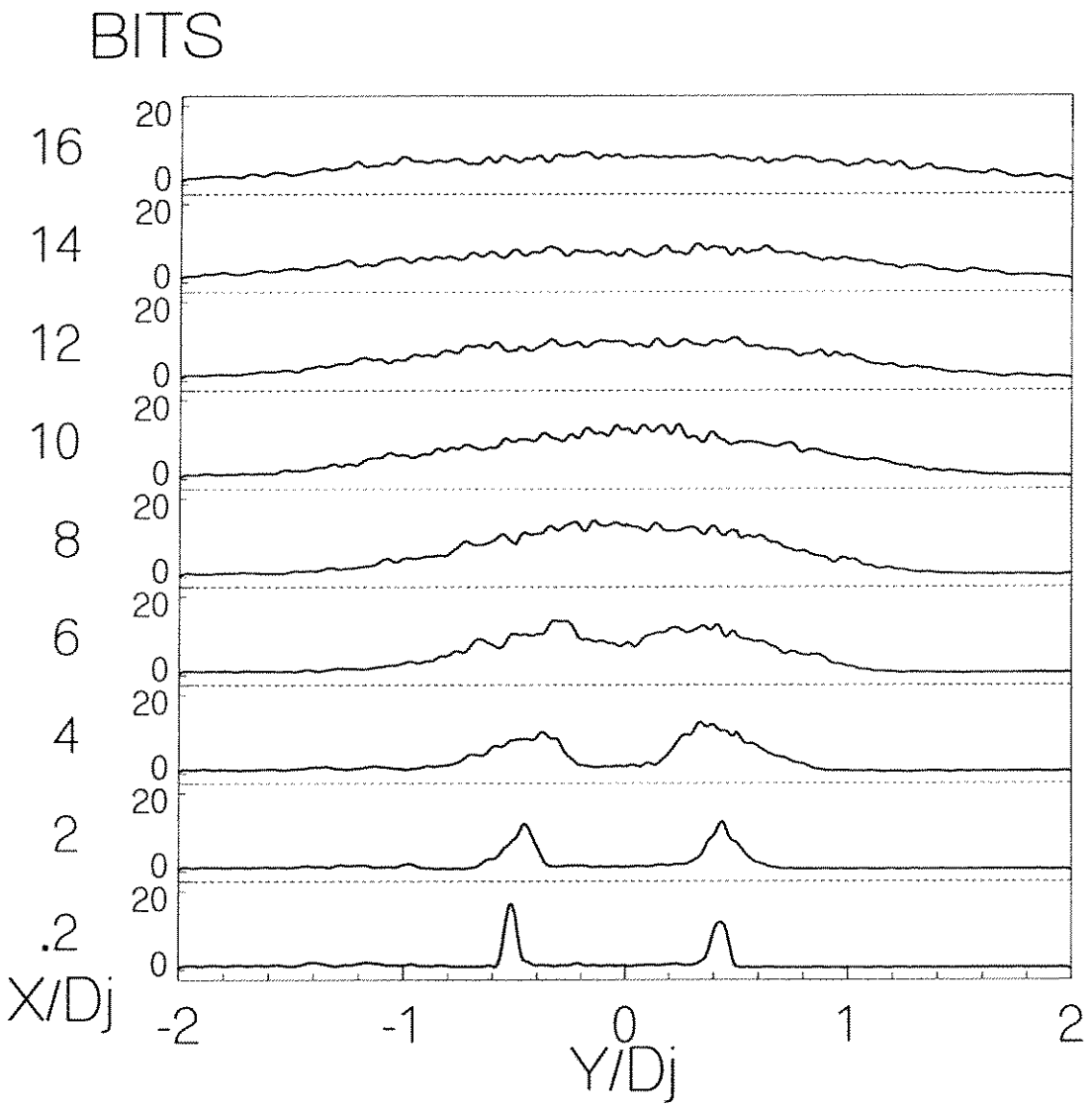

Figure D.2: Argon into Argon, Mach 1.41, RMS Data

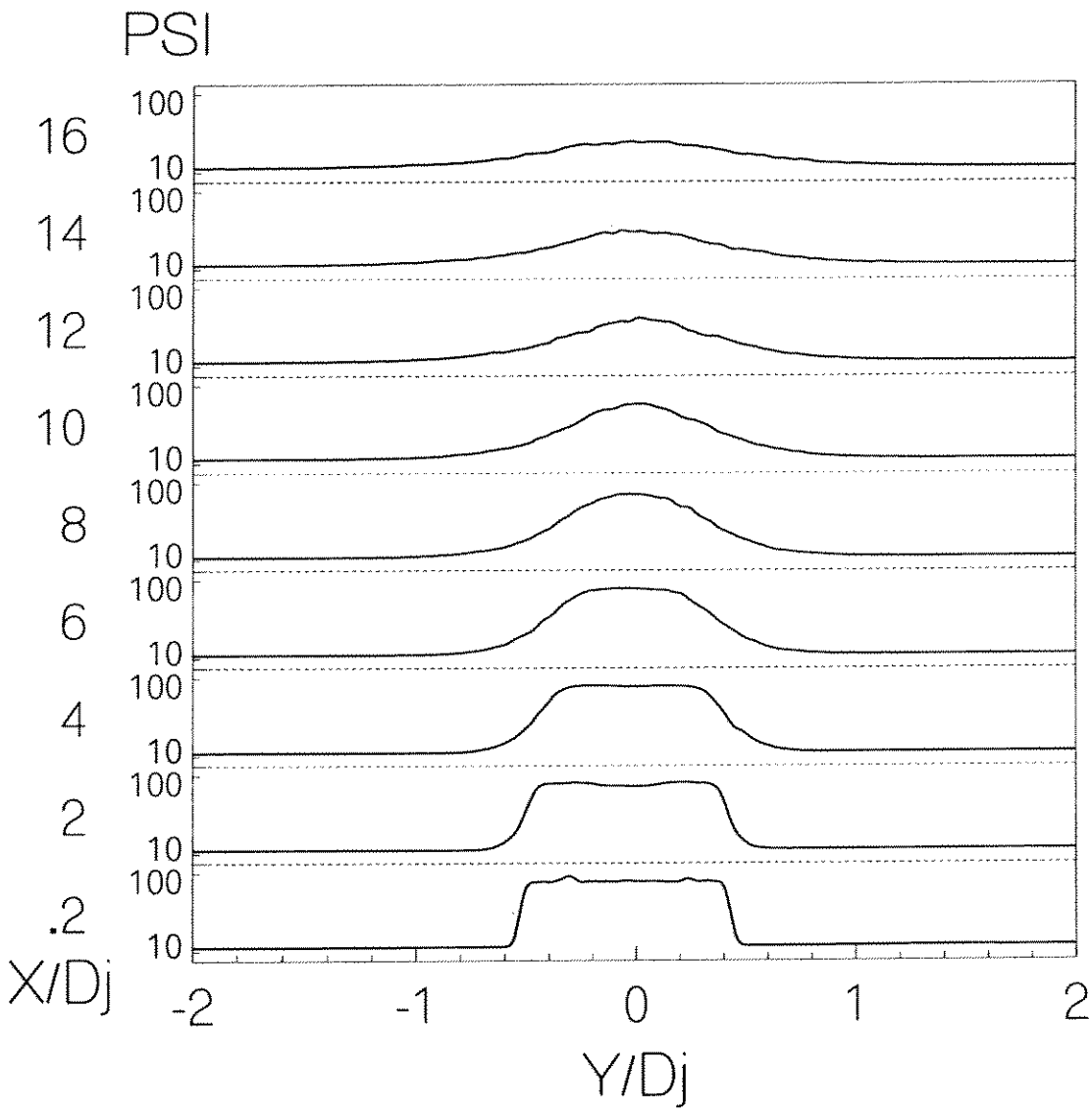

Figure D.3: Argon into Argon, Mach 2.0, Mean Pitot Pressures

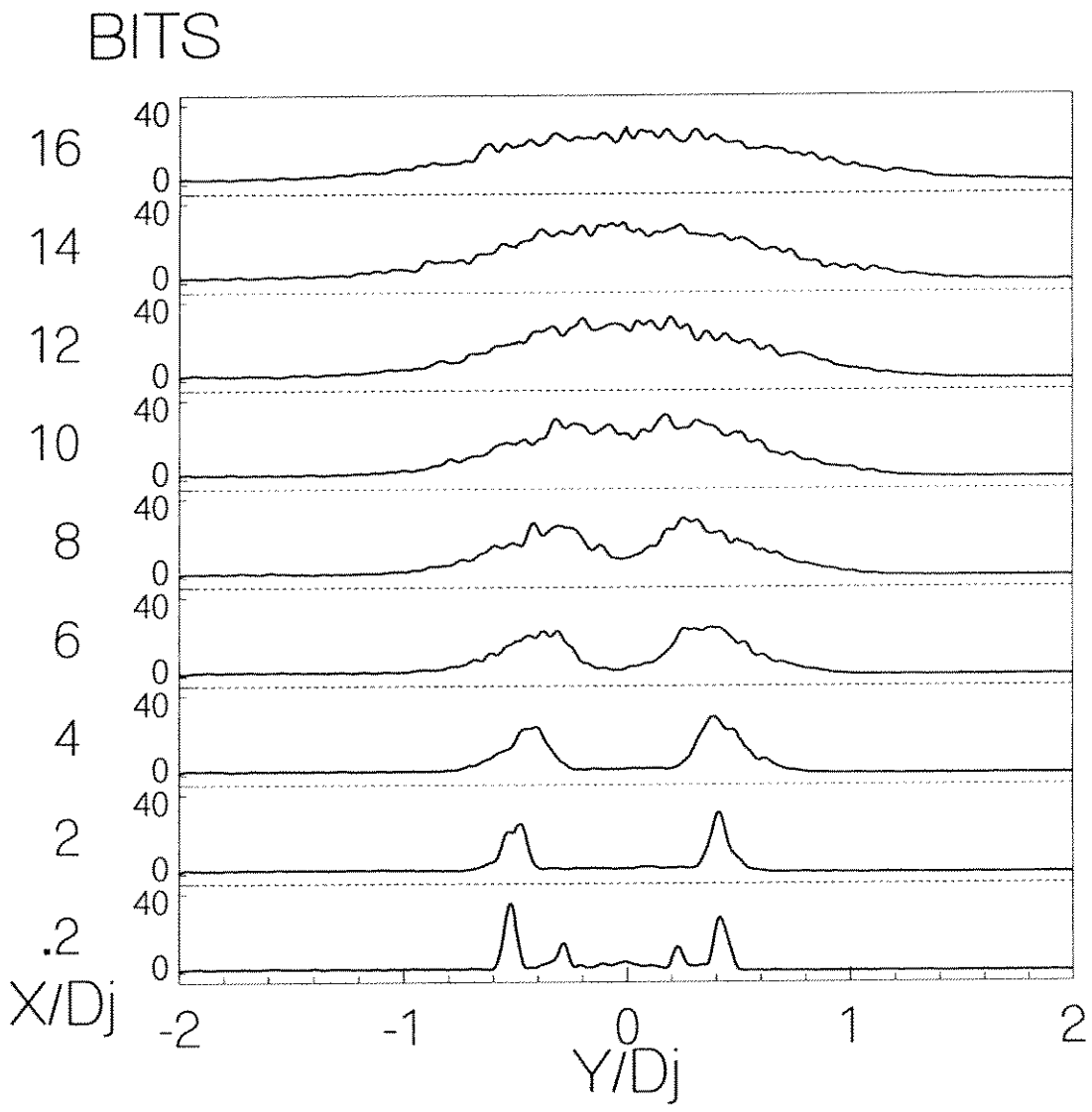

Figure D.4: Argon into Argon, Mach 2.0, RMS Data

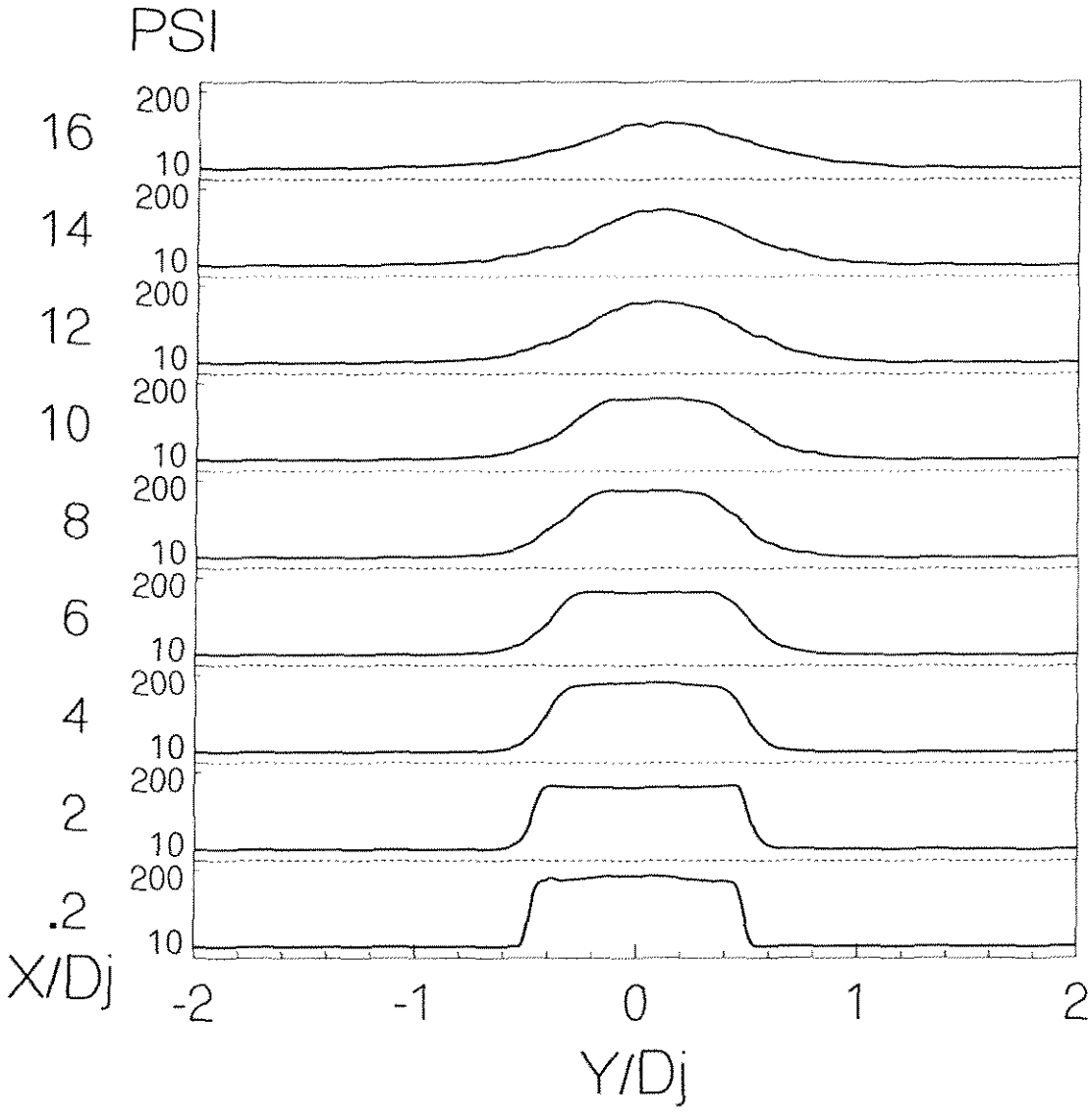

Figure D.5: Argon into Argon, Mach 3.0, Mean Pitot Pressures

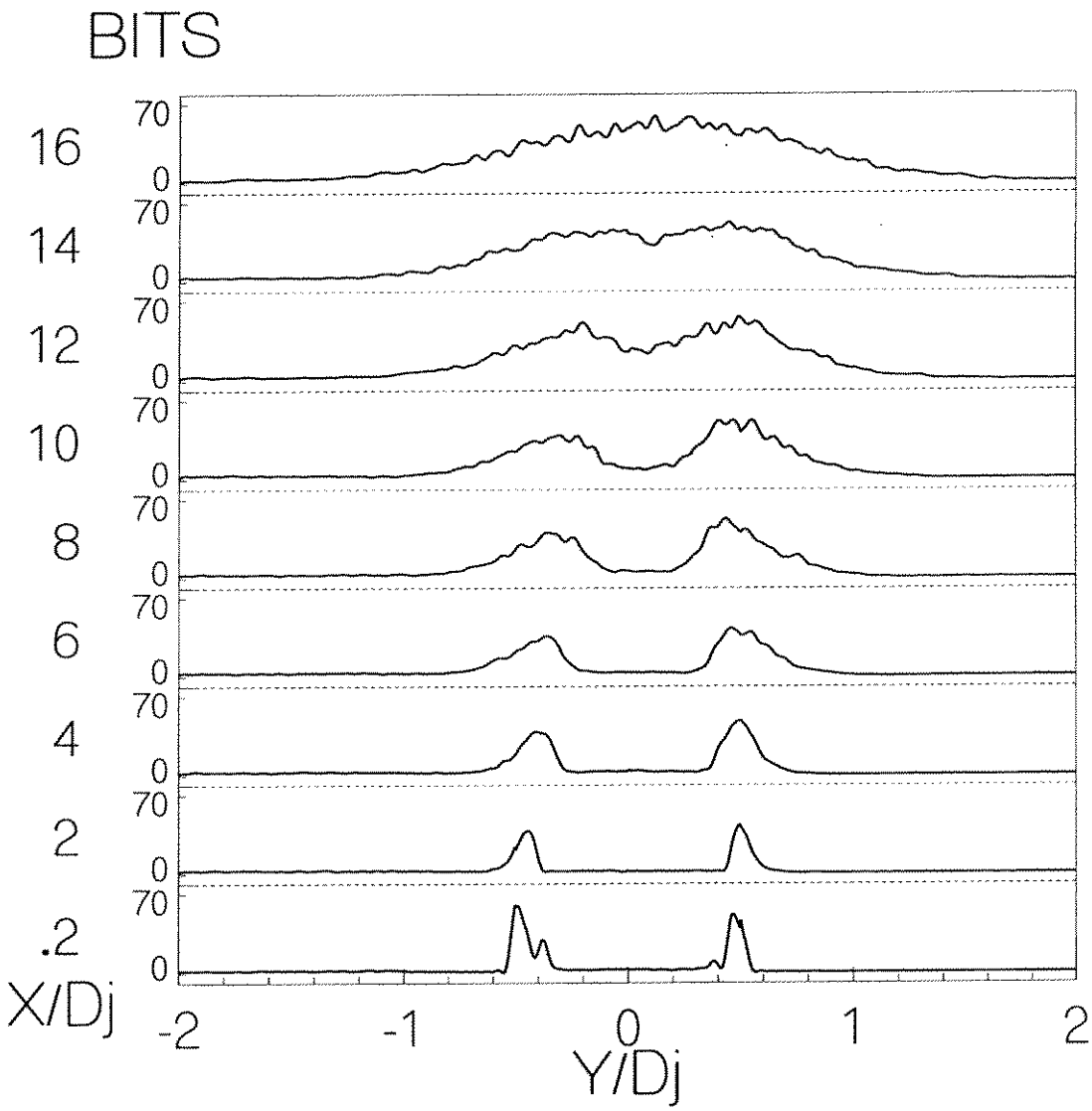

Figure D.6: Argon into Argon, Mach 3.0, RMS Data

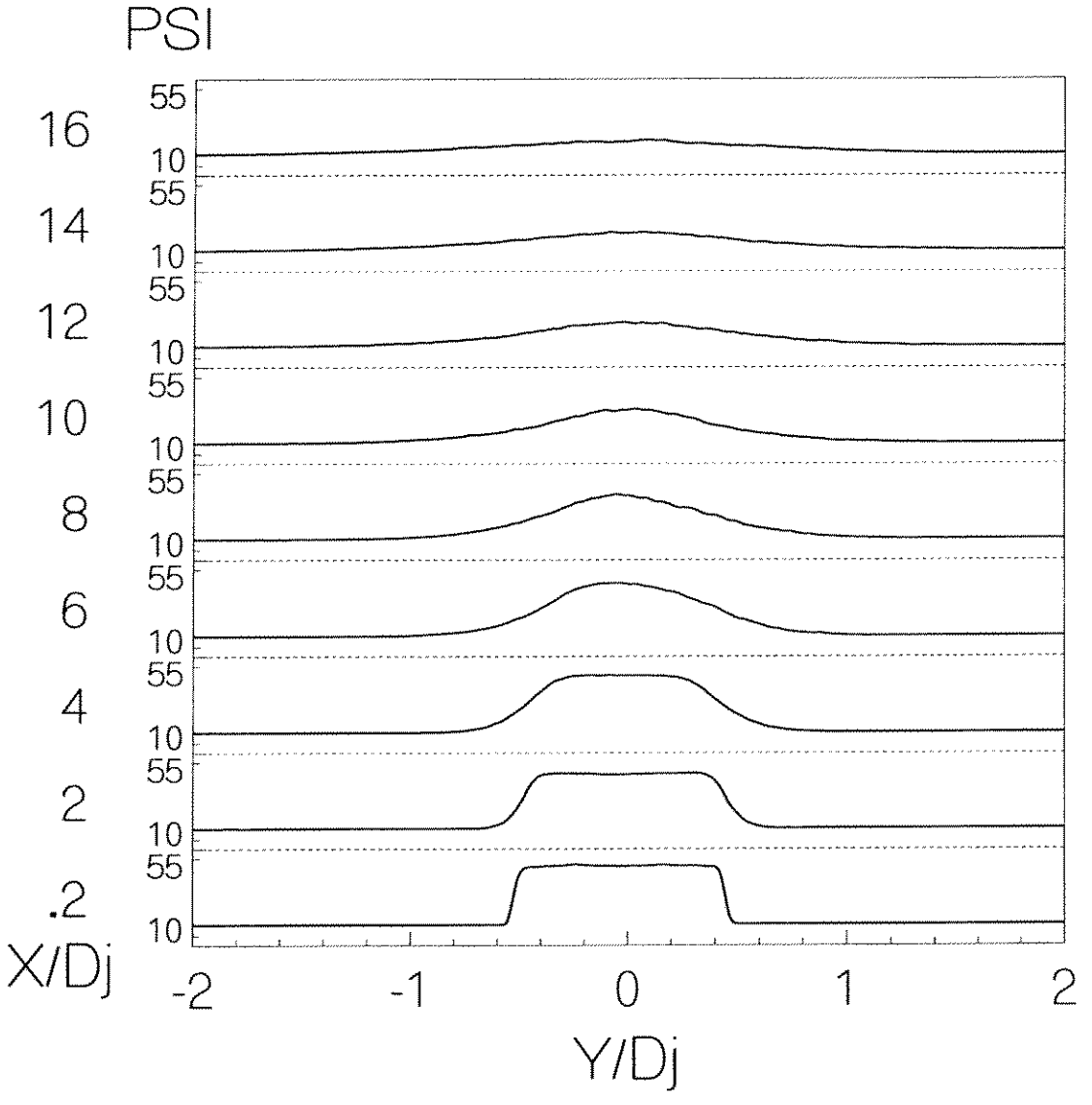

Figure D.7: Argon into Air, Mach 1.41, Mean Pitot Pressures

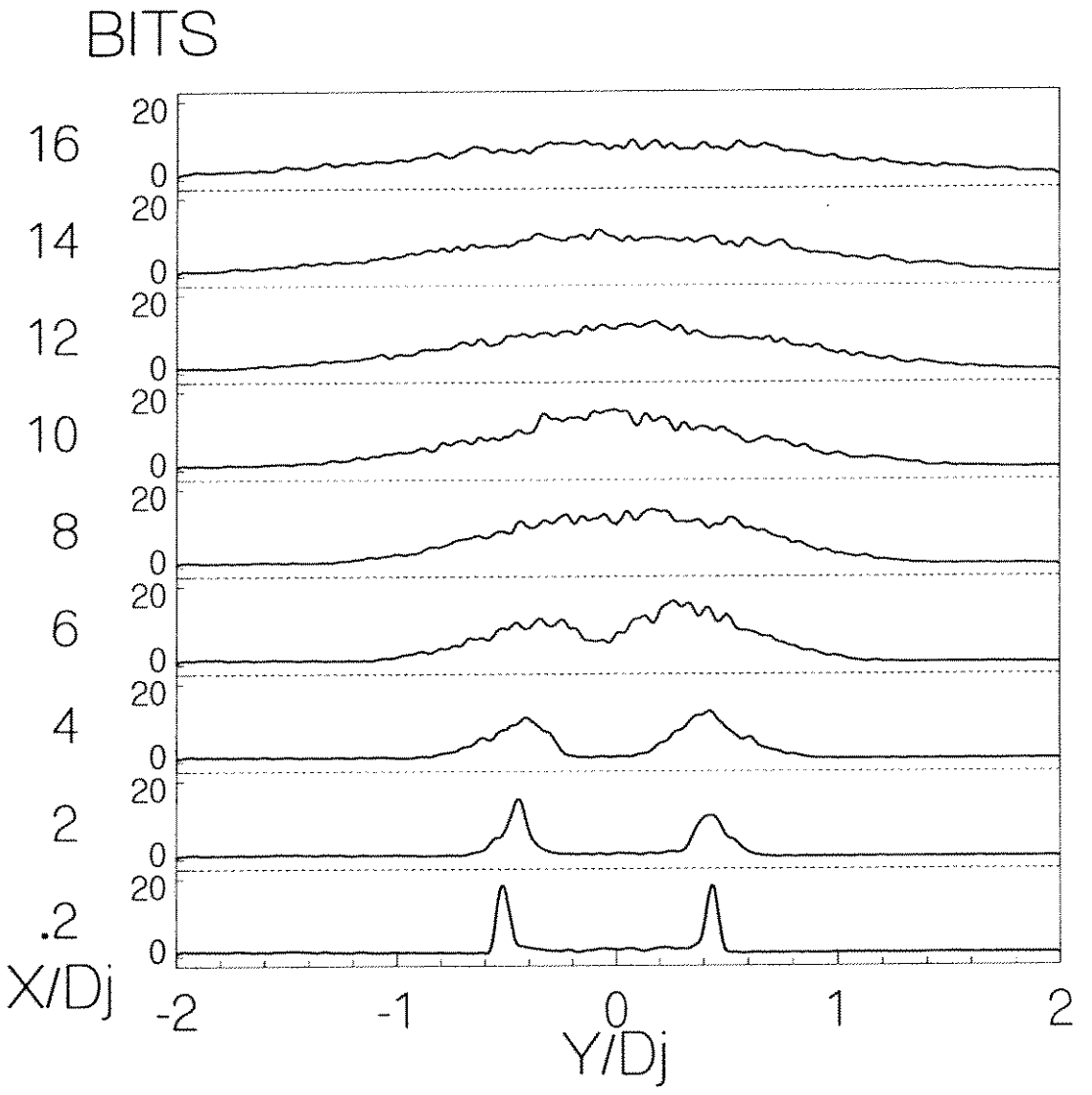

Figure D.8: Argon into Air, Mach 1.41, RMS Data

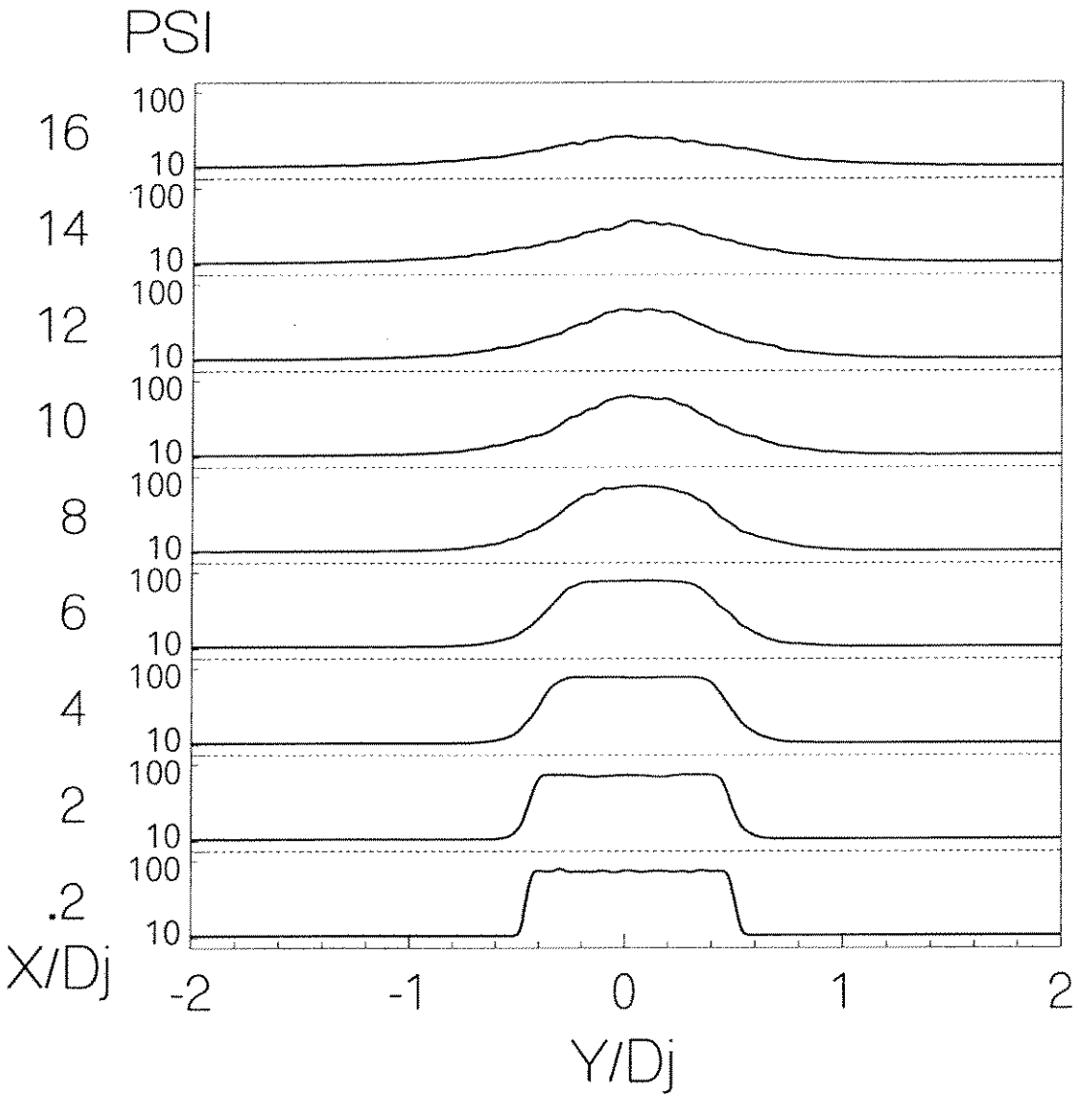

Figure D.9: Argon into Air, Mach 2.0, Mean Pitot Pressures

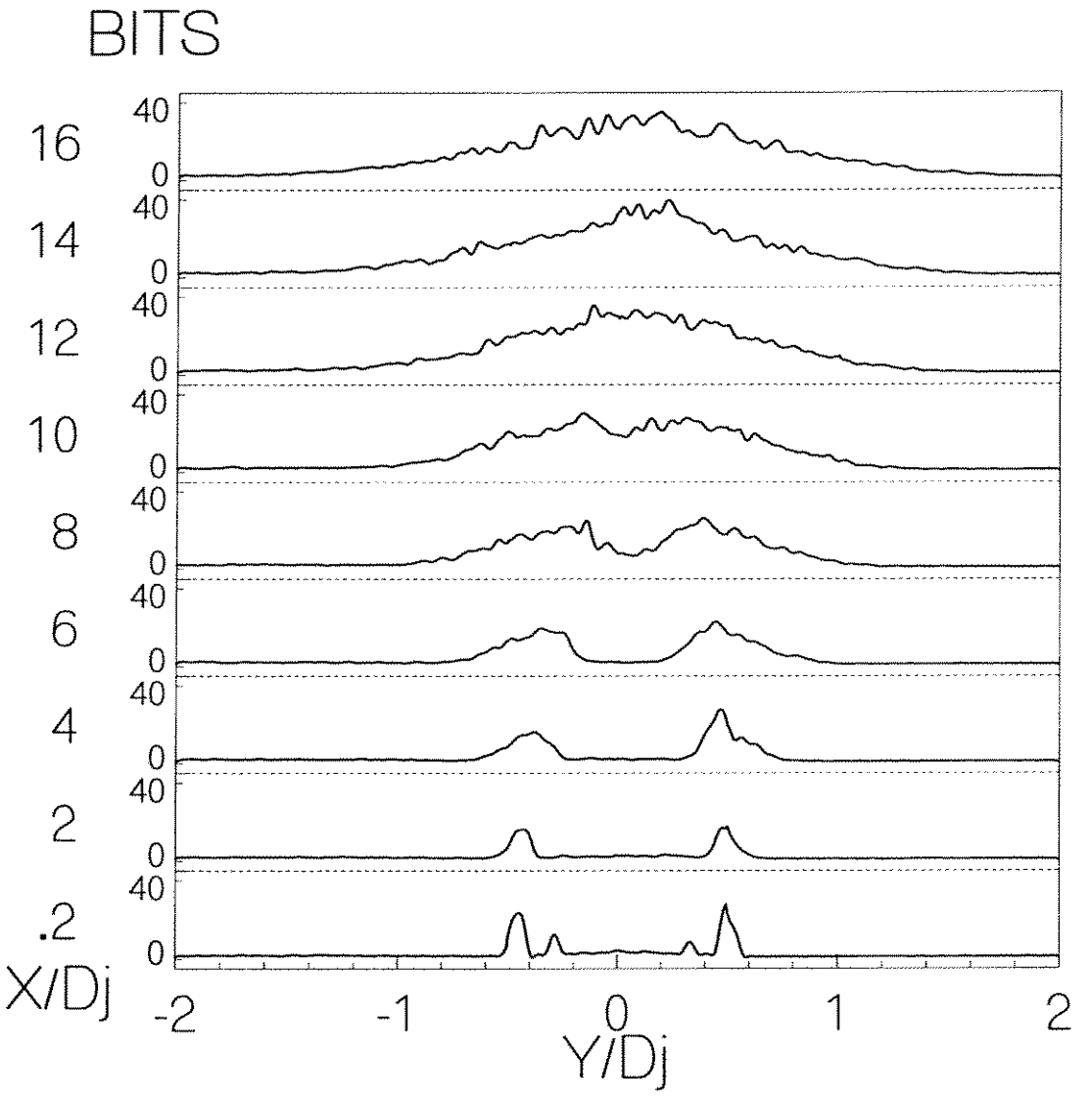

Figure D.10: Argon into Air, Mach 2.0, RMS Data

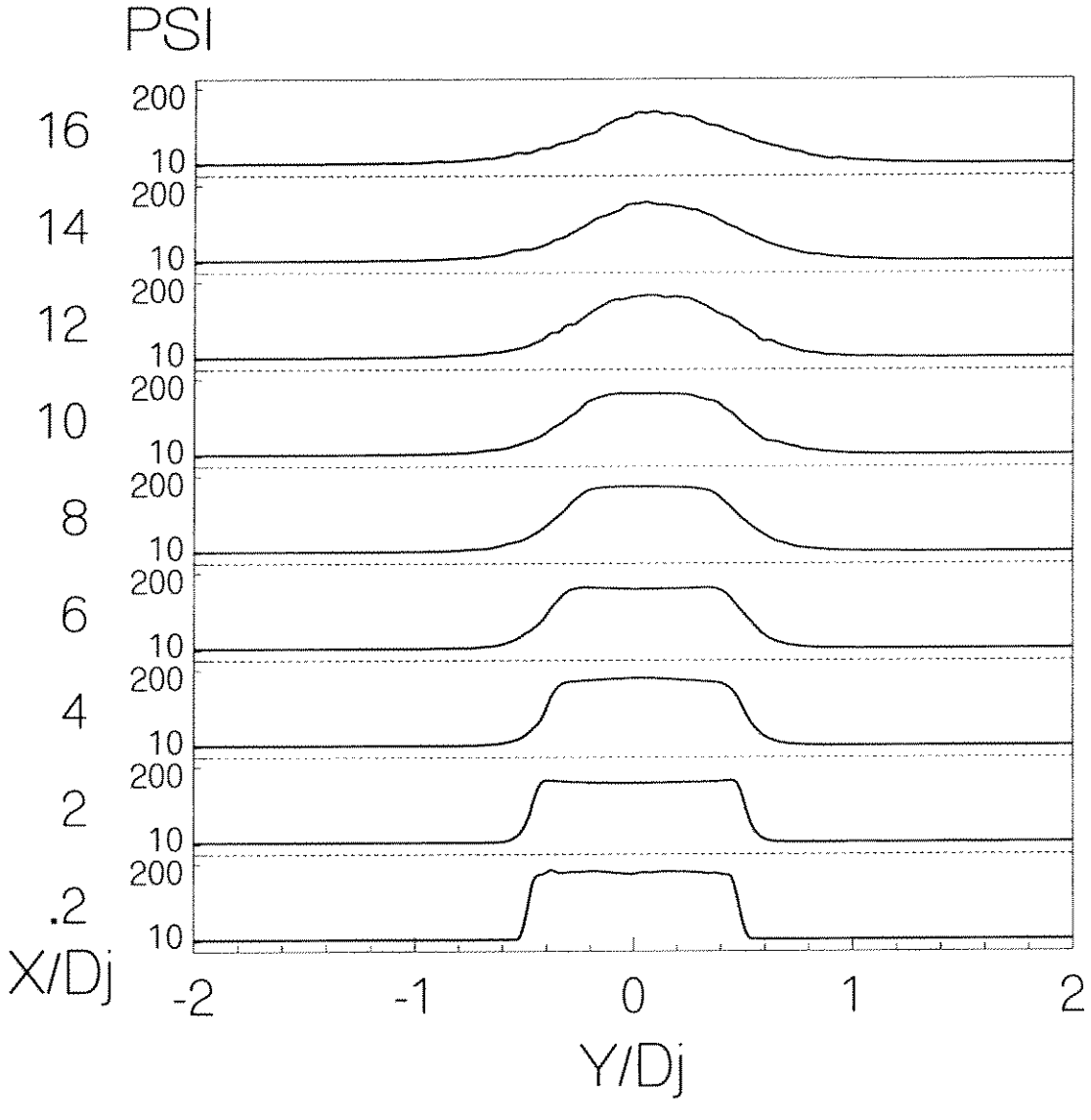

Figure D.11: Argon into Air, Mach 3.0, Mean Pitot Pressures

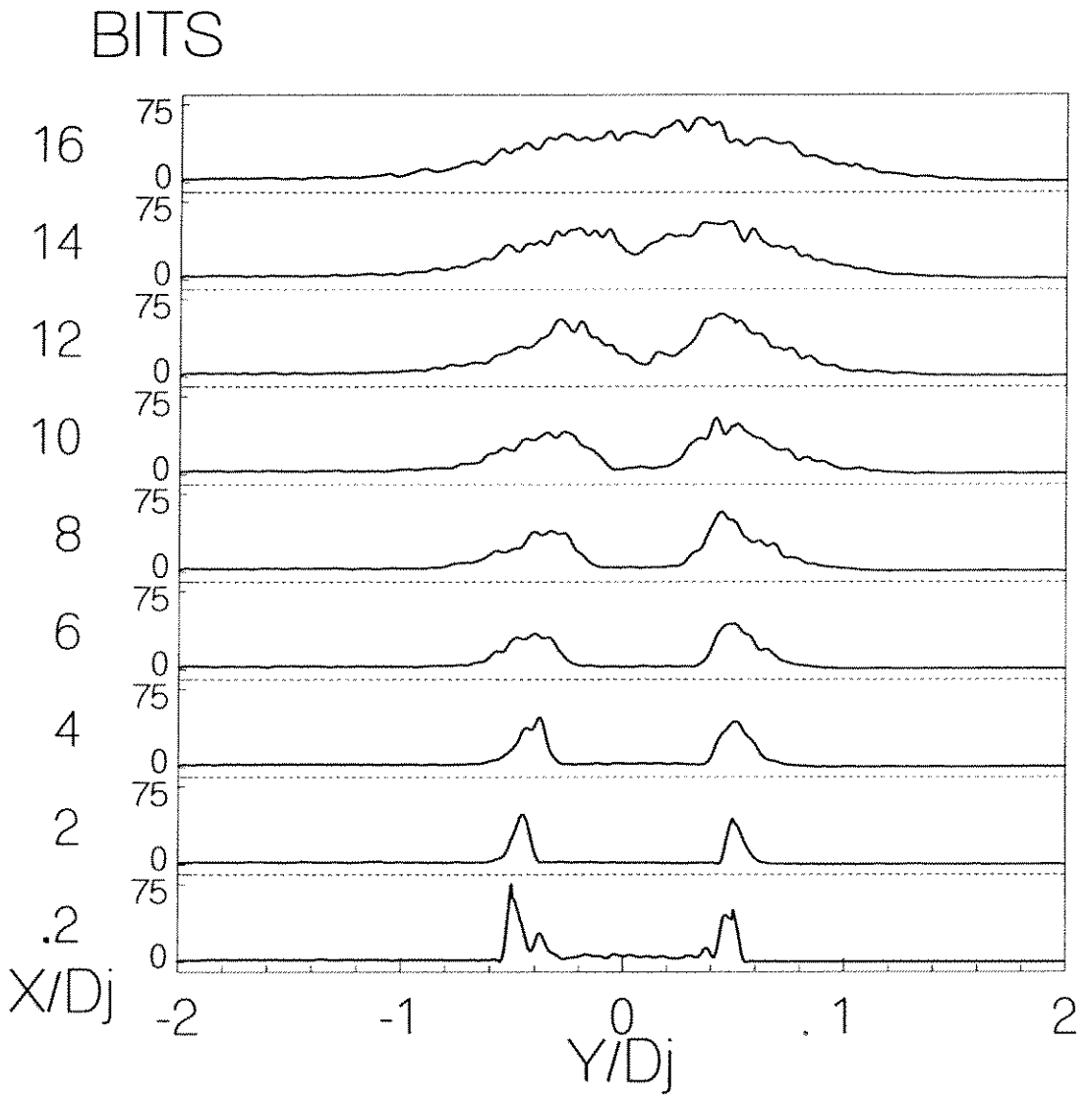

Figure D.12: Argon into Air, Mach 3.0, RMS Data

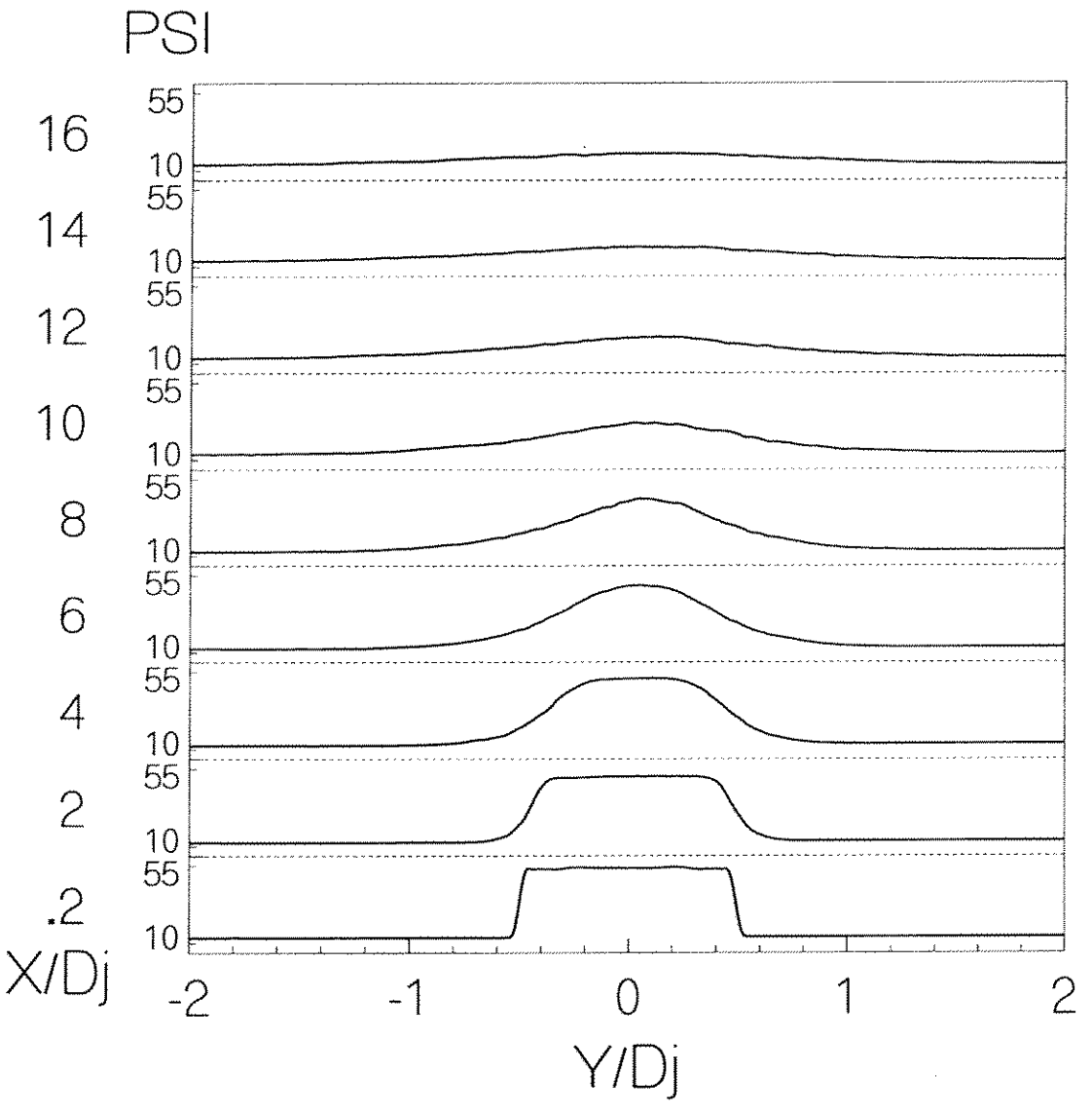

Figure D.13: Helium into Air, Mach 1.41, Mean Pitot Pressures

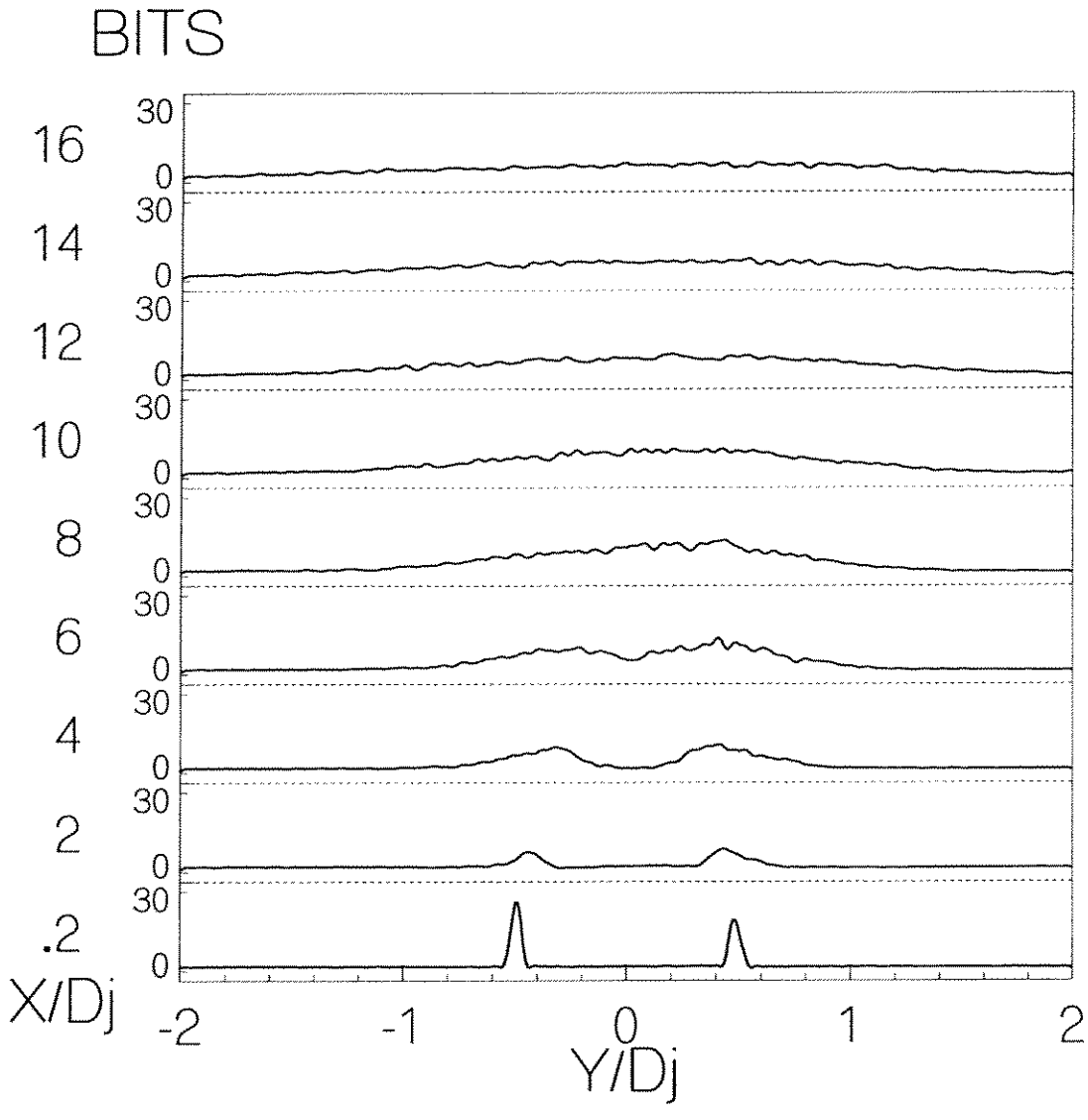

Figure D.14: Helium into Air, Mach 1.41, RMS Data

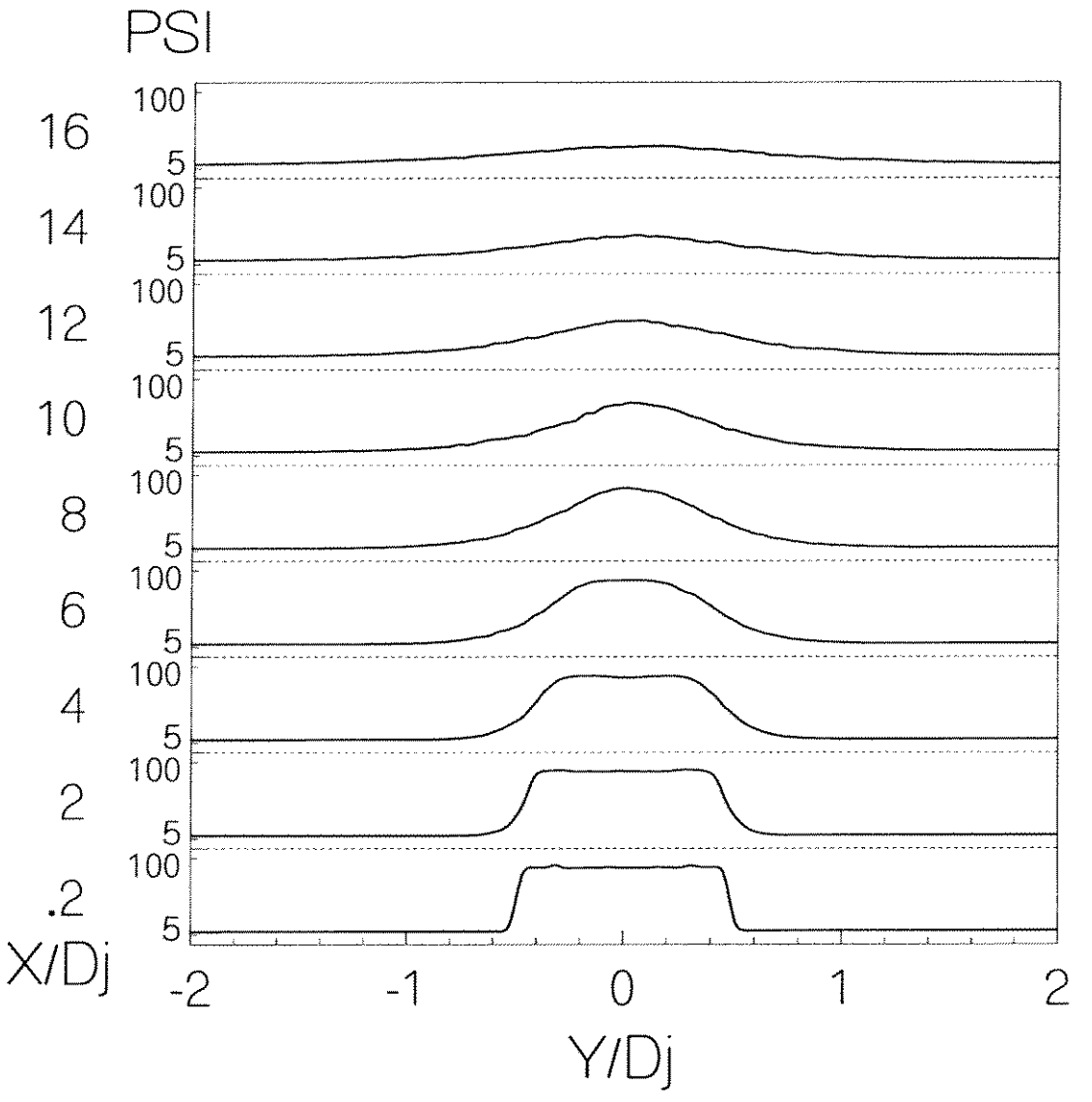

Figure D.15: Helium into Air, Mach 2.0, Mean Pitot Pressures

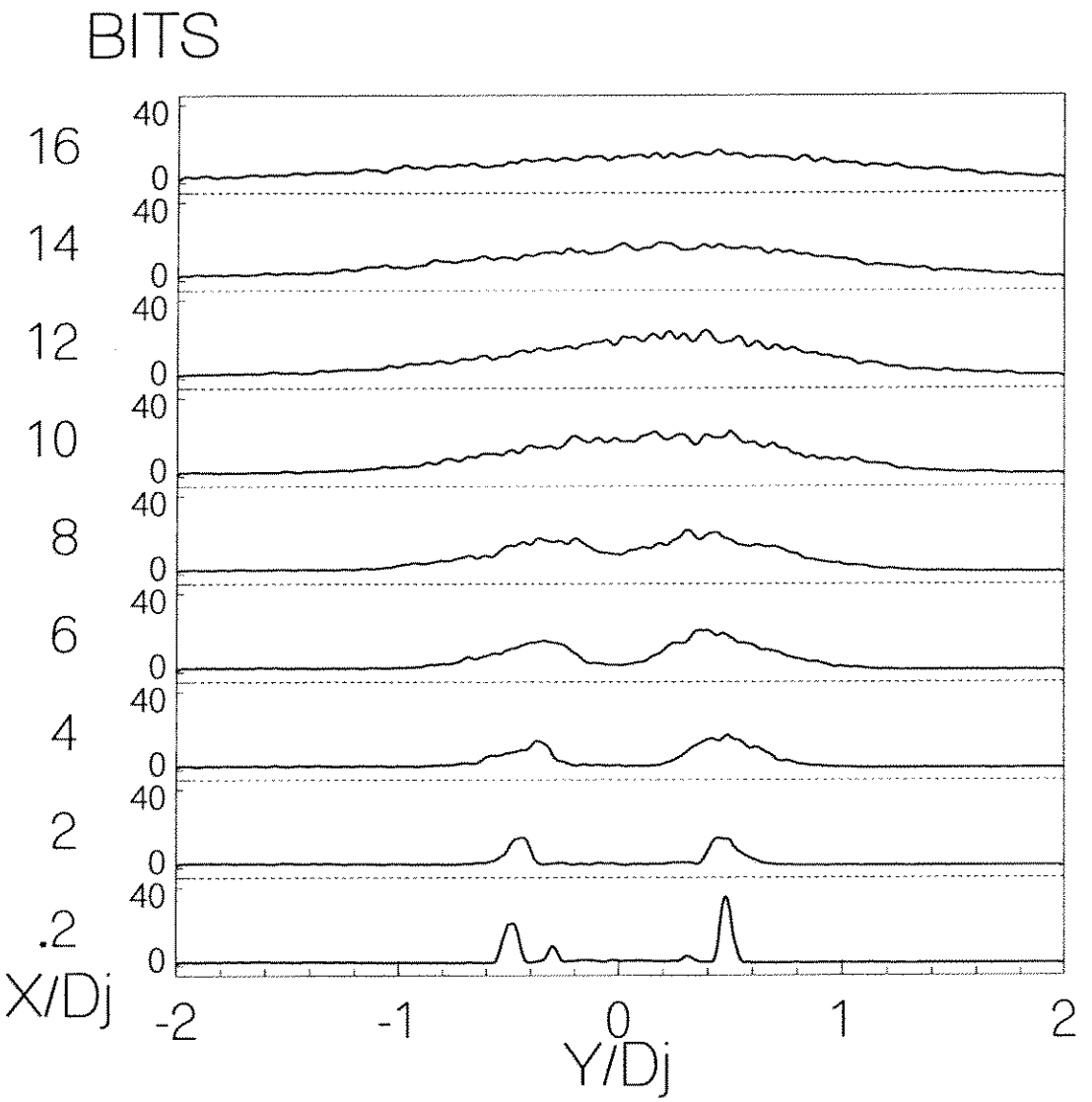

Figure D.16: Helium into Air, Mach 2.0, RMS Data

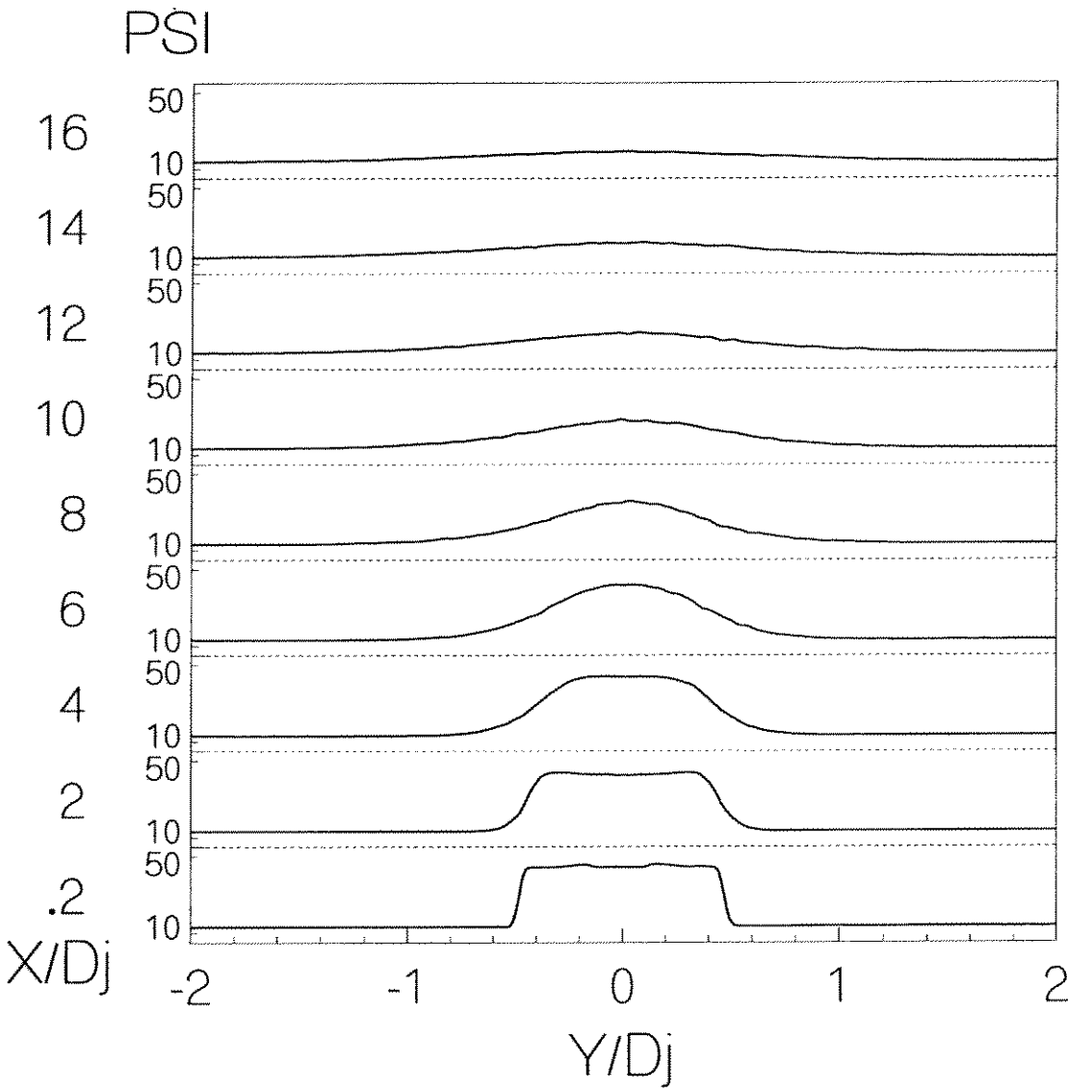

Figure D.17: Nitrogen into Air, Mach 1.41, Mean Pitot Pressures

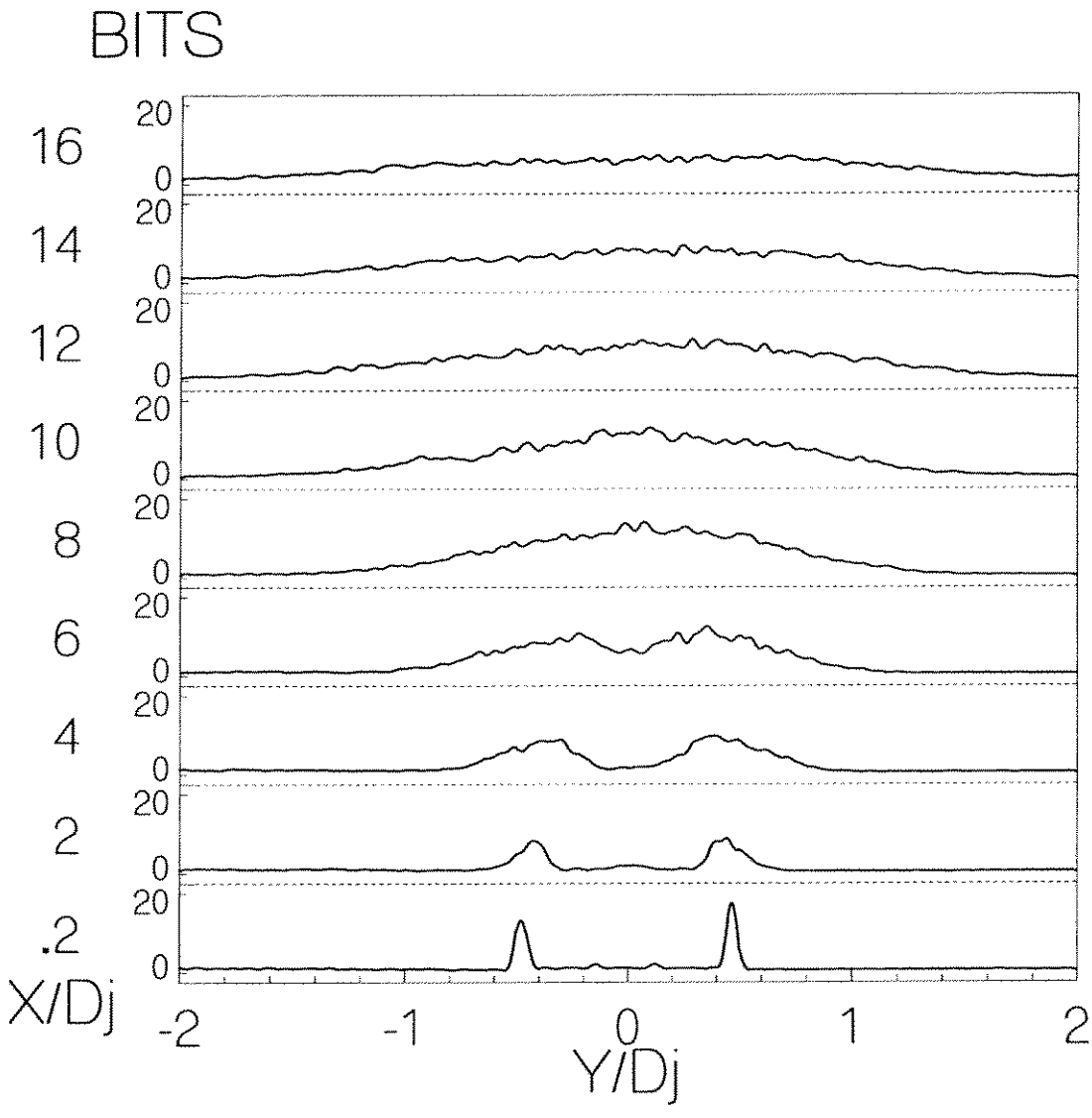

Figure D.18: Nitrogen into Air, Mach 1.41, RMS Data

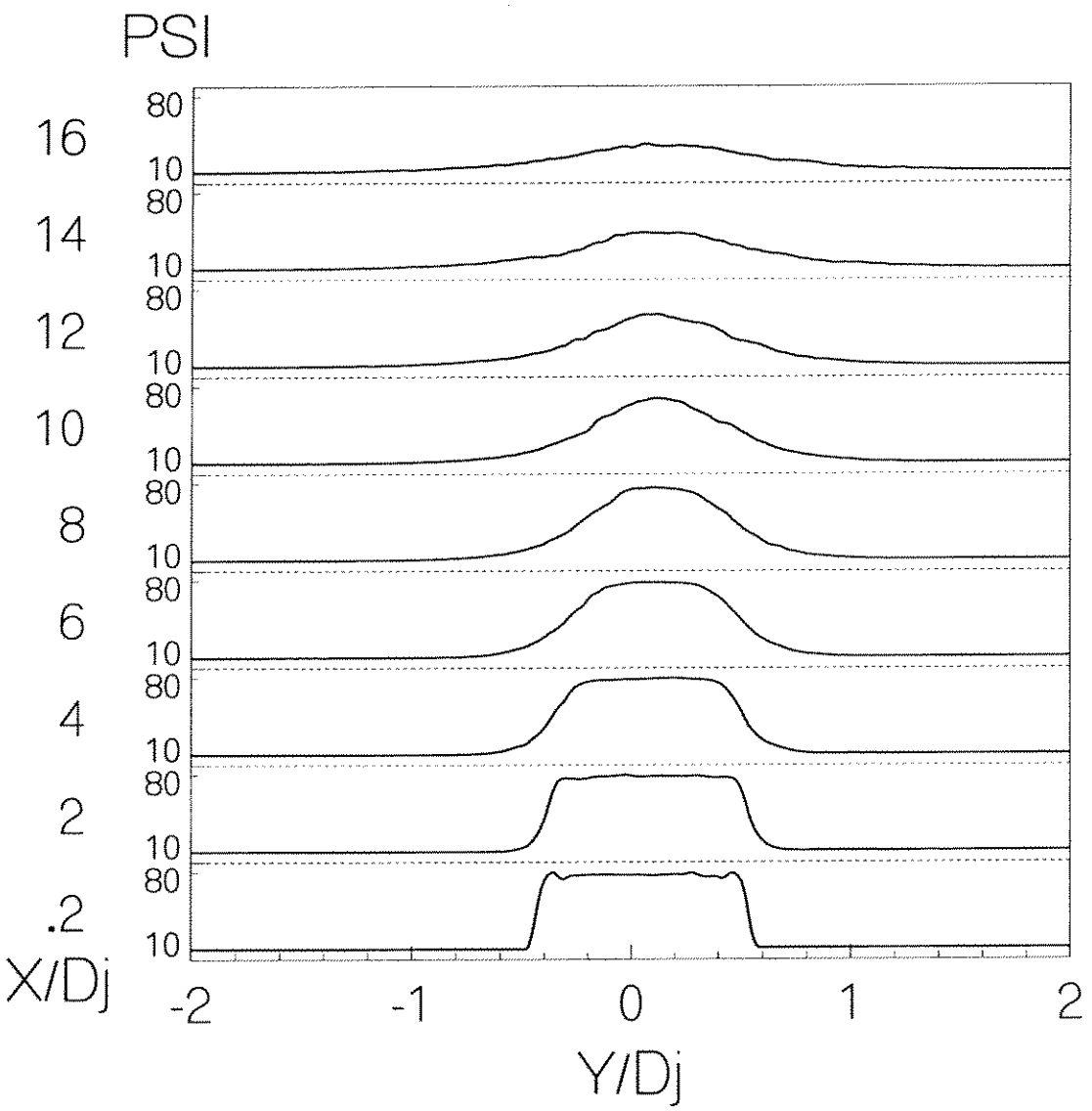

Figure D.19: Nitrogen into Air, Mach 2.0, Mean Pitot Pressures

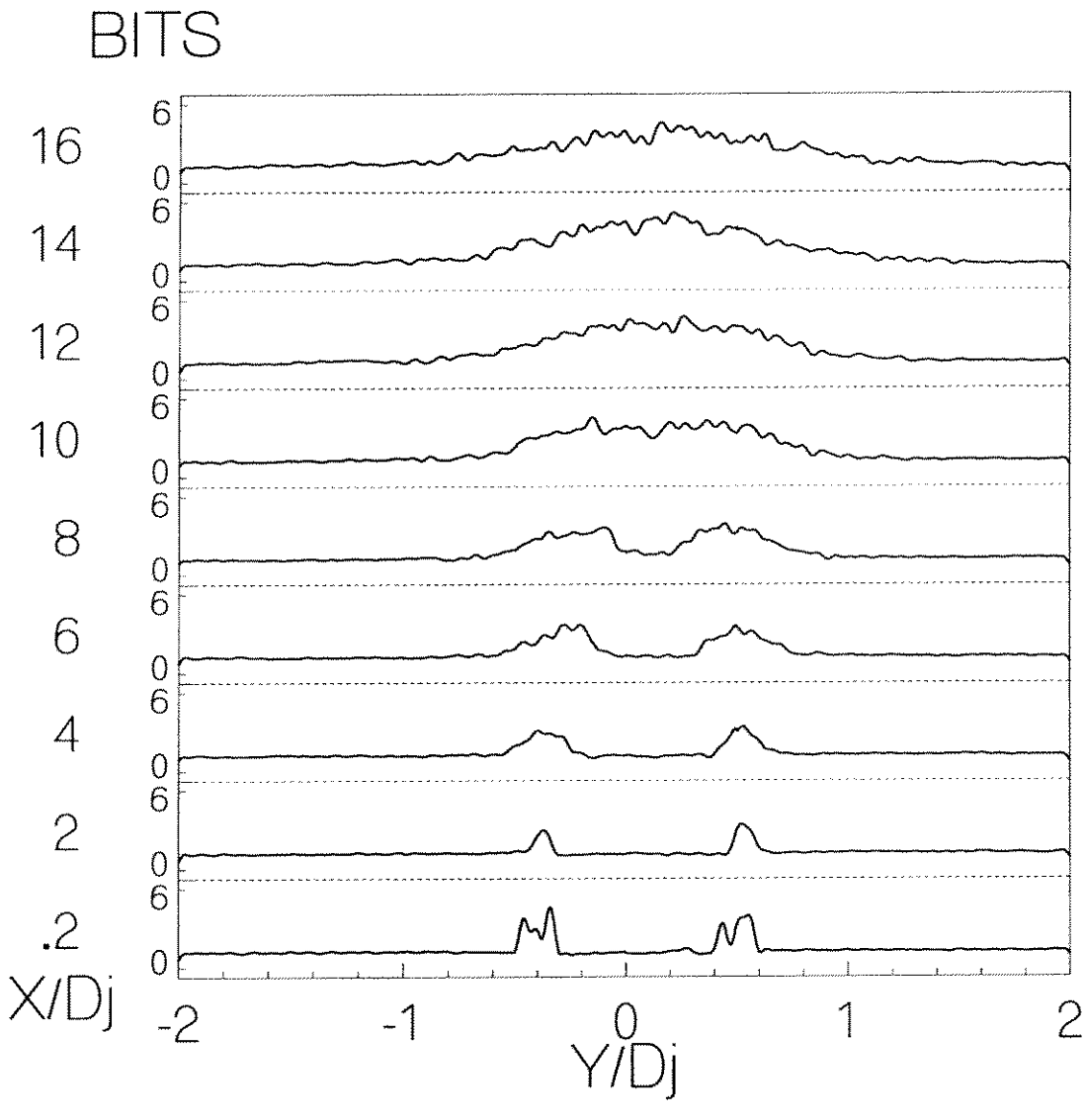

Figure D.20: Nitrogen into Air, Mach 2.0, RMS Data

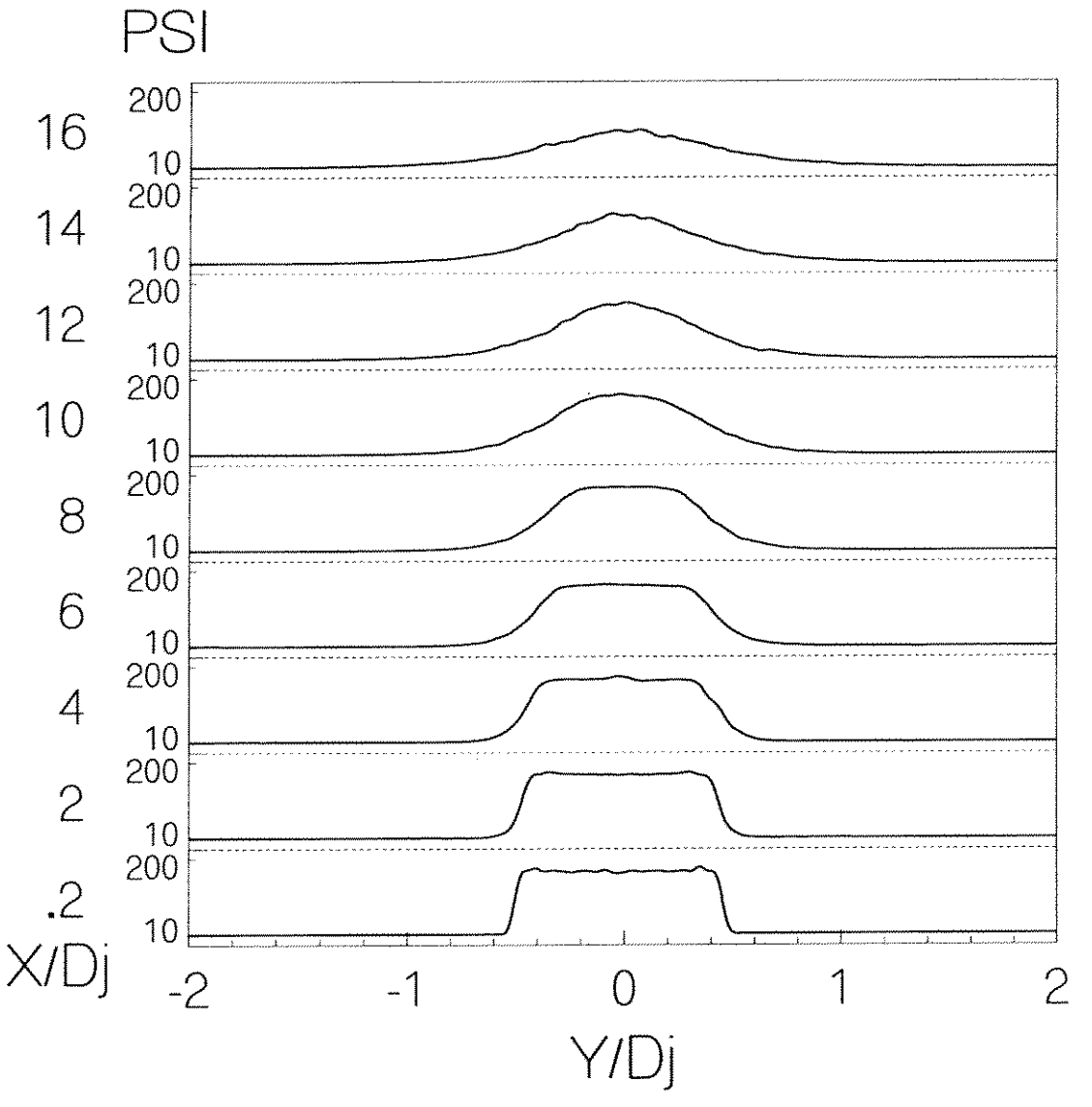

Figure D.21: Nitrogen into Air, Mach 3.0, Mean Pitot Pressures

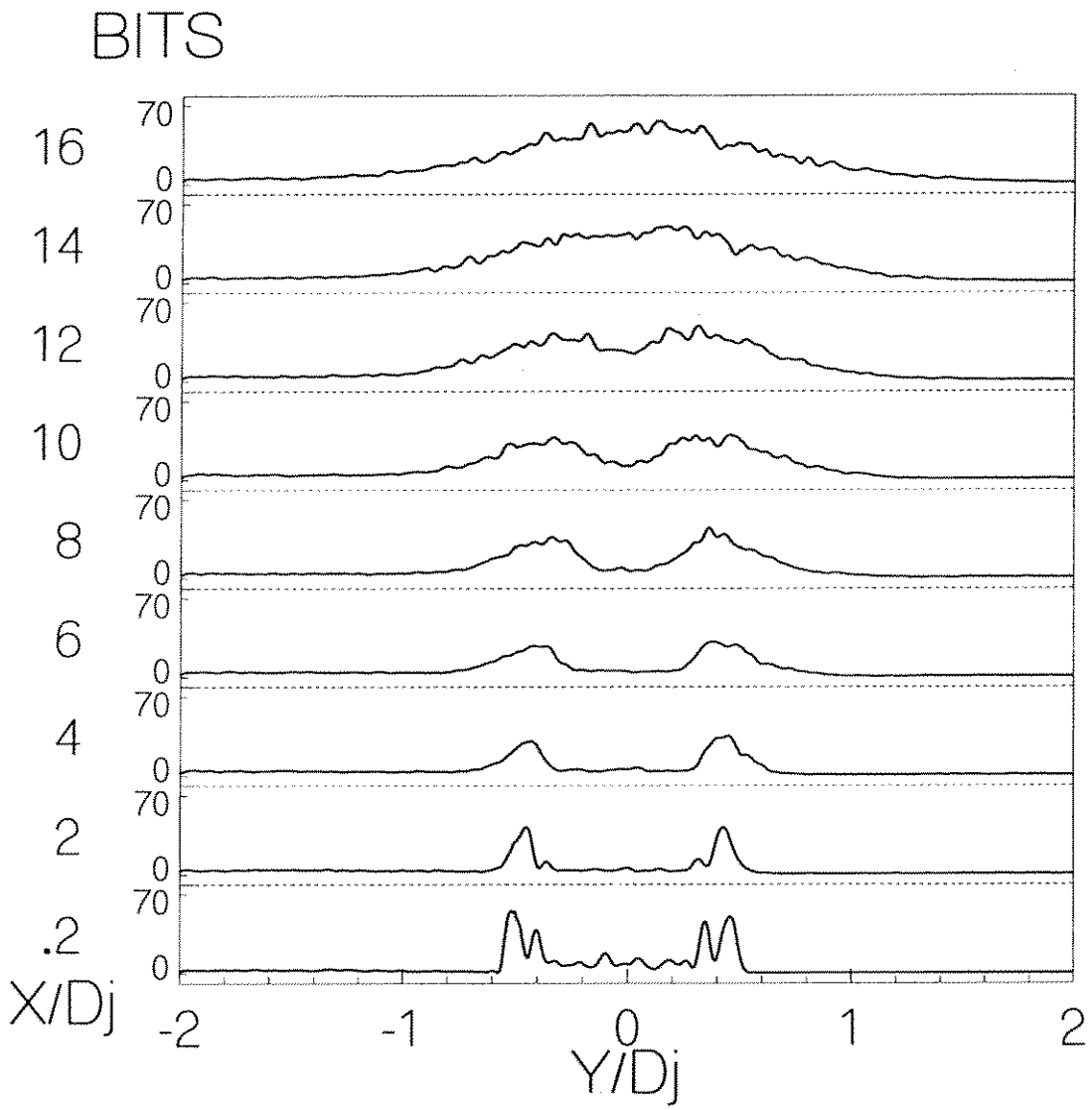

Figure D.22: Nitrogen into Air, Mach 3.0, RMS Data

Appendix E

Mach 3.0 Nitrogen Off-Design Data

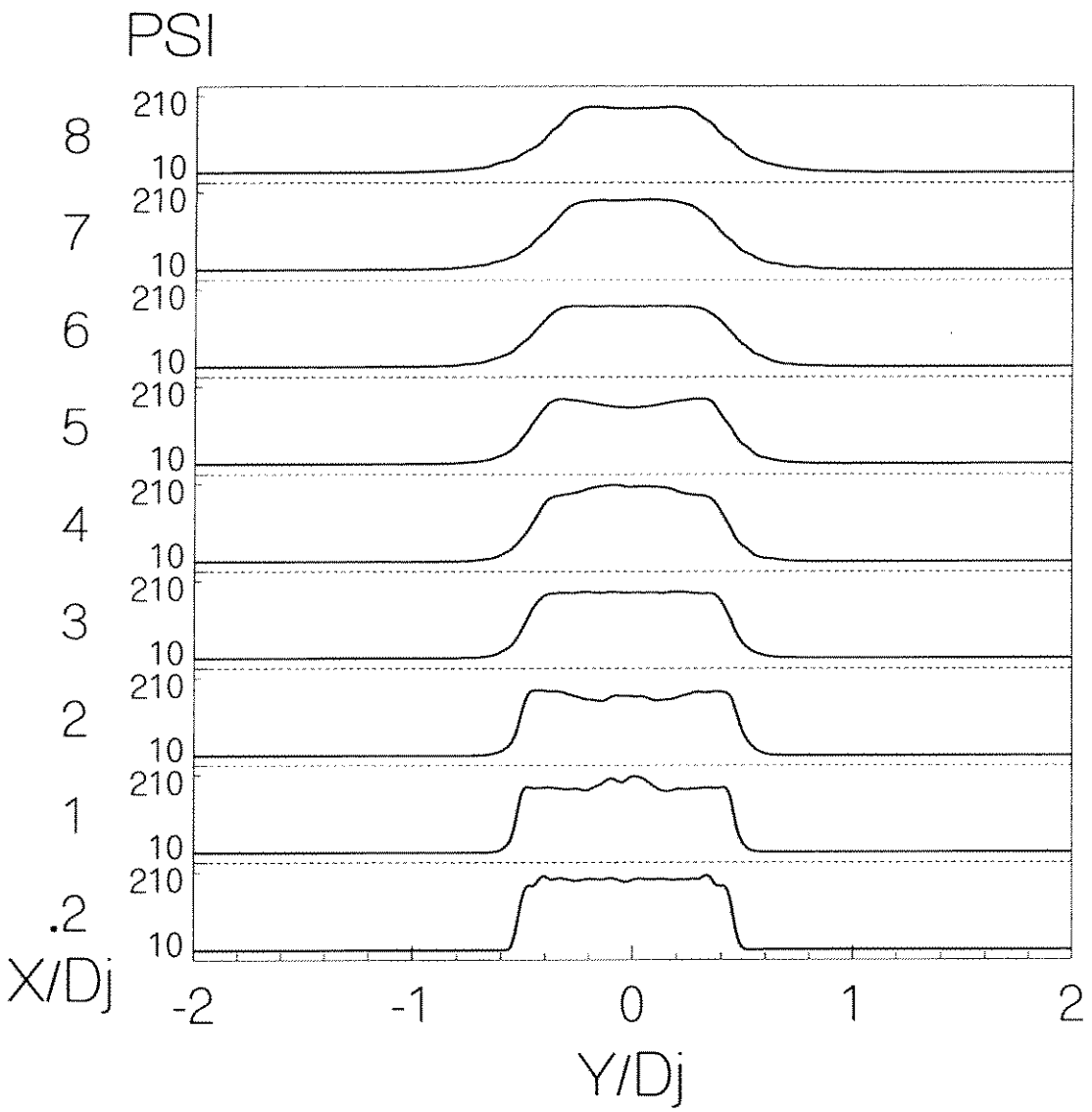

Figure E.1: Mean Pitot Pressures, M 3.0 N2, 534 psia, 0 to 8 diameters

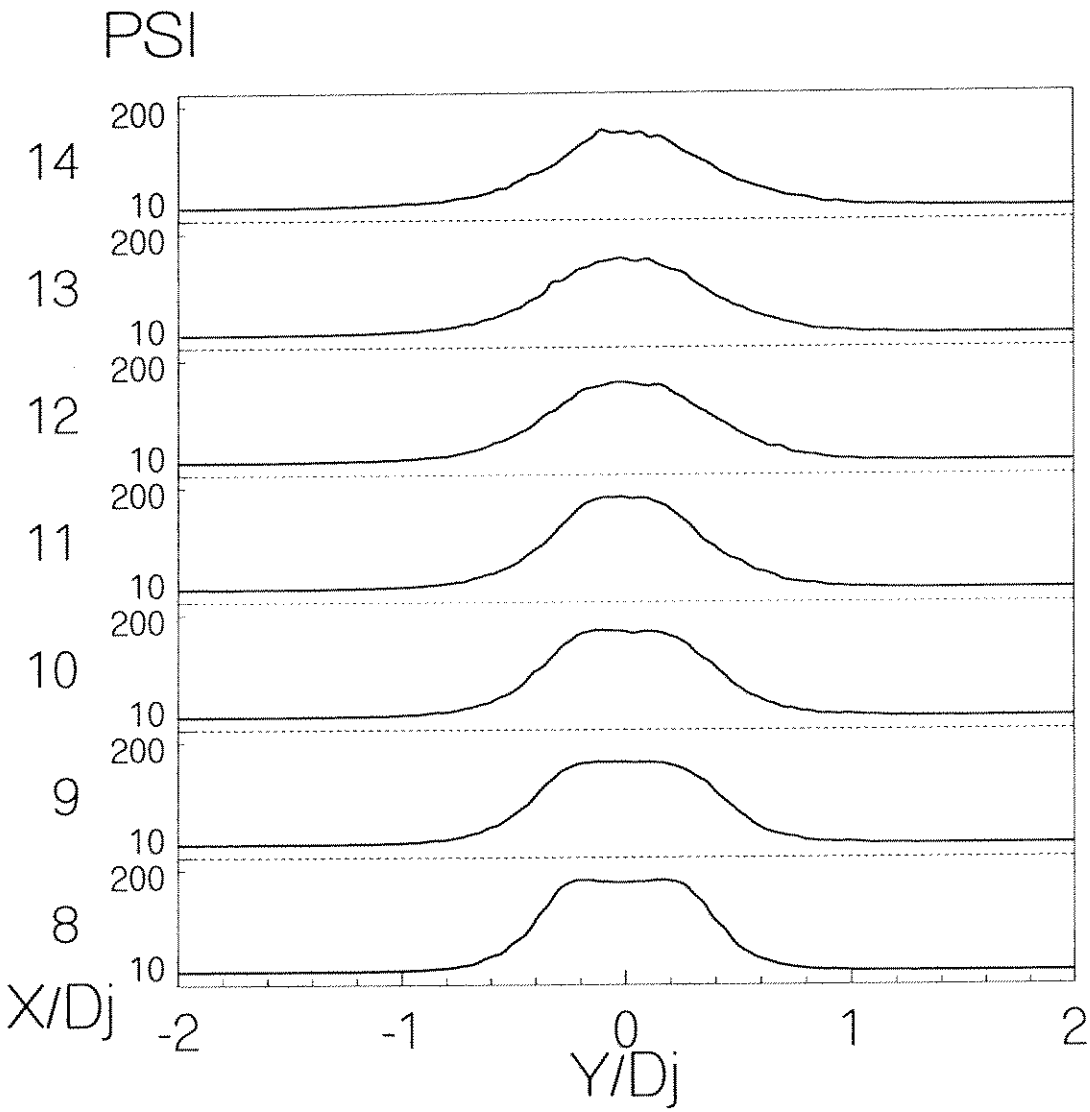

Figure E.2: Mean Pitot Pressures, M 3.0 N2, 534 psia, 8 to 14 diameters

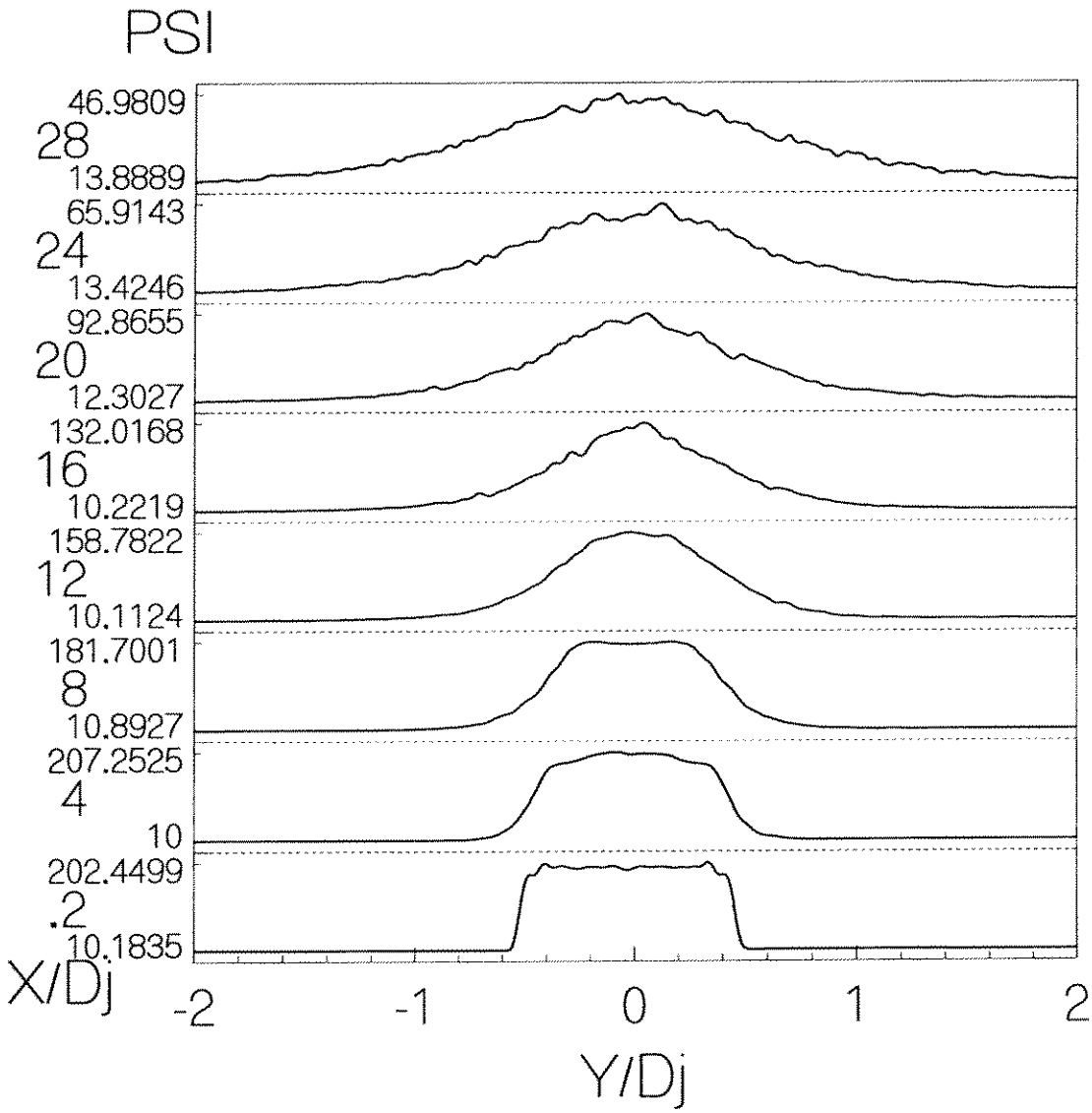

Figure E.3: Mean Pitot Pressures, M 3.0 N2, 534 psia, 0 to 28 diameters

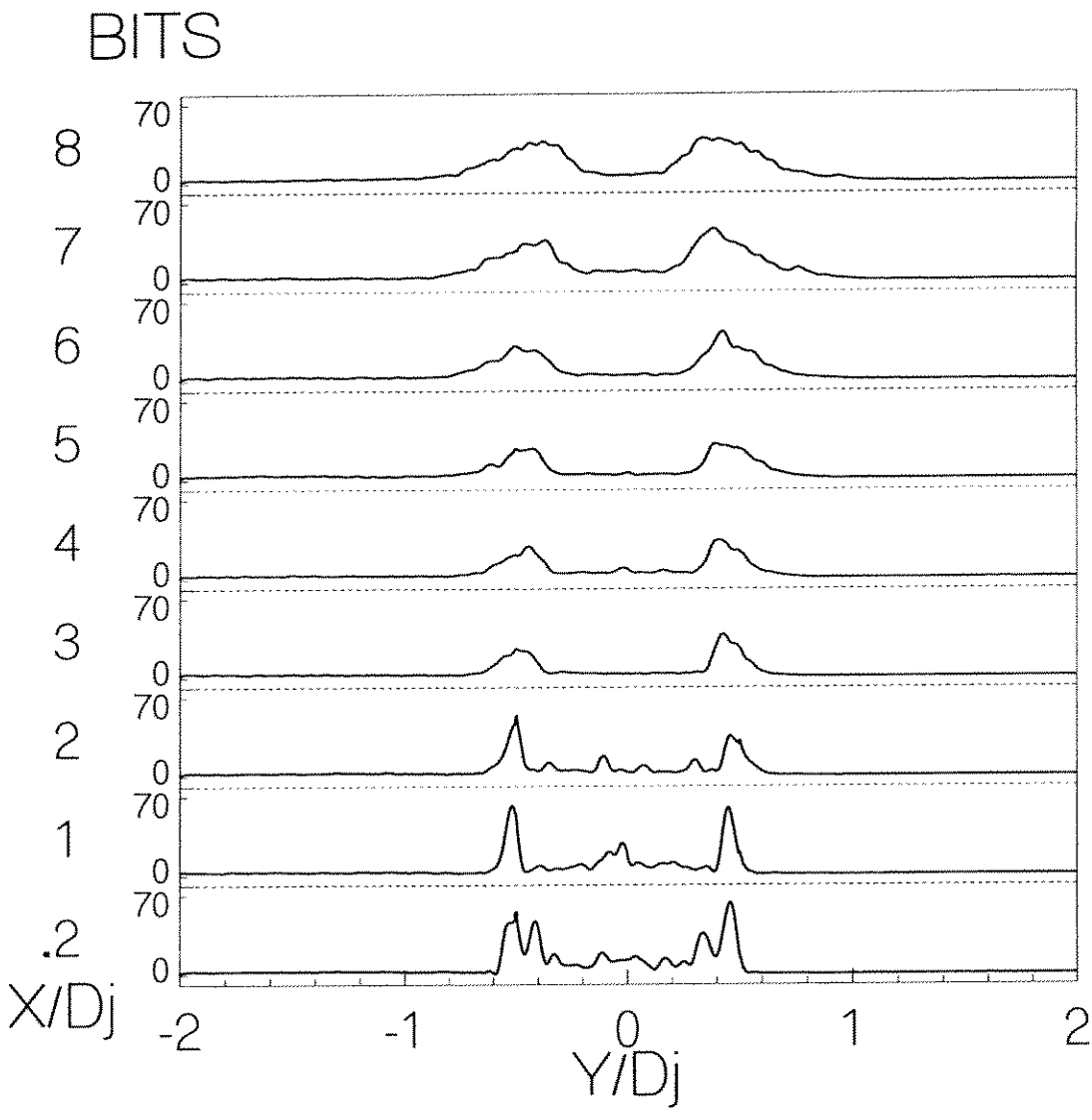

Figure E.4: RMS Pitot Pressures, M 3.0 N2, 534 psia, 0 to 8 diameters

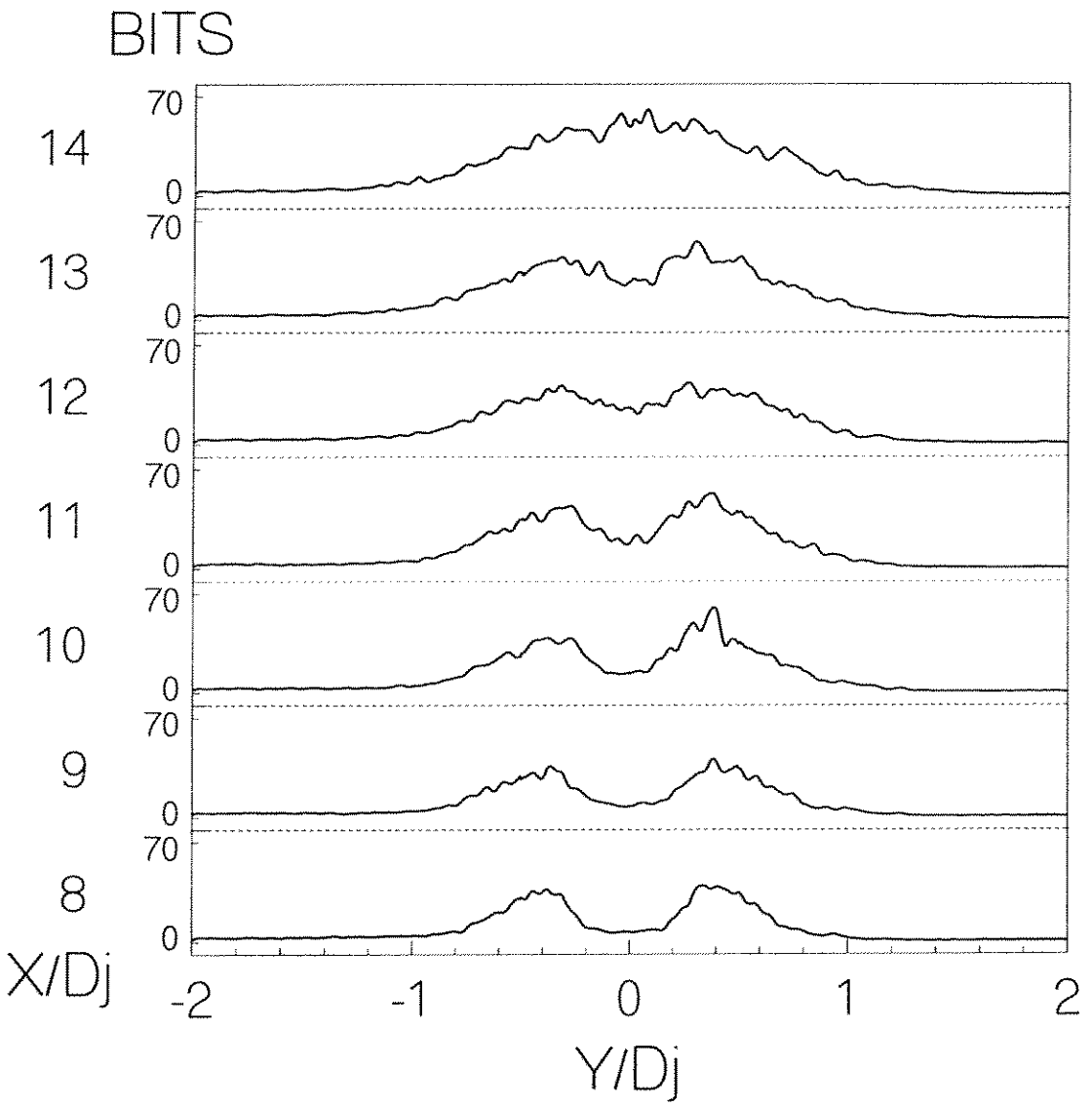

Figure E.5: RMS Pitot Pressures, M 3.0 N2, 534 psia, 8 to 14 diameters

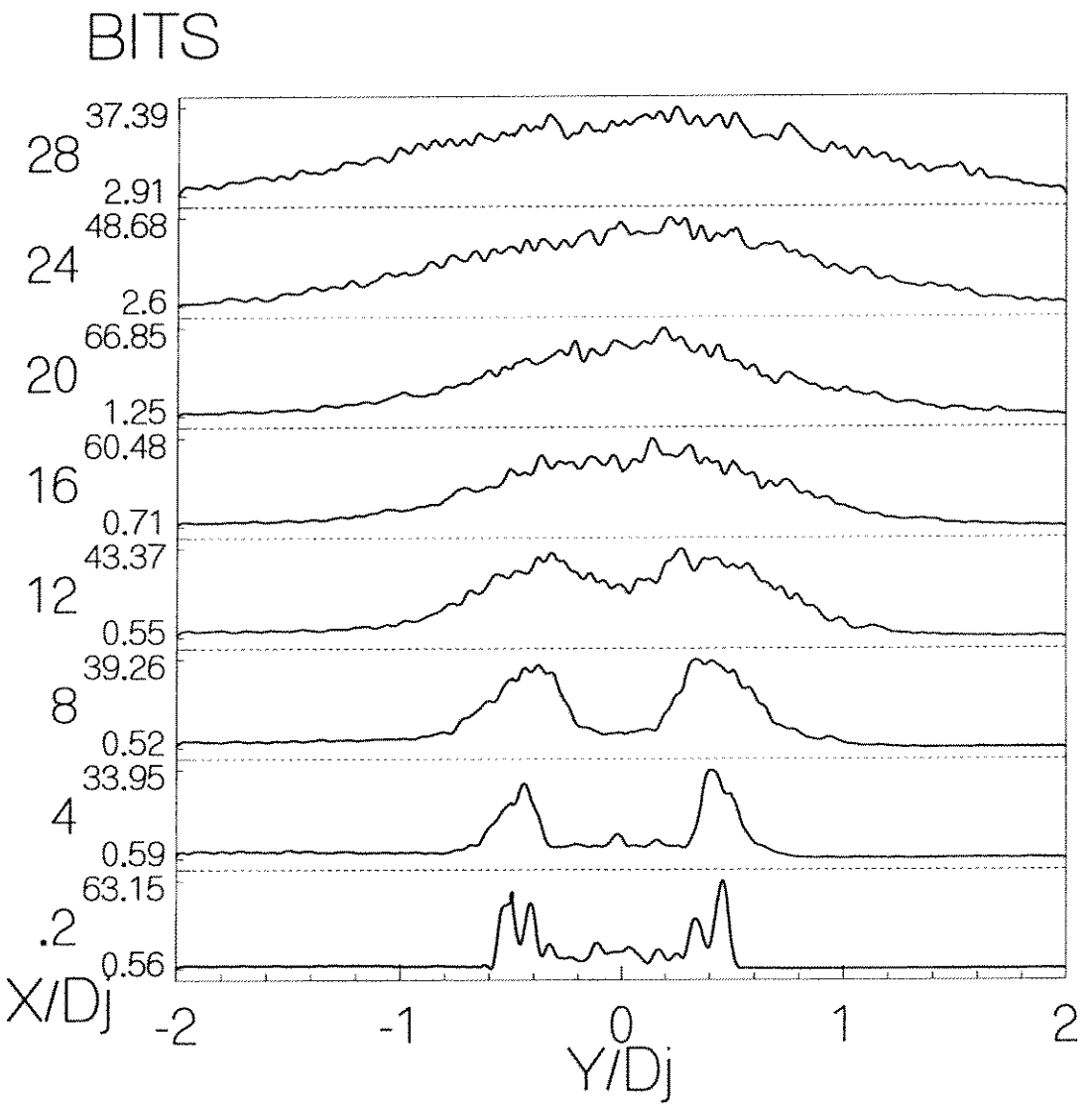

Figure E.6: RMS Pitot Pressures, M 3.0 N2, 534 psia, 0 to 28 diameters

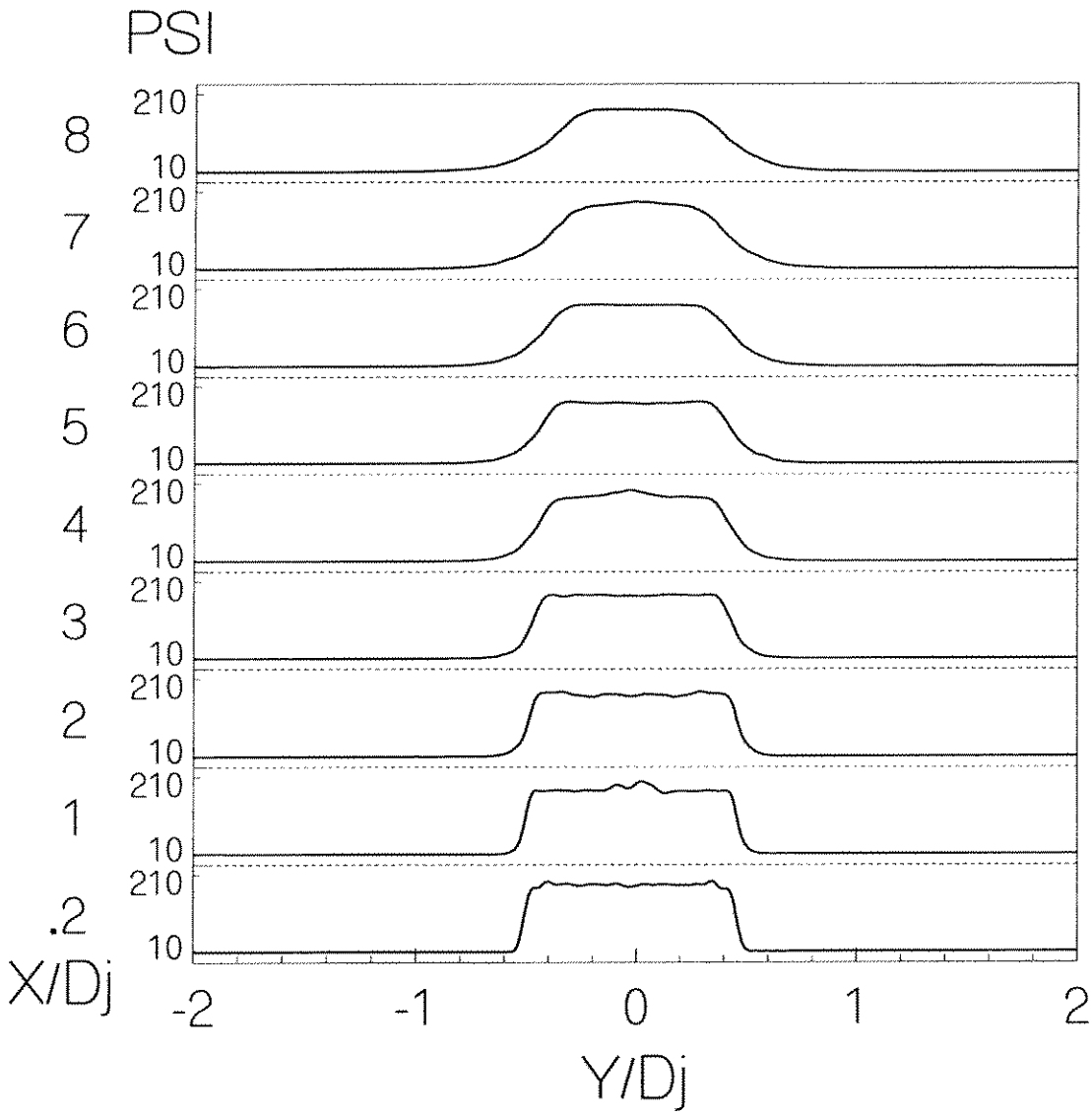

Figure E.7: Mean Pitot Pressures, M 3.0 N2, 491 psia, 0 to 8 diameters

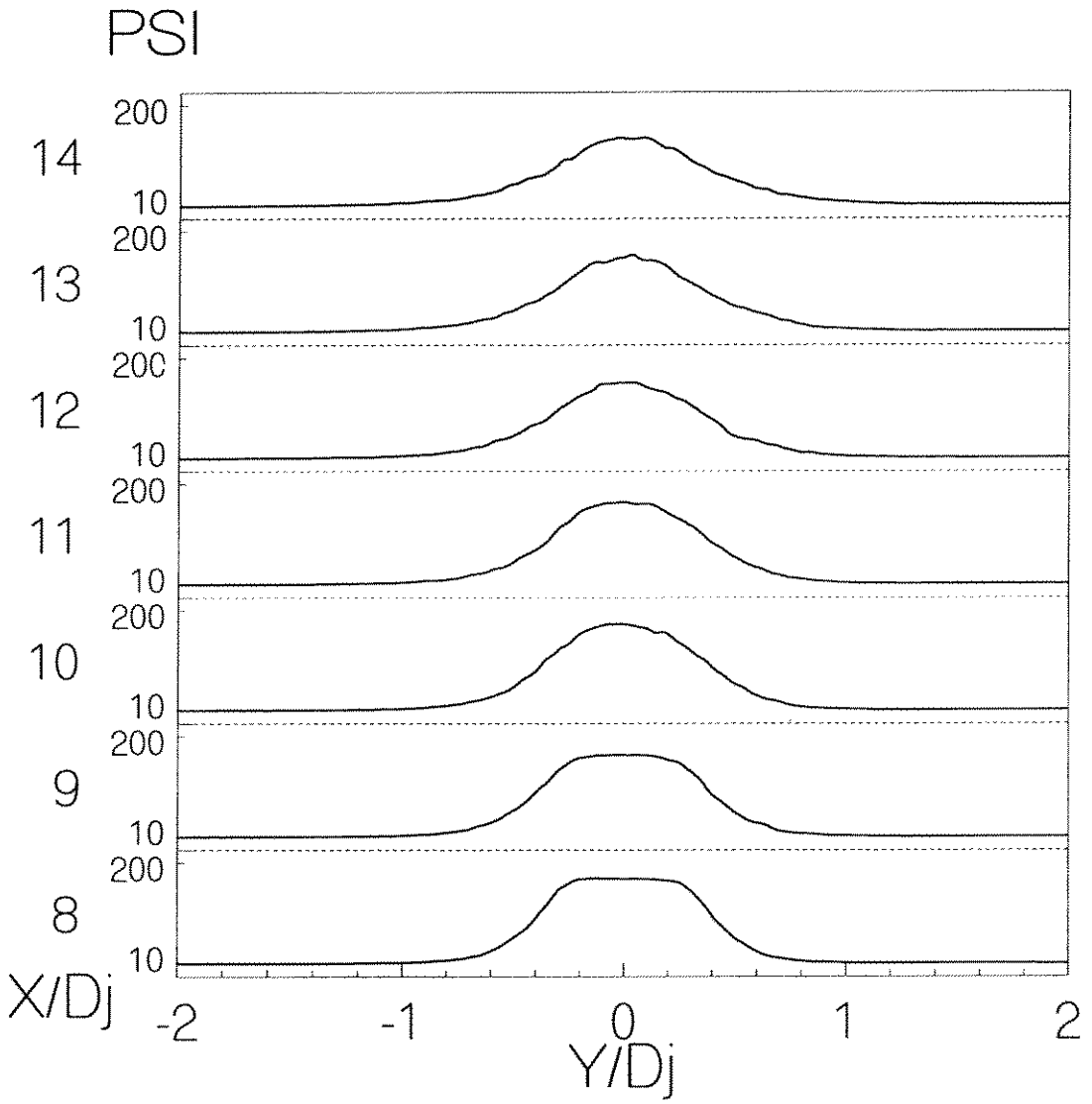

Figure E.8: Mean Pitot Pressures, M 3.0 N2, 491 psia, 8 to 14 diameters

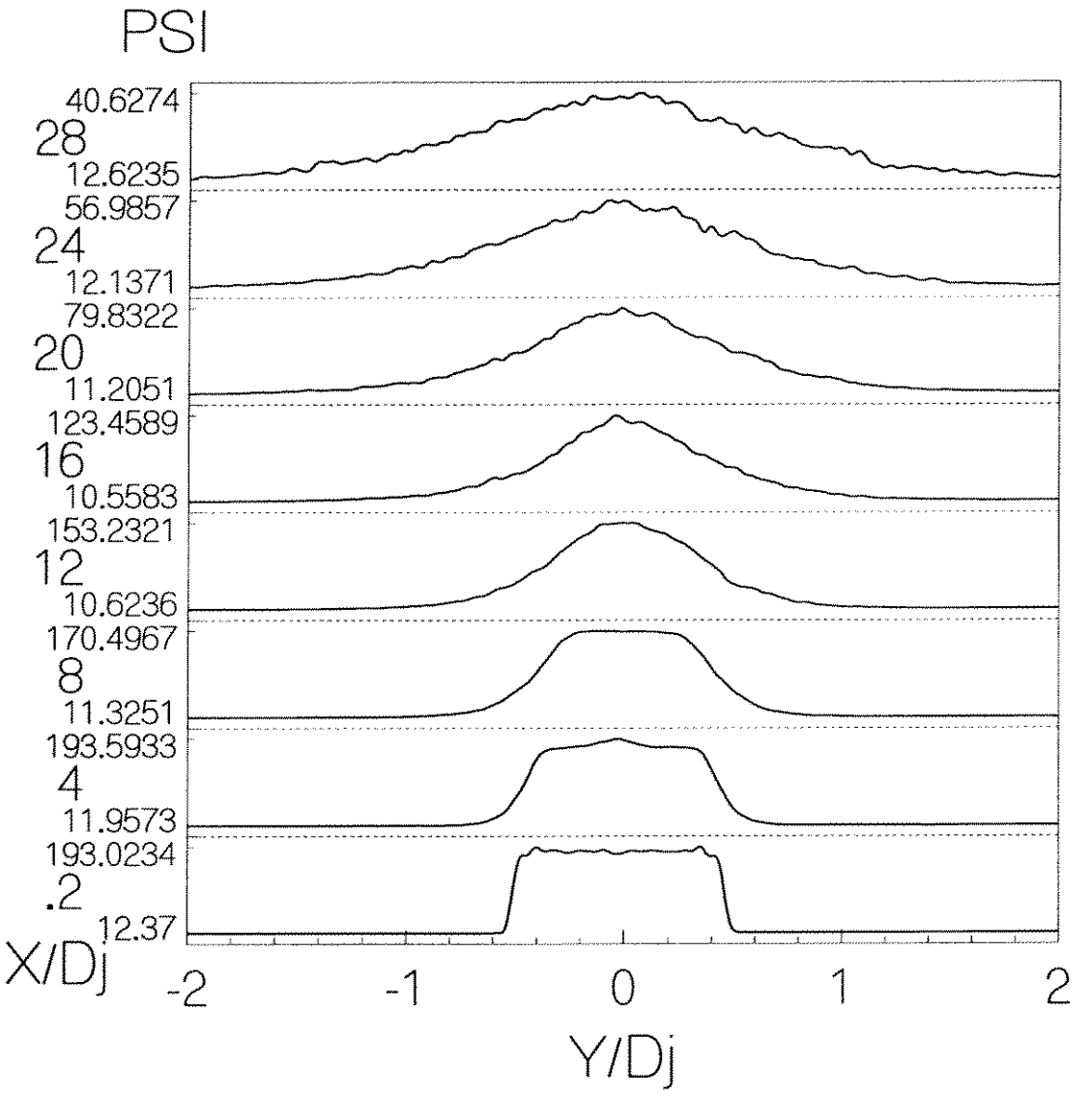

Figure E.9: Mean Pitot Pressures, M 3.0 N2, 491 psia, 0 to 28 diameters

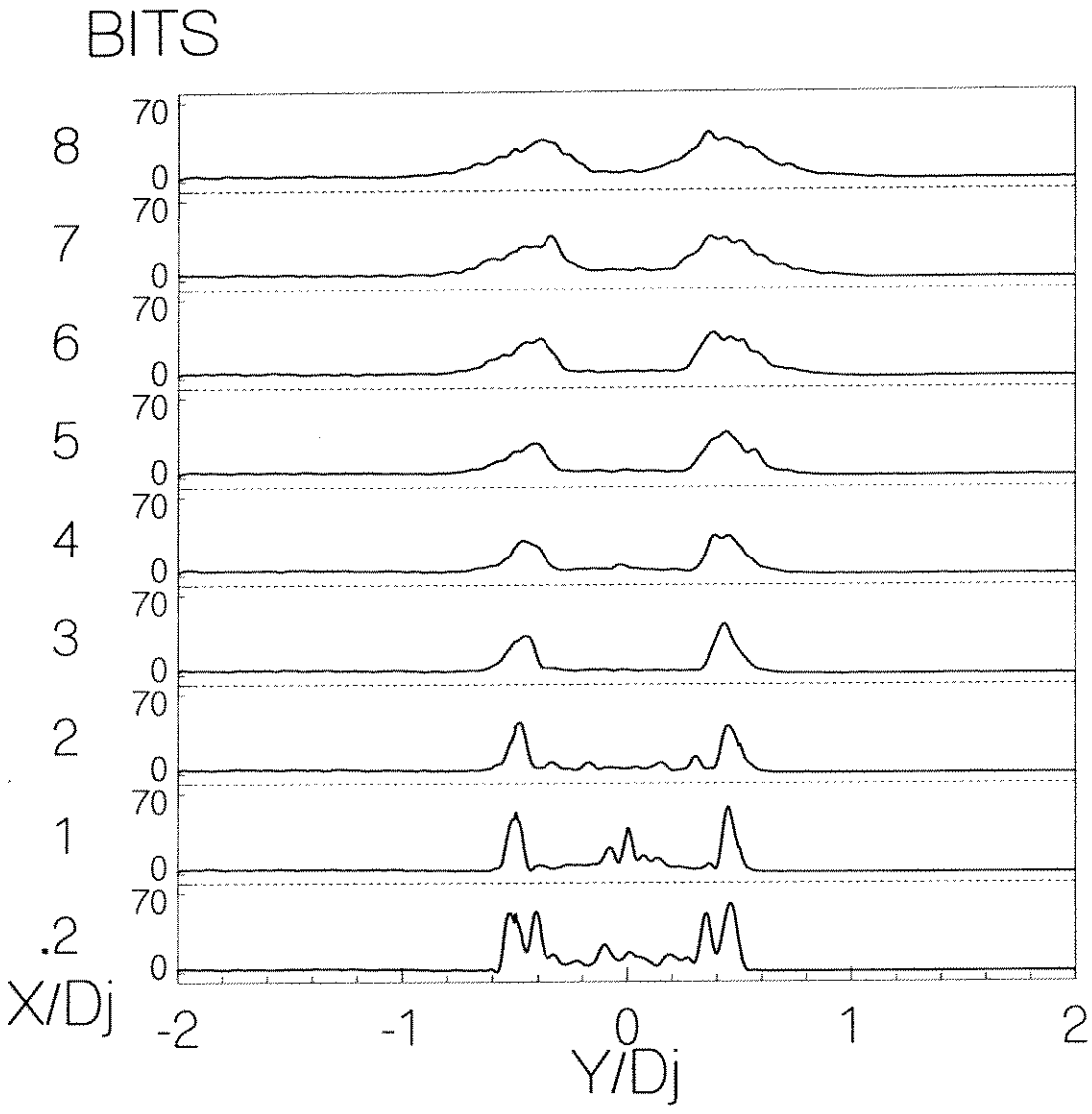

Figure E.10: RMS Pitot Pressures, M 3.0 N2, 491 psia, 0 to 8 diameters

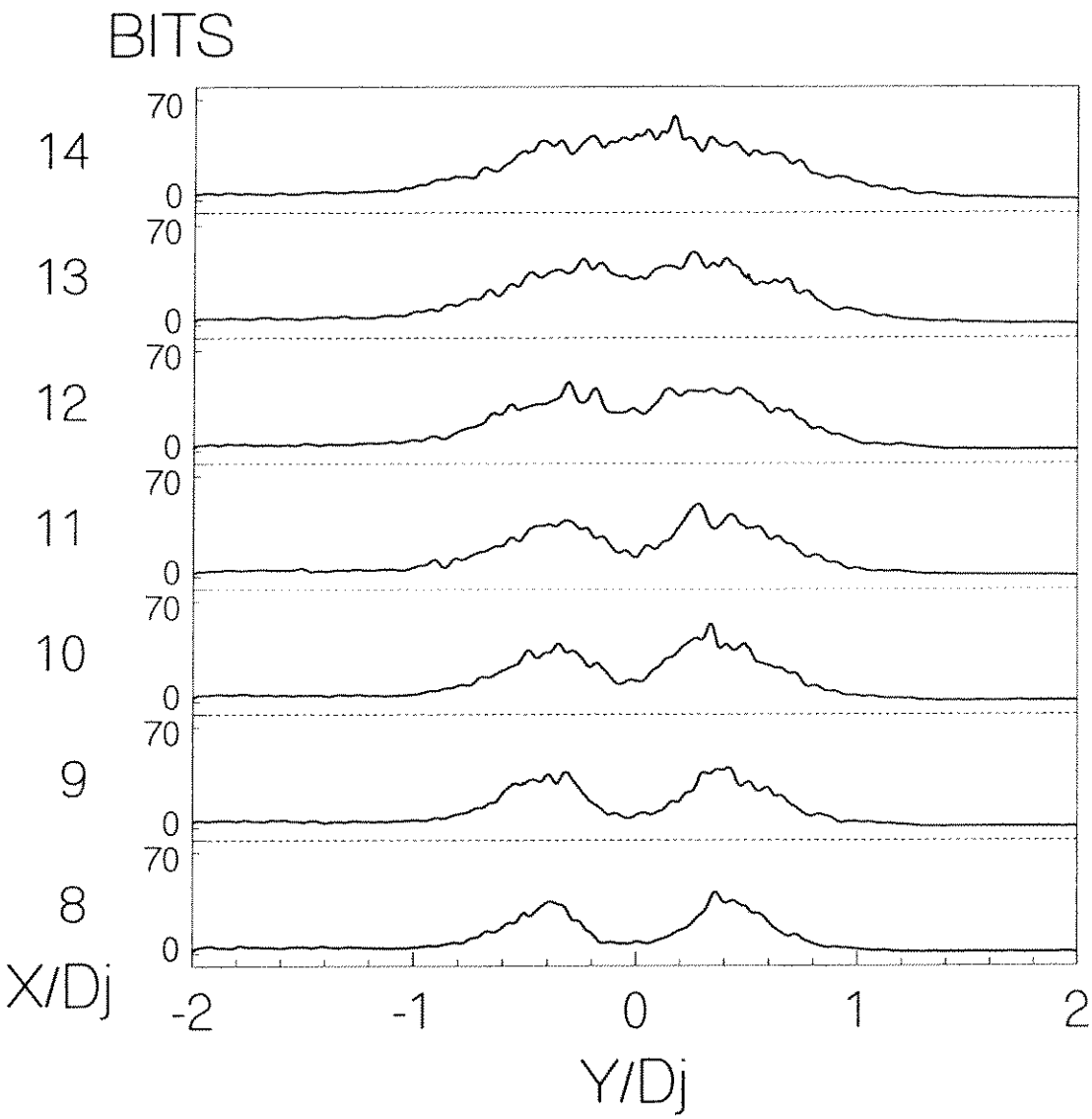

Figure E.11: RMS Pitot Pressures, M 3.0 N2, 491 psia, 8 to 14 diameters

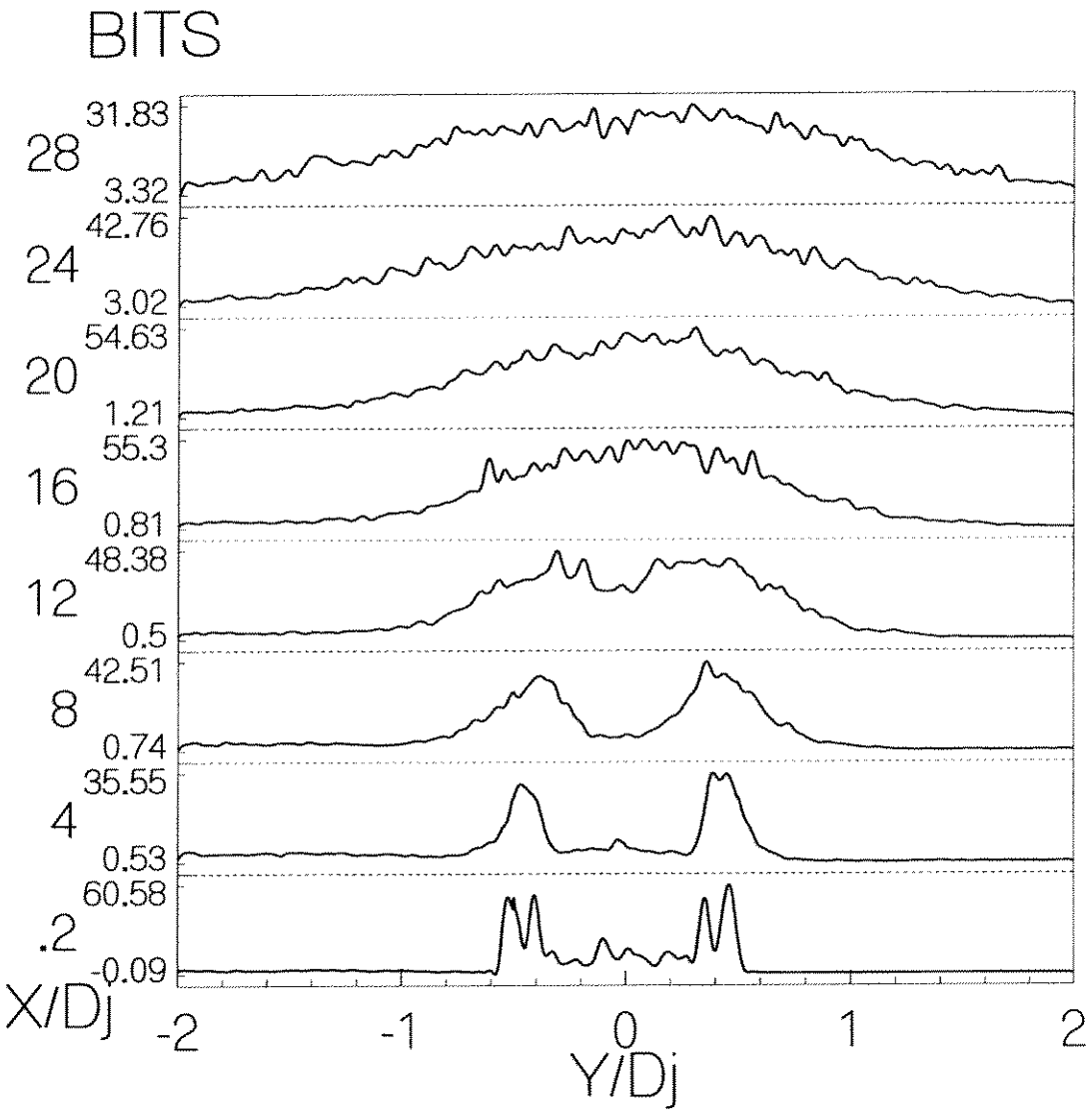

Figure E.12: RMS Pitot Pressures, M 3.0 N2, 491 psia, 0 to 28 diameters

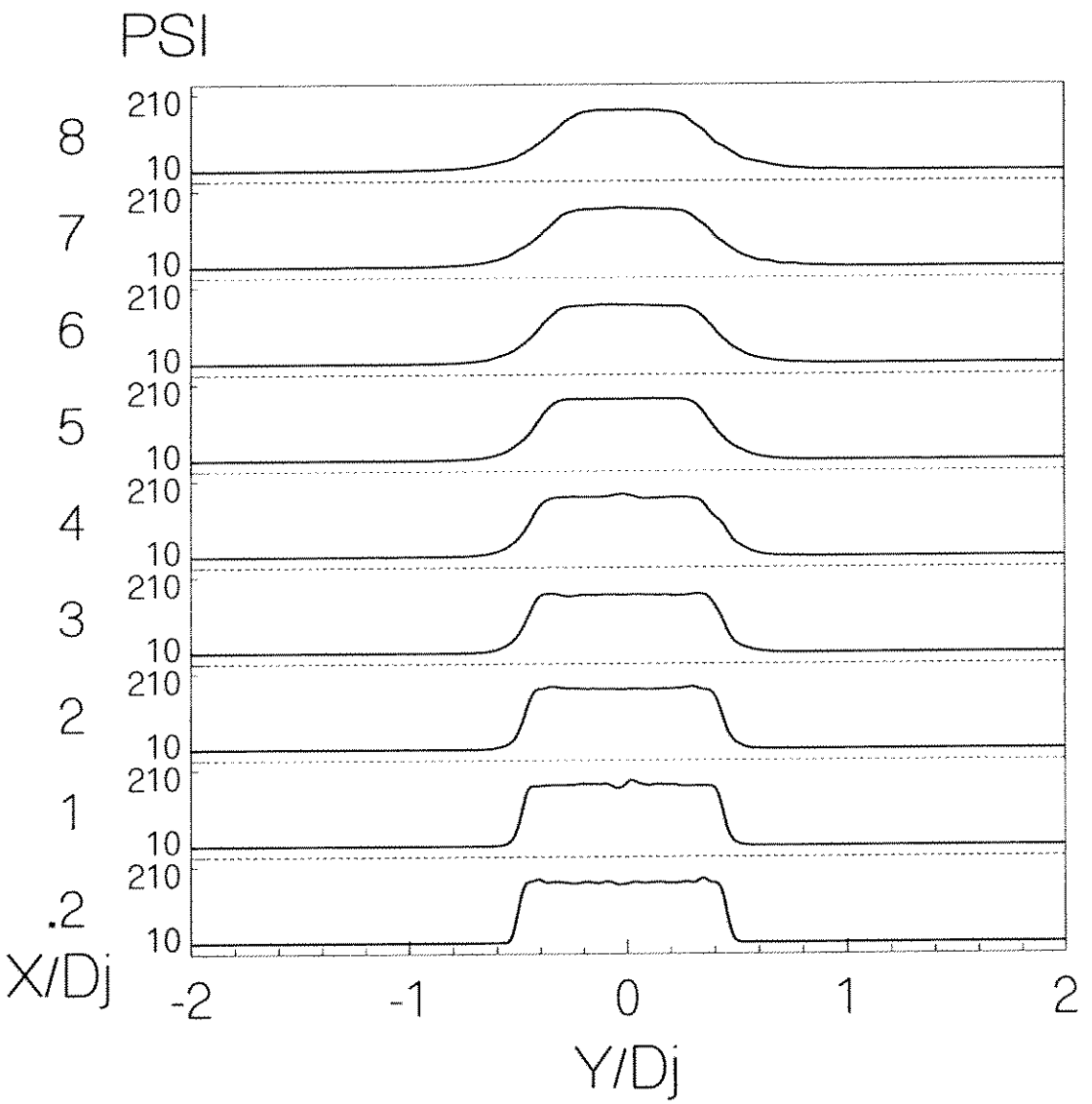

Figure E.13: Mean Pitot Pressures, M 3.0 N2, 454 psia, 0 to 8 diameters

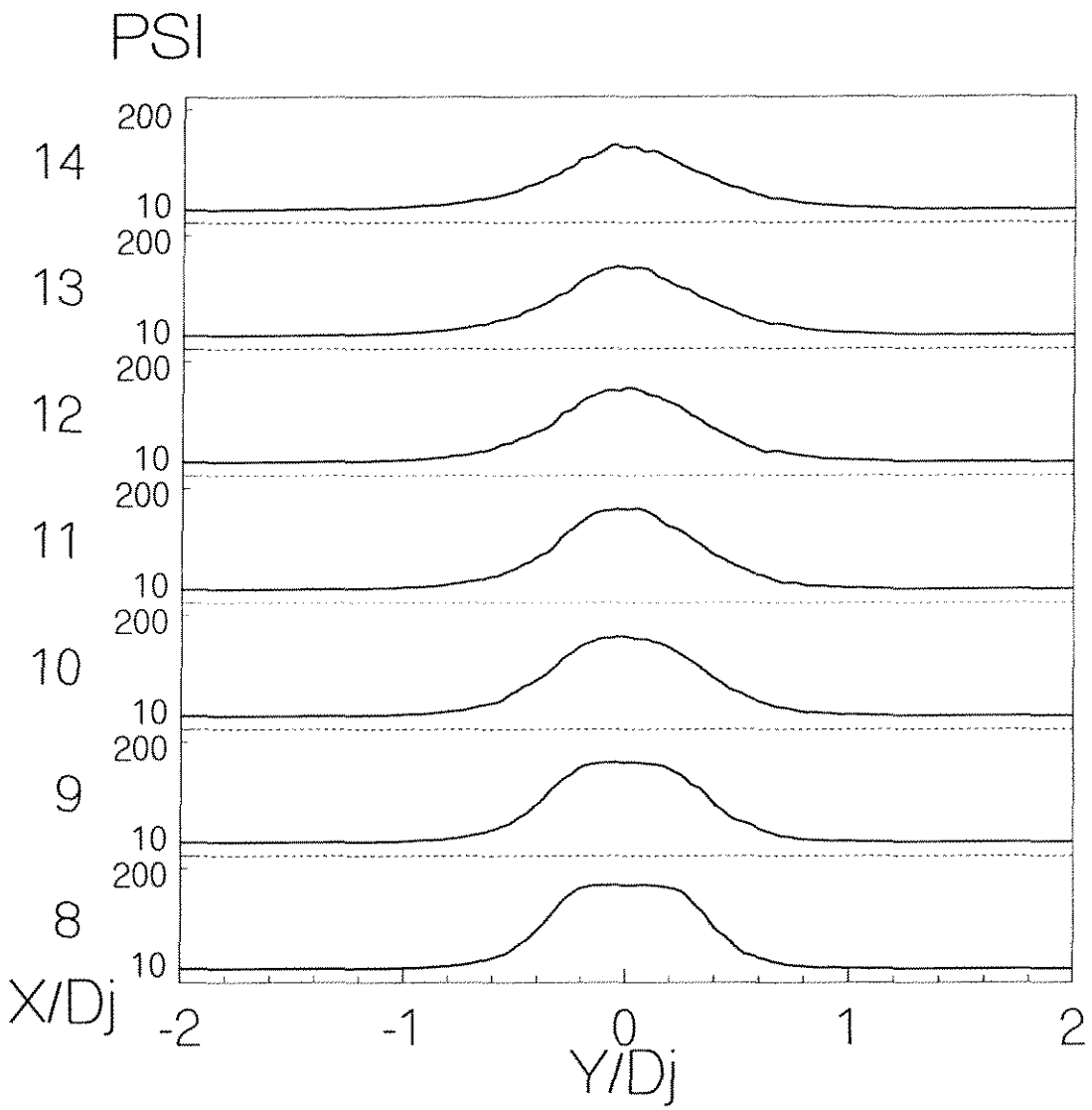

Figure E.14: Mean Pitot Pressures, M 3.0 N2, 454 psia, 8 to 14 diameters

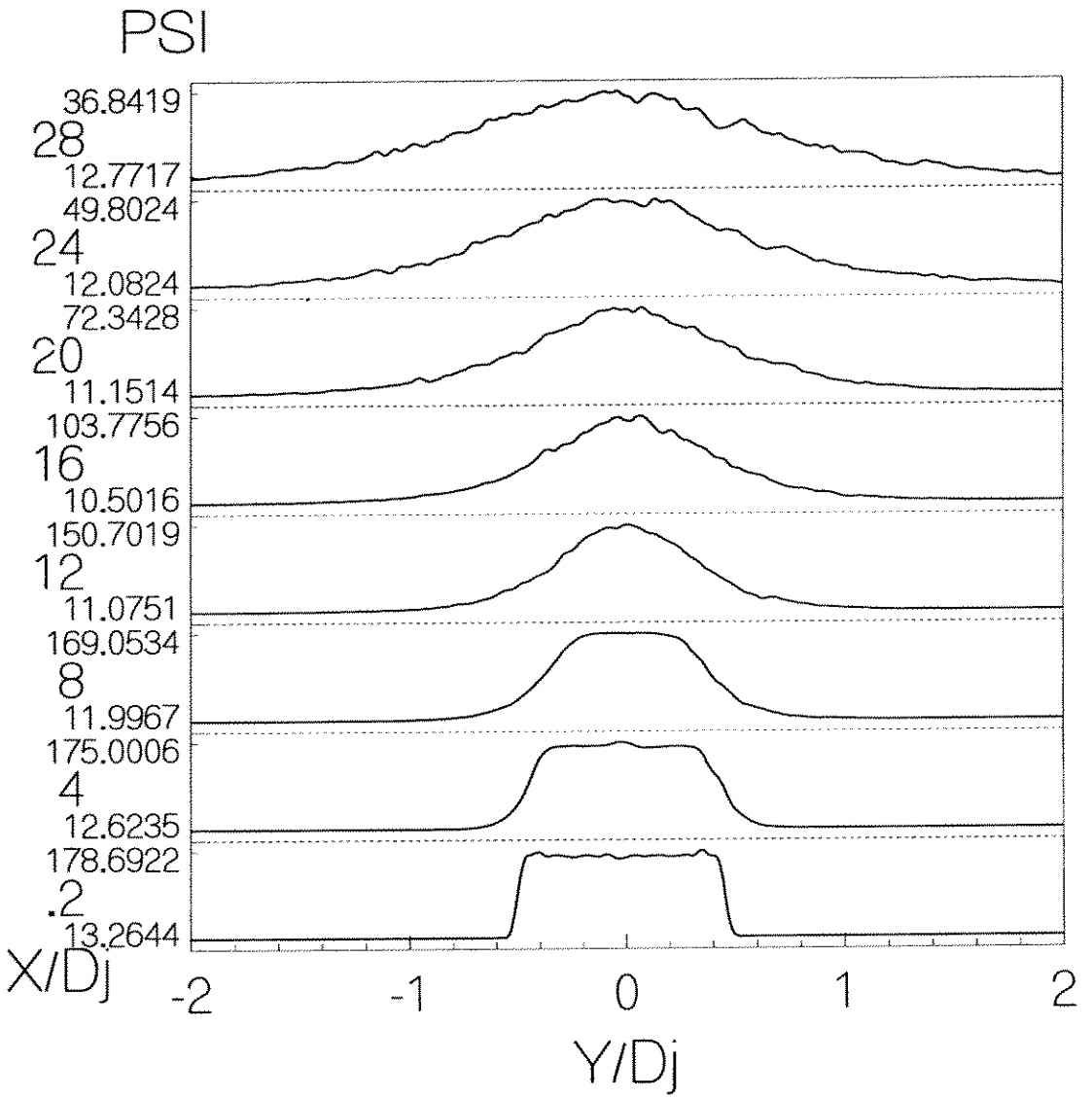

Figure E.15: Mean Pitot Pressures, M 3.0 N2, 454 psia, 0 to 28 diameters

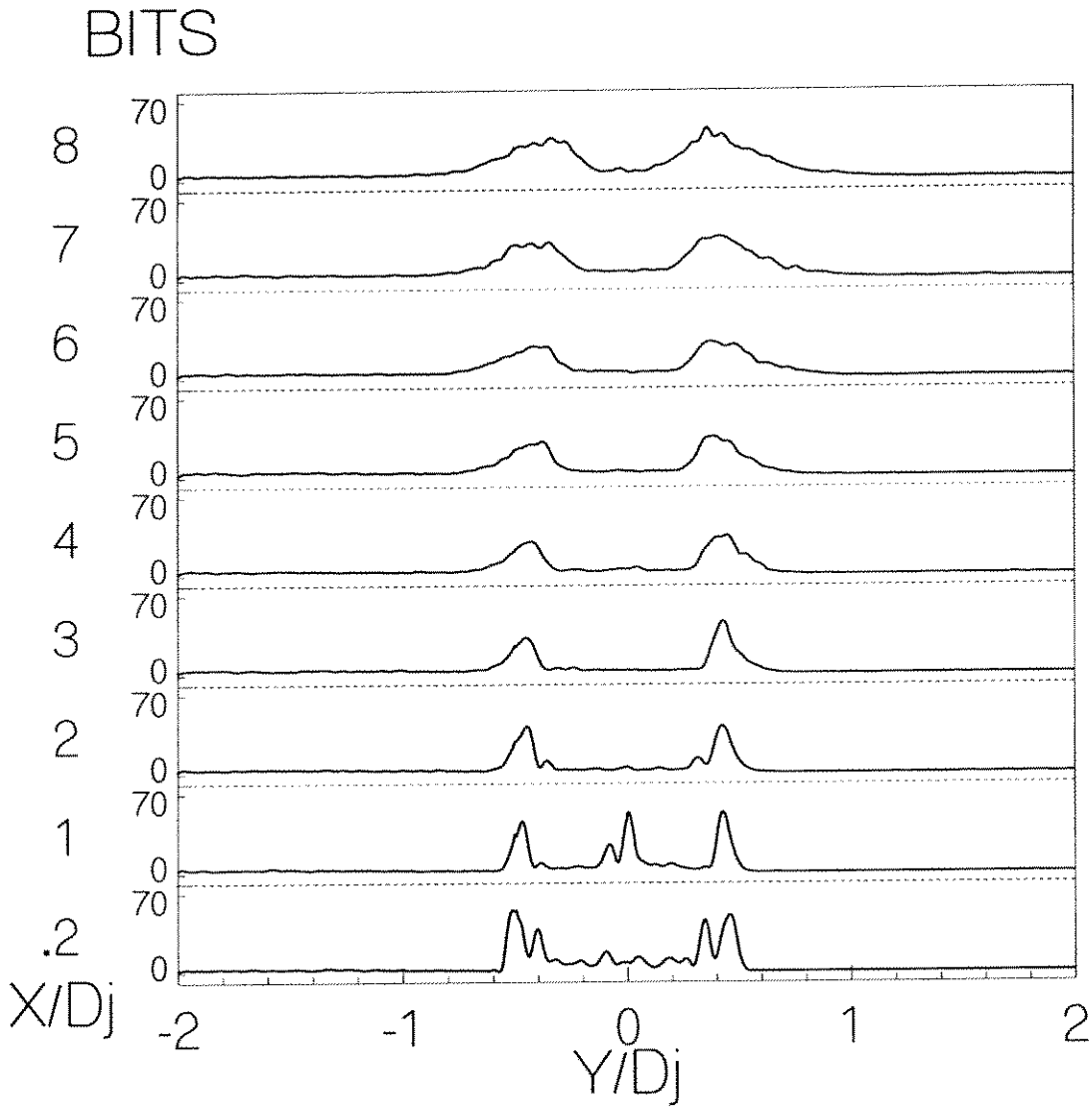

Figure E.16: RMS Pitot Pressures, M 3.0 N2, 454 psia, 0 to 8 diameters

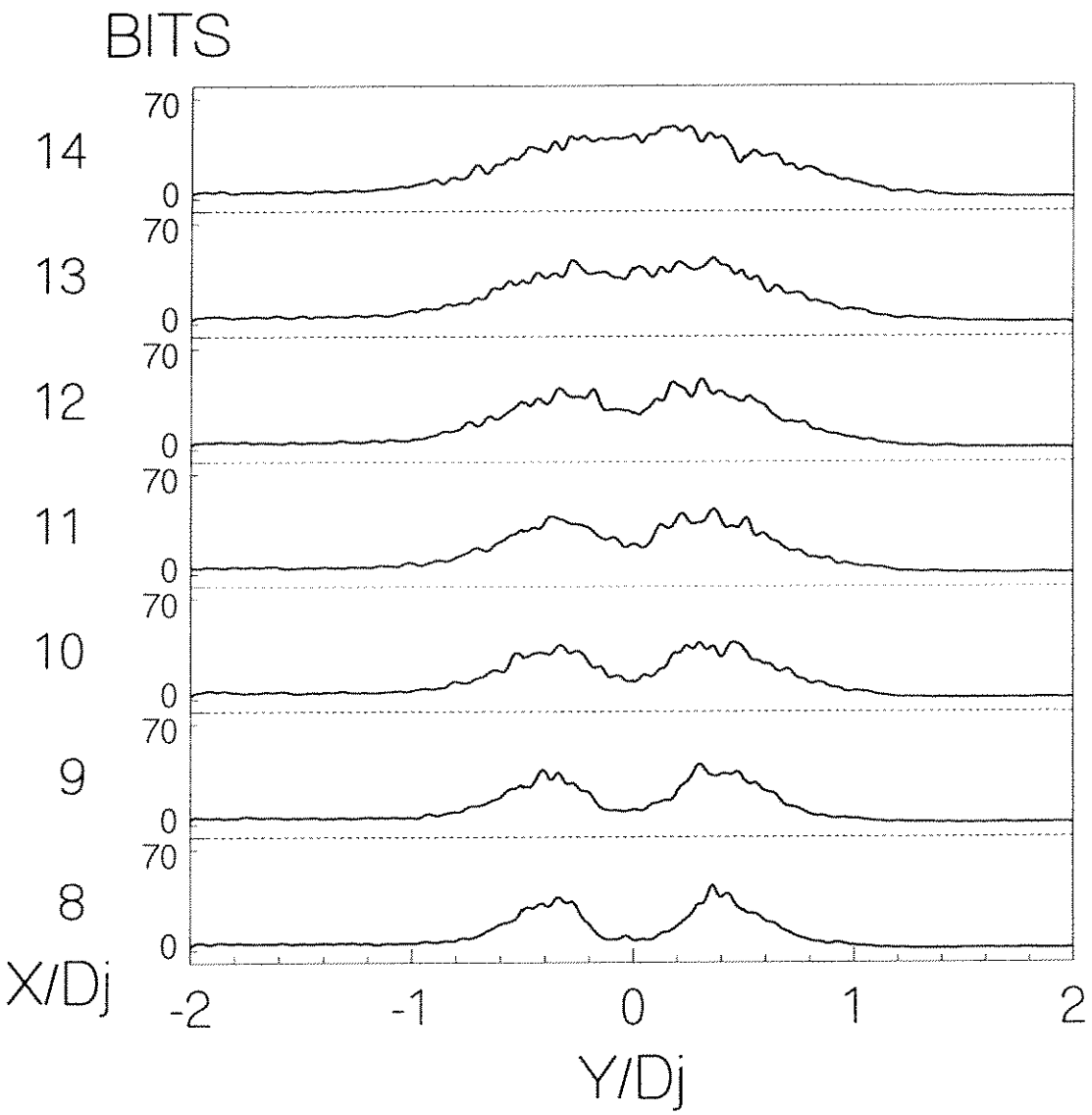

Figure E.17: RMS Pitot Pressures, M 3.0 N2, 454 psia, 8 to 14 diameters

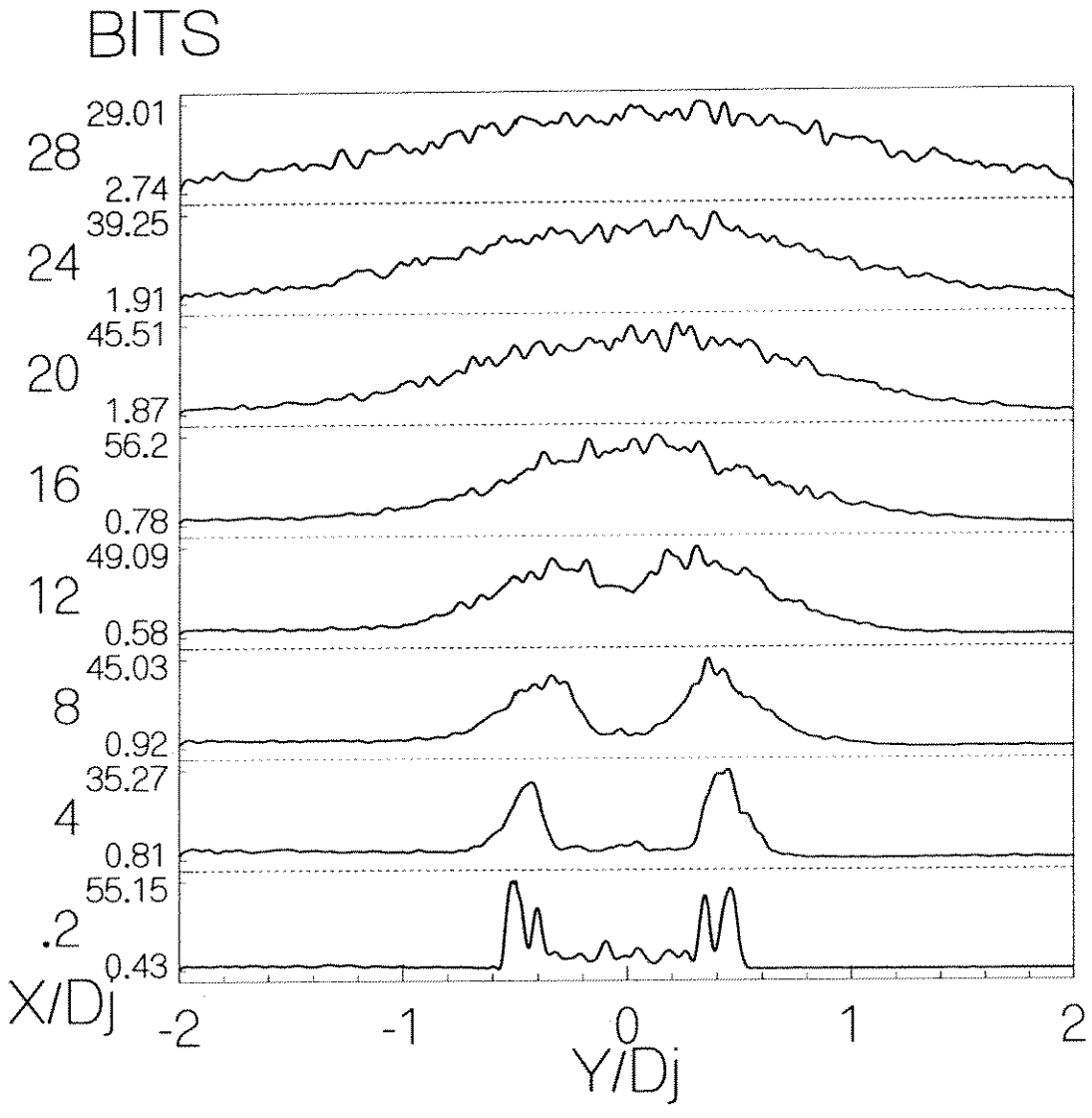

Figure E.18: RMS Pitot Pressures, M 3.0 N2, 454 psia, 0 to 28 diameters

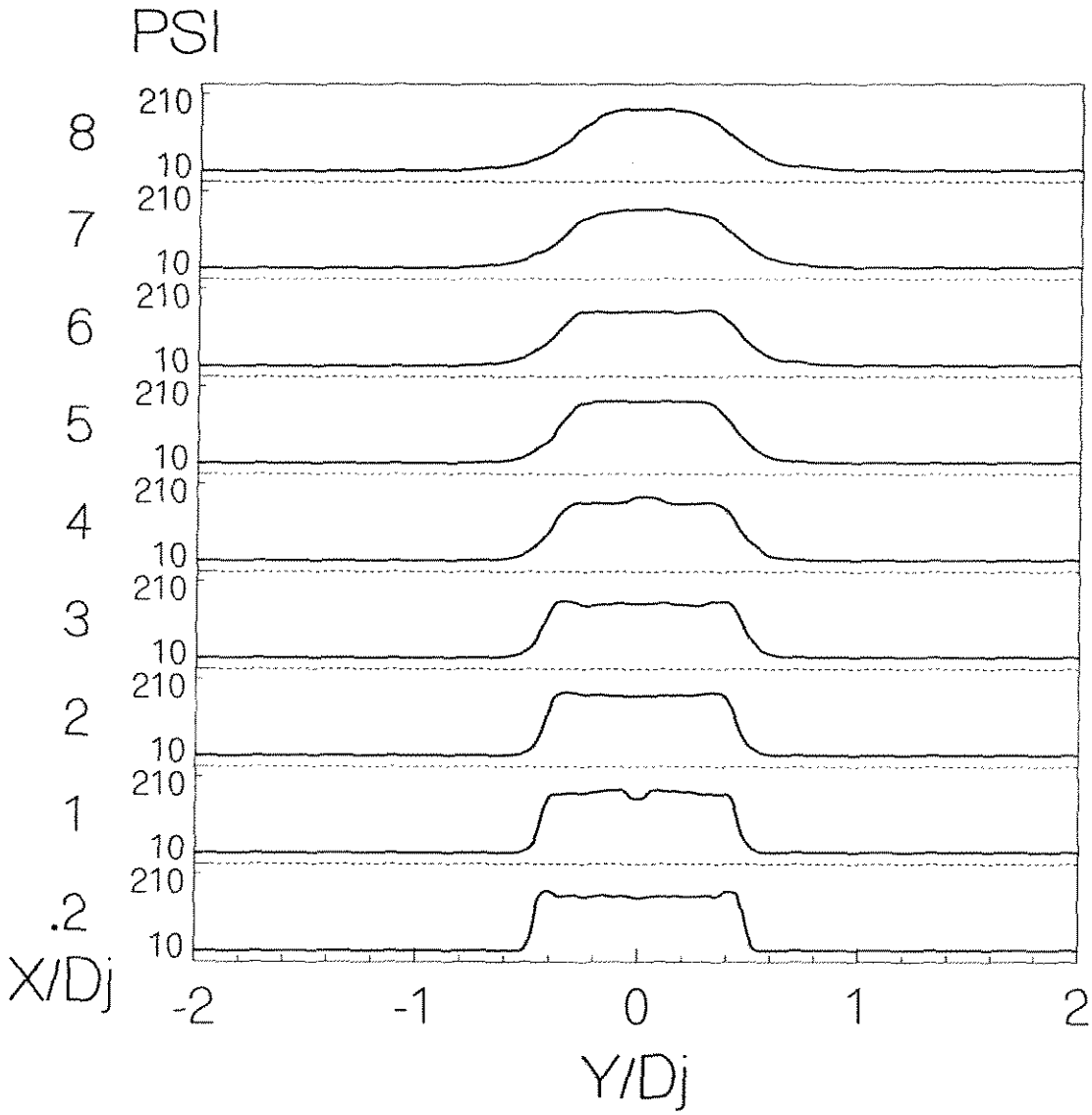

Figure E.19: Mean Pitot Pressures, M 3.0 N2, 417 psia, 0 to 8 diameters

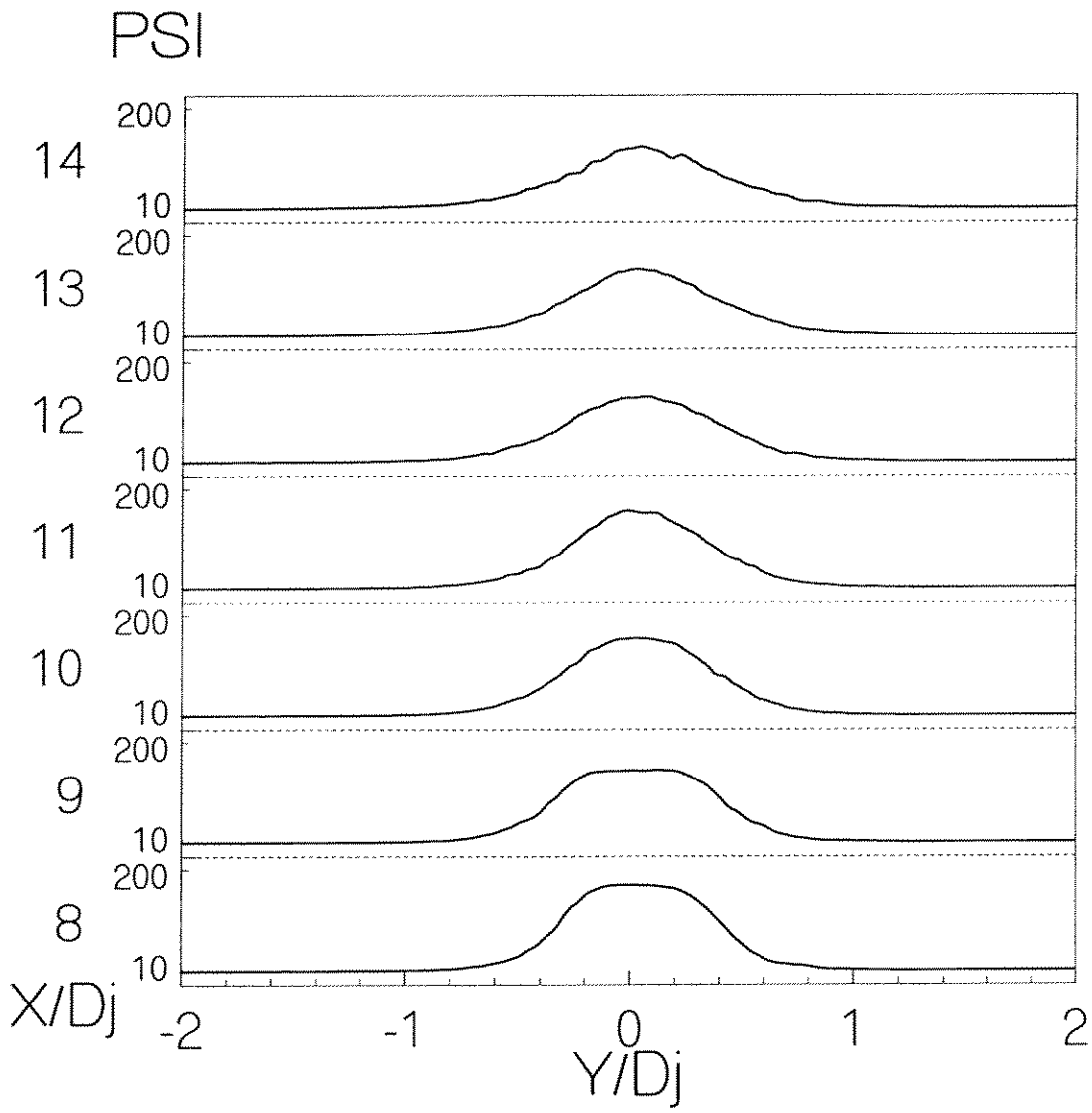

Figure E.20: Mean Pitot Pressures, M 3.0 N2, 417 psia, 8 to 14 diameters

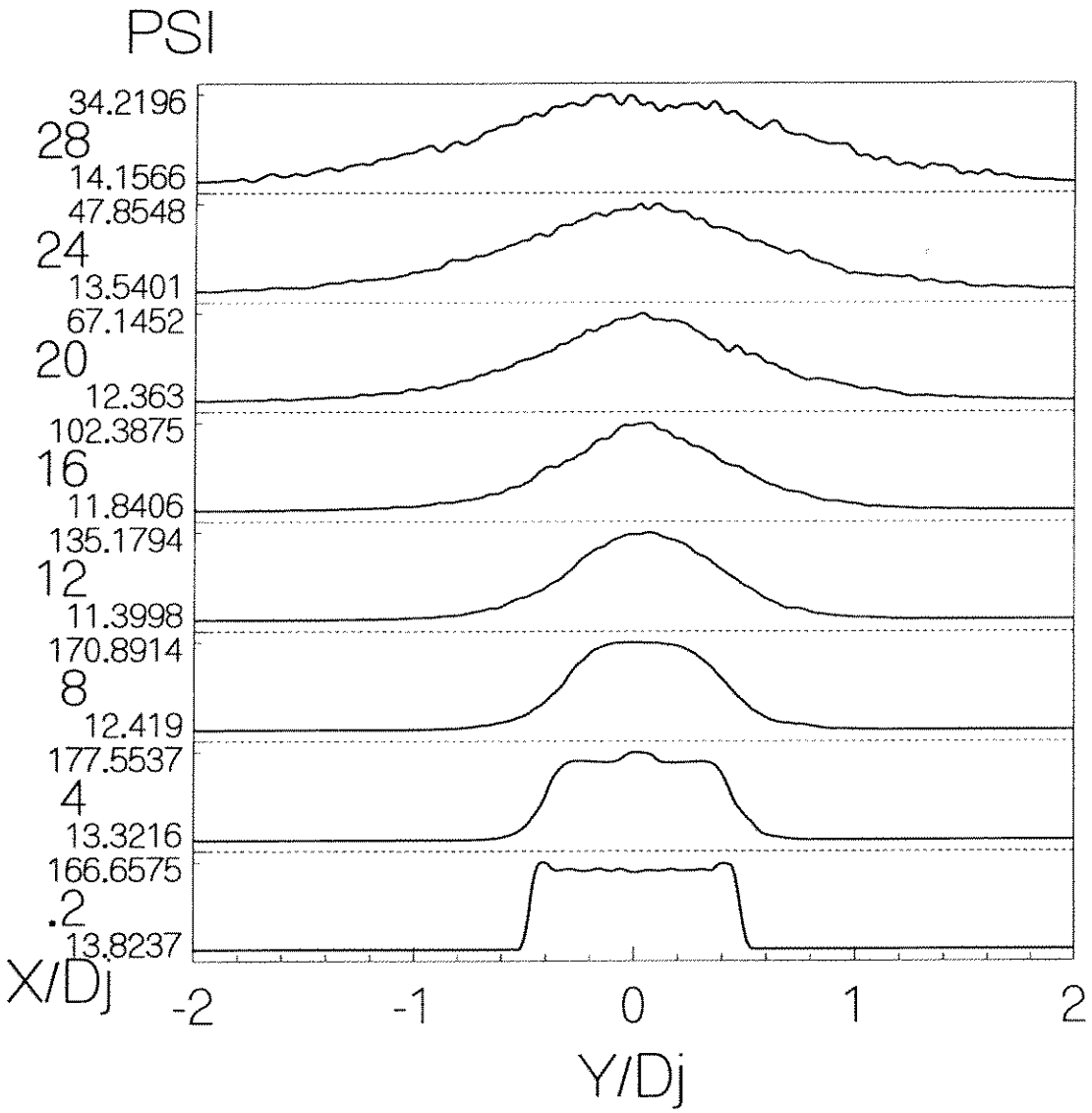

Figure E.21: Mean Pitot Pressures, M 3.0 N2, 417 psia, 0 to 28 diameters

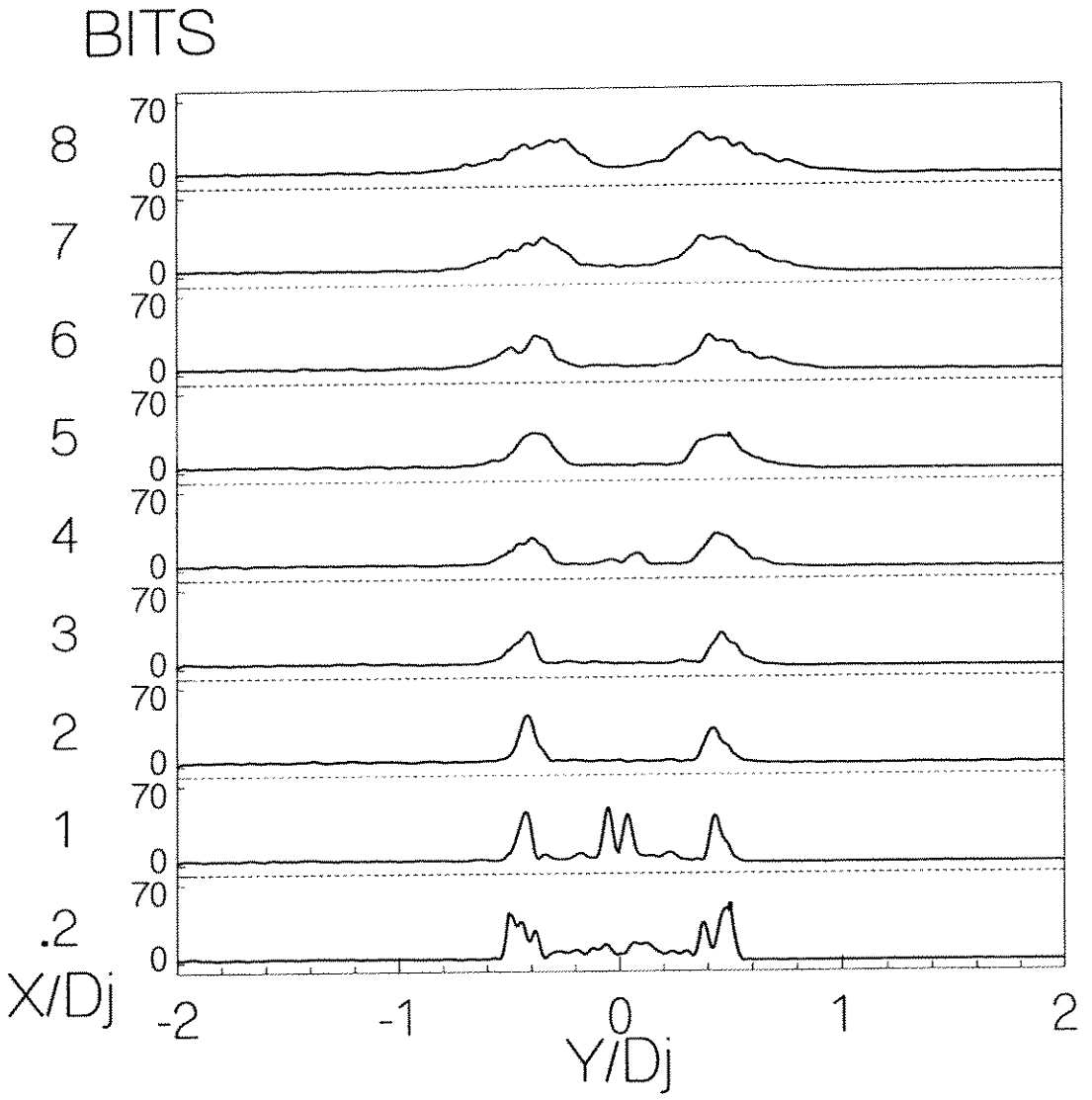

Figure E.22: RMS Pitot Pressures, M 3.0 N2, 417 psia, 0 to 8 diameters

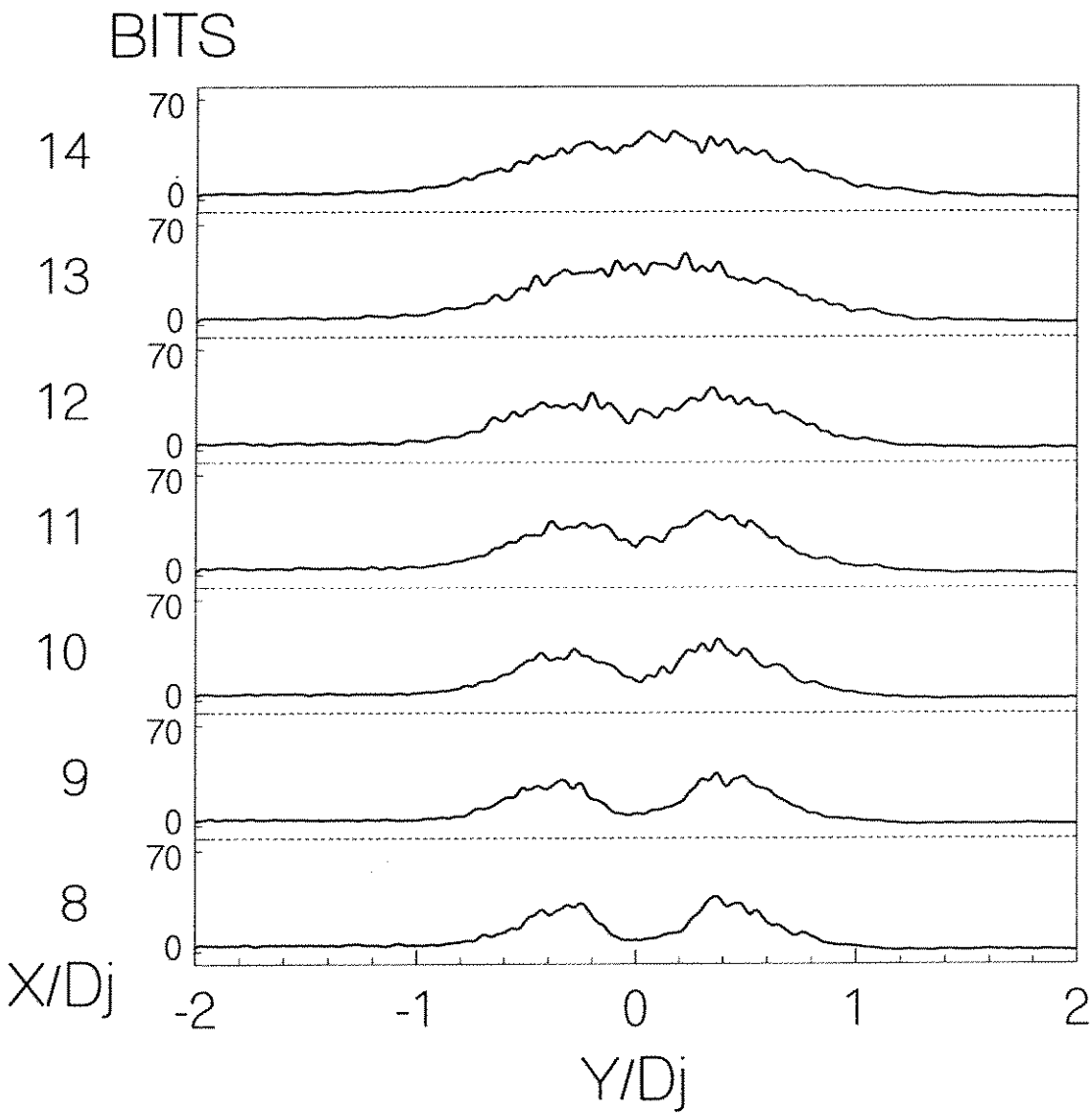

Figure E.23: RMS Pitot Pressures, M 3.0 N2, 417 psia, 8 to 14 diameters

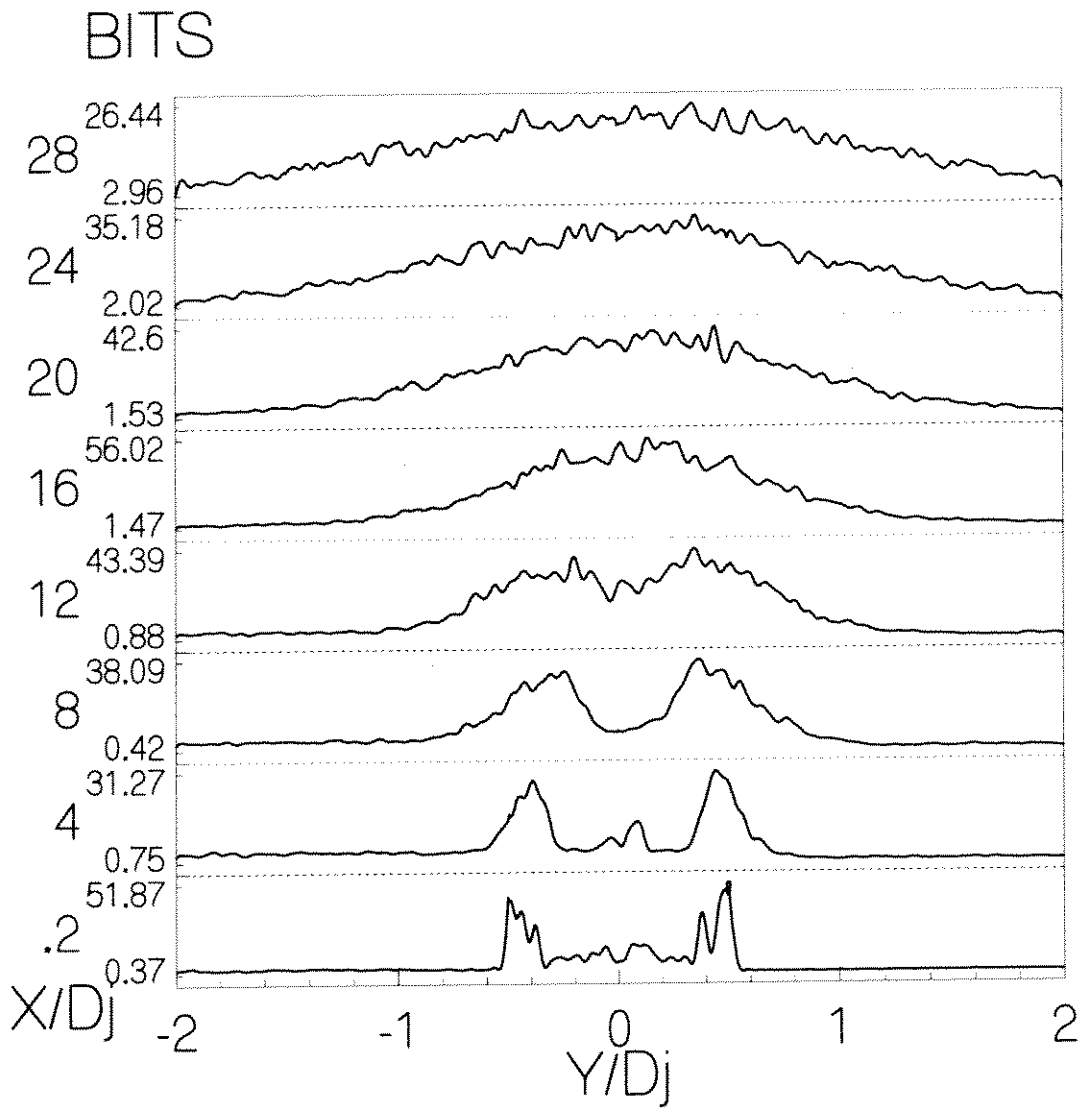

Figure E.24: RMS Pitot Pressures, M 3.0 N2, 417 psia, 0 to 28 diameters

Bibliography

[1] S. Birch and J. Eggers. A critical review of the experimental data for developed free turbulent shear layers. SP 321, NASA, 1972.

[2] G. Brown and A. Roshko. On density effects and large structures in turbulent mixing layers. *Journal of Fluid Mechanics*, 64:775–781, 1974.

[3] P. Bradshaw. The effect of the initial condition on the development of a free shear layer. *Journal of Fluid Mechanics*, 26(2):225–236, 1966.

[4] P.E. Dimotakis. Turbulent free shear layer mixing and combustion. In *High-Speed Flight Propulsion Systems*, volume 137 of *Progress in Astronautics and Aeronautics*, pages 265–340. AIAA, 1991.

[5] I. Tombach. *Velocity Measurements with a New Probe in Inhomogeneuos Turbulent Jets.* PhD thesis, California Institute of Technology, 1969.

[6] D. Papamoschou. *An Experimental Investigation of Heterogeneous Compressible Shear Layers.* PhD thesis, California Institute of Technology, 1986.

[7] G.L. Brown. Entrainment and large structures in turbulent mixing layers. In *Fifth Australian Conference on Hydraulics and Fluid Mechanics, University of Canterbury, Cristchurch, New Zealand*, 1974.

[8] J.H. Konrad. *An Experimental Investigation of Mixing in Two-Dimensional Turbulent Shear Flows with Applications to Diffusion-Limited Chemical Reactions.* PhD thesis, California Institute of Technology, 1976.

[9] P.E. Dimotakis. Two-dimensional shear-layer entrainment. *AIAA J*, 24(11):1791–1796, 1986.

[10] D.W. Bogdanoff. Compressibility effects in turbulent shear layers. *AIAA J*, 21(6):926–927, 1983.

[11] W. Forstall and A. Shapiro. Momentum and mass transfer in coaxial gas jets. *Journal of Applied Mechanics*, 17(4):399–408, 1950.

[12] G.N. Abramovich. *The Theory of Turbulent Jets.* M.I.T. Press, Cambridge, MA, 1963.

[13] S. Corrsin and M.S. Uberoi. Further experiments on the flow and heat transfer in a heated turbulent air jet. TN 1865, NACA, 1949.

[14] W.R. Keagy and A.E. Weller. A study of freely expanding inhomogeneous jets. In *Proceedings of the Heat Transfer and Fluid Mechanics Institute*, pages 89–98, Berkeley, CA, 1949.

[15] M.W. Thring and M.P. Newby. Combustion length of enclosed turbulent flames. In *Fourth Symposium (International) on Combustion*, pages 789–796, Pittsburgh, PA, 1953. The Standing Committee on Combustion.

[16] W.M. Pitts. Effects of global density ratio on the centerline mixing behavior of axisymmetric turbulent jets. *Experiments in Fluids*, 11:125–134, 1991.

[17] W.M. Pitts. Reynolds number effects on the mixing behavior of axisymmetric turbulent jets. *Experiments in Fluids*, 11:135–141, 1991.

[18] G.N. Abramovich et al. An investigation of the turbulent jets of different gases in a general stream. *Astronautica Acta*, 14:229–240, 1969.

[19] N.H. Johannesen. The mixing of free axially symmetrical jets of mach number 1.40. R&M 3291, A.R.C., 1957.

[20] N.H. Johannesen. Further results on the mixing of free axially symmetrical jets of mach number 1.40. R&M 3292, A.R.C., 1959.

[21] W.R. Warren. An analytical and experimental study of compressible free jets. Aero Report 381, Princeton University, 1959.

[22] W.R. Warren. The static pressure variation in compressible free jets. *Journal of Aeronautical Sciences*, 22:205–206, 1955.

[23] R. Maydew and J. Reed. Turbulent mixing of axisymmetric compressible jets (in the half jet region) with quiescent air. Technical Report SC-4764, Sandia Corporation, 1963.

[24] L. Crane. The laminar and turbulent mixing of jets of compressible fluid. *Journal of Fluid Mechanics*, 3, 1957.

[25] J.M. Eggers. Velocity profiles and eddy viscosity distributions downstream of a mach 2.22 nozzle exhausting to quiescent air. TN D 3601, N.A.S.A., 1966.

[26] J.C. Lau, P.J. Morris, and M.J. Fisher. Measurements in subsonic and supersonic free jets using a laser velocimiter. *Journal of Fluid Mechanics*, 93:1–27, 1979.

[27] V. Zakkay, E. Krause, and S. Woo. Turbulent transport properties for axisymmetric heterogeneous mixing. Technical Report ARL-64-103, U.S.A.F., 1964.

[28] R.P. Rhodes. Analysis of non-reactive supersonic turbulent mixing data. AFRPL-TR 82-52, USAF, 1983.

[29] C. Padova. Non-reacting turbulent mixing experiments. Report 6632-A-3, Calspan, 1983.

[30] E. Mollo-Christensen. Some aspects of free shear-layer instability and sound emission. Report 260, N.A.T.O., 1960.

[31] E. Mollo-Christensen. Jet noise and shear flow instability seen from an experimenter's point of view. *Journal of Applied Mechanics*, 34:1–7, 1967.

[32] J. Ffowcs Williams. The noise from turbulence convected at high speed. *Transactions of the Royal Society of London A.*, 255:459–503, 1963.

[33] K. Bishop, J. Ffowcs Williams, and W. Smith. On the noise sources of the unsuppressed high-speed jet. *Journal of Fluid Mechanics*, 50:21–31, 1971.

[34] C.K.W. Tam. Directional acoustic radiation from a supersonic jet generated by shear layer instability. *Journal of Fluid Mechanics*, 46:757–768, 1971.

[35] C.K.W. Tam. On the noise of a nearly ideally expanded supersonic jet. *Journal of Fluid Mechanics*, 51:69–95, 1972.

[36] C.K.W. Tam and P. Morris. The radiation of sound by the instability waves of a compressible plane turbulent shear layer. *Journal of Fluid Mechanics*, 98:349–381, 1980.

[37] C.K.W. Tam and D. Burton. Sound generated by instability waves of supersonic flows. part 1. two-dimensional mixing layers. *Journal of Fluid Mechanics*, 138:249–271, 1984.

[38] C.K.W. Tam and D. Burton. Sound generated by instability waves of supersonic flows. part 2. axisymmetric jets. *Journal of Fluid Mechanics*, 138:273–295, 1984.

[39] C.K.W. Tam and F.Q. Hu. On the three families of instability waves of high-speed jets. *Journal of Fluid Mechanics*, 201:447–483, 1989.

[40] C.K.W. Tam, P. Chen, and J. Seiner. Relationship between instability waves and noise of high-speed jets. *AIAA Journal*, 3(7):1747–1752, 1992.

[41] D.K. McLaughlin, G.R. Morrison, and T.R. Troutt. Experiments on the instability waves in a supersonic jet and their acoustic radiation. *Journal of Fluid Mechanics*, 69:73–95, 1975.

[42] D. Pack. A note on prandtl's formula for the wavelength of a supersonic gas jet. *Quarterly Journal of Mechanics and Applied Mathematics*, 3:173–181, 1950.

[43] E. Love, C. Grigsby, L. Lee, and M. Woodling. Experimental and theoretical studies of axisymmetric free jets. Technical Report R-6, NASA, 1959.

[44] D. McLaughlin, G. Morrison, and T. Troutt. Reynolds number dependence in supersonic jet noise. *AIAA Journal*, 15(4):526–532, 1977.

[45] J. Laufer, R. Schlinker, and R. Kaplan. Experiments on supersonic jet noise. *AIAA Journal*, 14(4):489–497, 1976.

[46] G. Morrison and D. McLaughlin. Instability process in low reynolds number supersonic jets. *AIAA Journal*, 18(7):793–800, 1980.

[47] P. Morris and C.K.W. Tam. Near and far field noise from large-scale instabilities of axisymmetric jets. Paper 77-1351, AIAA, 1977.

[48] T.R. Troutt and D.K. McLaughlin. Experiments on the flow and acoustic properties of a moderate reynolds number supersonic jet. *Journal of Fluid Mechanics*, 116:123–156, 1982.

[49] J. Seiner, D. McLaughlin, and C. Liu. Supersonic jet noise generated by large-scale instabilities. TP 2072, NASA, 1982.

[50] H. Oertel. Mach wave radiation of hot supersonic jets investigated by means of the shock tube and new optical techniques. In *Proceedings of the 12th International Symposium on Shock Tubes and Waves*, pages 266–275, Jerusalem, 1980.

[51] H. Oertel. *Coherent Structures Producing Machwaves Inside and Outside of the Supersonic Jet*, pages 334–343. Springer-Verlag, 1982.

[52] J. Lepicovsky, K.K. Ahuja, and M. Salikuddin. An experimental study of tine excited heated jets. Paper AIAA-84-2341, A.I.A.A., 1984.

[53] J. Lepicovsky, K.K. Ahuja, W.H. Brown, and R.H. Burrin. Coherent large-scale structures in high reynolds number supersonic jets. CR 3952, N.A.S.A., 1985.

[54] S. Arnette, M. Samimy, and G. Elliott. On streamwise vortices in high reynolds number supersonic axisymmetric jets. *Physics of Fluids A*, 5(1):187–202, 1993.

[55] J.C. Sivells. A computer program for the aerodynamic design of axisymmetric and planar nozzles for supersonic and hypersonic wind tunnels. TR 78-63, AEDC, 1978.

[56] H. Bergh and H. Tijdeman. Theoretical and experimental results for the dynamic response of pressure measuring systems. TR F 238, NLR, 1965.

[57] D. Fourguette, R. Dibble, and M. Mungal. Time evolution of the shear layer of a supersonic axisymmetric jet at matched conditions. Technical Report 90-0508, AAIA, 1990.

[58] J. Hall. *An Experimental Investigation of Structure, Mixing, and Combustion in Compressible Turbulent Shear Layers.* PhD thesis, California Institute of Technology, 1991.

[59] A. Pope and K. Goin. *High Speed Wind Tunnel Testing.* Wiley, New York, 1965.

[60] W. Gracey, W. Letko, and W. Russell. Wind-tunnel investigation of a number of total-pressure tubes at high angles of attack - subsonic speeds. TN 2331, NACA, 1951.

[61] W. Gracey, D. Coletti, and W. Russell. Wind-tunnel investigation of a number of total-pressure tubes at high angles of attack - supersonic speeds. TN 2261, NACA, 1951.

[62] T. Dudziniski and L. Krause. Effect of inlet geometry on flow-angle characteristics of miniature total-pressure tubes. TN D-6406, NASA, 1971.

[63] A. Young and J. Maas. The behaviour of a pitot tube in a transverse total-pressure gradient. R&M 1770, A.R.C., 1936.

[64] P.O.A.L. Davies. The behaviour of a pitot tube in transverse shear. *Journal of Fluid Mechanics*, 3:441–456, 1957.

[65] M. Lighthill. Contributions to the theory of the pitot-tube displacement effect. *Journal of Fluid Mechanics*, 2:493, 1957.

[66] N. Johannesen and W. Mair. Experiments with large pitot tubes in a narrow supersonic wake. *Journal of the Aeronautical Sciences*, 19:785–787, 1952.

[67] H. Tijdeman and H. Bergh. The influence of the main flow on the transfer function of a tube-transducer system used for unsteady pressure measurements. MP 72023U, NLR, 1972.